TESE DE DOUTORAMENTO

DETECTION, CHARACTERIZATION AND QUANTIFICATION OF NANOPARTICLES IN MARINE PRODUCTS AND DERIVATIVES

María Vanesa Taboada López

ESCOLA DE DOUTORAMENTO INTERNACIONAL
PROGRAMA DE DOUTORAMENTO EN CIENCIA E TECNOLOXÍA QUÍMICA

SANTIAGO DE COMPOSTELA
2020

USC
UNIVERSIDADE
DE SANTIAGO
DE COMPOSTELA

DECLARACIÓN DO AUTOR/A DA TESE

Detection, characterization and quantification of nanoparticles in marine products and derivatives

Dna. María Vanesa Taboada López

Presento a miña tese, seguindo o procedemento axeitado ao Regulamento, e declaro que:

1) A tese abarca os resultados da elaboración do meu traballo.
2) De selo caso, na tese faise referencia ás colaboracións que tivo este traballo.
3) A tese é a versión definitiva presentada para a súa defensa e coincide coa versión enviada en formato electrónico.
4) Confirmo que a tese non incorre en ningún tipo de plaxio doutros autores nin de traballos presentados por min para a obtención doutros títulos.

En Santiago de Compostela, 4 de Decembro de 2020

Asdo. María Vanesa Taboada López

USC
UNIVERSIDADE
DE SANTIAGO
DE COMPOSTELA

AUTORIZACIÓN DO DIRECTOR/TITOR DA TESE

D./Dna. **Pilar Bermejo Barrera**

En condición de: **Director/a**

Título da tese: **Detection, characterization and quantification of nanoparticles in marine products and derivatives**

INFORMA:

Que a presente tese, correspóndese co traballo realizado por D./Dna. María Vanesa Taboada López, baixo a miña dirección/titorización, e autorizo a súa presentación, considerando que reúne os requisitos esixidos no Regulamento de Estudos de Doutoramento da USC, e que como director/titor non incorre nas causas de abstención establecidas na Lei 40/2015.

En **Santiago de Compostela**, 4 de Decembro de 2020

Sinatura electrónica

USC
UNIVERSIDADE
DE SANTIAGO
DE COMPOSTELA

AUTORIZACIÓN DO DIRECTOR/TITOR DA TESE

D./Dna. **Antonio Moreda Piñeiro**

En condición de: **Titor/a e director/a**

Título da tese: **Detection, characterization and quantification of nanoparticles in marine products and derivatives**

INFORMA:

Que a presente tese, correspóndese co traballo realizado por D./Dna. María Vanesa Taboada López, baixo a miña dirección/titorización, e autorizo a súa presentación, considerando que reúne os requisitos esixidos no Regulamento de Estudos de Doutoramento da USC, e que como director/titor non incorre nas causas de abstención establecidas na Lei 40/2015.

En **Santiago de Compostela**, 4 de Decembro de 2020

Sinatura electrónica

USC
UNIVERSIDADE
DE SANTIAGO
DE COMPOSTELA

ACKNOWLEDGEMENT

USC
UNIVERSIDADE
DE SANTIAGO
DE COMPOSTELA

ACKNOWLEDGMENT

Cuatro años después de empezar esta aventura, ha llegado el momento de daros las gracias a todos aquellos que habéis formado parte de ella.

En primer lugar, quiero dar las gracias a mis directores, *Antonio Moreda* y *Pilar Bermejo*. Gracias por haber confiado en mí desde el momento en el que crucé la puerta del departamento y poner todos los medios para que esta tesis pudiese llegar lo más lejos posible.
Gracias a todos los miembros del grupo *GETEE*. A *Paloma*, por su inestimable ayuda a lo largo de todo este camino, por el apoyo, la paciencia y los buenos consejos. A *Raquel*, por involucrarse en esta tesis como una directora más y por sacar a relucir mi faceta de actriz. Gracias también a *Mari Carmen* y *Elena*, por nuestro "club del tupper" y por hacer de nuestras comidas y cafés momentos mucho más divertidos. A *Manolo*, por tener siempre la broma adecuada en el momento adecuado y por aportar esa alegría y buen humor.
Gracias a *Pili*, por cogerme de la mano desde que empecé esta etapa y no soltarla. Gracias por el apoyo, por la comprensión, por los mensajes de ánimo escondidos en las libretas del laboratorio, por 'poñerme a vivir' y por esos cafés (en Santiago o en Arzúa) tan necesarios y terapéuticos.
Gracias *Alá*, por haberme aportado sólo cosas buenas desde que nos conocimos. Gracias por tus detalles para levantarme el ánimo, por tu retranca gallega, por enseñarme tantas cosas y por ayudarme siempre que lo he necesitado sin tener ni que pedirlo.
Gracias *Iván*, por ese toque de sabiduría tan tuyo y por compartir conmigo comidas y cafés acompañados siempre de los mejores y más sinceros consejos.

Gracias a *Iria*, por dar nuestros primeros pasos juntas con el 'single particle'; a *Juanjo*, por los cafés en el Lago y en la terraza de la facultad; y a *Kolita* y *Thillini*, por enseñarme que todo esfuerzo tiene su recompensa y que hay luchar por nuestras metas. Gracias también a *Juan*, *Ana*, *Cristián*… por los momentos compartidos.
Gracias a todos los miembros del grupo *LIDSA*, por ser los mejores vecinos, por las comidas de departamento y por estar siempre dispuestos a ayudar, colaborar y organizar.
Gracias al grupo *GEAS*, de la universidad de Zaragoza, por la oportunidad de poder trabajar mano a mano con ellos. En especial, gracias a *David*, por las largas horas de AF4-ICP-MS, por los bocadillos de ingredientes sorprendentes y por ser el mejor anfitrión. A *Dani*, por poner hilo musical a las tardes de tratamiento de datos y por aportar ese toque de madurez y realidad. A *Laura*, por los menús compartidos de la cafetería y por hacerme de guía por el laberinto de pasillos de la facultad. Gracias también a *Ana Cris* y *Celia*, por acogerme de esa manera tan cercana y hacer de mi estancia una experiencia increíble.
Quiero agradecer también a *Heidi Goenaga* y a su '*Inorganic Team*' mi maravillosa y provechosa estancia en Reino Unido. Gracias a *Dorota*, por ser mi 'buddy' y enseñarme los entresijos del AF4. Gracias a *Susana* y *Estela*, por acogerme desde el primer momento con los brazos abiertos y por haber hecho de mi estancia una experiencia vital que me acompañará toda la vida. Me quedo con las cervezas en el 'Adelaide', los tés en los momentos de descanso para coger fuerzas y esas increíbles barbacoas los fines de semana.
Gracias a *Vicenta Devesa* y *Deni Vélez*, de *IATA-CSIC*, por darme la oportunidad de iniciarme en el mundo de los cultivos celulares y por haber sido tan cercanas conmigo. Gracias por haberos involucrado tanto en esta tesis. A *Gabi* que, a pesar de estar en la última etapa de su tesis doctoral, pudo sacar tiempo para ayudarme. Gracias también a *Carlos*, porque durante su estancia en Santiago me ayudó a dar mis primeros pasos en este campo que me era tan desconocido.
Gracias a la *Unidad de Proteómica* del *IDIS*. Gracias *Susana* y *María* por vuestra paciencia, cariño y esfuerzo.

Gracias a mis *amigas* de toda la vida, 'as de sempre', por permanecer a mi lado durante todos estos años, por aguantarme mientras hablo de química y por hacer que me olvidase de ella cuando estaba saturada. Gracias en especial a *Vane*, por estar siempre incondicionalmente, por ser mi fiel compañera y por borrarme de un plumazo las preocupaciones. Gracias a *Rocío*, por los más de veinte años compartidos, por animarme a dar este paso y por ejercer de mentora. Gracias a mis *amigos químicos*, por nuestros viajes y reencuentros. A *Patri* y *Chechu*, por los cafés en el Seu en los que nos ponemos al día; a *Andrea*, por ser la mejor anfitriona en Londres; y a *Bego*, por estar siempre ahí a pesar de la distancia.

Gracias a mi *familia*, los pilares fundamentales en los que sustenta esta tesis. Gracias *papá* y *mamá*, por darme siempre alas para tomar mis decisiones y por apoyarme en el camino que he escogido. Gracias por vuestro esfuerzo y trabajo duro para que yo haya podido llegar hasta aquí, por embarcaros en todas mis aventuras y por creer en mí. Gracias a *Marta*, mi mitad, por seguirme allá donde me lleve la vida y celebrar todos y cada uno de mis logros. Gracias por la comprensión y la paciencia y por ayudarme a desconectar cuando en mi cabeza no cogía nada más. Gracias a mis *abuelos*, por apoyarme al 100% en todas y cada una de las etapas de mi vida y ayudarme en todo lo que habéis podido.

Gracias *Dami*, por ser el primero en animarme a tomar este camino y ayudarme a alcanzar la meta. Gracias por tu fe en mí, por levantarme siempre que me caigo y por compartir mis alegrías.

USC
UNIVERSIDADE
DE SANTIAGO
DE COMPOSTELA

INDEX

USC
UNIVERSIDADE
DE SANTIAGO
DE COMPOSTELA

INDEX

USC
UNIVERSIDADE
DE SANTIAGO
DE COMPOSTELA

USC
UNIVERSIDADE
DE SANTIAGO
DE COMPOSTELA

ABBREVIATIONS

USC
UNIVERSIDADE
DE SANTIAGO
DE COMPOSTELA

ABBREVIATIONS

ADI	Acceptable Daily Intake
ADME	Absorption, Distribution, Metabolism and Excretion
AF4	Asymmetric Flow Field-Flow Fractionation
AFM	Atomic Force Microscopy
AFS	Atomic Fluorescence Spectrometry
ATR-FTIR	Attenuated Total Reflection-Fourier Transform Infrared Spectroscopy
BSA	Bovine Serum Albumin
CBB	Coomassie Brilliant Blue
CD	Circular Dichroism
CE	Capillary Electrophoresis
CER	Cation Exchange Reaction
CLP	Classification, Labelling and Packaging
CVG	Chemical Vapor Generation
DDA	Data-Dependent Acquisition
DIA	Data-Independent Acquisition
DLS	Dynamic Light Scattering
DMEM	Dulbecco's Modified Eagle Medium
DNA	Deoxyribonucleic Acid
DSC	Differential Scanning Calorimetry
DTT	Dithiothreitol
EC	European Commission
EC50	Median Effective Concentration
ECHA	European Chemicals Agency
EDL	Electrical Double-Layer
EDX	Energy Dispersive X-ray Spectroscopy
EELS	Electron Energy Loss Spectroscopy
EFSA	European Food Safety Authority

ERS	Electrical Resistance System
ESEM	Environmental Scanning Electron Microscopy
ESI	Electrospray Ionization
ET-AAS	Electrothermal-Atomic Absorption Spectroscopy
EU	European Union
FCS	Fluorescence Correlation Spectroscopy
FDA	Food and Drug Administration
FDR	False Discovery Rate
FESEM	Field-Emission Scanning Electron Microscopy
FFF	Field-Flow Fractionation
FlFFF	Flow Field-Flow Fractionation
FS	Fluorescence Spectroscopy
FTIR	Fourier Transform Infrared Spectroscopy
GE	Gel Electrophoresis
HBSS	Hanks' Balanced Salt Solution
HBV	Hepatitis B Virus
HDC	Hydrodynamic Chromatography
HIV	Human Immunodeficiency Virus
IAA	Iodoacetamide
IARC	International Agency for Research on Cancer
ICP	Inductively Coupled Plasma
ICP-MS	Inductively Coupled Plasma-Mass Spectrometry
ICP-MS/MS	Inductively Coupled Plasma-Tandem Mass Spectrometry
ICP-OES	Inductively Coupled Plasma-Optical Emission Spectrometry
IL	Interleukin
IR	Infrared Spectroscopy
IS	Internal Standard
ITC	Isothermal Titration Calorimetry
KED	Kinetic Energy Discrimination
LC	Liquid Chromatography
LC50	Median Lethal Concentration
LC-MS/MS	Liquid Chromatography coupled with tandem Mass Spectrometry
LOD	Limit Of Detection

LOQ	Limit of Quantification
MALDI	Matrix-Assisted Laser Desorption/Ionization
MALS	Multi-Angle Light Scattering
MS	Mass Spectrometry
MWCO	Molecular Weight Cut-Offs
ND	Non-Detected
NEAA	Non-Essential Aminoacids
NMR	Nuclear Magnetic Resonance
NMs	Nanomaterials
NMWL	Nominal Molecular Weight Limit
NOM	Non-Organic Matter
NPs	Nanoparticles
NSOM	Near-field Scanning Optical Microscopy
PBS	Phosphate-Buffered Saline
PCA	Principal Component Analysis
PCC	Particle Collision Coulometry
PDA	Photodiode Array
PPP	Plant Protection Products
PSD	Particle Size Distribution
PTA	Particle Tracking Analysis
PTFE	Poly(tetrafluoroethylene)
PVP	Polyvinylpyrrolidone
QDs	Quantum Dots
RC	Regenerated Cellulose
REACH	Registration, Evaluation, Authorisation and Restriction of Chemicals
ROS	Reactive Oxygen Species
RS	Raman Scattering
RSD%	Relative Standard Deviation %
SAXS	Small-Angle X-ray Scattering
SCENIHR	Scientific Committee on Emerging and Newly Identified Health Risks
SD	Standard Deviation
SdFFF	Sedimentation Field-Flow Fractionation
SDS	Sodium Dodecyl Sulphate

SDS-PAGE	Sodium Dodecyl Sulphate-Polyacrylamide Gel Electrophoresis
SEC	Size Exclusion Chromatography
SEM	Scanning Electron Microscopy
SERS	Surface-Enhanced Raman Scattering
SF-ICP-MS	Sector Field-Inductively Coupled Plasma-Mass Spectrometry
SLS	Static Light Scattering
sp-ICP-MS	Single Particle-Inductively Coupled Plasma-Mass Spectrometry
SPR	Surface Plasmon Resonance
STD	Standard
STEM	Scanning Transmission Electron Microscopy
STM	Scanning Tunnelling Microscopy
SWATH-MS	Sequential Window Acquisition of all Theoretical spectra-Mass Spectrometry
t_d	Dwell time
TE%	Transport Efficiency %
TEER	Transepithelial Electrical Resistance
TEM	Transmission Electron Microscopy
TERS	Tip-Enhanced Raman Scattering
TGA	Thermal Gravimetric Analysis
TMAH	Tetramethylammonium Hydroxide
TOF-MS	Time-Of-Flight-Mass Spectrometry
TTIP	Titanium Tetraisopropoxide
UK	United Kingdom
USA	United States of America
UV	Ultraviolet
UV-vis	Ultraviolet-visible spectroscopy
VIP	Voltammetry of Immobilized Particles
VSSA	Volume Specific Surface Area
VTG	Vitellogenin
XAS	X-ray Absorption Spectroscopy
XRD	X-ray Diffraction
ZP	Zona Pellucida

USC
UNIVERSIDADE
DE SANTIAGO
DE COMPOSTELA

USC
UNIVERSIDADE
DE SANTIAGO
DE COMPOSTELA

ABSTRACT

USC
UNIVERSIDADE
DE SANTIAGO
DE COMPOSTELA

ABSTRACT

Nanoscience was first introduced by Richard Feynman in 1959. Since then, nanotechnology has not stopped evolving. It includes several fields, such as chemistry, materials science, medicine, toxicology, ecotoxicology and industry. In 2011, the European Commission (EC) defined a nanomaterial (NM) as a natural, incidental or manufactured material where at least 50% of their particles and aggregates have one or more external dimensions between the size range from 1 to 100 nm. Nanofilms, nanotubes and nanoparticles (NPs) have one, two and three dimensions on that nanoscale, respectively. These NMs have novel physicochemical, electronic, optical and mechanical properties, besides a high reactivity.

Titanium dioxide (TiO_2) was first commercialized in 1916. It can be named as titanium oxide (IV), white titanium or pigment white 6 in paints and E171 as food additive. Traditionally, it was used as pigment in paints, coatings, plastics, inks and food. TiO_2 NPs have higher photocatalytic activity, light dispersion and opacity than bulk TiO_2. They are also antimicrobial agents. TiO_2 NPs are used in photovoltaics, photocatalysis and medicine. They are included in cosmetics as ultraviolet (UV) radiation blockers.

Silver (Ag) NPs are very popular due to their novel physicochemical properties, such as high electrical and thermal conductivity, chemical stability, catalytic activity and non-linear optical behavior. They have antimicrobial properties against Gram-positive and Gram-negative bacteria, fungi and viruses. Ag NPs are listed as one of the most commercialized NMs. They are used in several fields, such as catalysis, electronics, optics, environment, textiles, personal care products, food industry and medicine.

The potential effects of NMs on humans and on the environment are still unknown. Nanotoxicology aims to identify, manage and reduce the

potential adverse effects caused by NMs. Due to their novel properties, these NMs may have adverse effects different from that produced by bulk materials. Principal routes of exposure are ingestion, inhalation and dermal penetration. Their behavior is a combination of absorption, distribution, metabolism and excretion (ADME).

Nanotechnology is applied in several areas of food industry (processing, packaging, storage and consumption). There is concern about the direct use of NMs in food products, their migration from packaging and sensors to food matrix and their use during food production. All of them may lead to unintentional human exposure through ingestion. Digestion process may modify the physicochemical properties of NMs (dissolution and aggregation) and, hence, alter their toxicity. Bioaccessibility (fraction of a component that is released from a food matrix in the digestive fluids) and bioavailability (fraction of a component that pass through gastrointestinal epithelium and reach systemic circulation) studies are, therefore, very important.

NMs are considered emergent contaminants and their presence in the environment may have adverse effects. Once in the environment, NMs are subjected to physical, chemical and biological transformations. Properties of NMs and environmental conditions determine these processes. Aerial or atmospheric compartment, soils and water are susceptible to NMs exposure. Specifically, NMs may be released to seawater, where benthic bivalve organisms (sessile and filter-feeders) are targets for accumulation and toxicity of contaminants. They can penetrate inside the organisms through gills or digestive system and be translocated to hemolymph or other organs.

When NMs are in contact to biological fluids, the interaction between NMs and proteins leads to the formation of a protein corona. The composition, thickness and conformation of the corona depend on the properties of NMs, the nature of the media and the exposure time. Its structure is divided in “hard corona” (high affinity proteins that directly interact with the NM) and “soft corona” (weakly bound proteins that interact with “hard corona” proteins). Protein corona gives NMs a new identity that conditions their transport, uptake mechanism and subcellular location.

The analysis of NMs implies their detection and quantification (mass and number concentration), along with their physical (size, shape and surface properties) and chemical (core and coating composition) characterization. Sample pre-treatment methods are usually required, for example, enzymatic and acid digestion methods. Inductively coupled plasma-mass spectrometry (ICP-MS) and related techniques are used for characterization and quantification of NPs, such as single particle-ICP-MS (sp-ICP-MS) or ICP-MS coupled with asymmetric flow field-flow fractionation (AF4-ICP-MS). Scanning electron microscopy (SEM), transmission electron microscopy (TEM) and dynamic light scattering (DLS) are also commonly used to characterize NMs.

This Doctoral thesis is divided into four parts: (1) optimization of enzymatic extraction methods of TiO_2 NPs and Ag NPs from marine products (bivalve molluscs) and derivatives (crab sticks); (2) optimization of NPs separation in enzymatic extracts of bivalve molluscs by AF4 coupled with different detectors; (3) evaluation of potential risk of TiO_2 NPs and Ag NPs in humans through the ingestion of food products containing NPs; and (4) characterization of NP-associated protein corona in hemolymph of bivalve molluscs.

Part I. Enzymatic hydrolysis for NPs assessment by sp-ICP-MS

A. Enzymatic hydrolysis as a sample pre-treatment for TiO_2 NPs assessment in surimi (crab sticks) by sp-ICP-MS

A sample pre-treatment method, based on enzymatic hydrolysis, for TiO_2 NPs assessment in surimi samples has been optimized and validated. TiO_2 NPs were included in surimi as part of food additive E171. Surimi samples were bought in local supermarkets and homogenized by mechanical blending. Total titanium (Ti) concentration was determined by ICP-MS after microwave assisted acid digestion. For TiO_2 NPs extraction, 7.5 mL of a pancreatin and lipase solution (8 g L^{-1}), prepared in 0.2 M NaH_2PO_4/0.2 M NaOH at pH 7.4, were added to 1 g of sample. This mixture was stirred (200 rpm) and incubated at 37 ºC during 12 h. Enzymatic extracts were

centrifugated (8 ºC, 3900 rpm, 10 min) and stored at 4 ºC. Then, they were diluted with glycerol 1% (v/v) and analyzed by sp-ICP-MS.

There was no matrix effect, so aqueous ionic Ti calibrations were used. Good repeatability, in terms of relative standard deviations (RSD%), was obtained for TiO_2 NPs concentration (25%) and size (8%). The sensitivity was expressed using limit of detection (LOD) and limit of quantification (LOQ) for concentration and were as follows: 5.10×10^5 and 1.70×10^6 NPs g^{-1}. LOD in size varied between 31.3 and 37.1 nm. Analytical recovery values for standard solutions of 50 and 100 nm TiO_2 NPs were 108±5% and 105±4%, respectively.

Eleven out of the twenty-two analyzed samples contained Ti. The enzymatic hydrolysis method was applied to these samples. TiO_2 NPs levels were between 1.96×10^7 and 1.19×10^8 TiO_2 NPs g^{-1}. Size distributions were very different between samples, being the most frequent sizes between 42 and 75 nm, and mean sizes between 65 and 217 nm.

TiO_2 NPs presence in the enzymatic extracts was confirmed by an oxidative treatment with hydrogen peroxide and heating before TEM analysis.

B. Ultrasound assisted enzymatic hydrolysis for isolating TiO_2 NPs from bivalve mollusk before sp-ICP-MS

Characterization and quantification of TiO_2 NPs in bivalve molluscs were performed by sp-ICP-MS after ultrasound assisted enzymatic hydrolysis. Eleven bivalve mollusc (fresh and frozen) samples were acquired in local supermarkets. These samples were washed with ultrapure water and homogenized by mechanical blending. Total Ti concentration was determined by ICP-MS measurement after a microwave assisted acid digestion. For TiO_2 NPs extraction, a volume of 7.5 mL of pancreatin and lipase solution (3 g L^{-1}), prepared in buffer solution (0.2 M NaH_2PO_4/0.2 M NaOH at pH 7.4), were added to the sample (1 g). The mixture was ultrasonicated (60% amplitude) in an ice-bath for 10 min, centrifugated (8 ºC, 3900 rpm, 25 min) and diluted with glycerol 1% (v/v) prior their analysis by sp-ICP-MS.

Aqueous ionic Ti calibrations were used due to the absence of matrix effect. RSD% of 17 and 3% were obtained for TiO_2 NPs

concentration and size determinations. LOD and LOQ for TiO_2 NPs concentration were 5.28×10^6 and 1.76×10^7 NPs g^{-1}, respectively. LOD in size, calculated based on 3σ and 5σ criteria, were 24.4 and 30.4 nm, respectively. Mean analytical recovery was 95±6% for 50 nm TiO_2 NPs at two concentration levels (7 and 14 μg L^{-1}).

Clams, cockles, mussels, razor clams, oysters and variegated scallops were analyzed. All samples contained Ti and TiO_2 NPs. Total Ti concentrations were found in the range of 0.285-3.42 μg g^{-1}. Regarding TiO_2 NPs, the highest concentration was found in mussels ($1.25\times10^8\pm1.06\times10^7$ NPs g^{-1}), while a razor clam sample showed the lowest concentration ($2.36\times10^7\pm2.54\times10^6$ NPs g^{-1}). Most frequent size values were similar between different samples (53-69 nm).

The presence of TiO_2 NPs in enzymatic extracts was confirmed by DLS analysis. Most samples showed polydispersion indexes higher than 1.1 and two size distributions.

C. Determination and characterization of Ag NPs in bivalve molluscs by ultrasound assisted enzymatic hydrolysis and sp-ICP-MS

Bivalve molluscs (clams, cockles, mussels, razor clams, oysters and variegated scallops) were bought in local supermarkets, washed with ultrapure water and homogenized by mechanical blending. Then, 1 g of each sample was mixed with 10 mL of 2 g L^{-1} pancreatin and lipase solution (prepared in 0.2 M NaH_2PO_4/0.2 M NaOH at pH 7.4) and the mixture was ultrasonicated at 80% amplitude for 10 min in an ice-bath. The extracts were measured by sp-ICP-MS. A microwave assisted acid digestion followed by ICP-MS analysis was used for determining total Ag concentrations.

Due to the absence of matrix effect, aqueous ionic Ag calibrations were used. RSD% for Ag NPs concentration and size were 8 and 3%, respectively. Regarding the sensitivity, LOD and LOQ for Ag NPs concentration were 4.17×10^6 and 1.39×10^7 Ag NPs g^{-1}. The LOD in size was calculated following several methods obtaining values ranged from 13 to 23 nm. Analytical recovery values for 40 and 60 nm Ag NPs were 109±10% and 92±2%, respectively.

Ag was quantified in seven samples out of the eleven analyzed samples. Ag levels were found between 0.0841 and 3.72 μg g^{-1}. Four

samples were below the LOD (0.0247 μg g^{-1}). Regarding Ag NPs concentration (1.56×10^{7}-1.85×10^{9} Ag NPs g^{-1}), the highest levels were found in variegated scallops, oysters and Japanese clams, whereas the Atlantic surf clams showed the lowest Ag NPs concentration.

Ag NPs presence in the enzymatic extracts was confirmed by SEM analysis after an oxidative treatment (hydrogen peroxide and heating).

Part II. Optimization of separation of NPs by AF4 coupled with different detectors

D. AF4-UV-ICP-MS for detecting and quantifying Ag NPs in seafood after enzymatic hydrolysis

Detection and quantification of Ag NPs in bivalve molluscs (clams, oysters and variegated scallops) were performed by AF4 technique coupled with a UV spectrophotometer and ICP-MS. 1 g of sample was incubated with 10 mL of pancreatin and lipase solution (2.0 g L^{-1}) prepared in 0.2 M Trizma® (pH 7.4) for 12 h at 37 ºC in an oven equipped with a circular rotor. Solid residues were removed by centrifugation (8 °C, 3900 rpm, 25 min).

Separation in AF4 channel was performed with a regenerated cellulose membrane (10 kDa, 350 μm spacer) and 5 mM Tris-HCl as mobile phase. During the focusing step (4.0 min), tip and focus flow were 0.20 and 3.0 mL min^{-1}, respectively. In the elution step, cross flow was 3.0 mL min^{-1} for 15 min, followed by a linear decay over 7.5 min. Finally, a washing step (9.4 min) was included.

The total Ag concentrations (microwave assisted acid digestion and ICP-MS measurement) and Ag NPs levels (using the proposed method) were analyzed in four bivalve mollusc samples. The highest Ag concentrations in AF4 fractions was found in a frozen variegated scallop sample, while the lowest was found in oysters. All concentrations were within 4.1×10^{1}-2.3×10^{2} μg Ag kg^{-1}, whereas total Ag concentrations were between 1.6×10^{2} and 3.7×10^{3} μg Ag kg^{-1}. Fractograms of AF4-UV-ICP-MS showed different size distributions due to their different elution profile. Membrane recovery values were from 49 to 121%. According to the results obtained by UV spectra for

the analyzed samples, coelution of Ag NPs and proteins may indicate some kind of interactions between them.

Part III. Evaluation of potential risk of TiO_2 NPs and Ag NPs in humans through the ingestion of food products containing NPs

E. Biopersistence rate of metallic NPs in the gastrointestinal human tract (Stage 0 of the EFSA guidance for nanomaterials risk assessment)

Following the recommendations stablished by EFSA for the risk of the NMs usage in food and feed chain, an *in vitro* gastrointestinal digestion was performed to assess the biopersistence rate of TiO_2 NPs and Ag NPs in standards and foodstuff. Standards of two different sizes (50 and 100 nm TiO_2 NPs, and 40 and 60 nm Ag NPs) at three concentration levels were studied. In addition, food additive E171, bivalve molluscs and crab stick samples that contain NPs were also assessed. Convenient volumes of standard and E171 solutions, or 5 g of samples, were mixed with 50 mL of ultrapure water into Erlenmeyer flaks, and the pH was adjusted at 2.0 using a 0.6 M HCl solution. Gastric solution (0.16 g mL^{-1} pepsin in 0.1 M HCl) was added to get a final concentration of 7.5 mg mL^{-1}. Samples were incubated at 37 ºC for 2 h under orbital-horizontal stirring (150 rpm). Gastric digestion was stopped by introducing the samples in an ice-bath. Then, pH was adjusted to 7.0 with 0.2 M NaOH, and 25% (v/v) of intestinal solution (4 g L^{-1} pancreatin and 25 g L^{-1} bile salts in 0.1 M $NaHCO_3$) was added. Samples were incubated using the aforementioned conditions for 2 h. NPs concentration, size distribution and ionic content have been analyzed at the beginning of the digestion (T0) and at three times (30, 60 and 120 min) during gastric and intestinal stages. All measurements were performed by sp-ICP-MS.

In general, NPs agglomeration over gastric stage and NPs dispersion during intestinal digestion have been observed. Ag NPs have shown a size-dependent behavior. While 40 nm Ag NPs were agglomerated during gastric stage, 60 nm Ag NPs were ionized. In addition, sample matrix was found to influence the biopersistence rate of TiO_2 NPs and Ag NPs. TiO_2 NPs in bivalve molluscs were

progressively released, whereas TiO_2 NPs in crab sticks followed a similar behavior to the standards and E171. Ag NPs in bivalve molluscs showed distinct behavior depending on the sample.

TiO_2 NPs standards and food additive E171 were not degraded over the digestion. Ag NPs standards were less biopersistent than TiO_2 NPs. Higher degradation rate of Ag NPs compared to TiO_2 NPs were also observed in bivalve molluscs. All biopersistence rates were higher than the limit set by EFSA guidance (12%).

F. Caco-2 in vitro model of human gastrointestinal tract for studying the absorption of TiO_2 NPs and Ag NPs from seafood samples

Bivalve molluscs containing TiO_2 NPs and Ag NPs were subjected to an *in vitro* gastrointestinal digestion to determine the bioaccessibility of these NPs. Caco-2 cells were selected as human intestinal epithelium model to perform bioavailability studies (0-2 h). Bioaccessibility and bioavailability were assessed for total Ti and Ag (ICP-MS), and for TiO_2 NPs and Ag NPs (sp-ICP-MS).

Caco-2 were maintained in Dulbecco's modified Eagle medium (DMEM) which was supplemented with 10% (v/v) fetal bovine serum, 2 mM L-glutamine, 1% (v/v) penicillin/streptomycin, 1 mM sodium pyruvate and 1 mM non-essential aminoacids (NEAA) at 37 ºC, in a humidified atmosphere (95%) containing 5% CO_2. The medium was changed every 2 or 3 days at 80% confluence. Cells were detached using trypsin and seeded (7.5×10^4 cells cm^{-2}) on inserts with polyester membranes of Transwell® plates. Resuspended cells in DMEM were added to apical compartment (1.5 mL), while fresh DMEM was added to basolateral compartment (2.0 mL). Transepithelial electrical resistance (TEER) was monitored and 250 mΩ cm^2 was considered its optimal value. 7.5 mL of the bioaccesible fraction (digested samples following the protocol described above) were heated at 100 ºC for 5 min to inactivate enzymes. Glucose (1 g L^{-1}) was added, and 10 mM sodium chloride was used to adjust osmolarity (250-300 mOsm kg^{-1}). Bioavailability studies were performed by adding these treated bioaccesible fractions and Lucifer Yellow marker to apical compartment (1.5 mL), while Hank's balanced salt solution (HBSS) was added in basolateral compartment (2.0 mL). Transwell® plates

were incubated under the above-mentioned conditions (0-2 h). Finally, apical and basolateral fractions were collected, and phosphate-buffered saline (PBS) and trypsin were used to wash and detach cells.

Bioaccessibility percentages were in the range of 2.9-89% for total Ti and 6.5-51% for total Ag. The bioaccessibility values for TiO_2 NPs and Ag NPs were between 2.1 and 51% and 13 and 17%, respectively. Regarding transport studies, the obtained values were between 18 and 68% for Ti, and 0.016 and 0.017% for Ag. Bioavailability percentages for TiO_2 NPs and Ag NPs were 17-82% and 2.1-22%, respectively. Similar bioavailability percentages were found in Ti and TiO_2 NPs, while significant differences were observed between Ag and Ag NPs. Size distributions in bioaccesible fractions were higher than in apical, basolateral and cellular fractions for most of analyzed samples.

Part IV. Characterization of NPs protein corona in hemolymph of bivalve molluscs

G. TiO_2 NPs protein corona characterization and quantification in hemolymph of bivalve molluscs

A mesocosm system was settled to expose clams to TiO_2 NPs standards (50 and 100 nm) and food additive E171. Four tanks were prepared (1 control, 1 TiO_2 NPs 50 nm, 1 TiO_2 NPs 100 nm and 1 E171) with 30 specimens of clams each. Filtered marine seawater was used as medium and aeration systems were installed. Clams were fed with *in vitro* cultured phytoplankton every 2 days. TiO_2 NPs and E171 concentrations were progressively increased (2 mg L^{-1} increments) from 0 to 14 mg L^{-1} over 18 days. One specimen per tank was sampled before any addition (0 mg L^{-1}), at the 9th exposure day (8 mg L^{-1}) and at the last day of the experiment (14 mg L^{-1}). Hemolymph was extracted for all sampled specimens.

Centrifugation was selected as a separation technique of protein corona (pellet) and free proteins (supernatant) in hemolymph. Evolution profile of protein corona during the experiment was qualitatively and quantitatively studied by liquid chromatography coupled with tandem mass spectrometry (LC-MS/MS) and sequential window acquisition of all theoretical spectra mass spectrometry (SWATH-MS), respectively.

High variability between specimens was found even before the addition of NPs. NPs affinity for proteins changed over the time. During the exposure to 50 nm TiO_2 NPs, the concentrations of complement components (C3 and C1q) was reduced. In supernatants, superoxide dismutase (oxidative stress marker) and histone concentrations increased, but they did not interact with NPs. 100 nm TiO_2 NPs showed high affinity for histones (H2A and H2B) and low affinity for C3 complement component. Heat shock proteins, as well as ATP synthase (subunit beta) were part of the coronas. Food additive E171 showed high affinity for complement C1q-like protein, histones (H2A and H2B), talin-1, catalase and superoxide dismutase. The cytochrome c oxidase concentration progressively increased in supernatants, and the concentration of C3 complement component decreased. In general, due to the decrease in complement components and the increase in stress markers, TiO_2 NPs may cause alteration in immune system and oxidative stress.

USC
UNIVERSIDADE
DE SANTIAGO
DE COMPOSTELA

USC
UNIVERSIDADE
DE SANTIAGO
DE COMPOSTELA

I. INTRODUCTION

USC
UNIVERSIDADE
DE SANTIAGO
DE COMPOSTELA

1 INTRODUCTION TO NANOMATERIALS

Even though several nanomaterials (NMs), especially metallic nanoparticles (NPs), were detected in a lot of antiquities from Egypt, Mesopotamia and Rome, the concept of nanoscience was first introduced in 1959 by Richard Feynman during his talk "There's Plenty of Room at the Bottom". In 1974, the term "nanotechnology" was defined by Norio Taniguchi as "production technology allowing to reach ultrahigh precision and ultrasmall sizes of approximately 1 nm". It was established as a field in the 1980s. Nanotechnology evolution was only possible because of instrumental and tool development (Scanning Tunnelling Microscopy-STM and Atomic Force Microscopy-AFM). It involves several scientific fields, such as chemistry, materials science, medicine, toxicology, ecotoxicology and industry. The interest in nanotechnology grew in the 1990s and 2000s, and its breakthroughs do not stop increasing. The potential effects of NMs on human and the environment became a public concern and toxicological studies were established since there. Several efforts focused on developing frameworks and screening strategies for identifying, managing and reducing potential adverse effects of NMs have been performed. Worldwide companies are taking advantage of their novel properties and investigating new applications, while global regulatory agencies have been proposing regulations to control the use and classification of NMs [1, 2].

A NM was defined by the European Commission (EC) in 2011 as a natural, incidental or manufactured material containing unbound particles or aggregates where at least 50% of the particles have one or more external dimensions in size ranging from 1 to 100 nm [3]. When objects have three dimensions lower than a few hundred nanometres, they are considered NPs. If they have two dimensions lower than a few hundred nanometres, they are called "nanotubes" or "nanowires".

"Nanofilms" or "nanolayers" have only one dimension lower than 100 nm. NMs can also be classified based on their origin (i.e., natural or anthropogenic) and their elemental composition (i.e., metals, metal oxides, semiconductors or carbon NMs) [2]. They present different physicochemical, electronic, optical and mechanical (elasticity, hardness and ductility) properties from their bulk materials. Their reactivity increases because of the high surface-area-to-volume ratio, so many NMs can be used as catalysts. In semiconductors, the high electronic confinement is related to a high bandgap, optical absorption and photoluminescence. In addition, some NMs possess antibacterial, antifungal and antimicrobial activities [4].

Regarding preparation methods of NMs, they could be divided into top-down and bottom-up. In the top-down approach, the bulk material is treated to obtain reduced particle size by physical, chemical or mechanical processes. While in bottom-up methods, atoms or molecules are the starting material. Top-down approaches can be performed using mechanical milling (ball milling and mechanochemical synthesis), laser ablation, ion sputtering and lithography. Bottom-up treatments are divided in solid-, liquid- or gas-state synthesis methods. Physical and chemical vapor deposition methods are mainly used in the solid-state synthesis, while sol-gel, chemical reduction, colloidal (aqueous or organic), hydrothermal and solvothermal methods are applied in the liquid-state synthesis. The most common gas-phase synthesis methods are electrospray, inert gas condensation, laser and flame pyrolysis and biological methods. These biological or green synthesis methods are an emerging trend since they reduce the health and environmental impact. Their principles are clean chemistry, atom economy and environmentally friendly chemistry. They are based on bioreduction or biosorption processes performed by bacteria, fungi or plants. Other popular methods for NP synthesis are assisted procedures based on microwave energy, supercritical fluids or ultrasounds [5, 6].

The value chain of nanotechnology has four life cycle stages: NMs, nanointermediates, nanoenabled products and nanotools. This evolution reflects how nanotechnology is transformed into final products, so the number of nanoenabled products shows a rising trend for the future. In

terms of countries, the United States of America (USA) and Japan control all the four stages [7].
NMs and NPs have been applied in several fields, such as electronics and computing, energy, catalysis, photocatalysis, optics, biology and medicine, industry and personal care products. They are incorporated into various daily used products (sunscreens, cosmetics, textiles, food, packaging, transport, buildings, computers, sports goods…) [2, 8].

1.1 TITANIUM DIOXIDE NANOPARTICLES

Titanium dioxide (TiO_2) was discovered in 1791. It naturally exists as brookite, anatase and rutile. In 1916, TiO_2 was first manufactured and it is known as titanium (IV) oxide, titania, titanium white or pigment white 6 in building paints, and E171 as a food additive. The photocatalytic activity of TiO_2 was reported for the first time in 1929. The process consists of: 1) photoexcitation, when TiO_2 is exposed to ultraviolet (UV) light (280-400 nm) electrons are excited from the valence band to the conduction band and electron-hole pairs are formed; 2) electron-hole pairs are dissociated and migrate towards the reactive surface; and 3) free electrons/holes are transferred to the reactive species adsorbed on TiO_2 surfaces, and photoreduction/ photooxidation takes place. Traditionally, TiO_2 was used as a pigment in paints, coatings, plastics, papers, inks, food, medicine and toothpastes. It provides whiteness and opacity due to reflection and no absorption of visible light.
Compared to bulk TiO_2, TiO_2 NPs present higher light scattering and opacity and they also have higher photoactivity due to the increase of their surface-area-to-volume ratio. Size and shape of NPs control quantum confinement effect and, therefore, their catalytic activity. Anatase phase has the highest photocatalytic activity. TiO_2 NPs are used in photovoltaics, photocatalysis (water-splitting, environmental decontamination of organic and inorganic materials, biocides and antibacterial sterilization and photosynthesis) and photoinduced super-hydrophilicity. Oxygen defects, chemical doping (metal or anion doping) and sensitization can be applied to reduce the bandgap into the visible region [9, 10]. TiO_2 NPs can also be used as UV-blockers

due to their high refractive index, UV light absorption and discoloration resistance. They are also one of the Food and Drug Administration (FDA) approved inorganic filters for sunscreen formulas [11, 12]. Concerning biomedical applications, TiO_2 NPs can be applied in cancer photodynamic therapies, drug delivery systems, cell imaging, biosensors and genetic engineering [13, 14]. They act as antimicrobial agents by generating reactive oxygen species (ROS), damaging cell membrane by electrostatic interaction, generating disturbance in metal/metal ion homeostasis and causing protein and enzyme dysfunction, genotoxicity and photokilling [15]. The antibacterial activity of TiO_2 NPs under visible light can be improved if they are doped with metal and non-metal elements, carbon NMs or with other metal oxide semiconductors [16].

TiO_2 NPs are mainly synthesized by sol-gel methods and their variants, such as microemulsion synthesis, colloidal method, aerogel method and ultrasonic-assisted synthesis. Sol-gel methods consist of five key steps: 1) hydrolysis of precursors in water/alcohol; 2) polycondensation of adjacent molecules by forming metal oxide linkages; 3) aging process that happens along with polycondensation and reprecipitation; 4) drying process: atmospheric/thermal, supercritical or freeze drying; and finally 5) thermal decomposition or calcination. Physical and chemical vapor depositions, electrodeposition, hydrothermal and solvothermal processes, sonochemical synthesis, microwave-assisted methods, anodic and direct oxidation methods, hard template methods, reverse microemulsion synthesis, hydrolysis process, thermohydrolysis methods and coprecipitation are also used to synthesize TiO_2 NPs. Several plasma-based synthesis approaches such as thermal plasma method, supersonically expanded plasma jet synthesis, induction plasma torch, reactive plasma processing and plasma electrolytic oxidation are also applicable. The crystal structure of TiO_2 NPs has been found to depend on the preparation method [17-20]. Phytosynthesis methods of TiO_2 NPs have also been proposed. Several plant extracts, such as *Annona squamosa* (sugar apple), *Aloe vera*, *Citrus reticulata* (mandarin orange), *Murraya koenigii* (curry tree) and *Curcuma longa* (turmeric), among others, have been employed. Titanyl hydroxide ($TiO(OH)_2$), TiO_2 bulk particles and

titanium tetraisopropoxide (TTIP) were also used as precursors in these green synthesis methods [21].

1.2 SILVER NANOPARTICLES

Silver (Ag) NPs have been found in art pieces from the Roman era (Lycurgus Cup from 4th century AD), although their nature was unknown. The bactericidal effect of Ag^+ ions on microorganisms' cells was reported in the 19th century. The bactericidal activity of Ag NPs was discovered in the second half of the 20th century [22].

Ag NPs have novel physicochemical properties, such as high electrical and thermal conductivity, surface-enhanced Raman scattering, chemical stability, catalytic activity and non-linear optical properties. Moreover, they are very popular due to the well-documented antimicrobial properties against Gram-negative (*Escherichia coli*, *Pseudomonas aeruginosa*, *Vibrio cholerae*, *Acinetobacter baumannii*) and Gram-positive (*Staphylococcus aureus*, *Enterococcus faecalis*, *Staphylococcus epidermidis*, *Streptococcus pyogenes*, *Bacillus subtilis*) bacteria, fungi (*Trichophyton rubrum*, *Trichophyton mentagrophytes*, *Candida albanicans*, *Candida glabrata*) and viruses (influenza virus, Dengue virus, Human Immunodeficiency Virus -HIV, Hepatitis B Virus-HBV). Ag NPs interact with cell membranes and disturb their permeability. They penetrate inside cells causing further damage and interact with compounds that contain sulphur and phosphorous, such as proteins and deoxyribonucleic acid (DNA). They can also attack mitochondrial respiratory chain and induce oxidative stress. Antimicrobial activity is dependent on the size and shape of NPs.

Ag NPs have great marketing value and their presence in consumer products is widely advertised. They are included in 24% of products listed in Project on Emerging Nanotechnologies. Health and fitness market groups have the greatest number of Ag NPs containing-products, followed by appliances, medical applications, electronics and computers. They are listed as one of the most used NM in commerce. In 2025, their production is expected to reach 800 t. Due to their novel properties, Ag NPs are used in several fields such as catalysis (fuel cell catalyst and hydrogen production photocatalyst), electronics (cryogenic superconducting materials and integrated

circuit sensors), optics (biosensors and chemosensors), environmental (water and air disinfection, wastewater treatment and renewable energies), textiles (UV blocking textiles, anti-stain textiles and clinical clothing), health care (UV protection, cosmetics and nutraceutical), food and agriculture (food packaging and food quality sensors) and biomedical (cancer therapy, burnt treatment, dentistry materials, diagnosis, drug delivery, cell imaging, antiinflammatory and antiangiogenic therapies and antimicrobial catheters and gels).

They are synthesized in the liquid-phase via chemical methods: chemical reduction (ascorbic acid, alcohol, sodium citrate and borohydride are the most used reducing agents), electrochemical methods, photochemical methods, sonochemical methods, irradiation, microwave-assisted synthesis, microemulsion synthesis, sol-gel methods and biochemical methods. Physical approaches are based on evaporation-condensation, such as thermal-decomposition method, arc discharge method, laser ablation, physical vapor condensation, energy ball milling and direct-ion sputtering. The proposed biological synthesis methods are based on the use of reducing and stabilizing agents obtained from bacteria (*Shewanella oneidensis*, *Bacillus sp.*, *Lactobacillus sp.*, *Pseudomonas stutzeri*, among others), fungi (*Trichoderma viride*, *Fusarium oxysporum*, *Humicola sp.*, *Pleurotus cornucopiae*…), algae (*Chlamydomonas reinhardtii*, *Caulerpa racemosa*, *Arthrospira platensis*, among others) or plants (*Pongamia pinnata*, *Pelargonium endlicherianum*, *Sambucus nigra*, *Artocapus altilis*, *Aloe vera*…). These methods can be intracellular or extracellular, and the latter is preferable because they are cheap, allow large-scale production and require simpler processing [23-29]. Other biological synthesis methods use protein products from animal origin such as gelatine, albumins, biopolymer chitin and derivatives (chitosan) and polysaccharides (agar-agar) [22]. Also, viruses and DNA can be used as templates for Ag NPs synthesis. Viruses offer robust functional capsids and easy manipulation while stimulating nucleation and assembly of inorganic materials [30].

2 ANALYTICAL TECHNIQUES FOR NANOMATERIAL ANALYSIS

The consideration of NMs as analytes implies their detection and quantification in mass and number concentration, along with their physicochemical characterization. Physical properties (e.g., size, shape, surface charge or surface area) can be used for their characterization, in addition to their chemical composition [31]. All these physical and chemical properties influence the fate and distribution of NPs.

2.1 SAMPLE PREPARATION

Sample preparation methods are usually required prior to sample analysis. These methods consist of removing matrix without altering the nature of NMs by digestion or separation/preconcentration protocols.

There are different types of digestion protocols, such as acid-based, alkaline and enzymatic digestions. Acid digestions are oriented to assess the total element content since most NMs are dissolved under these conditions. They are used to digest organic matrices by conventional heating or with microwave assisted techniques. Tetramethylammonium hydroxide (TMAH) is one of the most common reagents in alkaline digestions for degradation of organic matter, while proteases and pectinases are used to solubilize proteins in enzymatic digestion (hydrolysis) processes.

Centrifugation, ultrafiltration, dialysis and liquid/solid-phase extraction are useful separation and preconcentration techniques when studying NPs. Extraction of NPs from an aqueous suspension and separation of NPs from dissolved species can be easily performed by centrifugation. Ultrafiltration and dialysis have been used for separating NPs from

dissolved species by using nanoporous permeable or semipermeable membranes made of several materials and molecular weight cut-offs (MWCO) between 1–100 kDa. Dialysis is a simple process based on the pure diffusion of the target analyte through a membrane, but it requires long times for completing the process. This may be considered inconvenient especially when comparing against ultrafiltration methods which are faster separation techniques because of the use of centrifugal forces. Liquid-phase extractions, such as hexane extraction and cloud point extraction, are used for the isolation of NMs from solid and liquid samples using organic solvents or water. Hexane extraction is used for defatting, while cloud point extraction allows the separation of NPs and their dissolved species. Solid-phase extraction of noble metal NPs can be also performed by anionic exchange resins. Functionalized magnetic NPs have also been proposed for this purpose [32].

2.2 PHYSICOCHEMICAL CHARACTERIZATION OF NANOMATERIALS

Several techniques have been applied for characterizing NMs (Table 1). Electron microscopy techniques are used to visualize NPs and, therefore, to obtain information about their size, shape, dispersion and aggregation state. In scanning electron microscopy (SEM), a beam of accelerated electrons scans the specimen surface and the interactions generate signals related to atomic composition and topography of the sample surface. Physical properties such as size, shape and size distribution can be studied. Due to the incident electron beam, sample electrons can be elastic or inelastic scattered and backscattered. In addition, low-energy secondary electrons and characteristic X-ray light can be emitted. The detection of secondary electrons is the most common detection mode in SEM. In environmental SEM (ESEM), samples can be imaged in their natural state because the sample chamber operates in a low-pressure and high humidity gaseous environment. Transmission electron microscopy (TEM) is the most frequently used technique for NMs characterization, and it provides direct images and chemical information based on the transmission of the incident electron beam through a thin sample. TEM has a better

spatial resolution than SEM and the capability of being coupled with additional analytical techniques such as energy dispersive X-ray spectroscopy (EDX) or electron energy loss spectroscopy (EELS). Wet scanning TEM (STEM) is a TEM technique that enables the visualization of species submerged in a liquid phase.

Near-field scanning optical microscopy (NSOM), STM and AFM are surface probe microscopes. NSOM combines both surface probe microscopy and optical microscopy for obtaining information about the size and shape of NMs. Laser light is emitted through the tip aperture closely to the object and the emerging light is evanescent in the near-field distance. So, the light field is highly confined and localized at the tip and the spatial resolution depends on the tip size. Simultaneous fluorescence and spectroscopy analysis can be therefore performed. STM is based on quantum tunnelling current to generate electron density images for conductive and semiconductive specimens. Small voltages are applied between the tip and the surface causing tunnelling of electrons, and variations can be recorded while the tip scans the surface in the xy-plane. AFM does not require conductive surfaces and it is based on a cantilever with a sharp tip. The cantilever can be deflected by electrostatic and van der Waals repulsion or attraction between atoms on the tip and atoms on the sample surface. Both STM and AFM provide information about size, shape, size distribution, structure and dispersion/aggregation of samples. In addition, certain modifications of the tip in AFM allow us to obtain information about surface properties.

Scattering techniques use the scattering of incident radiation through its interaction with a sample to acquire information about the size, shape, structure and aggregation of NMs. Dynamic light scattering (DLS) uses monochromatic light to monitor temporal intensity light variations induced by the Brownian movement of particles smaller than the incident light wavelength at a fixed scattering angle. Thus, the hydrodynamic size distribution is obtained. Other light scattering techniques are particle tracking analysis (PTA) and multi-angle light scattering (MALS). In fluorescence correlation spectroscopy (FCS), a laser interrogates the sample and the fluorescent variations are fitted to an autocorrelation function that can

be used to determine diffusion rates. Binding kinetics and hydrodynamic dimension can be studied. Zeta potential measurements are based on the application of an electric field across a sample and the measurement of the velocity at which charged species move in the direction of the electrode. The technique provides information about the net charge of NMs and their stability. Raman scattering (RS) measures the inelastically scattered photons of monochromatic radiation after their interaction with molecular dipoles. Surface-enhanced RS (SERS) can be applied for studying metallic NPs since they enhance RS signals, so spatial resolution is increased. In addition, tip-enhanced RS (TERS) uses an apertureless metallic tip for RS signals enhancement. SERS and TERS can provide topological information besides structural, chemical and electronic properties. While X-ray diffraction (XRD) is typically used to provide structural information about crystalline samples, Small-angle X-ray scattering (SAXS) technique can be used to analyze amorphous materials and samples in solution.

The most common spectroscopic techniques used to characterize NMs are UV-visible spectroscopy (UV-vis), circular dichroism (CD), fluorescence spectroscopy (FS), infrared spectroscopy (IR) and nuclear magnetic resonance (NMR). UV-vis absorbance spectroscopy can be used for determining the size, concentration, aggregation and bioconjugation of NMs. CD allows structure characterization of molecules by analyzing different absorptions of left and right circularly polarized radiation on asymmetric molecules. It gives information about conformational changes and thermal stability. FS is useful to study ligand binding or conformational changes of macromolecules. Absorption of IR radiation by a sample results from vibrational stretching, bending and twisting of covalent bonds. So, IR spectra are considered as a fingerprint of a molecule's structure. IR spectroscopy allows studying the surface properites via Fourier transform IR (FTIR), which is based on the expression of characteristic bands, and attenuated total reflection-FTIR (ATR-FTIR), that measures the total internal reflection. NMR technique measures the intrinsic magnetic moment of nuclei in the presence of an external magnetic

field. It provides information about size, structure, composition, purity and conformational changes.

Size characterization and quantification of NMs are possible by using electroanalytical techniques. Voltammetry of immobilized particles (VIP) is capable of determining the oxidation state of the elements, whereas particle collision coulometry (PCC) provides nanoinformation.

Thermal techniques are used for determining the thermal stability of NMs. Thermal gravimetric analysis (TGA) monitors temperature-dependent weight. Material transitions (melting, crystallization, glass transition or decomposition) can be studied via differential scanning calorimetry (DSC), whereas isothermal titration calorimetry (ITC) is used to analyze stoichiometry, affinity and enthalpy of NM-biomolecule.

Atomic techniques are used for elemental analysis. Electrothermal-atomic absorption spectroscopy (ET-AAS) and inductively coupled plasma-optical emission spectrometry (ICP-OES) are not nano-specific techniques, since they cannot provide any physicochemical information about an element, but they can be used for detection and quantification of elements in the NMs and the sample. X-ray absorption spectroscopy (XAS) provides element-specific qualitative information and quantitative distribution. Mass spectrometry (MS) is a useful tool for studying molecular weight, elemental composition and chemical structure of NMs. Different ionization techniques can be employed, such as matrix-assisted laser desorption/ionization (MALDI), electrospray ionization (ESI) and inductively coupled plasma (ICP). These techniques can be used as on-line element specific detectors coupled with continuous separation techniques [32-34].

Table 1. Analytical techniques for NMs characterization [32-34]

Technique	Analytical information
Electron Microscopy	
SEM	- Size and size distribution - Shape - Aggregation
ESEM	- Size and size distribution - Shape - Aggregation - Dispersion
TEM	- Size and size distribution - Shape - Aggregation - Dispersion - Elemental composition (+EDX) - Chemical structure (+EELS)
STEM	- Size and size distribution - Shape - Aggregation - Dispersion - Dynamic displacement
Surface Probe Microscopy	
NSOM	- Size and size distribution - Shape
STM	- Size and size distribution - Shape - Structure - Aggregation - Dispersion
AFM	- Size and size distribution - Shape - Structure - Aggregation - Dispersion - Sorption - Surface properties

Table 1. (Continued)

Technique	Analytical information
Scattering techniques	
DLS	- Hydrodynamic size distribution
PTA	- Size and size distribution - Number concentration
MALS	- Size - Shape
FCS	- Hydrodynamic dimension - Binding kinetics
Zeta potential	- Stability - Surface charge
RS	- Hydrodynamic size and size distribution - Conformational changes - Structural, chemical and electronic properties
SERS	- Hydrodynamic size and size distribution - Conformational changes - Structural, chemical and electronic properties - Topological information
TERS	- Hydrodynamic size and size distribution - Conformational changes - Structural, chemical and electronic properties - Topological information
XRD	- Size (crystalline materials) - Shape (crystalline materials) - Structure (crystalline materials)
SAXS	- Size and size distribution - Shape - Structure

Table 1. (Continued)

Technique	Analytical information
Spectroscopic techniques	
UV-vis	- Size and size distribution
CD	- Structure of biomolecules - Conformational changes
FS	- Size and size distribution - Structure
IR	- Structure of bioconjugates - Conformation of bioconjugates
ATR-FTIR	- Structure of bioconjugates - Conformation of bioconjugates - Surface charge - Surface properties
NMR	- Size - Structure - Composition - Purity - Conformational changes
Electroanalytical techniques	
VIP	- Elemental composition - Oxidation state - Average size
PCC	- NPs detection - Size and size distribution - Number and mass concentration

2.3 CONTINUOUS SEPARATION TECHNIQUES

Several separation techniques have been applied for particle separation based on their size, surface, density and charge. They are usually coupled with sensitive and selective detector systems.

In field-flow fractionation (FFF) techniques, separation occurs in a thin channel by applying an external field perpendicular to the laminar flow of the sample. No stationary phase is needed and there are

the most used FFF techniques for the analysis of NMs. Whereas centrifugal forces are applied in SdFFF, a perpendicular flow (cross flow) is used in FlFFF. Asymmetric FlFFF (AF4) is the most suitable FlFFF technique for the separation of NPs based on their hydrodynamic size, even in complex matrices. It can be on-line coupled with ICP-MS, UV-vis, DLS and PTA detectors, or off-line coupled with ET-AAS, ICP-OES and TEM.

In the electrophoresis techniques, the separation depends on the migration of charged species in presence of an applied electric field. Most frequent gel electrophoresis (GE) methods use polyacrylamide and agarose gels for separating proteins and charged biopolymers, respectively. Agarose gels have wider applications than polyacrylamide due to their largest pore size (10-100 nm). Optical extinction spectroscopy, hyperspectral imaging or TEM can be used as detectors for gels analysis. Separations in capillary electrophoresis (CE) takes place according to differences in the mobility of charged species into a thin capillary filled with an electrolyte when applying a high voltage at the end of the capillary. UV-vis, FS and ICP-MS are the most common detectors in CE.

In reference to the chromatographic techniques, hydrodynamic chromatography (HDC) uses columns packed with non-porous beads. Velocity gradient is generated within the capillaries between beads and separation takes place depending on the size of particles (there is no interaction between the targets and the stationary phase). HDC has been on-line coupled with UV-vis, FS, DLS and ICP-MS. Size exclusion chromatography (SEC) is similar to HDC, but stationary phases are porous materials and additional interaction between NMs and the stationary phase components is expected [32].

2.4 ICP-MS BASED TECHNIQUES FOR NANOMATERIAL ANALYSIS

2.4.1 Single particle-ICP-MS

Single particle-ICP-MS (sp-ICP-MS) combines the sensitivity and the elemental specificity of ICP-MS and the analysis of NPs on a particle-by-particle basis. The application of sp-ICP-MS for the analysis of colloids and NPs was first reported by McCarthy and Degueldre. A series of papers by Degueldre et al. summed up the principles of the sp-ICP-MS technique. The continuous growth in development, production and application of NMs, alongside the environmental and health concerns, have led to a significant increase of the interest in sp-ICP-MS to complete other available techniques [35].

sp-ICP-MS can be applied to NPs, colloids and microparticles, so it has a wide dynamic range. It provides information about the elemental composition, number concentration, size and size distribution. Dissolved forms of studied elements can be also determined at once. Besides, aggregation and agglomeration processes may be detected. Due to its low limit of detection (LOD), sp-ICP-MS is useful for the analysis of environmental samples containing very low concentrations of NPs.

Liquid samples are introduced to the ICP-MS instrument by using a nebulization system (a combination of a nebulizer and a spray chamber). An aerosol of polydisperse droplets is produced and, when the droplets reach the plasma, evaporation of the solvent, vaporization, atomization and ionization take place. Ions that passed through the interface are analyzed by a mass spectrometer based on their mass/charge (*m/z*) ratio. The concentration of the dissolved forms (ions) is homogenous within a solution, then, the produced signal can be considered constant (Figure 1A). On the contrary, NPs are discrete groups of atoms and when one NP arrives at the plasma, a transient signal is generated (Figure 1B). The measurement of individual NPs requires fast data acquisition systems (higher than 10^4-10^5 Hz).

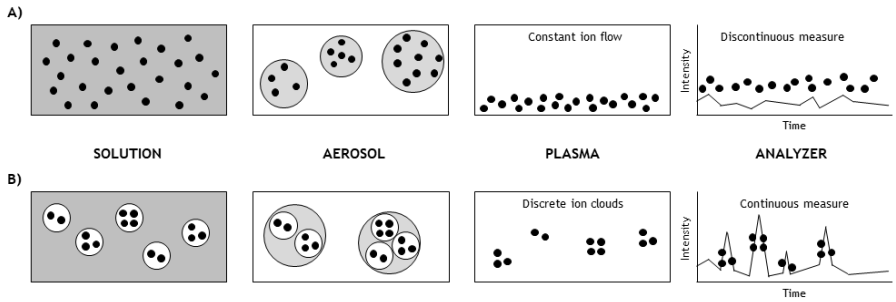

Figure 1. Comparison between A) classical ICP-MS for analysing dissolved ions and B) sp-ICP-MS for the analysis of NPs

sp-ICP-MS implies that each recorded pulse is produced by one single NP. Therefore, the number concentration of NPs depends on the frequency of the pulses (Equation 1) and the intensity of each pulse is related to the number of atoms in each detected NP (Equation 2). The use of sufficiently diluted suspensions is necessary to detect just one NP per reading.

$$n_p = \eta_{neb} \times Q_{sam} \times t_i \times C_p \qquad \text{(Equation 1)}$$

where n_p is the number of events counted during the acquisition time (t_i), η_{neb} is the nebulization efficiency, Q_{sam} is the sample introduction flow rate and C_p is the concentration of NPs.

$$I_p = K_{ICP\text{-}MS} \times K_M \times m_p \qquad \text{(Equation 2)}$$

where I_p is the total counts per reading, $K_{ICP\text{-}MS}$ is the detection efficiency (ratio of ions detected versus ions introduced into the ICP-MS) and m_p is the mass per NP. K_M (=A x N_{Av} / M_M) is related to the measured element, where A is the atomic abundance of the studied isotope, N_{Av} is the Avogadro's number and M_M is the atomic mass of the element.

By considering solid, spherical and pure NPs, Equation 2 can be written as a function of NP diameter, as follows (Equation 3):

$$I_p = \frac{1}{6} \times \pi \times \rho \times X_p \times K_{ICP\text{-}MS} \times K_M \times d^3 \qquad \text{(Equation 3)}$$

where ρ is the density of the NP, X_p is the mass fraction of the element in the NP and d is the diameter [31, 36].

There are different approaches to sp-ICP-MS calibration. The first one uses different size standards of NPs of the same element as the analyte. A calibration curve of signal intensity versus particle diameter

is generated. Dissolved standards of the analyte can be used to determine the mass of analyte per NP and the diameter of the NP when size standards are not available. The procedure has been described by Pace et al. [37] and it is based on the fact that atoms from a dissolved standard behave in a similar way when they reach the plasma to atoms from a NP. Previous knowledge about sample introduction flow rate and nebulization efficiency is required. The nebulization efficiency can be estimated as the ratio of NPs nebulized versus the known concentration of suspended NPs in the standard.

2.4.2 Asymmetric flow field-flow fractionation ICP-MS

FFF techniques were invented by J.C. Giddings in 1966. Fractionation takes place in a flat channel during the application of a separation field that is perpendicular to the direction of the sample flow (the separation field in AF4 is a liquid cross flow, F_c). The first AF4 system was assembled by Giddings and Wahlund in 1987, and nowadays it is the most used and versatile FFF technique.

The narrow channel is formed by a trapezoidal spacer placed between a porous and a nonporous plate. The membrane is on top of the porous plate that acts as an accumulation wall. F_c generates a force that leads particles and molecules to the membrane and diffusion exerts the opposite force. Based on the individual diffusion coefficients (D), concentration profiles of each particle are elongated to a greater or lesser extent into the channel. Depending on the position of particles in the channel, they are subjected to different streamlines of parabolic velocity flow.

There are two different elution modes: normal and steric modes. In normal or Brownian mode (Figure 2), translational diffusion controls the concentration profile of particles. Smaller particles diffuse to a greater extent, so they are more separated from the membrane and elute faster. If the size of particles is higher than 1 μm, retention behavior changes to steric mode (Figure 3). Elution is determined by the extension of particles in the channel, while the translational diffusion effect is not significant. Large particles elute first, unlike in the previous case.

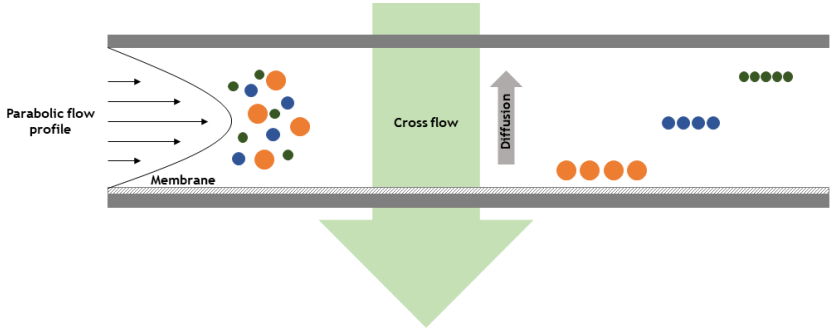

Figure 2. Fundamentals of separation in normal elution mode in AF4

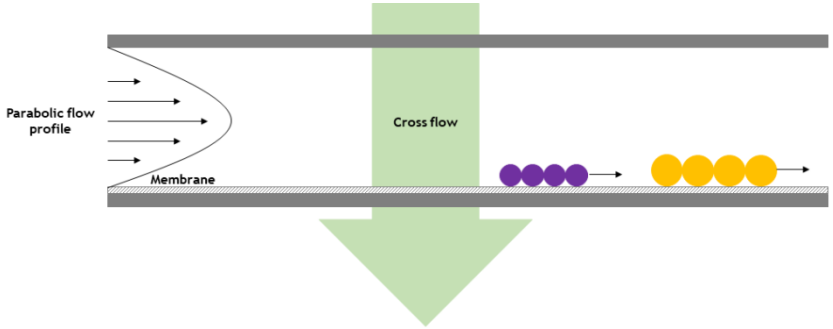

Figure 3. Fundamentals of separation in steric elution mode in AF4

Before the fractionation, the sample is injected into the channel (Figure 4A). Then, a focusing/relaxation step is applied to concentrate the analyte and avoid its spreading along the channel (Figure 4B). In the elution step, focus flow stops and fractionation starts (Figure 4C).

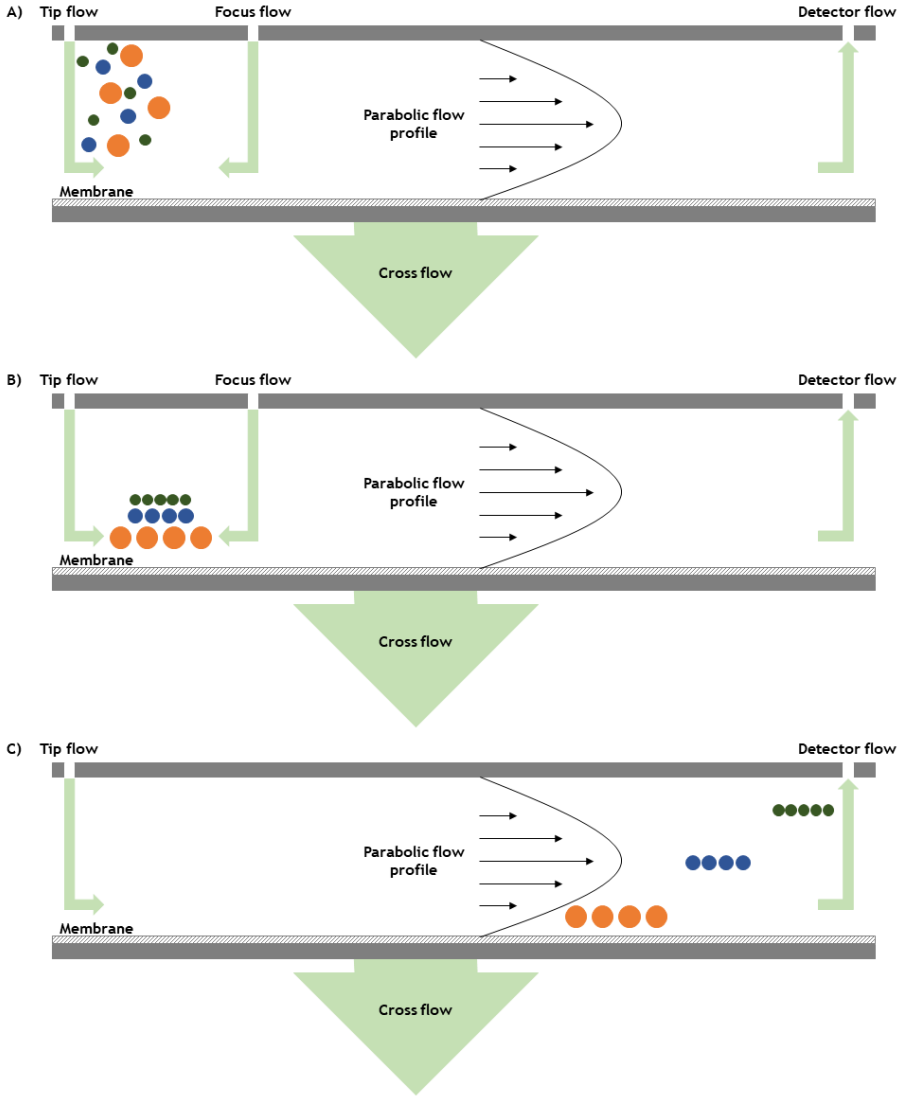

Figure 4. AF4 separation stages: A) injection, B) focusing/relaxation and C) elution

In normal elution mode, diffusion is the key parameter that determines the fractionation. D can be calculated considering the retention time of the analyte (t_R), the channel thickness (ω) and the flow profiles (Equation 4):

$$t_R = \frac{\omega^2}{6D} \times ln\left(1 + \frac{F_c}{F_d}\right) \qquad \text{(Equation 4)}$$

where F_d is the detector flow, or the outlet flow.

D can be used for hydrodynamic diameter (d_H) calculation by Stokes-Einstein equation (Equation 5):

$$\mathrm{D} = \frac{\mathrm{k_B} \times \mathrm{T}}{3 \times \pi \times \eta \times \mathrm{d_H}} \qquad \text{(Equation 5)}$$

where k_B is the Boltzmann constant (1.38×10^{-23} kg m^2 s^{-2} K^{-1}), T is the temperature of the channel (K), and η is the viscosity of the mobile phase (kg m^{-1} s^{-1}). Larger particles have lower D, so their t_R is higher.

Several experimental parameters can affect AF4 fractionation, such as mobile phase, F_c/F_d ratio, channel dimensions, injected sample volume, relaxation time and membrane material and its cut-off. Regarding the mobile phase, its chemical composition, ionic strength and pH must be taken into account. They control the electrical double-layer (EDL) on particles and membrane surface. In general, the carrier must provide the same electrical polarity to particles and membrane, positive or negative. The ionic strength can be manipulated to achieve a balance between avoiding strong electrostatic repulsive forces, that may cause pre-elution with the void peak, and providing enough repulsive interactions to prevent the irreversible adsorption of particles to the membrane. pH value also influences the net-charge of analytes and membrane, affecting attractive or repulsive electrostatic interactions. Another option is the use of surfactants, which can interact with analytes and membranes, as well as modify ionic strength and pH, which in turn alter electrostatic interactions. On the other hand, surfactants can change analyte size and its dispersion into the channel by steric repulsion. t_R depends on F_c/F_d ratio for a fixed ω. F_c must provide good resolution and reasonable time of analysis. High F_c values cause longer retention times, and it is suitable to separate smaller species, but it can cause sample loss. F_c gradients are useful for analyzing samples with a wide particle size range. Channel

dimensions depend on the spacer. For a fixed F_c, higher ω leads to increased retention times, so they are used for separating small particles. Membranes must prevent the loss of particles and their cut-off is an estimation of the smallest particles that can be retained. Injected sample volume is crucial since enough sample must be injected to have a good signal-to-noise ratio in the detector, however, overlapping phenomena is caused by an excessive amount of sample. Focusing/relaxation time must be adjusted to provide the equilibration of particles before the analysis and to remove dissolved species. Membrane charge is very important and high-charged membranes are preferred for separating low-charged particles. Several membrane materials, such as regenerated cellulose or polyether sulfone, can be considered.

Two different analytical parameters can be used to assess the suitability of AF4 fractionation. The recovery (*R*) is the ratio between the detected mass after the analysis (*m*) and the injected mass prior to the fractionation (m_0). It provides information about the ability of the method to fractionate different analytes with no significant sample loss. It can be defined as:

$$\mathrm{R}(\%) = \frac{\mathrm{m}}{\mathrm{m}_0} \times 100 \qquad \text{(Equation 6)}$$

Working with on-line approaches, the sample is measured with and without F_c (*m* and m_0, respectively) and the area under each peak is integrated.

Resolution (*Rs*) is related to the ability of the technique to separate two components and it can be calculated according to the following equation:

$$Rs = 1.176 \times \frac{t_{R2} - t_{R1}}{{\omega_1}^{0.5} + {\omega_2}^{0.5}} \qquad \text{(Equation 7)}$$

where $\omega^{0.5}$ is the width of the analyte peak at half height.

AF4 coupled with ICP-MS allows the quantification of the elemental composition of the injected species. External calibration and peak integration are used to convert the detector signals into concentrations [38-41].

3 NANOTOXICOLOGY

Nanotoxicology aims to address the adverse effects caused by NMs. The fate of foreign materials (xenobiotics) in the organism is a combination of their absorption, distribution, metabolism and excretion (ADME). Several physicochemical properties of NMs can drive adverse effects on biological systems that might not be seen with bulk materials. Interactions of NMs with living systems are complex because of the ability of NMs to bind and interact with biological components and change their surface characteristics. The interaction between NPs and biological mediums or fluids depends on the properties of NPs (chemical composition, particle size, state of dispersion and agglomeration, shape, crystallinity, surface area, surface charge and surface modifications) and the medium conditions. NMs in a biological environment do not consist of "bare" particles but they are surrounded by medium components generating a biological corona. This "corona" defines the properties and behavior of the formed complexes [42-44].

Since the tendency of NPs to form aggregates, *in vitro* experiments require to know (measure) the amount of NPs in the pre-treated solution that will be in contact with the cellular culture (initial conditions). Cellular uptake of NMs can involve several pathways: endocytosis mediated by clathrin and caveolae, independent endocytosis, phagocytosis, macrocytosis and pinocytosis. NMs are mostly captured via endocytosis due to their small size. Following this cellular uptake, NPs captured into vesicles (early endosomes) mature to late endosomes or multivesicular bodies and, later, in lysosomes which can be transported and fused with other intracellular organelles. Mitochondrial dysfunction, endoplasmic reticulum stress and

lysosomal rupture are some of the alterations in organelles caused by exposure to NPs. In addition, cells have exocytosis mechanisms for the excretion of NMs from cells that can be activated or inhibited based on calcium levels, lipid rafts (cholesterol) or metabolic inhibitors. NPs may induce cell death (necrosis, apoptosis, autophagy and pyroptosis) and decrease cellular metabolic activity, as well as alter cell function and morphology. The formation of biological corona should be taken into account. Chemical (production of ROS, dissolution and release of toxic ions, disturbance of cell membrane transport of electrons and ions, lipid peroxidation and oxidative damage) and physical (impairment of membranes, membrane activity, transport processes, protein conformation and protein misfolding/ fibrillation) mechanisms might take place on the corona bio-nanointerface. These processes generate a biological response in cells that can occur before or after the internalization of NPs. Extracellular and intracellular (mitochondrial, lysosomal and nuclear) membranes can be directly or indirectly damaged by NPs. NPs can affect membranes' integrity, morphology and stability, and even generate holes. Surface properties, as well as size and concentration, are key factors in NP-membrane interactions [45-48].

In vivo experiments are crucial to understanding mechanisms, pathways and entry routes of NMs into complex organisms. The main concern deals with the possibility of NPs access to other organs once they entered the body and reached the systemic circulation. Moreover, the bioaccumulation of NMs in several organs is possible. Excretion mechanisms are not yet clear. Potential toxicity mechanisms are related to protein misfolding/fibrillation and chronic inflammation [45]. Chronic liver toxicity has been observed due to the prolonged retention of inorganic NPs and their slow clearance rate. Lung disorders (pulmonary fibrosis, pneumoconiosis and exacerbation of asthma) may be produced as a response to inflammation caused by the accumulation of NPs in the lungs. The spleen is another target organ for NPs since splenic macrophages are responsible for the uptake of NPs and their metabolism. Accumulation of NPs in the spleen might cause an inflammatory response. In addition, some NPs tend to accumulate in renal blood vessels due to their special architecture,

causing an increase in mesangial cells, thickening of capsule and membrane, degeneration of proximal convoluted tubule and inflammation. Regarding neurotoxicity, NPs can reach the brain through the olfactory bulb nerves and cause toxicity. Some NMs were found to, moderately, decrease memory and learning activities, as well as damage in the hippocampus tissue and neurons. The accumulation of NPs in reproductive organs, such as ovaries, has been also observed. Oxidative stress, dysregulation of mineral elements distribution and sex hormones and decreased fertility were found after exposure to certain NMs. Physical changes to immune organs (bone marrow, thymus and spleen) and functional changes (immunostimulation or immunosuppression) on the immune system have been also linked to NMs exposure. In addition, changes in gene pattern and gene toxicity were found after exposure to several NMs, so they are potentially genotoxic [49].

3.1 ROUTES OF EXPOSURE TO NANOMATERIALS

The main routes of entry of NPs in the human body are via ingestion, inhalation and dermal penetration. Human body is mainly exposed to TiO_2 NPs by ingestion and dermal penetration because of their extensive use in sunscreens, food additives and paints. Ag NPs are used in food, antibacterial products, water disinfectants, textiles, diagnostic biosensors, imaging probes and conductive inks, so they can penetrate the human body via inhalation, ingestion and dermal penetration [42].

3.1.1 Ingestion

Human gastrointestinal tract is divided into upper (esophagus, stomach and duodenum) and lower tract (small and large intestines). A mucus coating is present throughout the gastrointestinal apparatus. NPs can reach the stomach when they are directly ingested or inhaled (via trachea and mucociliary escalator). Through the gastrointestinal tract, the pH value varies from one stage to another resulting in modifying the physicochemical properties of NPs alongside with the peristalsis. In the stomach, where the pH is between 1.2 and 2.0, NPs might be dissolved and degraded. Digestion and absorption processes

occur in the small intestine where the pH value is between 6.0 and 7.0. Translocation of NPs across gastrointestinal mucosa can occur via endocytosis by epithelial cells, transcytosis by M-cells uptake, crossing through villous gaps and paracellular uptake.

Daily ingestion of TiO_2 NPs, as food additive E171, and Ag NPs is 31.5 mg day^{-1} and 20-80 μg day^{-1}, respectively. Both induced cytokine secretion in intestinal cells. TiO_2 NPs are less genotoxic than Ag NPs, but both can produce the disruption of microvilli and tight junctions after exposure of Caco-2 cells and the collapse of the enteral epithelium at a concentration of 10 μg mL^{-1}. Rutile and anatase (50, 100 and 250 nm) TiO_2 NPs have shown a dose-dependent reduction of cell viability and ROS generation in Caco-2 cells and THP-1 monocyte macrophages at concentration levels ranged between 1 and 50 μg mL^{-1} for 24-72 h. They also induced the production of interleukin (IL)-1β in THP-1 macrophages and IL-8 in Caco-2 cells. They were unable to disrupt γ-catenin proteins, but they were found to alter microvilli on the apical surface and to increase calcium levels in Caco-2 cells exposed to TiO_2 NPs at 10 μg mL^{-1}. In addition, TiO_2 NPs (25, 80 and 155 nm), administered by single oral gavage to adult mice, were retained in the liver, spleen, kidneys and lungs with retention ratios similar to those observed after intravenous administration.

Ag NPs are usually deposited in the gastrointestinal tract, but they enter without forming large aggregates in the digestive fluids. Ag NPs (5-20 nm), orally administered for 21 days to mice (20 mg kg^{-1} of body weight), have been found to disrupt epithelial microvilli and intestinal glands. In addition, Ag NPs increased goblet cells in the intestine and the release of granule mucus. In general, Ag NPs are more toxic because they are highly susceptible to degrade at low pH. Systemic argyria was found after the ingestion of colloidal Ag [42, 44, 50].

3.1.2 Inhalation

The respiratory tract is divided into upper (nasal cavity, pharynx and larynx) and lower respiratory tract (trachea, bronchi and lungs). Each bronchus is branched into bronchioles, that are connected to alveoli, where gas exchange takes place. The upper respiratory tract

allows air intake and protects the lower tract. Airways are the conducting zone and the epithelium of the tracheobronchial region is protected by a mucus layer. The size distribution of NPs controls their ability to enter the human respiratory tract. Small particles (1-5 μm) can be deposited in the tracheobronchial region, whereas larger particles (5-30 μm) remain in the nasopharyngeal region. Only particles with sizes between 0.1 and 1 μm can reach the alveolar section. Accumulation of NPs in the deepest region may cause inflammation and ROS production. Their elimination via mucociliary clearance and coughing is slow, so expulsion is usually unsuccessful. Therefore, NPs can be translocated in the bloodstream through the epithelium formed by type I and type II epithelial cells. NPs can be removed from the alveoli by macrophages and neutrophils. They internalize NPs and degrade or carry them to the mucociliary escalator. This process takes place after 6-12 h deposition and it is more efficient for microparticles than for NPs.

Rats exposed to 15 mg m^{-3} of anatase TiO_2 NPs (20 nm) during 6 h have shown Ti accumulation in lungs, liver, kidney and spleen. Also, TiO_2 NPs were found to be excreted by faeces and urine. Lung tumours, bronchoalveolar adenomas and cystic keratinizing squamous cell carcinomas were produced after rutile TiO_2 NPs inhalation. Rats treated with 2, 10 and 50 mg m^{-3} TiO_2 NPs (25 nm) by inhalation, during 6 h day^{-1} for 5 days, have shown clearance rates around 50 days. Anatase TiO_2 NPs were found to penetrate the pulmonary interstitial space to a higher extent than larger particles at equivalent masses, and the translocation and clearance rate are higher in larger species than in rodents.

The exposure to Ag NPs promotes morphological changes and cell death in A549 cells after 24 h of exposure. DNA damage and overexpression of metallothioneins have been observed in these cells when they were exposed to 20 nm Ag NPs (0.6 nM) for 48 h. Cell shrinkage and cell elongation were observed in macrophages due to the exposure to uncoated and coated Ag NPs. Long term inhalation has produced lung functional alterations and inflammatory responses. Biodistribution and toxicity were found to be dependent on size, shape

and surface properties. While Ag NPs could be phagocytized by macrophages, their aggregates persisted for up to 7 days [42, 44, 50].

3.1.3 Dermal penetration

Skin is the largest primary defense organ. It gives protection against external agents and UV radiation, and it is a selective permeable barrier. Skin is structured in three layers: epidermis, dermis and hypodermis. The stratum corneum is the outer layer of the epidermis and it is made of corneocytes and a lipidic matrix. This matrix has a nonpolar portion (approximately 80%) and hydrophilic heads, which correspond to transepidermal intercellular nonpolar or lipidic route and transepidermal intercellular polar or hydrophilic route, respectively. The entry of NPs through the skin highly depends on the size. Particles smaller than 36 nm can penetrate the skin through aqueous pores, whereas particles smaller than 5-7 nm can use the transepidermal intercellular lipidic route and larger particles may penetrate through the transfollicular route. Epidermal keratinocytes are capable of phagocytized NPs and they may lead to inflammatory responses. The dermis has a high supply of blood and macrophages, lymph vessels, dendritic cells and sensory nerve endings. When NPs reach the dermis, they can be translocated to the systemic circulation via the lymphatic system and regional lymph. The exposure of the skin may be due to the use of NPs in cosmetics, textiles and topical drug treatments, or it may occur in working places.

TiO_2 NPs applied as dry powder and in water/surfactant suspension did not penetrate through the skin with an intact stratum corneum, and they can be easily removed by washing. Other studies showed penetration of TiO_2 NPs (20-100 nm) through 3-5 corneocytes layers and 13 cell layers into UV-damaged skin, and they even reached epidermis and dermis. In addition, transdermal permeation was found after 60 days of dermal exposure of hairless mice. TiO_2 NPs were detected in the liver, spleen and lungs with different surface characteristics, sizes and shapes. They had toxic effects on epidermal keratinocytes and fibroblasts by altering their gene and protein expression. The rutile phase has shown lower toxicity than anatase. Photoinduction seemed to promote TiO_2 NPs dermal penetration.

Artificial radiation along with the pH of skin can lead to disaggregation of these NPs.

Ag NPs dermal exposure can produce an abnormal increment of Ag levels and argyria in blood. Nanocrystalline Ag coated dressing was found to be cytotoxic for cultured keratinocyte. The shape of NPs was a key parameter since rods had higher penetration rates than spheres and triangles [42, 44, 50].

3.2 ADME PROCESS

3.2.1 Absorption

During the passage of NPs along the gastrointestinal tract, NPs agglomerate, aggregate, become soluble or react with some components (enzymes, intestinal microbiota or acids). Translocation depends on the properties of NMs (surface area, surface charge, size and presence of coatings) and the physiology and characteristics of the gastrointestinal tract. NPs can diffuse through intestinal mucus by cellular or paracellular transport and by contact with enterocytes and M-cells. In general, NMs are not absorbed to a large extent. Absorbed NMs will enter into the liver via the portal circulation.

Absorption via the skin is size-dependent. Several physiological barriers, such as the endothelial cells lining the blood vessels, prevent the transport of NMs from the skin to systemic circulation, the interstitial space or target tissues. Transcellular and paracellular transports are two pathways for the transport of NMs. Disturbance in the endothelial system may produce inflammation and oxidative stress responses, which can disturb the endothelial cell matrix by opening the cell-cell junctions and leads to an increase of paracellular transport [51].

3.2.2 Distribution

NMs can be transported to the liver, spleen and lymphatic system after passing through the gastrointestinal tract. The interaction of NMs with proteins may modify their structure and, therefore, their function. Membranes might be expanded, which increases cellular penetration and leads to apoptosis. Smaller particles can be detected in several organs (liver, spleen, kidney, lungs and brain), while larger particles

remain in the gastrointestinal tract. Information about the distribution of injected and inhaled NPs is limited, but it depends on NPs surface characteristics and size [51].

3.2.3 Metabolism

Metal containing NPs are usually dissolved in macrophages due to their acidic environment. After their entrance into a biological fluid, NPs are surrounded by a biological corona that controls their fate, transport and toxicity. This new identity may affect the internalization and clearance by the immune cells, and conformational changes in proteins of the corona may lead to an immune response [51].

3.2.4 Excretion

Information about the excretion of NPs is limited. NPs may be eliminated through urine, bile or faeces. In general, insoluble NMs might remain in tissues after long exposure periods [51, 52].

4 NANOMATERIALS IN FOOD INDUSTRY AND AGRICULTURE

Nanotechnology is involved in several areas of food production, such as processing, packaging, distribution, storage and consumption.
Major areas of NMs application in food and food packaging are foodstuff nanostructures; nanosized food additives and ingredients; NMs in coatings, packaging materials and nanosensors; and nano-pesticides, veterinary medicines and other agrochemicals. The most common methods in the area of processed nanostructures in foodstuffs are nano-emulsions, micelles (surfactant, double, multiple and reverse) and emulsion bilayers. They are used to improve food tasting, textures and mouth sensations. Nanosized or nanoencapsulated food additives (colours, preservatives and flavouring agents) and supplements (vitamins, antioxidants and probiotics) provide better solubility, absorption, uptake, stability and bioavailability. Nanocapsules, nanohydrogels, nanoemulsions, micelles and lipid NPs are some examples of nanoencapsulation, which preserves additives and supplements during processing and storage and control their release. They can be generated by spray drying, spray cooling, freeze drying, emulsification, emulsification-solvent evaporation, coacervation, nanoprecipitation, inclusion complexation and using supercritical fluid techniques. There are several types of food packaging materials (food contact materials) such as improved food packaging, active food packaging and intelligent or smart food packaging. Nanocomposites are a combination of a continuous phase (matrix) and a discontinuous nanophase. They improve physical and mechanical properties, such as flexibility, abrasion resistance, tensile strength, stiffness, toughness, shear strength, delamination resistance, temperature and moisture stability and flame resistance. They can also be eco-friendly and

biodegradable. The incorporation of fillers (nanophase) enhances the gas and water barrier properties, so nanocomposites are improved food packaging materials. In active packaging systems, active compounds (antimicrobial agents, preservatives, oxygen absorbers, water vapor absorbers, ethylene removers, UV protectors…) are incorporated into the food packaging for enhancing their protection function. These active components are produced by nanotechnology and they can be activated or released in response to internal or external factors. Several active food packaging materials incorporate Ag NPs for antimicrobial and oxygen scavenging activities, which extend the shelf-life of foodstuff. Other nanocoatings provide scratch resistance, antireflective properties, corrosion resistance and control release of enzymes, flavours, antioxidants and nutraceuticals. Nanosensors (array biosensors, nanoelectromechanical sensors, nanocantilevers or microfluidic devices) are useful for monitoring food quality and safety during transportation and storage, which ensure the integrity of the package. They can also show the relative humidity, oxygen and carbon dioxide exposure, temperature, time and pH variations, as well as the detection of the presence of gases, allergens, food pathogens, toxins, chemicals and pesticides. The use of nanosensors is part of intelligent or smart food packaging. The sensors interact with internal or external environmental factors and a response correlated with the state of the food is generated. Applications in food production and agriculture include novel formulations of nanopesticides, nanoveterinary medicines (minerals, vitamins and other supplements) and other nanoagrochemicals (fertilizers, plant growth regulators, herbicides, fungicides, bactericides and nanoagriparticles or bio-nanohybrid nanoparticles against phytopathogens). They allow the reduction of agrochemicals due to their better efficiency and dispersion in nanoform and the better control of dosage with slower and longer release of substances. The use of contaminated water in agriculture has deleterious effects on the environment, soil fertility and agricultural production, and also on humans. NMs are very useful in the design of coated water filters for removing organic pollutants, inorganic compounds and heavy metals from contaminated water. In

addition, nanosensors can be applied to onsite detection of pesticides, toxins, pathogens and other pollutants [53-58].

NMs used in the food industry can be classified into three main categories: inorganic, surface-functionalized and organic NMs. Inorganic NMs include transition metals (Ag, TiO_2), alkaline earth metals (calcium and magnesium) and non-metals (selenium and silicates), and they are mainly applied in food packaging. For example, Ag NPs are used as antimicrobial and antiodorant additive and in health supplements, whereas TiO_2 NPs provide UV protection and a barrier to moisture and oxygen. Conventional bulk TiO_2 is an approved food additive (E171) used as a white pigment. It contains a nanosized fraction of 17-36%. Other inorganic NMs used in the food industry are nanoselenium (food additive) and nanocalcium, nanoiron and nanomagnesium (health supplements). Surface-functionalized NMs provide additional functionalities to the matrix where NMs are included in. Antimicrobial and preservative properties were achieved, as well as improvement in mechanical strength and barrier against gases, volatile components or moisture. Organic NMs are vitamins, antioxidants, colorants, flavouring agents and preservatives encapsulated in nano-delivery systems. These systems provide a better dispersion of insoluble substances and control the release of certain substances [53].

There are consumer safety concerns about the use of NMs directly in food, their potential migration from packaging and sensors to the food matrix and their use in food production that may lead to unintentional human exposure through ingestion. The digestive tract acts as a barrier that prevents the penetration of unwanted substances into the body. As it was previously mentioned, the digestion process affects the physicochemical characteristics of NPs, mainly by dissolution or aggregation, and it may alter NPs toxicity. Ingested NPs may cross the epithelial barrier (transcytosis through epithelial and M-cells or paracellular transport) and reach the systemic circulation and other organs (liver, spleen, heart, lungs…), or they can be eliminated by faeces. Peristalsis, gut microbiota and mucus layer that cover the intestinal epithelium must be considered. The interaction of NMs with food components is also an important factor. NMs can directly affect nutrients absorption by disrupting microvilli or altering expression of

nutrient transporter and efflux pumps genes; food components may affect NMs absorption due to physicochemical modifications by protein and biological corona formation; and the presence of certain food components could also affect the oxidative stress generated by NMs. Potential toxic effects of TiO_2 NPs and Ag NPs via ingestion have been previously summarized in Section 3.1.1 [59, 60].

The safe use of NMs in agriculture and the food and feed industry is ensured by several regulations and guidance in the European Union (EU). The use of nanotechnology in food production as primary ingredients is covered by "Novel Food" and "Novel Food Ingredients" Regulation European Commission (EC) 258/97 which includes "foods and food ingredients with a new or intentionally modified primary molecular structure". Their risk assessment should be assessed before market approval. If NMs are food additives, Regulation (EC) 1333/2008 must be applied and NMs must be included in de EU register before being used. Regulations (EC) 1332/2008 and 1334/2008 must be applied for food enzymes and food flavourings substances, respectively. Regulation (EC) 1331/2008 establishes a common procedure for the assessment and pre-market authorization of food additives, enzymes and flavourings. Nanoforms of minerals and vitamins must be evaluated under the "Novel Food" Regulation. Regulation (EC) 1935/2004 covers all materials and articles that are in contact with food. There are two legislative pieces which explicitly refer to NMs: Regulation (EC) 450/2009 on "Active and Intelligent Materials and Articles", which requires a case-by-case assessment, and Regulation (EU) 10/2011 on "Plastic Food Contact Materials", which states that only substances in nanoform can be used if nanoform is explicitly authorized. Substances released for active food packaging are considered intentionally added to food and they must follow the aforementioned regulations for "Novel Food" and "Novel Food Ingredients". Pesticides are regulated by the Plant Protection Products (PPP) Regulation (EC) 1107/2009, which establishes a pre-market authorization. These active substances must be assessed on a case-by-case basis, but NMs are not explicitly mentioned. Pesticides that contain nanoforms of approved active substances must be considered as different pesticide products and they require a separate authorization.

Regulation (EC) 178/2002 regarding "General Principles and Requirements of Food Law" is the basis of protecting human and consumers' interests in relation to food. Biocides and chemical substances are regulated by (EU) No 528/2012 for non-agricultural pesticides. The European Chemicals Agency (ECHA) manages Registration, Evaluation, Authorisation and Restriction of Chemicals (REACH) and Classification, Labelling and Packaging (CLP) tasks. Substances used as plant protectors, biocides and food contact materials must be registered under REACH (Regulation (EC) 1907/2006). All ingredients included in food and biocidal products in the form of NMs must be indicated in the list of ingredients followed by the word "nano" in brackets. Feed for food producing and non-food producing animals is regulated by Regulation (EC) 767/2009, whereas Regulation (EC) 1831/2003 is applied to regulate the use of additives in animal nutrition. The EU Scientific Committee on Emerging and Newly Identified Health Risks (SCENIHR) recommends a case-by-case study for risk assessment of NMs. Several guidance for risk assessment of NMs have been published. The European Food Safety Authority (EFSA) has published a "Guidance for risk assessment of the application of nanoscience and nanotechnologies in the food and feed chain". This scientific opinion gives recommendations for assessing potential risk from the application of nanoscience and nanotechnology in food additives, enzymes, flavourings, food contact materials, novel foods, feed additives and pesticides. EFSA guidance recommends the analysis of NMs when they are produced, when they are used or presented in food and feed, when they are included in biological fluids and when a toxicological study is performed. EFSA Nanonetwork has been established for harmonizing of assessment methodologies and facilitating the exchange of information and data. In addition, they create an "Inventory of Nanotechnology applications in the agricultural, feed and food sector". ECHA has also published a "Guidance on Information Requirements and Chemical Safety Assessment", which addresses NMs specific requirements, and it has established a Nanomaterials Working Group. Compared to other non-EU countries, EU legislation is the strictest one [61, 62].

4.1 BIOACCESSIBILITY AND BIOAVAILABILITY

The bioaccessible fraction is the proportion of a component that is released from the food matrix into the digestive fluids. This fraction may be digested or remain intact, and then it may be absorbed through the gastrointestinal tract wall or be excreted. The bioavailable fraction, or absorbed fraction, is the portion of the bioaccessible fraction that crosses the gastrointestinal epithelium reaching lymph and blood.

There are various models that simulate human physiology, and they can be used to assess the solubility, digestion and epithelium permeability of food components in the gastrointestinal tract. The digestion process involves physical, chemical, enzymatic and microbial degradation of food, which takes place in the oral cavity, stomach, small intestine and large intestine. Ionic strength, pH, digestive enzymes, bile, microbiota, transit time and composition of the food matrix influence the digestion process.

Besides *in vivo* animal models, *ex vivo* tissue models, *in silico* computational models and *in vitro* non-cellular fluid models, *in vitro* cell models are a useful tool for screening the specific mechanisms of epithelial permeability. Immortalized cell lines form an adherent monolayer on semi-permeable membranes of transwell, that are used to assess the permeability of a compound from the donor or apical chamber (gut lumen) to the receiver or basolateral chamber (circulating basolateral lymph or blood) (Figure 5). Several cell lines are commonly used to mimic intestinal epithelium including Caco-2, HT-29 and Raji B lymphoma cells. They possess similar characteristics of the *in vivo* intestinal epithelial cells, such as the formation of tight junctions, the production of mucus and the formation of microvilli on their apical side. Caco-2 cells have been extensively used to study brush border formation. They mimic enterocytes, which are the most abundant epithelial cell type in the human intestine. Caco-2 cells were isolated from a patient with colon adenocarcinoma and an excellent correlation was found between *in vitro* permeability and *in vivo* absorption through transcellular, paracellular and carrier-mediated mechanisms. When they grow on transwell supports, monolayer cells become polarized with different apical and basolateral characteristics. They express microvillar proteins, such as villin, fimbrin, sucrase-

isomaltase, myosin I and myosin II. The absence of a mucus layer, which facilitates the transport to the basolateral chamber, is the main inconvenience of this model. Thus, cocultures with HT29 cells, which secret mucus, are more adequate models of gastrointestinal tract epithelium. In addition, Raji B lymphoma cells can be also cocultured to promote the differentiation of Caco-2 cells from microfold cells, or M-cells. These microfold cells are located in Peyer's patch and lymphoid nodules and they are the primary route of transcellular transport [59, 63, 64].

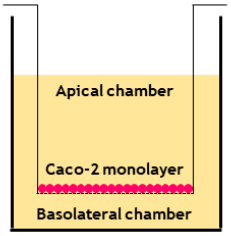

Figure 5. Scheme of a transwell system used for permeability studies

5 NANOMATERIALS IN THE ENVIRONMENT

Emerging contaminants are synthetic or natural chemicals that have recently been discovered and their environmental or public health risks are not known yet. NMs are considered emerging contaminants [65]. Due to their increased production and extensive use, NMs are released into the environment, where they may interact with biotic and abiotic components of ecosystems. Their presence in nature may cause deleterious effects and they may undergo bioaccumulation, biomagnification or biotransformation. Bioaccumulation is the increase in the concentration of contaminants or toxic chemicals in the organisms following their uptake from the environment. Biomagnification is the increase in the concentration of these toxic chemicals in the food chain. Biotransformation is defined as the bioactivation process that may generate reactive metabolites that are more toxic [66]. NPs can be classified as natural or engineered NPs, and their release can be intentional or unintentional. Natural NPs usually disappear from the environment by dissolution or aggregation, while engineered NPs may persist. Once released in the environment, NPs interact with several components and undergo dynamic transformations. These physical, chemical and biological processes are homo- and hetero-agglomeration, dissolution, sedimentation, adsorption, oxidation, reduction, sulfidation and photochemically and biologically mediated reactions. Physicochemical characteristics of NPs (size, surface area, zeta potential, surface charge, colloidal stability and core-shell composition) and environmental conditions (pH, ionic strength, organic and inorganic colloids, temperature, etc.) regulate these environmental transformations. All of them cause changes in the mobility and bioavailability of NPs. Potential toxicity mechanisms are associated with membrane integrity damage, protein destabilization

and oxidation, damage to nucleic acids, production of ROS, interruption of energy transduction and release of harmful and toxic components.

Regarding aerial or atmospheric channels, manufacturing facilities, transportation process, wastewater treatment plants, waste incineration and landfill sites are potential point sources. Non-point or diffuse sources of NPs may be abrasion and washing processes of paints, textiles, clothing, personal care products or cleaning agents. Only small amounts of NPs (8,300 t annually) have been released to the atmosphere compared to other environmental compartments and they usually have short residence times. They may deposit into land and surface waters. The main transformation processes that take place in the atmospheric component are coagulation, aggregation/ disaggregation and wet/dry deposition. Terrestrial flora is the main target for NPs in the atmosphere. Bioavailability is low because the probability of penetration of NMs through the surface of plant leaves is restricted and it depends on the size, shape and NPs concentration. NPs bigger than 50 nm are unable to cross the cell wall. In other cases, NPs can enter through stomatas or cell pores. NPs which pass through stomatas are deposited on the cell wall of substomatal cavity. Once there, NPs try to enter into protoplast by travelling through the cell wall. Only NPs smaller than 5 nm can cross the undamaged cell wall. Small spherical NPs are more toxic than other shapes (plates, rods or wires) because they can easily cross the cell wall through the pores. Foliar heating and alteration of gas exchange have been found due to the accumulation of NPs in stomatas and their obstruction, which may affect plant physiology. No significant impairment of the growth of foliage density of plants was observed. Low concentrations of NPs are considered more toxic than high concentrations due to the less inter-particle interactions in the first scenario, while clusters and agglomerates are not able to penetrate through the pores. Atmospheric NPs can also damage the climate and environmental and human health.

Potential intentional routes of entry of NMs into the soil, water and sediment systems are the discharges of wastewater and sewage sludge. Most NMs in soil tend to be aggregated, adsorbed on the surface,

sedimented and dissolved. Sulfidation and redox reactions are also very common. The fate of NMs in soils is highly dependent on their primary size, aggregation state and surface charge. Environmental conditions, such as pH, ionic strength, presence of non-organic matter (NOM), clay content and groundwater flow must be also considered. If NMs are able to move through the soil, they may enter into groundwater aquifers or move to other water bodies. Soil route may impact the growth cycle of territorial flora. Antifungal and antimicrobial NPs might affect free-living nitrogen-fixing bacteria and symbiotic relationships involving bacteria, fungi and plants. Plant nutrient availability can be modified and the ecosystem might be disturbed. Bacteria and fungi are essential food for soil animals, which regulate their activity and affect the physical condition of soils by digging and mixing. Endocytosis is the potential route of NPs entrance in plants, which was observed during the growth of root hair cells. NPs and their corresponding metal ions can act collectively. In addition, the presence of different types of NPs and contaminants in the soil promotes NP-NP and NP-contaminant interactions, which affect the amount of NPs, ionic forms (case of metallic NPs) and contaminants taken up by plants. Metallic NPs in soils produce a reduction of nodulation in plants and the shoot length and biomass show retarded growth. Genes related to nodulation are downregulated, while genes related to flavonoid biosynthesis, oxidative stress and metal tolerance are upregulated. The aforementioned alterations on plants and soil communities can, therefore, cause changes in the essential ecosystem services (biomass production, organic matter breakdown, nutrient recycling, groundwater purification, soil creation, stability and infiltration capacity).

The estimated amount of NMs released into surface waters is 66,000 t per year. NP behavior depends on their intrinsic physicochemical properties, as well as aquatic environmental conditions (pH, ionic strength, ionic composition and hydrodynamic conditions). Type and composition of water (freshwater, stormwater, groundwater and seawater) control the fate and transport of NMs. Interactions with organic matter, humic substances and dissolved molecules (phosphates and sulphates) can influence nanotoxicology due to their

effect on aggregation, dissolution and deposition. Algae productivity was compromised after their exposure to NPs. Direct and indirect toxic effects cause shadowing, increase in cellular weight and cell sinking. Both effects reduce the light availability for photosynthesis and, therefore, the biomass available for animals. In addition, antimicrobial NPs can have a direct effect on bacterioplankton. Aquatic life can be also exposed to nanotoxicity, which may affect fish growth. Several model systems, such as zebra fish, are very useful for ecotoxicology studies [67-71].

Median lethal concentration (LC50) is defined as the concentration of a material that causes the death of 50% of a group of test animals. Based on the median LC50 values for TiO_2 NPs and Ag NPs towards several groups of organisms of different environmental compartments (crustaceans, bacteria, algae, fish, ciliates, nematodes and yeasts), TiO_2 NPs and Ag NPs are classified as "harmful" and "extremely toxic", respectively. While algae are the most sensitive organism to TiO_2 NPs, crustaceans are very sensitive to Ag NPs [72]. TiO_2 NPs behavior is determined by catching pathway (processes that increase the tendency of NPs to stationary phases, as aggregation, sedimentation, bridging to NOM, incorporation to biofilms and attachment to surfaces) that results in a potential impact on sediment feeding organisms and biofilms. Ag NPs are masking-determined (processes which increase the tendency of the NPs to remain in the aqueous phase, including coating by NOM, partial oxidation, sulfidation and sorption of specific compounds) that results in higher mobility and potential effects on filter feeders. The dissolution of Ag NPs must also be taken into account since Ag NPs are more reactive than TiO_2 NP under certain environmental conditions [73].

5.1 NANOMATERIALS IN MARINE AQUATIC ENVIRONMENT

NMs may enter in the marine environment directly (aerial deposition, effluents, landfill, run-off and sunscreens) and indirectly (rivers). Once in marine systems, NPs are exposed to a highly dynamic environment and they can undergo several chemical, physical and biological transformations, as well as interaction with macromolecules, that will modify their physicochemical properties. Redox reactions and

oxidation-dissolution processes, followed by the interaction with other environmental compounds (chloride, sulphide and phosphate), are the main chemical transformations in the marine environment. Physical transformations, such as aggregation, agglomeration and sedimentation, are also very frequent. Interaction with macromolecules, such as NOM and polysaccharides, causes the formation of a corona layer that enhances the stability of NMs and affects their dissolution rate. The extent of each transformation is dependent on both physicochemical properties of NPs and environmental factors (pH, temperature, ionic strength, salinity and NOM) [74-77]. If NPs continue in suspension in the aquatic environment, the horizontal transport of these materials at large distances increases. If NPs tend to settle, the horizontal transport is reduced and the local exposure is increased [78].

Several types of NMs have shown toxic effects on marine organisms, such as bacteria, algae, rotifers, arthropods, annelids, molluscs (bivalve and gastropods), echinoderms, teleosts and estuarine, brackish, diadromous and euryhaline fishes. Two different mechanisms are responsible for NMs toxicity: 1) chemical toxicity caused by the release of ions or the formation of ROS; and 2) physical stress by NPs size, shape and surface properties. All effects are NP-, environmental-, and species-dependent [74, 75, 78].

Benthic bivalve species, which are sessile and filter-feeders, are targets for accumulation and toxicity of NPs due to the high tendency to sedimentation of these materials and organisms' feeding habits. The digestive gland is a target organ for NMs accumulation. During water-bone exposure, NMs aggregates or agglomerates may be broken in the gills by cilia action or in the digestive gland by the microvillous border. NMs in the gut may induce digestive disorders that can lead to reduced growth or death. The state of aggregation and agglomeration, size, shape and charge of NMs can be modified during ingestion and digestion processes. All these alterations may facilitate the degradation, dispersion, aggregation, agglomeration and distribution of NMs in tissues. NMs can be translocated from the digestive system to the systemic circulation and hemolymph. Regarding subcellular localization, they can be freely dispersed in the cytoplasm, be associated with the cytoskeleton or be inside endocytic vesicles,

lysosomes, mitochondria or the nucleus. Endocytic and lysosomal pathways are the most common locations in bivalve species. Metal-based NMs and metal oxide NMs can release free metal ions after the intracellular digestion process in the lysosomes due to the acidic environment. Adverse effects on lysosomes may cause diseases, cell injury, cell death and alterations in the development of bivalve embryos. Mitochondria are also a target for NMs toxicity. In general, major modes of action of NMs in bivalve molluscs are related to dissolution and release of toxic ions, oxidative stress and cell injury in proteins, membrane and DNA. All processes are directly or indirectly controlled by the production of ROS and free radicals. Oxidative stress in bivalve molluscs may lead to the breakdown of the antioxidant defense system, cytoskeleton disorganization, lipid peroxidation, protein oxidation, mitochondrial disruption and DNA damage. Immunotoxic, genotoxic, neurotoxic and behavioral effects have been found [78].

Ag NPs are very toxic to microalgae, while cnidarians and echinoderms showed adverse effects at 0.1 mg L^{-1}. Toxicity in molluscs and annelids was dependent on their life stage and way of exposure, and it was detected between 0.0007 and 250 mg L^{-1}. By considering behavioral endpoints, crustaceans were highly sensitive to Ag NPs. Adverse effects on fish also depended on the life stage and exposure way. The median effective concentration (EC50), defined as the concentration of a substance in an environmental medium that is expected to produce an effect in 50% of test organism, for water-bone exposed juveniles and dietary exposed adults were 3.46 and 0.2-1 mg L^{-1}, respectively. Bacteria showed no toxicity towards Ag NPs. TiO_2 NPs were found to be more toxic in early life stages. Fish embryos showed negative effects at concentrations between 0.03 and 14 mg L^{-1}, while molluscs showed embryotoxicity between 0.1 and 10 mg L^{-1}. Toxicity in crustacean larvae and adults was detected at 10 and 100 mg L^{-1}, respectively. EC50 values for bacteria and algae exposed to TiO_2 NPs were 100 and 89-179 mg L^{-1}, respectively. Annelids were the less sensitive organism in sediment exposure. Rotifers did not show any effect [79].

Trophic transfer of NMs, or the accumulation of chemicals by an organism following the consumption of another organism previously exposed to NMs, is an important topic that needs to be addressed [74].

6 PROTEIN CORONA FORMATION IN BIOLOGICAL FLUIDS

Once NPs enter in contact with biological fluids, the physicochemical interactions between NPs and medium components, such as proteins, result in a new bio-nanointerface. This structure is called protein corona and the formation is a dynamic and complex process. Protein corona composition, thickness and conformation depend on the physicochemical properties of the NP (size, shape, curvature, solubility, composition, hydrophobicity/hydrophilicity, surface functional groups and surface charge), the nature of the medium and the exposure rate. Temperature is another important factor that alters the composition of protein corona.

First, proteins with high abundance bind to the surface of NPs and, then, they can be replaced by lower concentrated proteins that have higher affinity and slower exchange ratio. This competitive absorption is the "Vroman effect". Protein corona is divided into two parts: hard corona, which is made up of proteins with high affinity that do not desorb from NPs; and soft corona, which includes loosely bound proteins with low affinity. Exchange times are higher in the hard corona than in the soft corona. Protein-NP interactions, as well as protein-protein interactions, govern the absorption of proteins on the surface of NPs. While hard corona proteins interact directly with the surface of the NP, soft corona proteins interact with hard corona proteins.

Protein corona gives NPs a new identity that determines their transport, uptake mechanisms and subcellular localization. It governs the stability, immunogenicity, circulation lifetime, signalling, accumulation, clearance rates, organ distribution and toxicity of the

NP within an organism. Hard corona defines the physiological response to a greater extent than soft corona.
When a protein is linked to a NP, it may lose its conformation and, therefore, its function. These protein conformational changes are usually irreversible [80-82].

7 REFERENCES

[1] A. Santamaria, Historical Overview of Nanotechnology and Nanotoxicology, in J. Reineke (Ed.), Nanotoxicity Methods and Protocols, Humana Press, New Jersey, USA, 2012, pp. 1–12.
[2] D. Schaming, H. Remita, Nanotechnology: from the ancient time to nowadays, Found. Chem. 17 (2015) 187–205.
[3] The European Commission. Commission, Recommendation (EU) 2011/696 of 18 October 2011 on the definition of nanomaterial, Official Journal of the European Union L 275. 58 (2011) 38–40.
[4] A. López-Serrano, R.M. Olivas, J.S. Landaluze, C. Cámara, Nanoparticles: a global vision. Characterization, separation, and quantification methods. Potential environmental and health impact, Anal. Methods 6 (2014) 38–56.
[5] P.G. Jamkhande, N.W. Ghule, A.H. Bamer, M.G. Kalaskar, Metal nanoparticles synthesis: An overview on methods of preparation, advantages and disadvantages, and applications, J. Drug Deliv. Sci. Technol. 53 (2019) 101174–101185.
[6] T. Kodanek, S. Sánchez, F. Lübkemann, D. Dorfs, N.C. Bigall, Fundamentals of Nanotechnology, in P. Grunwald (Ed.), Biocatalysis and Nanotechnology, Pan Stanford Publishing, Singapore, 2017, pp. 1–44.
[7] G. Wang, J. Guan, Value chain of nanotechnology: A comparative study of some major players, J. Nanoparticle Res. 14 (2012) 702–716.
[8] G.L. Hornyak, J.J. Moore, H.F. Tibbals, J. Dutta, Introduction, in Fundamentals of Nanotechnology, CRC Press, Boca Raton, USA, 2008, pp. 3–52.

[9] Y. Lan, Y. Lu, Z. Ren, Mini review on photocatalysis of titanium dioxide nanoparticles and their solar applications, Nano Energy. 2 (2013) 1031–1045.
[10] Y. Nam, J.H. Lim, K.C. Ko, J.Y. Lee, Photocatalytic activity of TiO_2 nanoparticles: A theoretical aspect, J. Mater. Chem. A. 7 (2019) 13833–13859.
[11] B. Faure, G. Salazar-Alvarez, A. Ahniyaz, I. Villaluenga, G. Berriozabal, Y.R. De Miguel, L. Bergström, Dispersion and surface functionalization of oxide nanoparticles for transparent photocatalytic and UV-protecting coatings and sunscreens, Sci. Technol. Adv. Mater. 14 (2013) 023001 (DOI: 10.1088/1468-6996/14/2/023001).
[12] S.L. Schneider, H.W. Lim, A review of inorganic UV filters zinc oxide and titanium dioxide, Photodermatol. Photoimmunol. Photomed. 35 (2019) 442–446.
[13] Z. Fei Yin, L. Wu, H. Gui Yang, Y. Hua Su, Recent progress in biomedical applications of titanium dioxide, Phys. Chem. Chem. Phys. 15 (2013) 4844–4858.
[14] D. Ziental, B. Czarczynska-Goslinska, D.T. Mlynarczyk, A. Glowacka-Sobotta, B. Stanisz, T. Goslinski, L. Sobotta, Titanium dioxide nanoparticles: Prospects and applications in medicine, Nanomaterials 10 (2020) 387–418.
[15] A. Raghunath, E. Perumal, Metal oxide nanoparticles as antimicrobial agents: a promise for the future, Int. J. Antimicrob. Ag. 49 (2017) 137–152.
[16] C. Liao, Y. Li, S.C. Tjong, Visible-light active titanium dioxide nanomaterials with bactericidal properties, Nanomaterials 10 (2020) 124–180.
[17] D.P. MacWan, P.N. Dave, S. Chaturvedi, A review on nano-TiO_2 sol-gel type syntheses and its applications, J. Mater. Sci. 46 (2011) 3669–3686.
[18] X. Chen, S.S. Mao, Titanium dioxide nanomaterials: Synthesis, properties, modifications and applications, Chem. Rev. 107 (2007) 2891–2959.

[19] M. Parashar, V.K. Shukla, R. Singh, Metal oxides nanoparticles via sol–gel method: a review on synthesis, characterization and applications, J. Mater. Sci. Mater. Electron. 31 (2020) 3729–3749.
[20] Y. Wang, Y. He, Q. Lai, M. Fan, Review of the progress in preparing nano TiO_2: An important environmental engineering material, J. Environ. Sci. 26 (2014) 2139–2177.
[21] G. Nabi, Qurat-ul-Aain, N.R. Khalid, M.B. Tahir, M. Rafique, M. Rizwan, S. Hussain, T. Iqbal, A. Majid, A Review on Novel Eco-Friendly Green Approach to Synthesis TiO_2 Nanoparticles Using Different Extracts, J. Inorg. Organomet. Polym. Mater. 28 (2018) 1552–1564.
[22] O. V. Mikhailov, E.O. Mikhailova, Elemental silver nanoparticles: Biosynthesis and bio applications, Materials 12 (2019) 3177–3210.
[23] Q.H. Tran, V.Q. Nguyen, A.T. Le, Silver nanoparticles: Synthesis, properties, toxicology, applications and perspectives, Adv. Nat. Sci. Nanosci. Nanotechnol. 4 (2013) 033001 (DOI: 10.1088/2043-6262/4/3/033001).
[24] R. Ladj, A. Bitar, M. Eissa, Y. Mugnier, R. Le Dantec, H. Fessi, A. Elaissari, Individual inorganic nanoparticles: Preparation, functionalization and *in vitro* biomedical diagnostic applications, J. Mater. Chem. B. 1 (2013) 1381–1396.
[25] B. Calderón-Jiménez, M.E. Johnson, A.R. Montoro Bustos, K.E. Murphy, M.R. Winchester, J.R.V. Baudrit, Silver nanoparticles: Technological advances, societal impacts, and metrological challenges, Front. Chem. 5:6 (2017) 21 (DOI: 10.3389/fchem.2017.00006).
[26] E. Abbasi, M. Milani, S.F. Aval, M. Kouhi, A. Akbarzadeh, H.T. Nasrabadi, P. Nikasa, S.W. Joo, Y. Hanifehpour, K. Nejati-Koshki, M. Samiei, Silver nanoparticles: Synthesis methods, bio-applications and properties, Crit. Rev. Microbiol. 42 (2016) 173–180.
[27] K.S. Siddiqi, A. Husen, R.A.K. Rao, A review on biosynthesis of silver nanoparticles and their biocidal properties, J. Nanobiotechnol. 16 (2018) 14–42.
[28] S. Mukherji, S. Bharti, G. Shukla, S. Mukherji, Synthesis and characterization of size- and shape-controlled silver nanoparticles, Phys. Sci. Rev. 4 (2018) 20170082 (DOI: 10.1515/psr-2017-0082).

[29] X.F. Zhang, Z.G. Liu, W. Shen, S. Gurunathan, Silver nanoparticles: Synthesis, characterization, properties, applications, and therapeutic approaches, Int. J. Mol. Sci. 17 (2016) 1534–1568.
[30] T.A. Jorge de Souza, L.R. Rosa Souza, L.P. Franchi, Silver nanoparticles: An integrated view of green synthesis methods, transformation in the environment, and toxicity, Ecotoxicol. Environ. Saf. 171 (2019) 691–700.
[31] F. Laborda, E. Bolea, J. Jiménez-Lamana, Single particle inductively coupled plasma mass spectrometry: A powerful tool for nanoanalysis, Anal. Chem. 86 (2014) 2270–2278.
[32] F. Laborda, E. Bolea, G. Cepriá, M.T. Gómez, M.S. Jiménez, J. Pérez-Arantegui, J.R. Castillo, Detection, characterization and quantification of inorganic engineered nanomaterials: A review of techniques and methodological approaches for the analysis of complex samples, Anal. Chim. Acta. 904 (2016) 10–32.
[33] K.E. Sapsford, K.M. Tyner, B.J. Dair, J.R. Deschamps, I.L. Medintz, Analyzing nanomaterial bioconjugates: A review of current and emerging purification and characterization techniques, Anal. Chem. 83 (2011) 4453–4488.
[34] P.C. Lin, S. Lin, P.C. Wang, R. Sridhar, Techniques for physicochemical characterization of nanomaterials, Biotechnol. Adv. 32 (2014) 711–726.
[35] M.D. Montaño, J.W. Olesik, A.G. Barber, K. Challis, J.F. Ranville, Single Particle ICP-MS: Advances toward routine analysis of nanomaterials, Anal. Bioanal. Chem. 408 (2016) 5053–5074.
[36] F. Laborda, E. Bolea, J. Jiménez-Lamana, Single particle inductively coupled plasma mass spectrometry for the analysis of inorganic engineered nanoparticles in environmental samples, Trends Environ. Anal. Chem. 9 (2016) 15–23.
[37] H.E. Pace, N.J. Rogers, C. Jarolimek, V.A. Coleman, C.P. Higgins, J.F. Ranville, Determining transport efficiency for the purpose of counting and sizing nanoparticles via single particle inductively coupled plasma mass spectrometry, Anal. Chem. 83 (2011) 9361–9369.

[38] J. Gigault, J.M. Pettibone, C. Schmitt, V.A. Hackley, Rational strategy for characterization of nanoscale particles by asymmetric-flow field flow fractionation: A tutorial, Anal. Chim. Acta. 809 (2014) 9–24.
[39] M. Wagner, S. Holzschuh, A. Traeger, A. Fahr, U.S. Schubert, Asymmetric flow field-flow fractionation in the field of nanomedicine, Anal. Chem. 86 (2014) 5201–5210.
[40] F. von der Kammer, S. Legros, T. Hofmann, E.H. Larsen, K. Loeschner, Separation and characterization of nanoparticles in complex food and environmental samples by field-flow fractionation, Trac - Trends Anal. Chem. 30 (2011) 425–436.
[41] E. Bolea, J. Jiménez-Lamana, F. Laborda, J.R. Castillo, Size characterization and quantification of silver nanoparticles by asymmetric flow field-flow fractionation coupled with inductively coupled plasma mass spectrometry, Anal. Bioanal. Chem. 401 (2011) 2723–2732.
[42] V. De Matteis, Exposure to inorganic nanoparticles: Routes of entry, immune response, biodistribution and *in vitro/in vivo* toxicity evaluation, Toxics. 5 (2017) 29–50.
[43] A. Elsaesser, C.V. Howard, Toxicology of nanoparticles, Adv. Drug Deliv. Rev. 64 (2012) 129–137.
[44] S. Arora, J.M. Rajwade, K.M. Paknikar, Nanotoxicology and *in vitro* studies: The need of the hour, Toxicol. Appl. Pharmacol. 258 (2012) 151–165.
[45] A. Elsaesser, C.V. Howard, Toxicology of nanoparticles, Adv. Drug Deliv. Rev. 64 (2012) 129–137.
[46] L.C. Cheng, X. Jiang, J. Wang, C. Chen, R.S. Liu, Nano-bio effects: interaction of nanomaterials with cells, Nanoscale. 5 (2013) 3547–3569.
[47] R. Sakhtianchi, R.F. Minchin, K.B. Lee, A.M. Alkilany, V. Serpooshan, M. Mahmoudi, Exocytosis of nanoparticles from cells: Role in cellular retention and toxicity, Adv. Colloid Interface Sci. 201–202 (2013) 18–29.
[48] N. Liu, M. Tang, Toxic effects and involved molecular pathways of nanoparticles on cells and subcellular organelles, J. Appl. Toxicol. 40 (2020) 16–36.

[49] R. Mohammadpour, M.A. Dobrovolskaia, D.L. Cheney, K.F. Greish, H. Ghandehari, Subchronic and chronic toxicity evaluation of inorganic nanoparticles for delivery applications, Adv. Drug Deliv. Rev. 144 (2019) 112–132.
[50] R. Landsiedel, E. Fabian, L. Ma-Hock, W. Wohlleben, K. Wiench, F. Oesch, B. Van Ravenzwaay, Toxico-/biokinetics of nanomaterials, Arch. Toxicol. 86 (2012) 1021–1060.
[51] Z. Piperigkou, K. Karamanou, A.B. Engin, C. Gialeli, A.O. Docea, D.H. Vynios, M.S.G. Pavão, K.S. Golokhvast, M.I. Shtilman, A. Argiris, E. Shishatskaya, A.M. Tsatsakis, Emerging aspects of nanotoxicology in health and disease: From agriculture and food sector to cancer therapeutics, Food Chem. Toxicol. 91 (2016) 42–57.
[52] J. Zhao, V. Castranova, Toxicology of nanomaterials used in nanomedicine, J. Toxicol. Environ. Heal. - Part B Crit. Rev. 14 (2011) 593–632.
[53] Q. Chaudhry, L. Castle, R. Watkins, Nanomaterials in Food and Food Contact Materials – Potential Implications for Consumer Safety and Regulatory Controls, in L.J. Frewer, W. Norde, A. Fischer, F. Kampers (Ed.), Nanotechnology in the Agri-Food Sector: Implications for the Future, Wiley-VCH, Weinheim, Germany, 2011, pp. 191–208.
[54] M. Shafiq, S. Anjum, C. Hano, I. Anjum, B.H. Abbasi, An overview of the applications of nanomaterials and nanodevices in the food industry, Foods. 9 (2020) 148–175.
[55] M.Â. Cerqueira, A.C. Pinheiro, O.L. Ramos, H. Silva, A.I. Bourbon, A.A. Vicente, Advances in Food Nanotechnology, in R. Busquets (Ed.), Emerging Nanotechnologies in food science, Elsevier, Amsterdam, Netherlands, 2017, pp. 11–38.
[56] M. Thiruvengadam, G. Rajakumar, I.M. Chung, Nanotechnology: current uses and future applications in the food industry, 3 Biotech. 8 (2018) 74–87.
[57] S. Baker, T. Volova, S. V. Prudnikova, S. Satish, N. Prasad, Nanoagroparticles emerging trends and future prospect in modern agriculture system, Environ. Toxicol. Pharmacol. 53 (2017) 10–17.
[58] S.D.F. Mihindukulasuriya, L.T. Lim, Nanotechnology development in food packaging: A review, Trends Food Sci. Technol. 40 (2014) 149–167.

[59] C. McCracken, P.K. Dutta, W.J. Waldman, Critical assessment of toxicological effects of ingested nanoparticles, Environ. Sci. Nano. 3 (2016) 256–282.
[60] Y. Cao, J. Li, F. Liu, X. Li, Q. Jiang, S. Cheng, Y. Gu, Consideration of interaction between nanoparticles and food components for the safety assessment of nanoparticles following oral exposure: A review, Environ. Toxicol. Pharmacol. 46 (2016) 206–210.
[61] C.A. dos Santos, A.P. Ingle, M. Rai, The emerging role of metallic nanoparticles in food, Appl. Microbiol. Biotechnol. 104 (2020) 2373–2383.
[62] V. Amenta, K. Aschberger, M. Arena, H. Bouwmeester, F. Botelho Moniz, P. Brandhoff, S. Gottardo, H.J.P. Marvin, A. Mech, L. Quiros-Pesudo, H. Rauscher, R. Schoonjans, M.V. Vettori, S. Weigel, R.J. Peters, Regulatory aspects of nanotechnology in the agri/feed/food sector in EU and non-EU countries, Regul. Toxicol. Pharmacol. 73 (2015) 463–476.
[63] D.E. Lefebvre, K. Venema, L. Gombau, L.G. Valerio, J. Raju, G.S. Bondy, H. Bouwmeester, R.P. Singh, A.J. Clippinger, E.M. Collnot, R. Mehta, V. Stone, Utility of models of the gastrointestinal tract for assessment of the digestion and absorption of engineered nanomaterials released from food matrices, Nanotoxicology 9 (2015) 523–542.
[64] S. Yee, *In vitro* permeability across Caco-2 cells (colonic) can predict *in vivo* (small intestinal) absorption in man - Fact or myth, Pharm. Res. 14 (1997) 763–766.
[65] R. Naidu, V.A. Arias Espana, Y. Liu, J. Jit, Emerging contaminants in the environment: Risk-based analysis for better management, Chemosphere 154 (2016) 350–357.
[66] M.N. Uddin, F. Desai, E. Asmatulu, Engineered nanomaterials in the environment: bioaccumulation, biomagnification and biotransformation, Environ. Chem. Lett. 18 (2020) 1073–1083.
[67] M.S. Bakshi, Impact of nanomaterials on ecosystems: Mechanistic aspects *in vivo*, Environ. Res. 182 (2020) 109099–109114.

[68] X. Ma, J. Geiser-Lee, Y. Deng, A. Kolmakov, Interactions between engineered nanoparticles (ENPs) and plants: Phytotoxicity, uptake and accumulation, Sci. Total Environ. 408 (2010) 3053–3061.
[69] Q. Abbas, B. Yousaf, Amina, M.U. Ali, M.A.M. Munir, A. El-Naggar, J. Rinklebe, M. Naushad, Transformation pathways and fate of engineered nanoparticles (ENPs) in distinct interactive environmental compartments: A review, Environ. Int. 138 (2020) 105646–105664.
[70] K.L. Garner, A.A. Keller, Emerging patterns for engineered nanomaterials in the environment: A review of fate and toxicity studies, J. Nanoparticle Res. 16 (2014) 2503–2531.
[71] E. Navarro, A. Baun, R. Behra, N.B. Hartmann, J. Filser, A.J. Miao, A. Quigg, P.H. Santschi, L. Sigg, Environmental behavior and ecotoxicity of engineered nanoparticles to algae, plants, and fungi, Ecotoxicology 17 (2008) 372–386.
[72] A. Kahru, H.C. Dubourguier, From ecotoxicology to nanoecotoxicology, Toxicology 269 (2010) 105–119.
[73] G.E. Schaumann, A. Philippe, M. Bundschuh, G. Metreveli, S. Klitzke, D. Rakcheev, A. Grün, S.K. Kumahor, M. Kühn, T. Baumann, F. Lang, W. Manz, R. Schulz, H.J. Vogel, Understanding the fate and biological effects of Ag- and TiO_2-nanoparticles in the environment: The quest for advanced analytics and interdisciplinary concepts, Sci. Total Environ. 535 (2015) 3–19.
[74] T.J. Baker, C.R. Tyler, T.S. Galloway, Impacts of metal and metal oxide nanoparticles on marine organisms, Environ. Pollut. 186 (2014) 257–271.
[75] G. Vale, K. Mehennaoui, S. Cambier, G. Libralato, S. Jomini, R.F. Domingos, Manufactured nanoparticles in the aquatic environment-biochemical responses on freshwater organisms: A critical overview, Aquat. Toxicol. 170 (2016) 162–174.
[76] R.F. Lehutso, Y. Tancu, A. Maity, M. Thwala, Aquatic toxicity of transformed and product-released engineered nanomaterials: An overview of the current state of knowledge, Process Saf. Environ. Prot. 138 (2020) 39–56.

[77] M. Amde, J.-fu Liu, Z.Q. Tan, D. Bekana, Transformation and bioavailability of metal oxide nanoparticles in aquatic and terrestrial environments. A review, Environ. Pollut. 230 (2017) 250–267.
[78] T.L. Rocha, T. Gomes, V.S. Sousa, N.C. Mestre, M.J. Bebianno, Ecotoxicological impact of engineered nanomaterials in bivalve molluscs: An overview, Mar. Environ. Res. 111 (2015) 74–88.
[79] D. Minetto, A. Volpi Ghirardini, G. Libralato, Saltwater ecotoxicology of Ag, Au, CuO, TiO_2, ZnO and C60 engineered nanoparticles: An overview, Environ. Int. 92–93 (2016) 189–201.
[80] I. Lynch, T. Cedervall, M. Lundqvist, C. Cabaleiro-Lago, S. Linse, K.A. Dawson, The nanoparticle-protein complex as a biological entity; a complex fluids and surface science challenge for the 21st century, Adv. Colloid Interface Sci. 134–135 (2007) 167–174.
[81] A.L. Capriotti, G. Caracciolo, C. Cavaliere, V. Colapicchioni, S. Piovesana, D. Pozzi, A. Laganà, Analytical methods for characterizing the nanoparticle-protein corona, Chromatographia 77 (2014) 755–769.
[82] M. Rahman, S. Laurent, N. Tawil, L. Yahia, M. Mahmoudi, Nanoparticle and protein corona, in B. Martinac (Ed.) Protein-Nanoparticle Interactions, Springer, Berlin, Germany, 2013, pp. 21–44.

USC
UNIVERSIDADE
DE SANTIAGO
DE COMPOSTELA

II. OBJECTIVES AND HYPOTHESIS

USC
UNIVERSIDADE
DE SANTIAGO
DE COMPOSTELA

OBJECTIVES AND HYPOTHESIS

This Doctoral thesis focuses on developing analytical nanometrological platforms for detection, characterization and quantification of NPs in marine products (bivalve molluscs) and their derivatives (crab sticks); studying the behavior of these NPs present in bivalve molluscs and crab sticks in the human gastrointestinal tract; and evaluating the NPs-protein interactions in hemolymph of bivalve molluscs.
The present work aims to:

1. Develop analytical methods for characterizing and quantifying TiO_2 NPs and Ag NPs (Chapters 1, 2, 3 and 4).

2. Develop methods of extraction and digestion of TiO_2 NPs and Ag NPs from bivalve molluscs and crab sticks without affecting the integrity of NPs (Chapter 1, 2 and 3).

3. Separate NPs using FFF techniques, specifically by AF4 (Chapter 4).

4. Study the degradation rate of TiO_2 NPs and Ag NPs in the human gastrointestinal tract (Stage 0 of EFSA guidance) (Chapter 5).

5. Study the bioaccessibility and bioavailability of TiO_2 NPs and Ag NPs in bivalve molluscs (Chapter 6).

6. Characterize protein corona associated with NPs in the hemolymph of bivalve molluscs (Chapter 7).

Because of the increasing use of NPs-containing products, they are expected to be found in environmental samples, such as bivalve molluscs. We decide to focus on TiO_2 NPs and Ag NPs because they are two of the most used NPs. Due to the presence of TiO_2 NPs in food additive E171, it is presumed to find them in food products that contain this whitening agent, like crab sticks. The presence of NPs in food may have adverse effects on the human health since some NPs are expected to be biopersistent under human gastrointestinal conditions and they may be able to cross the gastrointestinal epithelium and reach the bloodstream and other organs. Finally, the interaction of NPs with proteins in hemolymph of bivalve molluscs might lead to protein corona formation that controls their transport, behavior and toxicity, so studying the protein corona composition will be of great importance.

USC
UNIVERSIDADE
DE SANTIAGO
DE COMPOSTELA

USC
UNIVERSIDADE
DE SANTIAGO
DE COMPOSTELA

III. METHODOLOGY

USC
UNIVERSIDADE
DE SANTIAGO
DE COMPOSTELA

METHODOLOGY

This Doctoral thesis consists of the following stages:

Stage 1. Characterization and quantification of TiO_2 NPs and Ag NPs. Electron microscopy techniques, SEM and TEM, were used for the characterization of NPs, as well as DLS. sp-ICP-MS allows simultaneous characterization and quantification of NPs with LOD below ng L^{-1}. The benefits of sp-ICP-MS were evaluated and the obtained information (mass and number concentrations, most frequent and mean sizes and dissolved concentrations) was validated.

Stage 2. Separation of NPs by FFF techniques, mainly AF4.
AF4 system was coupled on-line with several detectors, such as UV-vis spectroscopy and ICP-MS. Analyzed samples were enzymatic extracts from bivalve molluscs containing NPs. Information about size distribution, elemental composition of NPs and concentration were obtained.

Stage 3. Development of extraction and digestion methods of TiO_2 NPs and Ag NPs from bivalve molluscs and crab sticks without affecting the integrity of NPs.
Enzymatic hydrolysis procedures were optimized, working at neutral pH and moderate temperature, to extract NPs from bivalve molluscs and crab sticks. These procedures were assisted and accelerated by ultrasounds. All measurements were performed by sp-ICP-MS. Acid digestions were used for sample preparation before total concentration analysis by ICP-MS.

Stage 4. Study the degradation rate of TiO_2 NPs and Ag NPs in the human gastrointestinal tract (Stage 0 of EFSA guidance).
Following the recommendations set by the EFSA guidance, several standards of TiO_2 NPs and Ag NPs of different sizes at three concentration levels were subjected to an *in vitro* human gastrointestinal digestion. Changes in number concentration, size distribution and dissolved content were studied over the digestion process (30, 60 and 120 min of gastric and intestinal stages). Similar studies were performed for the E171 food additive, bivalve molluscs and crab sticks containing TiO_2 NPs and Ag NPs. Measurements were performed by sp-ICP-MS.

Stage 5. Study the *in vitro* bioavailability of TiO_2 NPs and Ag NPs in bivalve molluscs.
Caco-2 cell line was used to mimic the transport of NPs through the human intestine after bivalve mollusc ingestion. Bivalve mollusc samples, that contained TiO_2 NPs and Ag NPs, were subjected to a gastrointestinal digestion simulation. *In vitro* intestinal absorption was studied using the soluble extract (bioaccessible fraction) from samples. We analyzed changes in concentrations and size distributions of NPs in bivalve mollusc samples, soluble fractions (after gastrointestinal digestion), apical fractions (fraction that did not pass through Caco-2 monolayer) and basolateral fractions (fraction that was translocated through Caco-2 monolayer). NPs present in the basolateral fractions were considered bioavailable. sp-ICP-MS and ICP-MS were selected as measurement techniques.

Stage 6. Characterization of protein corona associated with NPs in the hemolymph of bivalve molluscs.
Separation of protein corona from free proteins and free NPs in hemolymph of clams exposed to TiO_2 NPs and E171 was performed by centrifugation. LC-MS/MS and SWATH-MS were used for protein identification and quantification, respectively. The evolution of corona composition was analyzed over time for clams exposed to TiO_2 NPs of different sizes and food additive E171 at different concentration levels.

USC
UNIVERSIDADE
DE SANTIAGO
DE COMPOSTELA

USC
UNIVERSIDADE
DE SANTIAGO
DE COMPOSTELA

IV. RESULTS

USC
UNIVERSIDADE
DE SANTIAGO
DE COMPOSTELA

PART I. ENZYMATIC HYDROLYSIS FOR NANOPARTICLES ASSESSMENT BY SP-ICP-MS

USC
UNIVERSIDADE
DE SANTIAGO
DE COMPOSTELA

CHAPTER 1

ENZYMATIC HYDROLYSIS AS A SAMPLE PRE-TREATMENT FOR TITANIUM DIOXIDE NANOPARTICLES ASSESSMENT IN SURIMI (CRAB STICKS) BY SINGLE PARTICLE ICP-MS

MARÍA VANESA TABOADA-LÓPEZ, PALOMA HERBELLO-HERMELO, RAQUEL DOMÍNGUEZ-GONZÁLEZ, PILAR BERMEJO-BARRERA AND ANTONIO MOREDA-PIÑEIRO

TALANTA (2019), 195: 23-32
ISSN: 0039-9140
DOI: 10.1016/J.TALANTA.2018.11.023

USC
UNIVERSIDADE
DE SANTIAGO
DE COMPOSTELA

CHAPTER 2

ULTRASOUND ASSISTED ENZYMATIC HYDROLYSIS FOR ISOLATING TITANIUM DIOXIDE NANOPARTICLES FROM BIVALVE MOLLUSK BEFORE SP-ICP-MS

MARÍA VANESA TABOADA-LÓPEZ, SARA IGLESIAS-LÓPEZ, PALOMA HERBELLO-HERMELO, PILAR BERMEJO-BARRERA AND ANTONIO MOREDA-PIÑEIRO

ANALYTICA CHIMICA ACTA (2018), 1018: 16-25
ISSN: 0003-2670
DOI: 10.1016/J.ACA.2018.02.075

USC
UNIVERSIDADE
DE SANTIAGO
DE COMPOSTELA

CHAPTER 3

DETERMINATION AND CHARACTERIZATION OF SILVER NANOPARTICLES IN BIVALVE MOLLUSCS BY ULTRASOUND ASSISTED ENZYMATIC HYDROLYSIS AND SP-ICP-MS

MARÍA VANESA TABOADA-LÓPEZ, NEREA ALONSO-SEIJO, PALOMA HERBELLO-HERMELO, PILAR BERMEJO-BARRERA AND ANTONIO MOREDA-PIÑEIRO

MICROCHEMICAL JOURNAL (2019), 148: 652-660
ISSN: 0026-265X
DOI: 10.1016/J.MICROC.2019.05.023

USC
UNIVERSIDADE
DE SANTIAGO
DE COMPOSTELA

PART II. OPTIMIZATION OF SEPARATION OF NPS BY AF4 COUPLED WITH DIFFERENT DETECTORS

USC
UNIVERSIDADE
DE SANTIAGO
DE COMPOSTELA

CHAPTER 4

AF4-UV-ICP-MS FOR DETECTING AND QUANTIFYING SILVER NANOPARTICLES IN SEAFOOD AFTER ENZYMATIC HYDROLYSIS

MARÍA VANESA TABOADA-LÓPEZ, DOROTA BARTCZAK, SUSANA CUELLO-NÚÑEZ, HEIDI GOENAGA-INFANTE, PILAR BERMEJO-BARRERA AND ANTONIO MOREDA-PIÑEIRO

USC
UNIVERSIDADE
DE SANTIAGO
DE COMPOSTELA

4 AF4-UV-ICP-MS FOR DETECTING AND QUANTIFYING SILVER NANOPARTICLES IN SEAFOOD AFTER ENZYMATIC HYDROLYSIS

María Vanesa Taboada-López[1], Dorota Bartczak[2], Susana Cuello-Núñez[2], Heidi Goenaga-Infante[2], Pilar Bermejo-Barrera[1], Antonio Moreda-Piñeiro[1]

[1]Trace Element, Spectroscopy and Speciation Group (GETEE), Strategic Grouping in Materials (AEMAT), Department of Analytical Chemistry, Nutrition and Bromatology. Faculty of Chemistry. Universidade de Santiago de Compostela. Avenida das Ciencias, s/n. 15782 – Santiago de Compostela, Spain.
[2]LGC Limited. Queen's Road, TW11 0LY, Teddington, United Kingdom.

Abstract

A method based on asymmetric flow field-flow fractionation (AF4) coupled to ultraviolet-visible (UV-vis) spectroscopy and inductively coupled plasma-mass spectrometry (ICP-MS) has been developed for silver nanoparticles (Ag NPs) detection and quantification in bivalve molluscs. Samples were pre-treated using a conventional enzymatic (pancreatin and lipase) hydrolysis procedure (37 °C, 12 h). AF4 was performed using a regenerated cellulose (RC) membrane (10 kDa, 350 µm spacer) and aqueous 5 mM Tris-HCl (pH 7.4) as a carrier. Focusing implied tip and focus flows of 0.20 and 3.0 mL min^{-1}, respectively, and an injection time of 4.0 min. Elution step was performed using a cross flow of 3.0 mL min^{-1} for 15 min, followed to lineal cross flow decrease for 7.5 min and a washing step for 9.4 min. Several bivalve molluscs (clams, oysters and variegated scallops) were analyzed for total Ag content (ICP-MS after microwave assisted acid

digestion) and for Ag NPs by the presented here method. Results show that Ag NPs are detected at the same elution time that proteins (UV monitoring at 280 and 405 nm), which suggests a certain interaction between Ag NPs and proteins in the enzymatic extracts. AF4-UV-ICP-MS fractograms also suggest different Ag NPs size distributions for selected samples. Membrane recoveries, determined by peak area comparison of fractograms with and without application of cross flow, were within the 49-121% range.

Keywords
Silver nanoparticles, bivalve molluscs, ultrasonic probe, enzymatic hydrolysis, sp-ICP-MS

4.1 INTRODUCTION

Because of the novel properties of nanomaterials (NMs), nanotechnology is a constantly growing field. Between 1990 and 2018, the number of papers related to this topic increased exponentially from 667 to 10142 [1]. The European Commission (EC) defined in 2011 a NM as a natural, incidental or manufactured material which contains at least 50% of particles with one or more dimensions between 1 and 100 nm [2]. If the NM has one, two or three dimensions within the above-mentioned range, it is a nanofilm, a nanotube or a nanoparticle, respectively.
There are currently more than 1800 listed consumer products which contain NMs, 443 of them contain silver nanoparticles (Ag NPs) [3]. These products containing Ag NPs can be included in different fields like electronics, paints, coatings, glass and ceramics, textiles, cosmetics, medical devices and food [4]. Ag NPs show innovative physical (high electrical and thermal conductivity [5]), optical (surface-enhanced Raman scattering [6] and non-linear optical behavior [7]) and photocatalytic properties [8]. However, Ag NPs are mainly known because of their antimicrobial [9], antifungal [10] and antibacterial activity against Gram-positive and Gram-negative bacteria [11, 12].
Ag NPs can be synthetized by physical, biological and chemical methods. Gas phase deposition, laser burning, mechanical grinding and ion sputtering are common physical methods used for NPs synthesis.

Chemical methods are based reduction mechanisms using certain reducing reagents or assisted methods (electrochemistry and microwave irradiation), whereas biological methods take the advantage of certain plants or plant extracts to perform chemical reduction from metallic ions [13]. Chemical and biological methods are the most commonly used because of the possibility of controlling the morphology of Ag NPs [14] and because they are environmentally friendly and non-toxic [15], respectively.

Because of the numerous applications of Ag NPs, there are concerns over the public health and environmental effects of Ag NPs and other engineered NM. Actions to ensure the safety and health of human, terrestrial and aquatic lives and environment are therefore needed [16]. The presence of Ag NPs has been studied in environmental samples such as river water [17] and soils [18]. Regarding the marine ecosystem, studies performed at different trophic levels have shown that the effect of Ag NPs depends on the type of organism [19, 20]. Ag NPs have found to be toxic to marine microalgae, and toxicity was found to be dependent on Ag NPs size and coating [21, 22] causing photo-inhibition [23]. In annelids [24] and amphipods [25], Ag NPs are related to mortality and abnormal larval development and changes on swimming pattern in response to light, respectively. Molluscs are traditionally considered as sentinels of environmental health because they are filtration feeders and they accumulate in their organism pollutants present in seawater. There are some studies about mussels (*Mytilus galloprovincialis*) [26], clams (*Scrobicularia plana*) [27, 28] and periwinkle (*Littorina littorea*) exposed to Ag NPs [29] which demonstrate a concentration-dependent bioaccumulation and a different distribution for ionic Ag and Ag NPs. The study of different biochemical parameters shows a potential toxicity of Ag NPs, which is related to reactive oxygen species (ROS), apoptosis and genotoxicity.

The consideration of NPs as analytes requires methods which give chemical (composition and mass/number concentration) and physical information (size, shape and aggregation state) [30]. Sample preparation is a crucial step and it is led to remove matrix sample and/or to separate NPs from other sample components. For the first purpose, digestion methods (acid, alkaline or enzymatic) are the most used techniques.

Centrifugation, filtration and extraction (liquid or solid phase) can also be applied to separate NPs. Electron microscopy techniques (Transmission Electron Microscopy TEM, Field-Emission Scanning Electron Microscopy FESEM, Environmental Scanning Electron Microscopy ESEM) provide physical information about NPs and information about elemental composition in combination with energy dispersive X-ray spectroscopy (EDX). Light scattering techniques like Dynamic Light Scattering (DLS) and Particle Tracking Analysis (PTA) can be also used for determining NPs diameter based on Brownian motion of particles. Elemental analytical techniques such as Electrothermal-Atomic Absorption Spectroscopy (ET-AAS), Inductively Coupled Plasma-Optical Emission Spectroscopy (ICP-OES) and Inductively Coupled Plasma-Mass Spectrometry (ICP-MS), although they are not nano-specific, can be used for detection and quantification of elements included in the NPs. ICP-MS working in the so-called single particle mode (single particle-ICP-MS, sp-ICP-MS) provides physical (most frequent diameter, mean diameter and particle diameter distribution) and chemical information (mass/number concentration) at once, and its use is therefore in constant increase. Field-Flow Fractionation (FFF), electrophoresis and liquid chromatography (LC) are mainly used to separate NPs based on their size, density, surface chemistry or charge, and they can be easily coupled with several elemental analysis detectors [31].

Asymmetric Flow FFF (AF4) was selected to perform the current study. AF4 separation implies the injection of analytes in a flat channel with a laminar tangential flow and then a cross flow perpendicular to the channel is applied. NPs are separated according to diffusion coefficients, which are related to their size [32]. AF4 is versatile, simple and compatible with different materials, particle sizes and mobile phases [33]. It can be coupled online with different detectors such as UV-vis spectroscopy (useful technique because of the Surface Plasmon Resonance, SPR, inherent to metallic NPs) and ICP-MS (technique of choice for elemental quantification) [34]. Despite some studies regarding Ag NPs separation by AF4, the developed procedures have been focused on spiked soils (several Ag NPs standards for spiking and AF4-UV for assessment) [33], on nutraceuticals and beverages

(AF4-UV-ICP-MS) [32] and on characterizing/quantifying Ag NPs standards of different sizes by AF4-ICP-MS [35, 36]. Therefore, AF4-UV-ICP-MS methods have not been developed/applied to complex matrices containing Ag NPs concentration at environmental levels. This represents a current analytical challenge.

The aim of the current work has been the detection and quantification of Ag NPs in commercial bivalve molluscs (clams, oysters and variegated scallops) containing environmental (basal) Ag NPs levels. Samples were pre-treated overnight (12 h) using an enzymatic digestion with a pancreatin/lipase mixture at physiological temperature (37 °C), and Ag NPs content was quantified by AF4-UV-ICP-MS. Fractions separated by AF4 were monitored using a UV detector, set at 280 nm (proteins) and 405 nm (related to Ag NPs), and ICP-MS optimized for m/z 107 and 109 Ag.

4.2 MATERIALS AND METHODS

4.2.1 Instrumentation

AF4 system (AF2000, Postnova Analytics, Landsberg am Lech, Germany), with an analytical ceramic-frit channel with nominal dimensions of 355 mm×60 mm, equipped with 350μm spacer and loaded with 10 kDa RC membrane (all from Postnova), was used throughout the current work. Manual injection was performed using a 20 μL loop. AF4 was on-line connected to a photodiode array (PDA) Accela UV-vis detector (Thermo Scientific, Massachusetts, USA) set at 280 and 405 nm. The outlet from PDA was connected to an 8900 ICP-MS (Agilent Technologies, California, USA) equipped with a concentric nebulizer, a cyclonic spray chamber and a torch. Total Ag determinations were performed with a NexION 300X ICP-MS system (Perkin Elmer, Massachusetts, USA) equipped with a SeaFast SC2 DX autosampler (Elemental Scientific, Nebraska, USA), a concentric nebulizer (PFA-ST) and a PC^3 glass cyclonic spray chamber. Enzymatic hydrolysis was performed in a Heraeus oven (Thermo Scientific, Massachusetts, USA) equipped with a circular rotator (Bibby Sterilin, Staffordshire, UK). Acid digestion was performed using an Ethos Plus microwave from Milestone

Milestone (Sorisole, Italy) with 100 mL Teflon vessels and covers. A Scanning Electron Microscope (SEM) from JEOL (Tokyo, Japan) was used for obtaining images of NPs in the enzymatic extracts. Extracts were pre-treated in a 6223MG domestic microwave oven (700 W) from Nevir (Madrid, Spain). Other used equipment were a pH-meter model Hydrus 300 (Fisherbrand, Pittsburgh, USA), a Kerry ultrasonic cleaner water-bath from Guyson (North Yorkshire, UK), a centrifuge 5804 R (Eppendorf, Hamburg, Germany), a domestic Taurus blade grinder (Taurus, Barcelona, Spain) and a KNF Laboport ® vacuum pump (New Jersey, USA).

4.2.2 Reagents

Ultrapure water (18.2 MΩ cm) was obtained from an Elga water purification system (Marlow, UK). Ionic Ag ($AgNO_3$ 1000 mg L^{-1}), used for ICP-MS calibration for total Ag quantification, was purchased from Merck (Darmstadt, Germany). Ionic silver ($AgNO_3$ 1000 mg L^{-1} in 0.5 M HNO_3) from Romil (Cambridge, UK) was used for AF4-UV-ICP-MS calibration. Rhodium (1000 mg L^{-1} in 5% HNO_3) was from Merck and germanium ($(NH_4)_2GeF_6$, 1000 mg L^{-1} in 0.1M HF) from Romil. Porcine pancreatin and lipase from *Candida rugose* were from Sigma Aldrich (Osterode, Germany). Enzymes were dissolved in Trizma® base solution (Sigma Aldrich) which was adjusted to pH 7.4 with 36% (w/v) hydrochloric acid from Promochem (LGC Standards, Wesel, Germany). This solution was also used to prepare the mobile phase for AF4. NovaChem 0.05% (v/v) (Postnova Analytics) was tested as a carrier. Mobile phases were vacuum filtered every day through a 0.22 μm filter (Millipore, Massachusetts, USA). 33% (w/v) hydrogen peroxide and 69% (w/v) hyperpure nitric acid (Panreac, Barcelona, Spain) were used for acid digestion.

4.2.3 Seafood samples

Four seafood samples were purchased in markets and supermarkets in Santiago de Compostela (Spain). Studied samples were Atlantic surf clams, *Spisula solidissima* (ABB); oysters, *Ostrea edulis* (OP) and fresh and frozen variegated scallop, *Chlamys varia* (Z24 and Z28). Flesh was separated from byssus and shell from approximately 1 kg of each sample, and they were then washed with ultrapure water and homogenized by mechanical blending. Homogenized samples were kept in polyethylene bottles at -20 °C until their analysis.

4.2.4 Microwave assisted acid digestion

Each sample was subjected to microwave assisted acid digestion in triplicate by weighting 1.0 g of sample into the Teflon reactors and adding 4 mL of ultrapure water, 3 mL of 69% (w/v) HNO_3 and 1 mL of 33% (w/v) H_2O_2. Closed reactors were then subjected to a four-stage microwave program [37]. The first ramp heating from room temperature to 90 °C in 2 min; then another ramp heating from 90 to 140 °C in 5 min; a third ramp heating from 140 to 200 °C for 5 min; and a final heating stage at 200 °C for 11 min. All steps were carried out at 1000 W microwave power. After 2 h for cooling-down, acid digests were made up to 25 mL with ultrapure water, and they were kept in clean plastic tubes at room temperature before measurements.

4.2.5 Total Ag quantification

Total Ag quantification was performed by ICP-MS after 1:10 dilution of acid digests with ultrapure water. Operating ICP-MS conditions are listed in Table 4.1. Standard addition calibration method was performed at seven levels of Ag concentrations (0, 1, 5, 10, 50, 100 and 200 μg L^{-1}). Rhodium (^{103}Rh) at a concentration of 10 μg L^{-1} was selected as internal standard (IS). The limit of detection (LOD) and the limit of quantification (LOQ) were calculated based on the 3 SD and 10 SD criteria (SD is the standard deviation of eleven measurements of a reagent blank), respectively, and they were found to be 6.2 (LOD) and 21 μg kg^{-1} (LOQ).

Table 4.1. ICP-MS operating conditions for total Ag quantification

ICP-MS operating conditions		
Radiofrequency power		1600 W
Gas Flows	Nebulization	0.87 mL min^{-1}
	Auxiliary	1.2 mL min^{-1}
	Plasma	16 mL min^{-1}
Ion optics	Analogic phase voltage	−1862 V
	Pulses voltage	1650 V
	Discriminant limit	12
	Deflector voltage	−11.25 W
	Entrance cell voltage	−5 V
	Exit cell voltage	−5 V
	Collision cell offset	−16
Analyte (*m*/*z*)	Ag	107
	Rh (IS)	103

4.2.6 Enzymatic hydrolysis for Ag NPs extraction

Based on a previous study [38], approximately 1.0 g of sample was weighted into 10 mL plastic tubes and 10 mL of enzymatic solution (2.0 g L^{-1} of pancreatin and 2.0 g L^{-1} lipase solution prepared in 0.2 M Trizma® solution, pH 7.4) were added. The pH of the Trizma® solution was adjusted at 7.4 with diluted hydrochloric acid. Mixtures were incubated at 37 °C for 12 h in an oven equipped with a circular rotator. Enzymatic digests were separated from the solid residues by centrifugation (8 °C, 3900 rpm, 25 min). Each sample was digested by duplicate. Extracts were protected from light with aluminium foil and were kept in plastic tubes at 8 °C.

4.2.7 AF4-UV-ICP-MS measurements for Ag NPs

Enzymatic extracts were sonicated (ultrasound water-bath) for 10 min to prevent NPs aggregation before measurements. They were analyzed freshly prepared and analyzed by triplicate.

4.2.7.1 AF4 operating conditions

Parameters affecting AF4 separation, such as mobile phase composition and focusing and elution flows were optimized. Two mobile phases (NovaChem 0.05% (v/v) in ultrapure water and 5 mM Tris-HCl (pH 7.4) solution prepared in ultrapure water from 0.2 M Trizma®

solution), were tested. The elution profile of Ag NPs in the enzymatic extracts was analyzed using both carriers under several cross flows.

4.2.7.2 UV operating conditions

UV-vis detector was set at two different wavelengths (280 nm for proteins monitoring and 405 nm for Ag NPs).

4.2.7.3 ICP-MS operating conditions

ICP-MS detection after AF4 separation of Ag NPs was performed using hydrogen and oxygen as reaction gases in the collision/reaction cell (operating conditions are listed in Table 4.2). AF4-UV eluates were mixed with the IS (10 μg kg^{-1} Ge in 1% (v/v) nitric acid) via a polyether ether ketone tee-piece. Monitored ions for Ag were m/z 107 and 109, whereas m/z 72 was used for the IS (Ge).

Post-channel calibration was performed by replacing the post-channel diluting nitric acid/IS with calibration standards, containing increasing Ag concentrations (0, 20, 100, 200 and 500 μg kg^{-1}) and the same concentration of IS (10 μg kg^{-1} of Ge) [39, 40] prepared in 1 % (v/v) nitric acid. The same flow rates as during sample analysis were used. To calculate the Ag content in the samples, fractograms were normalized against IS signal and converted into mass flow fractograms using the calculated regression parameters obtained from the post-channel calibration curve and sample flow rates (measured daily). Total peak area present in the background-corrected fractograms was calculated using sum of trapezoid approximation accounting for the sample volume injected into AF4 and the dilution factor of injected sample.

4.2.8 SEM analysis

Enzymatic extracts were pre-treated to reduce the amount of organic matter prior to SEM analysis. 2 mL of 33% (v/v) hydrogen peroxide was added to 1 mL of the enzymatic extracts. Samples were subjected to microwave irradiation (330 W) for 2 min followed by a cooling stage (ice-bath) for 10 min (five cycles). Digests were finally made up to 2 mL with ultrapure water. This procedure has found to not affect Ag NPs stability [38].

SEM measurements (80 kV accelerating voltage) were performed using carbon-coated grid (dropping 10 µL of clean/treated enzymatic extract and air-drying at room temperature).

Table 4.2. ICP-MS operating conditions for AF4 coupling

ICP-MS operating conditions		
Radiofrequency power		1550 W
Gas flows	Nebulization	1.15 mL min^{-1}
	Auxiliary	0.9 L min^{-1}
	Plasma	15.0 L min^{-1}
	Collision (H_2)	4.0 mL min^{-1}
	Collision (O_2)	1.0 mL min^{-1}
Ion optics	Analogic phase voltage	2170 V
	Pulses voltage	1453 V
	Discriminant limit	3.7 mV
	Deflector voltage	6.0 V
Analyte (*m*/*z*)	Ag	107
	Ge (IS)	72

4.3 RESULTS AND DISCUSSION

4.3.1 Mobile phase composition and cross flow optimization

As previously indicated, mobile phase composition and focusing and elution flows must be optimized. For this purpose, aliquots from enzymatic extracts from samples coded as ABB and Z28 were analyzed at different conditions. AF4 elution program consists on a focusing step with tip and focus flows at 0.20 and 3.0 mL min^{-1}, respectively, during an injection time of 4.0 min. Elution step was performed at several cross flows (2.0, 3.0 and 3.5 mL min^{-1}) using two mobile phases (NovaChem 0.05% (v/v) and 5 mM Tris-HCl (pH 7.4) buffers). Cross flow was kept constant for 15 min, followed by a linear decrease for 7.5 min and a final washing step without cross flow for 9.4 min. Results regarding the use of NovaChem 0.05% (v/v) as a carrier have shown that there is improvement in separation by increasing the cross flow; however, there was not separation from the void peak, so quantification was not possible (Figure 4.1A). The use of 5 mM Tris-HCl (pH 7.4) led to Ag NPs separation from the void peak in all fractograms (Figure 4.1B), which allowed quantification. Recoveries (%) were calculated as a ratio

between Ag concentrations obtained from the fractogram and Ag concentrations found after enzymatic extract injection into the channel but without applying any cross flow. Ag recoveries were improved when increasing the cross flow from 2 to 3 mL min^{-1}, and the highest concentrations were obtained with a cross flow of 3 mL min^{-1} (Table 4.3). Based on these results, 5 mM Tris-HCl was selected as a mobile phase, and the applied cross flow was set at 3 mL min^{-1} (Table 4.4).

Finally, recoveries and Ag concentrations were calculated using both ^{107} Ag and ^{109}Ag isotopes. This helped conclude that there were not spectral interferences during measurements.

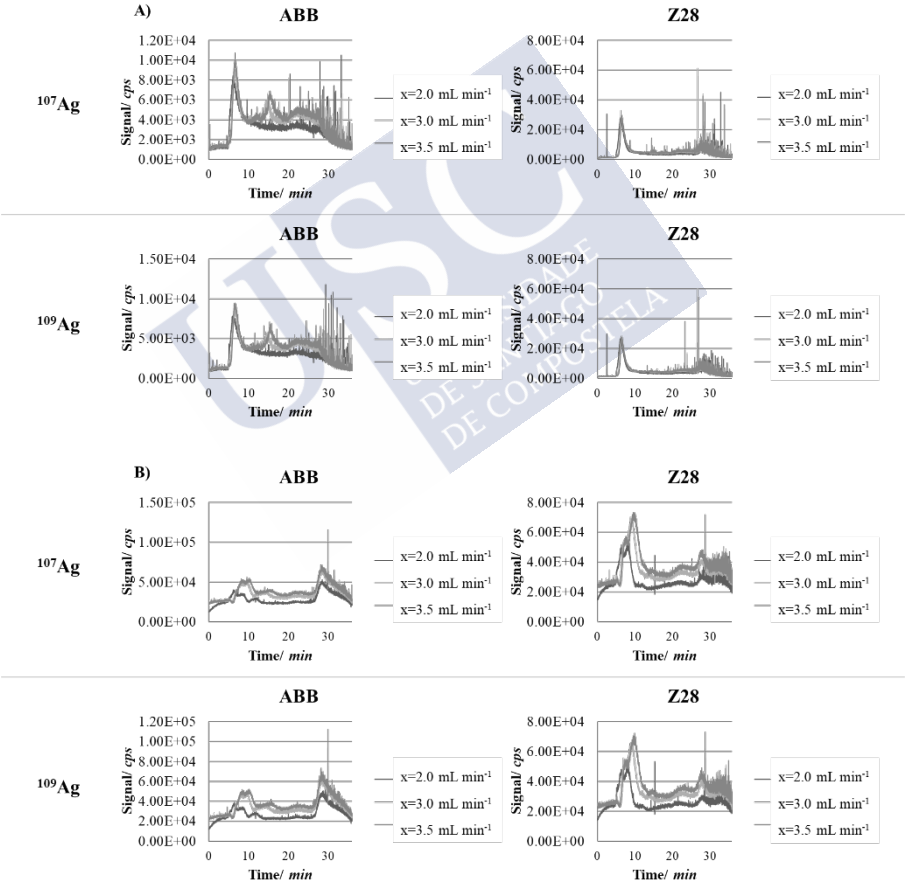

Figure 4.1. Fractograms of enzymatic extracts of samples ABB and Z28 at different values of cross flow with A) NovaChem 0.05% (v/v) and B) 5 mM Tris-HCl as carriers for the monitorization of ^{107}Ag and ^{109}Ag

Table 4.3. Ag concentration and recoveries for different cross flows with 5 mM Tris-HCl solution as carrier for ^{107}Ag and ^{109}Ag monitorization

	Recovery (%)						Concentration (µg Ag kg^{-1})					
Cross flow (mL min^{-1})	2.0		3.0		3.5		2.0		3.0		3.5	
Isotope	^{107}Ag	^{109}Ag	^{107}Ag	^{109}Ag	^{107}Ag	^{109}Ag	^{107}Ag	^{109}Ag	^{107}Ag	^{109}Ag	^{107}Ag	^{109}Ag
ABB	110	109	139	138	145	145	-	2.5×10^{1}	1.4×10^{2}	1.2×10^{2}	1.1×10^{2}	1.1×10^{2}
Z28	91	91	86	83	92	90	2.6×10^{2}	2.9×10^{2}	4.1×10^{2}	3.8×10^{2}	3.8×10^{2}	3.7×10^{2}

Table 4.4. AF4 optimized program

AF4 optimized program			
Step	Time (min)	Regime	Cross flow (mL min^{-1})
Focusing	4.0	Injection flow 0.2 mL min^{-1}	3.0
Elution	15	Constant	3.0
	7.5	Linear decay	3.0-0.0
	9.4	Constant	0.0

4.3.2 Application to Ag NPs quantification in molluscs

Calibration curve and sample flow rates for AF4-UV-ICP-MS were measured daily. Mean calculated regression parameters for ^{107}Ag and ^{109}Ag were y = 2.23x - 0.736 (R^2=0.999) and y = 2.21x - 0.759 (R^2=0.999), respectively. Results regarding Ag content in AF4 fractions (Table 4.5) have shown that the highest Ag concentration were found in the variegated scallop Z28 ($2.6\times10^2\pm2.5\times10^1$ µg Ag kg^{-1} and $2.2\times10^2\pm2.2\times10^1$ µg Ag kg^{-1} for ^{107}Ag and ^{109}Ag detection, respectively), followed by the Atlantic surf clam ABB ($8.9\times10^1\pm1.5\times10^1$ µg Ag kg^{-1} and $8.9\times10^1\pm1.4\times10^1$ µg Ag kg^{-1}, by monitoring ^{107}Ag and ^{109}Ag). Samples Z24 and OP were found to contain the lowest amounts of Ag. Membrane recoveries within 49 and 121% were found. The highest recovery was obtained for Z24 (fresh scallop) and the lowest was calculated for Z28 (frozen scallop). Low recovery values might be due to poor AF4 membrane recovery or due to dissolution of Ag NPs over the elution. Different elution profiles in each sample were related to different size distribution of Ag NPs. UV spectra showed a co-elution of Ag NPs (absorption at 405 nm) and proteins (280 nm absorbance) in all samples due to the huge interaction between them. AF4 fractograms and UV spectra for each sample are shown in Figures 4.2 to 4.5.

Table 4.5. Total Ag content, Ag concentration in AF4 fractions and channel recoveries in AF4 for four mollusc samples for a) ^{107}Ag and b) ^{109}Ag monitorization (mean±SD, n=3)

	Total Ag (µg kg^{-1})	Ag in AF4 fractions (µg kg^{-1})	Channel Recovery (%)
ABB	$1.6\times10^2\pm1.1\times10^1$ [a]	$8.9\times10^1\pm1.5\times10^1$ [a] $8.9\times10^1\pm1.4\times10^1$ [b]	94±11 [a] 94±9 [b]
OP	$9.9\times10^2\pm8.8\times10^1$ [a]	$4.1\times10^1\pm0.8\times10^1$ [a] $4.1\times10^1\pm0.9\times10^1$ [b]	54±1 [a] 55±2 [b]
Z24	$1.5\times10^2\pm1.0\times10^1$ [a]	$5.9\times10^1\pm0.5\times10^1$ [a] $5.5\times10^1\pm0.8\times10^1$ [b]	121±8 [a] 115±7 [b]
Z28	$3.7\times10^3\pm3.6\times10^2$ [a]	$2.3\times10^2\pm2.5\times10^1$ [a] $2.2\times10^2\pm2.2\times10^1$ [b]	49±1 [a] 49±1 [b]

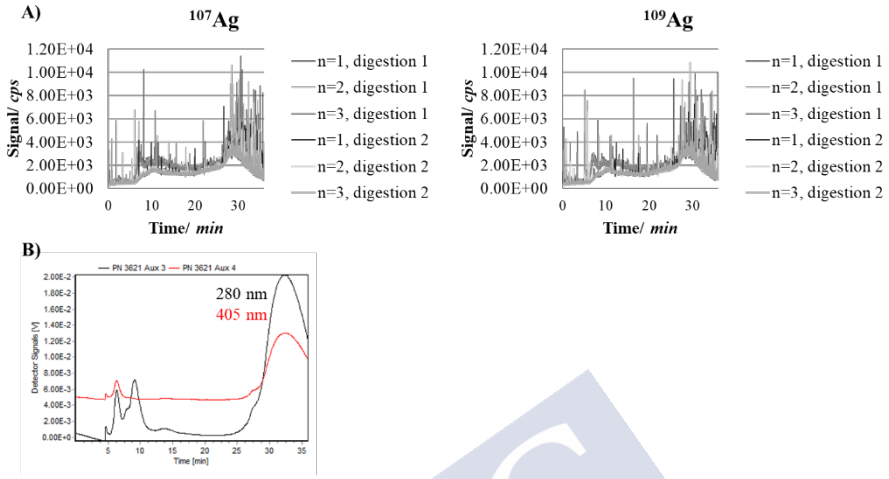

Figure 4.2. Fractogram of enzymatic extract of ABB as detected by A) ICP-MS and B) UV-vis (280 and 405 nm)

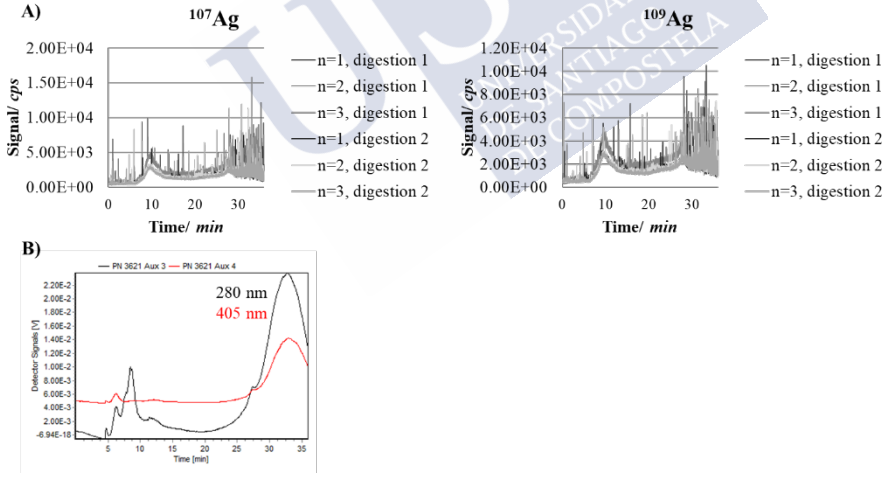

Figure 4.3. Fractogram of enzymatic extract of OP as detected by A) ICP-MS and B) UV-vis (280 and 405 nm)

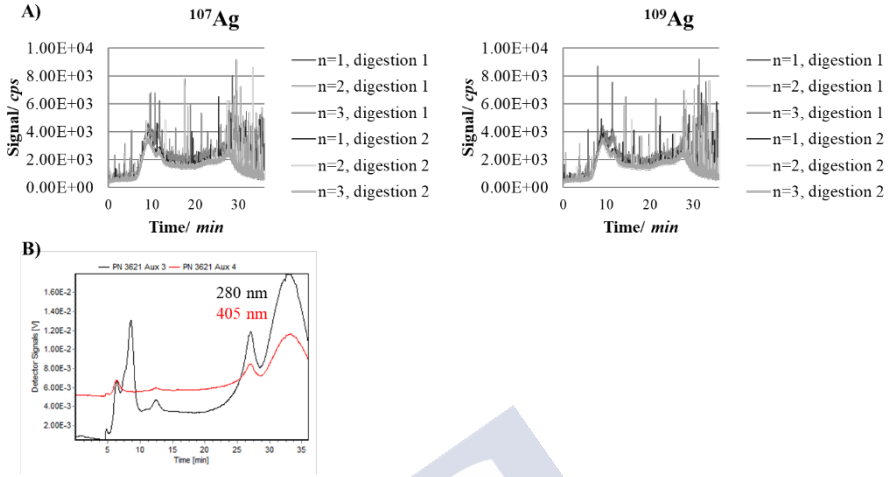

Figure 4.4. Fractogram of enzymatic extract of Z24 as detected by A) ICP-MS and B) UV-vis (280 and 405 nm)

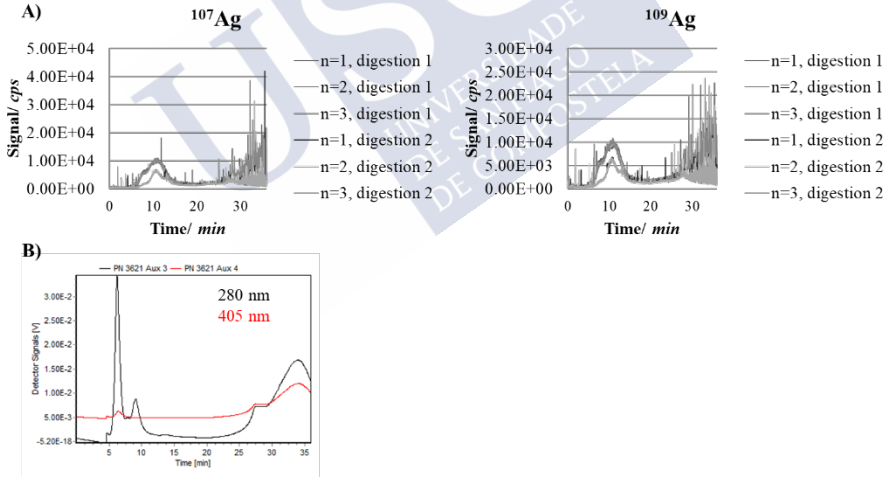

Figure 4.5. Fractogram of enzymatic extract of Z28 as detected by A) ICP-MS and B) UV-vis (280 and 405 nm)

SEM analysis of enzymatic extracts after a microwave oxidative digestion of the organic matter in the extracts confirms the presence of metallic NPs in the extracts (Figure 4.6).

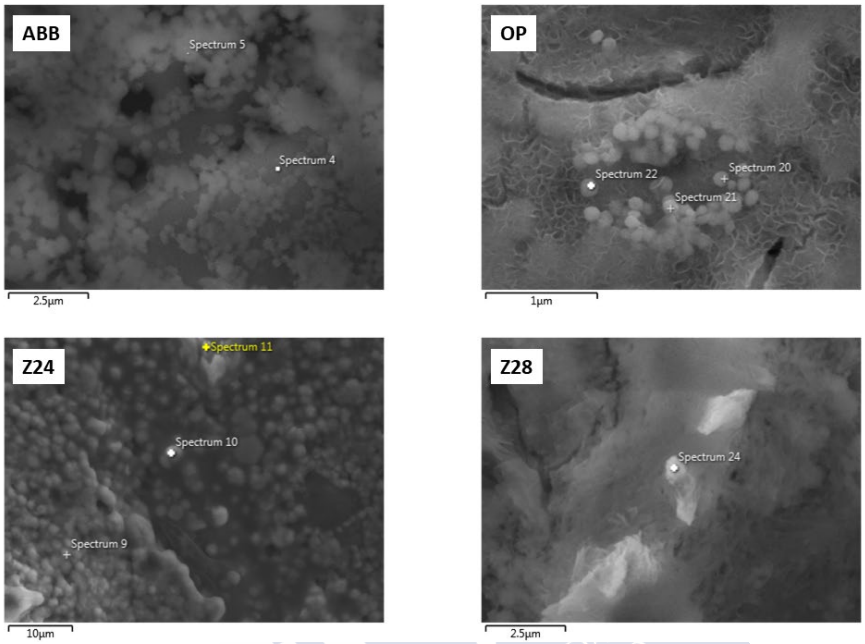

Figure 4.6. SEM images for enzymatic extracts from ABB, OP, Z24 and Z28 samples after a microwave oxidative digestion

Finally, total Ag concentrations in the four bivalve molluscs (microwave assisted acid digestion and ICP-MS) were found to vary from 1.6×10^2 to 3.7×10^3 µg kg^{-1} (Table 4.5). Percentages of Ag detected in AF4 fractograms relative to the total Ag content were 4% (OP), 6% (Z28), 39% (Z24) and 56% (ABB). This percentages are quite higher than those previously reported using ultrasound assisted enzymatic hydrolysis and sp-ICP-MS measurement for the same samples [38], probably due to the more moderate hydrolysis conditions.

4.4 CONCLUSIONS

In this study, an AF4-UV-ICP-MS method has been developed for the detection and quantification of Ag NPs in enzymatic extracts from bivalve molluscs. Total Ag concentrations were within the 1.6×10^{2}-3.7×10^{3} µg kg^{-1} range. AF4 parameters, such as mobile phase and focusing and elution flows, have been optimized for the best Ag NPs separation. Successful quantification of Ag NPs in the enzymatic extracts for four seafood samples (clams, oysters and variegated scallops) was achieved under these optimized conditions. Measured concentrations were within 4.1×10^{1} and 2.3×10^{2} µg Ag kg^{-1} range. Co-elution of Ag NPs and proteins was observed in UV-vis spectra for all samples due to the strong interaction between them. AF4-UV-ICP-MS fractograms suggest different size distribution of Ag NPs in each sample. Calculated membrane recoveries (%) were found to vary from 49 to 121%. Direct analysis of enzymatic extracts is possible with the developed Ag NPs extraction and AF4-UV-ICP-MS measurement, so this methodology could be useful for simple and fast silver speciation in complex matrices. The presence of Ag NPs in these enzymatic extracts has been also demonstrated by SEM analysis after an oxidative pre-treatment based on hydrogen peroxide and microwave irradiation.

Acknowledgements

The authors wish to acknowledge the financial support of the *Ministerio de Economía y Competitividad* (project INNOVANANO, reference RT2018-099222-B-100), the European Union (Interreg POCTEP, project ACUINANO, reference 07-12-ACUINANO_1_E), and the *Xunta de Galicia* (*Grupo de Referencia Competitiva*, grant number ED431C2018/19; and Program for Development of a Strategic Grouping in Materials – AEMAT, grant number ED431E2018/08). The authors are also grateful to Dr. Enrique Carbo and Dr. Laura Rodríguez-Lorenzo from the International Iberian Nanotechnology Laboratory (Braga, Portugal) for TEM assistance. M.V. Taboada-López would like to thank the *Xunta de Galicia* and the European Social Fund (FSE) for a pre-doctoral grant.

4.5 REFERENCES

[1] Scopus. http://www.scopus.com (accessed on July 10th 2019).
[2] The European Commission. Commission, Recommendation (EU) 2011/696 of 18 October 2011 on the definition of nanomaterial, Official Journal of the European Union L 275, 58 (2011) 38–40.
[3] Consumer Products Inventory. An inventory of nanotechnology-based consumer products introduced on the market, http://www.nanotechproject.org/cpi (accessed on July 10th 2019).
[4] Danish Ministry of the Environment, Environmental Protection Agency (EPA). Nanomaterials in waste; Issues and new knowledge. Environmental Project No. 1608 (2014).
[5] C.S. Shivananda, B.L.R. Sangappa, Structural, thermal and electrical properties of silk fibroin-silver nanoparticles composite films, J. Mater. Sci.: Mater. Electron. 30 (2019) 1–11.
[6] R. Premkumar, S. Hussain, T. Mathavan, K. Anitha, A.M.F. Benial, Surface-enhanced Raman scattering and quantum chemical studies of 2-trifluoroacetylpyrrole chemisorbed on colloidal silver and gold nanoparticles: A comparative study, J. Mol. Liq. 290 (2019) 111209–11221.
[7] S.H. Lee, B.H. Jun, Silver Nanoparticles: Synthesis and Application for Nanomedicine, Int. J. Mol. Sci. 20 (2019) 865–889.
[8] M.F.A. Messih, M.A. Ahmed, A. Soltan, S.S. Anis, Synthesis and characterization of novel Ag/ZnO nanoparticles for photocatalytic degradation of methylene blue under UV and solar irradiation, J. Phys. Chem. Solids 135 (2019) 109086–109099.
[9] S. Hamed, M. Emara, R.M. Shawky, R.A. El-domany, T. Youssef, Silver nanoparticles: Antimicrobial activity, cytotoxicity and synergism with N-acetyl cysteine, J. Basic Microb. 57 (2017) 659–668.
[10] S. Küünal, S. Kutti, P. Rauwel, M. Guha, D. Wragg, E. Rauwel, Biocidal properties study of silver nanoparticles used for applications in green housing, Int. Nano. Lett. 6 (2016) 191–197.
[11] J. Chumpol, S. Siri, Simple green production of silver nanoparticles facilitated by bacterial genomic DNA and their antibacterial activity, Artif. Cell. Nanomed. B. 46 (2018) 619–625.

[12] G.A. Kahrilas, W. Haggren, R.L. Read, L.M. Wally, S.J. Fredrick, M. Hiskey, A.L. Prieto, J.E. Owens, Investigation of Antibacterial Activity by Silver Nanoparticles Prepared by Microwave-Assisted Green Synthesis with Soluble Starch, Dextrose and Arabinose, ACS Sustain. Chem. Eng. 2 (2014) 590–598.
[13] Y. Ren, H. Yang, T. Wang, C. Wang, Bio-synthesis of silver nanoparticles with antibacterial activity, Mater. Chem. Phys. 235 (2019) 121746–121753.
[14] W. Zhang, G. Hu, W. Zhang, Y. Zhang, J. He, Y. Yuan, L. Zhang, J. Fei, A facile strategy for the synthesis of silver nanostructures with different morphologies, Mater. Chem. Phys. 235 (2019) 121629–121638.
[15] F. Zia, N. Ghafoor, M. Iqbal, S. Mehboob, Green synthesis and characterization of silver nanoparticles using *Cydonia oblong* seed extract, Appl. Nanosci. 6 (2016) 1023–1029.
[16] E. Rezvani, A. Rafferty, C. McGuiness, J. Kennedy, Adverse effects of nanosilver on human health and the environment, Acta Biomater. 94 (2019) 145–159.
[17] A. Wimmer, A.A. Markus, M. Schuster, Silver Nanoparticle Levels in River Water: Real Environmental Measurements and Modeling Approaches-A comparative study, Environ. Sci. Technol. 6 (2019) 353–358.
[18] L. Torrent, F. Laborda, E. Marguí, M. Hidalgo, M. Iglesias, Combination of cloud point extraction with single particle inductively coupled plasma mass spectrometry to characterize silver nanoparticles in soil leachates, Anal. Bioanal. Chem. 41 (2019) 5317–5329.
[19] H. Wang, K.T. Ho, K.G. Scheckel, F. Wu, M.G. Cantwell, D.R. Katz, D.B. Horowitz, W.S. Boothman, R.M. Burgess, Toxicity, Bioaccumulation and Biotransformation of Silver Nanoparticles in Marine Organisms, Environ. Sci. Technol. 48 (2014) 13711–13717.
[20] C. Gambardella, E. Costa, V. Piazza, A. Fabbrocini, E. Magi, M. Faimali, F. Garaventa, Effect of silver nanoparticles on marine organisms belonging to different trophic levels, Mar. Environ. Res. 11 (2015) 41–49.
[21] M. Sendra, M.P. Yeste, J.M. Gatica, I. Moreno-Garrido, J. Blasco, Direct and indirect effects of silver nanoparticles on freshwater and marine microalgae (*Chlamydomonas reinhardtii* and *Phaedactylum tricornutum*), Chemosphere 179 (2017) 279–289.

[22] A. Tsiola, P. Pitta, A.J. Callol, M. Kagiorgi, I. Kalantzi, K. Mylona, I. Santi, C. Toncelli, S. Pergantis, M. Tsapakis, The impact of silver nanoparticles on marine plankton dynamics: Dependence on coating, size and concentration, Sci. Total Environ. 601-602 (2017) 1838–1848.
[23] J. Huang, J. Cheng, J. Yi, Impact of silver nanoparticles on marine diatom *Skeletonema coastatum*, J. Appl. Toxicol. 36 (2016) 1343–1354.
[24] J. García-Alonso, N. Rodríguez-Sanchez, S.K. Misra, E. Valsami-Jones, M.N. Croteau, S.N. Luoma, P.S. Rainbow, Toxicity and accumulation of silver nanoparticles during development of the marine polychaete *Platynereis dumerilii*, Sci. Total Environ. 476-477 (2014) 688–695.
[25] M. Vannuci-Silva, S. Kohler, G.de A. Umbuzeiro, A.T. Ford, Behavioural effects on marine amphipods exposed to silver ions and silver nanoparticles, Environ. Pollut. 252 (2019) 1051–1058.
[26] A. Ale, G. Liberatori, M.L. Vannuccini, E. Bergami, S. Ancora, G. Mariotti, N. Bianchi, J.M. Galdopórpora, M.F. Desimone, J. Cazenave, I. Corsi, Exposure to a nanosilver-enabled consumer product results in similar accumulation and toxicity of silver nanoparticles in the marine mussel *Mytilus galloprovincialis*, Aquat. Toxicol. 211 (2019) 46–56.
[27] P.E. Buffet, A. Zalouk-Vergnoux, A. Châtel, B. Berthet, I. Métais, H. Perrein-Ettajni, L. Poirier, A. Luna-Acosta, H. Thomas-Guyon, E. Valsami-Jones, C. Mouneyrac, A marine mesocosm study on the environmental fate of silver nanoparticles and toxicity effects on two endobenthic species: The ragworm *Hediste diversicolor* and the bivalve mollusc *Scrobicularia plana*, Sci. Total Environ. 470-471 (2014) 1151–1159.
[28] C. Mouneyrac, P.E. Buffet, L. Poirier, A. Zalouk-Vergnoux, M. Guibbolini, C. Risso-de Faverney, D. Gilliland, D. Berhanu, A. Dybowska, A. Châtel, H. Perrein-Ettajni, J.F. Pan, H. Thomas-Guyon, P. Reip, E. Valsami-Jones, Fate and effects of metal-based nanoparticles in two marine invertebrates, the bivalve mollusc *Scrobicularia plana* and the annelid polychaete *Hediste diversicolor*, Environ. Sci. Pollut. Res. 21 (2014) 7889–7912.
[29] H. Li, A. Turner, M.T. Brown, Accumulation of Aqueous and Nanoparticulate Silver by the Marine Gastropod *Littorina littorea*, Water Air Soil Pollut. 224 (2013) 1354–1363.

[30] H. Rauscher, A. Mech, N. Gibson, D. Gilliland, A. Held, V. Kestens, R. Koeber, T.P.J. Linsinger, E.A. Stefaniak, Identification of Nanomaterials through Measurements, JRC Science for Policy Report JRC118158 (2019).
[31] F. Laborda, E. Bolea, G. Cepriá, M.T. Gómez, M.S. Jiménez, J. Pérez-Arantegui, J.R. Castillo, Detection, characterization and quantification of inorganic engineered nanomaterials: A review of techniques and methodological approaches for the analysis of complex samples, Anal. Chim. Acta 904 (2016) 10–32.
[32] J. Gigault, J.M. Pettibone, C. Schmitt, V.A. Hackley, Rational strategy for characterization of nanoscale particles by asymmetric-flow field flow fractionation: A tutorial, Anal. Chim. Acta 809 (2014) 9–24.
[33] K. Ramos, L. Ramos, C. Cámara, M.M. Gómez-Gómez, Characterization and quantification of silver nanoparticles in nutraceuticals and beverages by asymmetric flow field flow fractionation coupled with inductively coupled plasma mass spectrometry, J. Chromatogr. A 1371 (2014) 227–236.
[34] G.F. Koopmans, T. Hiemstra, I.C. Regelink, B. Molleman, R.N.J. Comans, Asymmetric flow field-flow fractionation of manufactured silver nanoparticles spiked into soil solution, J. Chromatogr. A 1392 (2015) 100–109.
[35] D.M. Mitrano, A. Barber, A. Bednar, P. Westerhoff, C.P. Higgins, J.F. Ramville, Silver nanoparticle characterization using single particle ICP-MS (SP-ICP-MS) and asymmetrical flow field flow fractionation ICP-MS (AF4-ICP-MS), J. Anal. At. Spectrom. 27 (2012) 1131–1143.
[36] B. Meermann, A.L. Fabricius, L. Duester, F. Vanhaecke, T. Ternes, Fraction-related quantification of silver nanoparticles *via* on-line species-unspecific post-channel isotope dilution in combination with asymmetric flow-field flow fractionation (AF4)/sector field ICP-mass spectrometry (ICP-SF-MS), J. Anal. At. Spectrom. 29 (2014) 287–297.
[37] U. Araujo-Barbosa, E. Peña-Vazquez, M.C. Barciela-Alonso, S.L. Costa-Ferreira, A.M. Pinto-dos-Santos, P. Bermejo-Barrera, Simultaneous determination and speciation analysis of arsenic and chromium in iron supplements used for iron-deficiency anemia treatment by HPLC-ICP-MS, Talanta 170 (2017) 523–529.

[38] M.V. Taboada-López, N. Alonso-Seijo, P. Herbello-Hermelo, P. Bermejo-Barreara, A. Moreda-Piñeiro, Determination and characterization of silver nanoparticles in bivalve molluscs by ultrasound assisted enzymatic hydrolysis and sp-ICP-MS, Microchem. J. 148 (2019) 652–660.
[39] V. Nischwitz, A. Berthele, B. Michalke, Speciation analysis of selected metals and determination of their total contents in paired serum and cerebrospinal fluid samples: An approach to investigate the permeability of the human blood-cerebrospinal fluid-barrier, Anal. Chim. Acta 627 (2008) 258–269.
[40] J. Heroult, V. Nischwitz, D. Bartczak, H. Goenaga-Infante, The potential of asymmetric flow field-flow fractionation hyphenated to multiple detectors for the quantification and size estimation of silica nanoparticles in a food matrix, Anal. Bioanal. Chem. 406 (2014) 3919–3927.

USC
UNIVERSIDADE
DE SANTIAGO
DE COMPOSTELA

USC
UNIVERSIDADE
DE SANTIAGO
DE COMPOSTELA

PART III. EVALUATION OF POTENTIAL RISK OF TiO_2 NPS AND Ag NPS IN HUMANS THROUGH THE INGESTION OF FOOD PRODUCTS CONTAINING NPS

USC
UNIVERSIDADE
DE SANTIAGO
DE COMPOSTELA

CHAPTER 5

BIOPERSISTENCE RATE OF METALLIC NANOPARTICLES IN THE GASTROINTESTINAL HUMAN TRACT (STAGE 0 OF THE EFSA GUIDANCE FOR NANOMATERIALS RISK ASSESSMENT)

MARÍA VANESA TABOADA-LÓPEZ, GEMMA VÁZQUEZ-EXPÓSITO, RAQUEL DOMÍNGUEZ-GONZÁLEZ, PALOMA HERBELLO-HERMELO, PILAR BERMEJO-BARRERA AND ANTONIO MOREDA-PIÑEIRO

USC
UNIVERSIDADE
DE SANTIAGO
DE COMPOSTELA

5 BIOPERSISTENCE RATE OF METALLIC NANOPARTICLES IN THE GASTROINTESTINAL HUMAN TRACT (STAGE 0 OF THE EFSA GUIDANCE FOR NANOMATERIALS RISK ASSESSMENT)

María Vanesa Taboada-López, Gemma Vázquez-Expósito, Raquel Domínguez-González, Paloma Herbello-Hermelo, Pilar Bermejo-Barrera, Antonio Moreda-Piñeiro

Trace Element, Spectroscopy and Speciation Group (GETEE), Strategic Grouping in Materials (AEMAT), Department of Analytical Chemistry, Nutrition and Bromatology. Faculty of Chemistry. Universidade de Santiago de Compostela. Avenida das Ciencias, s/n. 15782 – Santiago de Compostela, Spain.

Abstract

The European Food Safety Authority (EFSA) has recently published a guidance regarding risk assessment of nanomaterials in the food and feed chain (human and animal health). Following these recommendations, an *in vitro* gastrointestinal digestion approach has been developed to study the biopersistence rate of titanium dioxide and silver nanoparticles (TiO_2 NPs and Ag NPs) in standards and in foodstuff (molluscs and crab sticks). For the standards, two nominal sizes and three different concentration levels were studied for each type of NP. In addition, food additive E171 (food coloring containing micro- and nano-titanium) was also evaluated. Particle size distribution (PSD) and NPs concentration were assessed at three times (30, 60 and 120 min) during the gastric and the intestinal stages. Inductively coupled plasma-mass spectrometry operating in single particle mode (sp-ICP-MS) was used for assessing NPs concentration and PSD. TiO_2 NPs standards and TiO_2 NPs/TiO_2

microparticles from E171 were not found to be degraded under simulated gastrointestinal conditions. Ag NPs proved to be more degradable than TiO_2 NPs, but the biopersistence rates calculated for Ag NPs were higher than 12% (the limit set by the EFSA), which means that Ag NPs are also biopersistent. Findings for molluscs and crab sticks are quite similar to those obtained for TiO_2 NPs and Ag NPs standards, although the calculation of the biopersistence rate proposed by the EFSA was not found to be straightforward for foodstuff, and a modification consisting of using the NPs concentration in the sample instead of the NPs concentrations at T0 (sample mixed with the gastric solution before enzymatic hydrolysis) has been proposed.

Keywords
Titanium dioxide nanoparticles, silver nanoparticles, seafood, crab sticks, *in vitro* gastrointestinal digestion, EFSA guidance

5.1 INTRODUCTION

A nanomaterial (NM) is defined by the European Commission (EC) as a natural, incidental or manufactured material which contains at least 50% of particles with one or more dimensions between 1 and 100 nm [1]. The novel mechanical, thermal, optical and antimicrobial properties of NMs make them valuable ingredients in food science as additives for improving food appearance and lengthening shelf-life [2]. There are 119 listed NMs used in the food and beverage industry [3]. Inorganic nanoparticles (NPs), and more specifically metal and metal-oxide NPs, are widely used as food additives and as active ingredients in films for food packaging due to their excellent mechanical and antimicrobial properties [2]. However, the impacts that engineered NMs have on environmental and human health are unclear, and research for elucidating these impacts is a current challenge [4].

Titanium dioxide (TiO_2) as a bulk material is the authorized food additive E171, which is used as a pigment for its resistance to discoloration, high refractive index and brightness [5]. Candies, sweets, chewing gums, cheese and cheese products, edible ices, crab sticks (surimi), dressings and non-dairy creamers are some of the food products that contain E171 [6].

Several studies on food-grade E171 have reported the presence of TiO_2 NPs in a number-based fraction of 17-36% [7].
The antimicrobial activity exhibited by TiO_2 NPs and silver (Ag) NPs has led to their use as active ingredients in food packaging [8-11]. TiO_2 NPs show a strong oxidizing power when illuminated with ultraviolet (UV) light (385 nm), which enhances the production of reactive oxygen species (ROS) and promotes the breakdown of bacteria membranes [12, 13]. Similarly, the antibacterial mechanism of Ag NPs is related to the formation of ROS [14], and there are some insights regarding Ag NPs transcellular transport and endocytosis after crossing the cytoplasmic membrane and oxidizing into Ag^+ ions [15, 16]. Nevertheless, the antibacterial activity of TiO_2 NPs has been demonstrated to depend on the food composition (mainly total phenolics and protein content), as well as turbidity and oxygen, that cause a decrease of the microbicidal activity of TiO_2 NPs [17].
There is great concern regarding the migration of NPs from packaging to food products or their direct use as additives because of their consequent release inside the human gastrointestinal tract. The interaction between NPs and food matrix can affect the physicochemical and morphological properties of NPs, as well as their biotransformation, gastrointestinal fate and bioactivity. Food constituents (water, proteins, carbohydrates, lipids and minerals), molecular interactions and structural organization are some of the most important food properties that have a potential impact on NPs behavior [18]. Physicochemical properties of NPs can also be modified during food ingestion, digestion and fermentation. The presence of enzymes, ionic strength and pH changes are important factors that can modify the bioavailability of assessed NPs by *in vitro* protocols [19]. Intestinal cells and gut microbiota have been widely used to evaluate NPs toxicity. The assessment of cell number, enzymatic activity, deoxyribonucleic acid (DNA) and protein contents are typically used in these cytotoxicity studies [20].
Due to the growing presence of nanoscience/nanotechnology products in the food industry, the European Food Safety Authority (EFSA) published a guidance in 2018 to evaluate the risks of the application of nanoscience and nanotechnologies in the food and feed chain [21]. Regarding manufactured materials, the guidance establishes a first

physicochemical characterization to determine whether or not the materials meet the EC definition of NM. Particle size, particle size distribution (PSD) and volume specific surface area (VSSA) must be considered in this preliminary study, and size of NPs must be measured by two independent methods including one electron microscopy technique. Indicators of potential toxicity, such as antimicrobial activity, specific morphology, persistence/high stability and bioaccumulation, should be also considered. If the material meets the established specification of NM, further studies must be performed. Stage 0 of the EFSA guidance consists of investigating the degradation rate of NMs to non-nanomaterial under representative gastrointestinal conditions. If a high degradation rate is found, a further nano-specific risk assessment procedure is not necessary. Studies must be done at three different concentration levels and at several gastrointestinal times. The guidance recommends at least two replicates per sample and gastrointestinal time. Particle number concentrations, PSD and dissolved metal concentration must be assessed. The EFSA guidance defines NMs as highly degradable if 12% or less of the material (in mass fraction) remains as NPs after completing 30 min of the simulated intestinal digestion. Physical forces, temperature, pH, enzymes, salts and bile concentration are expected to have a considerable effect on NM degradation and dissolution [21].

Particle number concentration, PSD and dissolved content can be assessed by using single particle-inductively coupled plasma-mass spectrometry (sp-ICP-MS), which is the only currently available technique for simultaneous characterization and quantification of NPs with limits of detection (LOD) below 10 μg L^{-1} [22]. Metal and metal oxide NPs reach ICP-MS plasma as clouds of metal ions which are detected as pulses at a corresponding mass-to-charge ratio (*m/z*) in the mass spectrometer. Concentration of NPs in the sample is related to the frequency of detected signal pulses. The metal mass detected in each pulse can be used to estimate particle size by assuming spherical shape and density values [23, 24].

The aim of the current work has focused on the study of the potential biopersistence of TiO_2 NPs and Ag NPs after an *in vitro* gastrointestinal human digestion following EFSA recommendations. The biopersistence

of TiO_2 NPs and Ag NPs standards of two different sizes at three concentration levels and the food additive E171 was compared with TiO_2 NPs and Ag NPs biopersistence in foodstuff such as seafood (molluscs) and crab sticks. Changes between gastric and intestinal stages were analyzed taking into account NPs concentration, NPs size and the metal dissolved content after sp-ICP-MS analysis.

5.2 MATERIALS AND METHODS

5.2.1 Instrumentation

A NexION 300X ICP-MS system was used for TiO_2 NPs and Ag NPs characterization and quantification with the Syngistix™ Nano Application software (Perkin Elmer, Massachusetts, USA). JEM-1010 transmission electron microscope (TEM) from JEOL (Tokyo, Japan) was used for comparative purposes (TEM images). *In vitro* digestion was performed in a Boxcult temperature-controlled incubation chamber (Stuart Scientific, Surrey, UK) equipped with a Rotabit orbital-rocking platform shaker (J.P. Selecta, Barcelona, Spain). Other pieces of equipment were a pH-meter model pH 50+DHS (XS Instruments, Carpi, Italy), a Raypa UCI–150 ultrasonic cleaner water-bath (ultrasound frequencies of 17 and 35 kHz, power of 325 W) from R. Espinar S.L. (Barcelona, Spain), a Laborcentrifugen 2K15 centrifuge (Sigma, Osterode, Germany), a heating bath from J.P. Selecta and a domestic Taurus blade grinder (Barcelona, Spain). Minisart® Syringe Filters (5µm cellulose acetate filters) from Sartorius (Göttingen, Germany), plastic syringes from Dispomed (Gelnhausen, Germany) and spin filters (Amicon® Ultra 0.5 mL centrifugal filters of 30K) from Merck (Darmstadt, Germany) were used to prepare samples prior to TEM analysis.

5.2.2 Reagents

Ultrapure water was from a Milli-Q purification device (Millipore Co., Massachusetts, USA). TiO_2 NPs stock solutions were prepared from TiO_2 nanopowder (99.9% rutile) of 50 and 100 nm from US Research Nanomaterials (Texas, USA). E171 (titanium dioxide) was from Minerals-

Water (Rainham, UK). Ag NPs solutions of 40 and 60 nm with sodium citrate as stabilizer were from Sigma Aldrich (Missouri, USA). NIST8013 Au NPs (60 nm) certified reference material was from NIST (Maryland, USA). Ionic titanium ($(NH_4)_2TiF_6$ 1000 mg L^{-1}) and ionic silver ($AgNO_3$ 1000 mg L^{-1}) stock standard solutions were from Merck. NexION Setup Solution (10 µg L^{-1} Be, Ce, Fe, In, Li, Mg, Pb and U in 1% nitric acid) was from Perkin Elmer. Pepsin from porcine gastric mucosa, pancreatine from porcine pancreas and bile salts were from Sigma Aldrich. Hydrochloric acid 37%, nitric acid 65% and sodium hydrogen carbonate were from Panreac (Barcelona, Spain); 99.5% glycerol was from Merck.

To avoid metal contamination, glassware and plasticware were washed with ultrapure water, kept in 10% (v/v) nitric acid for 48 h and fully rinsed with ultrapure water before use.

5.2.3 Bivalve mollusc and crab stick samples

Biopersistence rate of TiO_2 NPs was studied in mussels (*Mytilus galloprovincialis*), sample denoted as M; and fresh variegated scallops (*Chlamys varia*), denoted as Z24. Ag NPs biopersistence studies were performed with oysters (*Ostrea edulis*), coded as OP; and frozen variegated scallops (coded as Z28). Approximately 1 kg of byssus and shell were removed from each specimen. Soft tissues were washed with ultrapure water and homogenized by mechanical blending.

Surimi (crab stick) samples consisted of a fresh (FH6) and a frozen product (FZ12) which were also homogenized by mechanical blending (approximately 100 g of each sample).

The total Ti and Ag contents, as well as TiO_2 NPs and Ag NPs concentrations in seafood and surimi samples, were previously quantified by ICP-MS and sp-ICP-MS, respectively [25-27].

5.2.4 *In vitro* gastrointestinal digestion procedure

The applied simulated *in vitro* digestion was based on the protocol described by Domínguez-González et al. [28]. Regarding standards and E171 food additive, several volumes of TiO_2 NPs (50 and 100 nm) standards, Ag NPs (40 and 60 nm) standards and food additive E171

suspensions were added into Erlenmeyer flasks, and ultrapure water was then added up to 50 mL (tested concentrations listed in Table 5.1). When working with foodstuff, a mass of 5.0 g (wet weight) of molluscs/crab sticks were directly mixed with 50 mL of ultrapure water. For all cases, the pH was adjusted to 2.0 by adding 0.6 M HCl dropwise. Gastric solution (0.16 g mL^{-1} pepsin in 0.1 M HCl) was added to provide a concentration of 7.5 mg of gastric solution per mL. Samples were digested at 37 ºC in an incubation chamber under orbital-horizontal shaking (150 rpm) for 2 h, and the gastric digestion was then stopped by placing the flasks in an ice-bath. The pH of the mixture was then adjusted to 7.0 with 0.2 M NaOH. 5.0 mL of intestinal solution (4 g pancreatin and 25 g bile salts in 1 L of 0.1 M $NaHCO_3$) were added and samples were incubated for 2 h under the same conditions mentioned above.

Table 5.1. TiO_2 and Ag concentrations used in the *in vitro* digestion assays

	STD 50 nm (g TiO_2 L^{-1})	*STD 100 nm (g TiO_2 L^{-1})*	*E171 (g TiO_2 L^{-1})*	*STD 40 nm (g Ag L^{-1})*	*STD 60 nm (g Ag L^{-1})*
Level 1	6.00×10^{-6}	6.00×10^{-5}		5.40×10^{-6}	1.20×10^{-5}
Level 2	6.00×10^{-5}	6.00×10^{-4}	1.33×10^{-3}	7.40×10^{-6}	1.60×10^{-5}
Level 3	6.00×10^{-4}	6.00×10^{-3}		9.40×10^{-6}	2.00×10^{-5}

STD: standard

Four replicates per sample and two blanks were performed for each *in vitro* digestion set. An extra replicate and an extra blank were also prepared to measure NPs concentrations and PSD after pH 2.0 adjustment and gastric solution addition (experiment coded as T0). Aliquots of 5.0 mL were taken at 30, 60 and 120 min of the gastric (G30, G60 and G120) and intestinal (I30, I60 and I120) stages. Enzymatic digests from NPs standards and E171 were directly stored at -20ºC, whereas enzymatic fractions from seafood and crab sticks were first subjected to centrifugation (3900 rpm, 8 ºC, 10 min) and the supernatants were kept until the analysis (-20 ºC storage). Before sp-ICP-MS analysis, thawed enzymatic digests were heated at 90 ºC for 5 min to inactivate the residual enzymes (pepsin and pancreatin) in the enzymatic fractions.

5.2.5 sp-ICPMS measurements

Instrumental ICP-MS conditions (Table 5.2) were daily adjusted using a solution prepared from the NexION Setup Solution and Ti or Ag standards (10 μg L^{-1} of Ti or Ag and 1.0 μg L^{-1} of Be, Ce, Fe, In, Li, Mg, Pb and U). Sample flow rate (0.41-0.45 mL min^{-1}) was assessed by pumping ultrapure water for 1 min at 4 rpm pumping speed and calculating the flow rate by means of the difference of weights before and after ICP-MS aspiration. Transport efficiency (TE%) values within the 1-5% range were directly assessed by Syngistix™ Nano Application software using a gold NPs suspension (60 nm and 518 ng L^{-1}).

Table 5.2. sp-ICP-MS operating conditions for TiO_2 NPs and Ag NPs determination

Operating parameters regarding single particle measurements		
Analyte	Ti	Ag
Mass	48.9479 uma	106.905 uma
Density	4.23 g cm^{-3}	10.49 g cm^{-3}
Mass Fraction	59.9 %	100 %
Ionization efficiency	100 %	100 %
Sample Flow Rate	0.41-0.45 mL min^{-1}	0.41-0.45 mL min^{-1}
Dwell time	100 μs	50 μs
Sampling time	100 s	100 s
Mode	Standard	Standard
Operating conditions of ICP-MS		
Nebulization gas flow: 0.95 mL min^{-1}; Auxiliary gas flow:1.2 mL min^{-1}; Plasma gas flow: 16 mL min^{-1}; Radiofrequency power: 1600 W		

Aqueous calibrations of ionic Ti and Ag were prepared ranging from 0 to 10 μg L^{-1}. Syngistix™ Nano Application software was capable of directly calculating NPs concentration, PSD and dissolved concentration using the TE% value, the ionic (dissolved) aqueous calibration fit, the sample flow rate and NPs density and mass fraction [29]. Enzymatic digests were diluted with 1.0 % (v/v) glycerol and sonicated (water-bath, 37 kHz) for 10 min before analysis.

LOD and limit of quantification (LOQ) were calculated based on three and ten times the standard deviation of eleven measurements of a blank, respectively, and the slope of the calibration curve. Calculated values of LOD and LOQ for TiO_2 NPs concentration were 1.27×10^4 and 4.24×10^4 NPs mL^{-1}, respectively. In the case of Ag NPs, LOD was

1.89×10^3 NPs mL^{-1} and LOQ was 9.22×10^3 NPs mL^{-1}. LOD values for dissolved (ionic) Ti and Ag were 0.295 µg Ti L^{-1} and 0.678 ng Ag L^{-1}; whereas the LOQs were 0.982 µg Ti L^{-1} and 2.26 ng Ag L^{-1}. Finally, LOD in size, based on the 3σ and 5σ criteria [30], were 29.1 nm for TiO_2 NPs and 10.1 nm for Ag NPs (3σ), or 34.5 nm for TiO_2 NPs and 12.0 nm for Ag NPs (5σ).

5.2.6 TEM analysis of gastric and intestinal fractions

Gastric (0.5 mL of diluted sample 1:20 with ultrapure water) and intestinal fractions (0.5 mL), previously filtered through 5 µm cellulose filters, were ultracentrifuged using 30K Nominal Molecular Weight Limit (NMWL) regenerated cellulose centrifugal filters. Centrifugation was performed at 14000 g during 20 min at 10 ºC. For the gastric fractions, filtrate was discarded and the filter was washed 9 times with sample dilution (0.5 mL) by centrifugation 14000 g for 20 min at 10 ºC, followed by one more centrifugation for 10 min. For the intestinal fractions, filtrate was discarded and the filter was washed 19 times with ultrapure water (0.5 mL) under centrifugation (14000 g for 20 min at 10 ºC), followed by another centrifugation for 10 min. Finally, the concentrated solute in the filter was recovered by placing the filter upside down in a clean microcentrifuge tube and centrifuging at 1000 g for 2 min at 10 ºC. 10 µL of the clean enzymatic extracts were dropped onto a copper grid, wicking on filter paper and air-drying at room temperature.

5.2.7 Statistical Analysis

Statgraphics Centurion 18 v18.1.12 (Manugistics Inc., Maryland, USA) software was used for statistical analysis. The Cochran test was performed (at 95% confidence level) for standard deviation comparison for NPs concentrations and mean sizes (p-values lower than 0.05 imply a statistically significant difference amongst standard deviations and if p-values are higher than 0.05, standard deviation are not significantly different). In both scenarios, a Multiple Range Test was

applied for mean values comparison (detection of homogeneous groups with comparable values of concentrations or sizes).

5.3 RESULTS AND DISCUSSION

5.3.1 TiO_2 NPs biopersistence rate in standards

As shown in Figures 5.1 and 5.2, no TiO_2 NPs concentration changes were found during the simulated gastric stage ($p<0.05$). TiO_2 NPs concentrations at 30, 60 and 120 min (G30, G60 and G120 solutions) remain constant and similar to the TiO_2 NPs concentration found at zero time (T0). However, gastric digests from the lowest TiO_2 NPs concentration standards (level 1 for both 50 and 100 nm, Tables S5.1 and S5.2) showed small differences amongst TiO_2 NPs concentrations at zero time (T0) and after carrying out the simulated gastric digestion at the selected times. These findings could be attributed to the low concentration of these standards (6.00×10^{-6} and 6.00×10^{-5} g Ti L^{-1}), which could be close to the LOQ (4.24×10^{4} TiO_2 NPs mL^{-1}). Regarding PSDs, the most frequent sizes, instead of the mean sizes of the PSD, were used for comparison due to the spread range of size and the high degree of agglomeration of the TiO_2 NPs standards used in this study (characterization confirmed by TEM analysis as shown in Figure S5.1 in supplementary material). The most frequent size at the selected gastric digestion times were found to be similar and close to the most frequent size of the solution at T0 ($p<0.05$). TiO_2 NPs dissolution (ionization) during the gastric step was not significant because ionic Ti (dissolved) concentrations were very small, constant along the whole gastric digestion stage and quite similar to ionic Ti contents at T0. However, it must be taken into account that the presence of enzymes and electrolytes could affect the stability of TiO_2 NPs (aggregation) because of enzyme-NPs interactions and the decreased electrostatic repulsion between particles attributed to electrolytes [31]. Therefore, TiO_2 NPs aggregation is expected in the studied solutions, and the measured TiO_2 NPs concentration and PSD could be different from those obtained in the absence of the gastric and intestinal constituents.

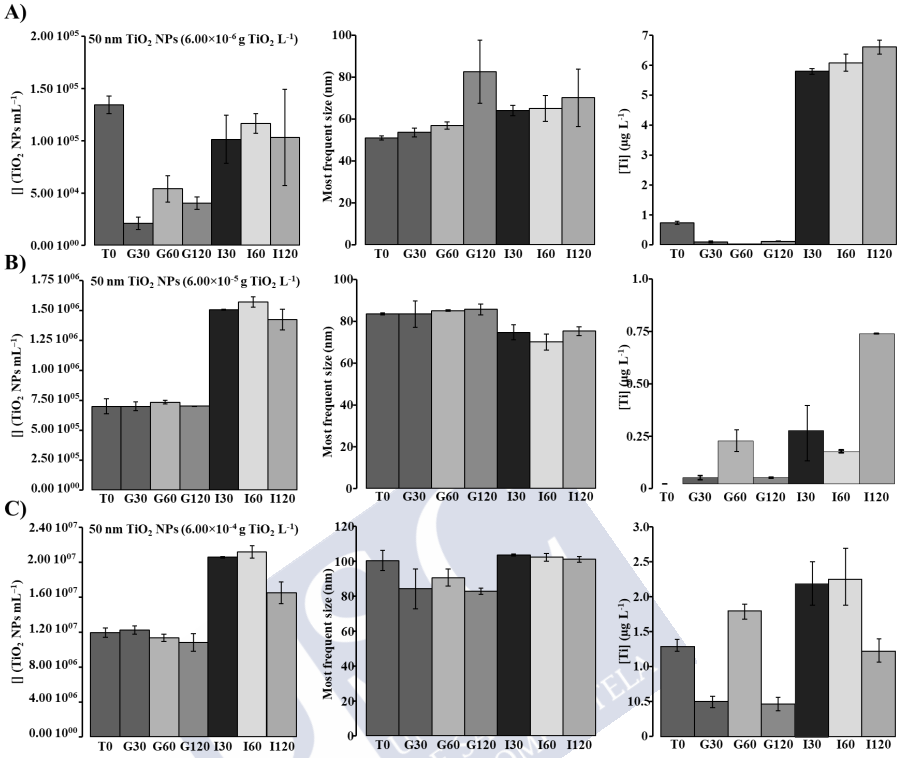

Figure 5.1. TiO_2 NPs concentrations, most frequent sizes and dissolved Ti concentrations at several stages of an *in vitro* gastrointestinal digestion of 50 nm TiO_2 NPs standard at three concentration levels: A) 6.00×10^{-6} g TiO_2 L^{-1}, B) 6.00×10^{-5} g TiO_2 L^{-1} and C) 6.00×10^{-4} g TiO_2 L^{-1}

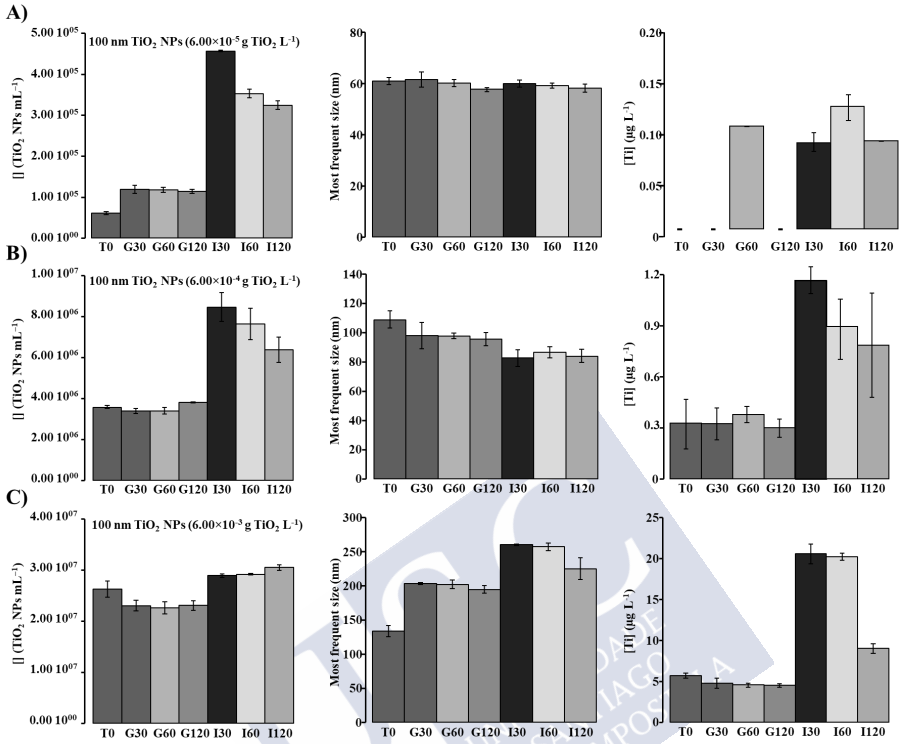

Figure 5.2. TiO_2 NPs concentrations, most frequent sizes and dissolved Ti concentrations at several stages of an *in vitro* gastrointestinal digestion of 100 nm TiO_2 NPs standard at three concentration levels: A) 6.00×10^{-5} g TiO_2 L^{-1}, B) 6.00×10^{-4} g TiO_2 L^{-1} and C) 6.00×10^{-3} g TiO_2 L^{-1}

Important differences have been observed during the simulated intestinal digestion stage (Figures 5.1 and 5.2, and Tables S5.1 and S5.2), and TiO_2 NPs concentrations were found to be increased during this stage for all experiments (TiO_2 NPs standards of both sizes and concentration levels) when comparing to TiO_2 NPs concentration in the simulated gastric step. Intestinal conditions must promote TiO_2 NPs ionization and TiO_2 NPs dispersion. The higher ionic Ti contents in the simulated intestinal digests compared to those found in simulated gastric digests (Figures 5.1 and 5.2, and Tables S5.1 and S5.2) suggest that TiO_2 NPs are partially ionized during the intestinal stage. However, this result does not always agree with TiO_2 NPs PSDs because the most frequent sizes

These findings agree with those previously reported for the *in vitro* bioaccessibility studies of TiO_2 NPs [32] and other engineered oxide-based nanomaterials (i.e., Fe_3O_4 NPs, CuO NPs, CeO_2 NPs, ZnO NPs [32] and SiO_2 NPs [33]), where DLS and SEM analysis support NPs aggregation during the gastric step and NPs dispersion under intestinal conditions. The pH of the digestive solutions has been suggested to be an important parameter. Separated (dispersed) individual NPs are found when the pH is increased from acid (gastric digestion) to neutral (intestinal digestion) [33]. As reported for SiO_2 NPs [33], EDX analysis showed the presence of chloride in the SiO_2 agglomerates, which is expected because hydrochloric acid is a component of the gastric juices. TEM analysis of the gastric fractions from 50 nm TiO_2 NPs standard at the highest concentration level (Figure 5.3) showed highly agglomerated TiO_2 NPs (500 nm) embedded in a diffuse matrix, and EDX microanalysis confirmed the presence of chloride in the aggregates (chloride bridges among TiO_2 NPs as previously reported for SiO_2 NPs [33]). On the other hand, chloride was not detected by EDX microanalysis in the intestinal fractions, and small aggregates and disperse NPs containing Ti were found.

In accordance to EFSA [21], the biopersistence rate was calculated as the mass fraction taking into account the TiO_2 NPs concentration before the *in vitro* digestion (T0) and after 30 min of the intestinal stage (I30). The mass of an individual TiO_2 NP was calculated by assuming spherical shape and using the mean size of the PSD and the TiO_2 density. The mass concentration was then obtained by multiplying the mass of one TiO_2 NP by the TiO_2 NPs concentration. Calculated rates were higher than 100% and 80% for 50 nm and 100 nm TiO_2 NPs at the three concentration levels, respectively. Biopersistence rates higher than 100% are explained taking into account that TiO_2 NPs dispersion is promoted during the intestinal stage, which implies higher TiO_2 NPs concentrations of lower PSD when comparing with gastric extracts. Agglomeration/dispersion of TiO_2 NPs could lead to a misleading deduction of the biopersistence rate because the dispersion of TiO_2 NPs during the intestinal stage (I30) leads to a higher TiO_2 NPs concentration than that measured in extracts from the gastric stage and at T0.

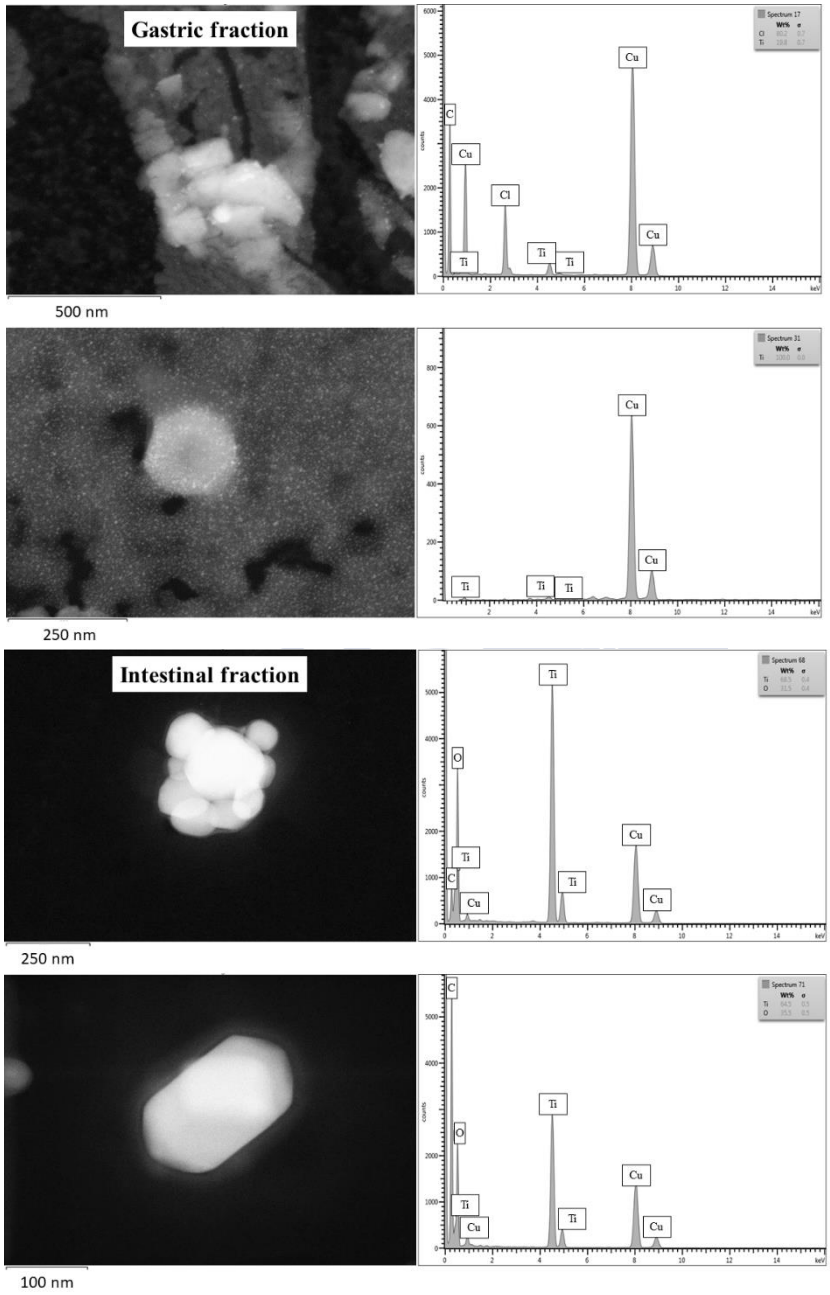

Figure 5.3. TEM images and EDX spectra of gastric and intestinal fractions from 50 nm TiO_2 NPs standard at the highest concentration level

The assessed biopersistence rates are higher than the stipulated limit by EFSA (12%) [21], which implies that TiO_2 NPs (50 and 100 nm) are unaltered and poorly degradable under gastrointestinal digestion conditions. These findings agree with those reported for nano-sized metal oxides, TiO_2 NPs included, solubility (*in vitro* bioaccessibility experiments) studies which have showed a low bioaccessibility of TiO_2 NPs and low toxic effects from the released metal ions [32].

5.3.2 TiO_2 NPs biopersistence rate in food additive E171

Similar results to those obtained for 50 and 100 nm TiO_2 NPs standards have been obtained for E171 experiments (Table S5.3 and Figure S5.2), where TiO_2 NPs concentrations were found to be slightly lower after gastric digestion (G30, G60 and G120) than at T0, and no statistically significant differences ($p<0.05$) were found in the concentrations of TiO_2 NPs during the gastric digestion process. Similarly, there were no statistically significant differences ($p<0.05$) found for mean sizes and ionic Ti contents over the simulated gastric digestion. Regarding the intestinal digestion stage, higher TiO_2 NPs concentrations than those found in the gastric digests were measured, results which are in good agreement with those obtained for 50 and 100 nm TiO_2 NPs standards and reported in the literature on *in vitro* bioaccessibility [32, 33]. Also, no statistically significant differences ($p<0.05$) were found on the TiO_2 NPs concentrations, TiO_2 NPs PSD and dissolved Ti during the intestinal digestion process. However, as shown in Table S5.3 and Figure S5.2, mean sizes in the intestinal digests were lower than the mean sizes in gastric aliquots, results which agree to the higher ionic Ti concentrations in the intestinal digests. Similar to 50 and 100 nm TiO_2 NPs standards, partial degradation of TiO_2 NPs and TiO_2 microparticles occurred during the intestinal digestion.

Regarding the biopersistence rate, TiO_2 NPs and TiO_2 microparticles in E171 do not seem to be degradable under gastrointestinal conditions. In accordance with results from 50 and 100 nm TiO_2 NPs standards, biopersistence rate of TiO_2 NPs and TiO_2 microparticles in E171 was higher than 100%. However, as stated for 50 and 100 nm TiO_2 NPs standards, agglomeration/dispersion phenomena could misrepresent the biopersistence rate.

5.3.3 Ag NPs biopersistence rate in standards

Tables S5.4 and S5.5 and Figures 5.4 and 5.5 show the Ag NPs concentrations, the PSD data and the ionic Ag concentrations in gastric and intestinal digests when 40 and 60 nm Ag NPs standards are subjected to the *in vitro* digestion process. Gastric conditions induce a slight increase on Ag NPs concentration at the beginning of the process (G30 experiments for 40 nm and 60 nm Ag NPs at low and intermediate concentrations), which is more important for 40 nm Ag NPs. Afterward, Ag NPs concentrations are gradually reduced (G60 and G120), except for the experiment with 40 nm Ag NPs at the highest concentration (Figure 5.4). The decrease of Ag NPs concentrations match, in some cases, with the decrease of the mean sizes (G60 and G120 for 40 nm Ag NPs at the low and intermediate concentrations and for 60 nm Ag NPs at the highest concentration). On other occasions (60 nm Ag NPs standards at low and intermediate concentration), mean sizes remain constant. Similarly, an increase in the ionic Ag in the gastric digests was observed in some experiments which could imply Ag NPs degradation during the *in vitro* gastric step. These findings agree with those reported by Bove et al. for TEM and DLS analysis of simulated gastric and intestinal digests (dynamic mode) from NM300k Ag NPs [34], which have also revealed a high degree of Ag NPs dissolution during the gastric digestion and the simultaneous presence of smaller Ag NPs and large Ag NPs agglomerates (attributed to the organic matrix). sp-ICP-MS, DLS and SEM-EDX also showed Ag NPs agglomeration during the gastric stage in the presence of proteins (pepsin) for experiments with 60 nm Ag NPs, and revealed that reduction in number of particles was caused by their clustering (clusters composed of Ag NPs and chloride) [35].

Regarding the intestinal stage, an important increase on the Ag NPs concentrations was observed for experiments with the largest size (60 nm NPs, Figure 5.5), whereas a clear trend was not observed for 40 nm Ag NPs standards (Figure 5.4). PSD was found to be unchanged (gastric and intestinal digests), although ionic Ag concentrations were found to be increased in intestinal digest from 40 nm Ag NPs. However, ionic Ag in intestinal digests from 60 nm Ag NPs standards were quite lower than those found in gastric digests. In general, these

results agree with results by Walczak et al. [35], who also found that the number of Ag NPs rise back to original values after the intestinal digestion.

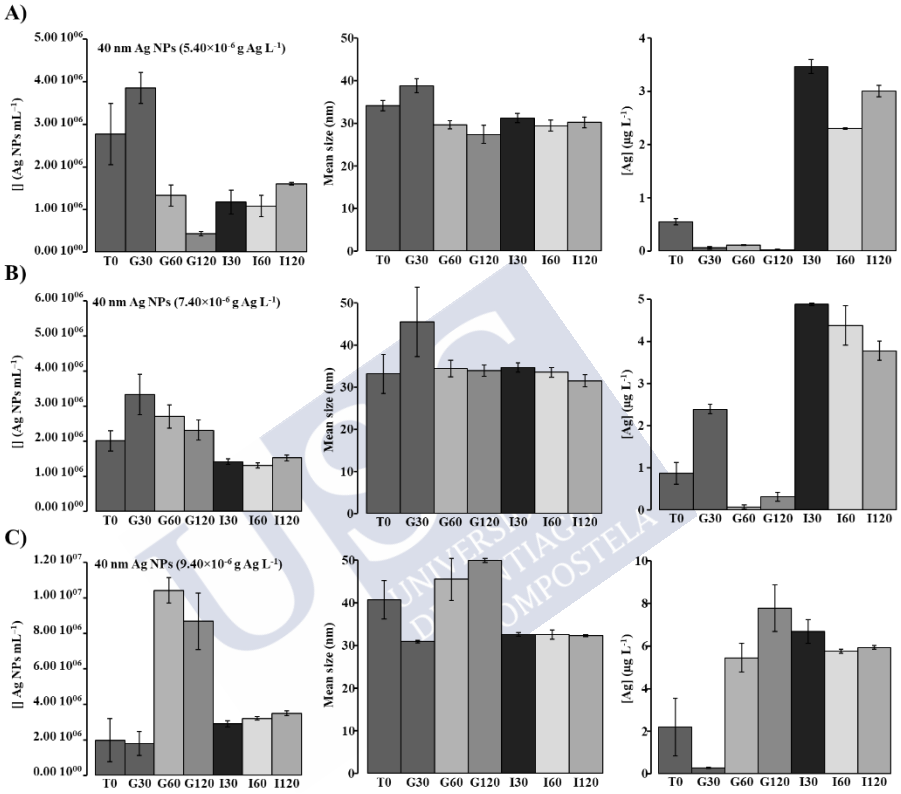

Figure 5.4. Ag NPs concentrations, mean sizes and dissolved Ag concentrations at several stages of an *in vitro* gastrointestinal digestion of 40 nm Ag NPs standard at three concentration levels: A) 5.40×10^{-6} g Ag L^{-1}, B) 7.40×10^{-6} g Ag L^{-1} and C) 9.40×10^{-6} g Ag L^{-1}

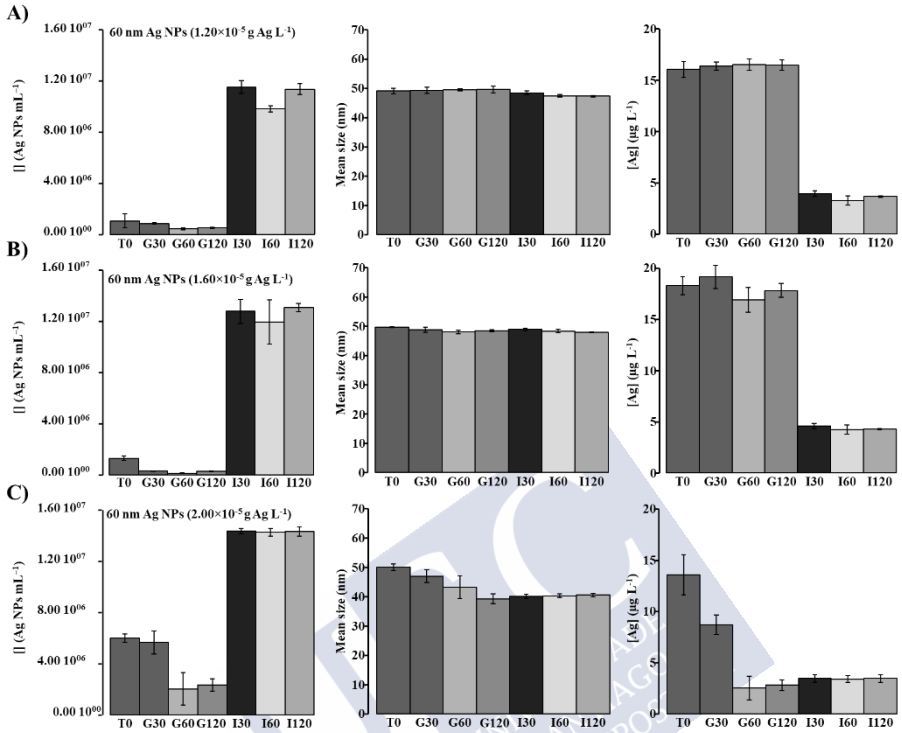

Figure 5.5. Ag NPs concentrations, mean sizes and dissolved Ag concentrations at several stages of an *in vitro* gastrointestinal digestion of 60 nm Ag NPs standard at three concentration levels: A) 1.20×10^{-5} g Ag L^{-1}, B) 1.60×10^{-5} g Ag L^{-1} and C) 2.00×10^{-5} g Ag L^{-1}

Conclusive results based on Ag NPs concentration, PSD and ionic metal content are therefore difficult to obtain due to the varied behavior of NPs in different environments. Agglomeration/dispersion phenomena plays an important role in an accurate characterization of NPs in complex mediums. However, Ag NPs appear to be more degradable than TiO_2 NPs under gastrointestinal conditions and biopersistence rates lower than 60% (22, 58 and 31% for 40 nm Ag NPs at low, intermediate and high concentrations, respectively) were calculated according to the EFSA protocol [21]. However, biopersistence rates were higher than 100% for 60 nm Ag NPs, which could mean that 60 nm Ag NPs are more stable than 40 nm Ag NPs under gastrointestinal conditions and NPs degradability could be dependent on the NPs size.

5.3.4 TiO_2 NPs biopersistence rate in mollusc and surimi samples

The degradability of TiO_2 NPs used as a food additive in two surimi samples, and TiO_2 NPs "naturally" present in a mussel and in a variegated scallop, has been studied in accordance with the EFSA guidance. Results (TiO_2 NPs and dissolved Ti concentrations) and mean sizes are listed in Tables S5.6 and S5.7 and plotted in Figures 5.6 and 5.7. Stability and degradability of TiO_2 NPs appears to be highly dependent of the sample matrix. TiO_2 NPs releasing from surimi during the simulated gastric stage appear to be inefficient and TiO_2 NPs and TiO_2 microparticles from E171 contained in surimi are highly clustered under gastric conditions as shown in Figure 5.6. High TiO_2 NPs concentrations were measured in enzymatic digests from the intestinal stage (Figure 5.6), which is also in good agreement with results from the literature [32] and *in vitro* digestion simulations of E171 and 50 and 100 nm TiO_2 NPs standards.

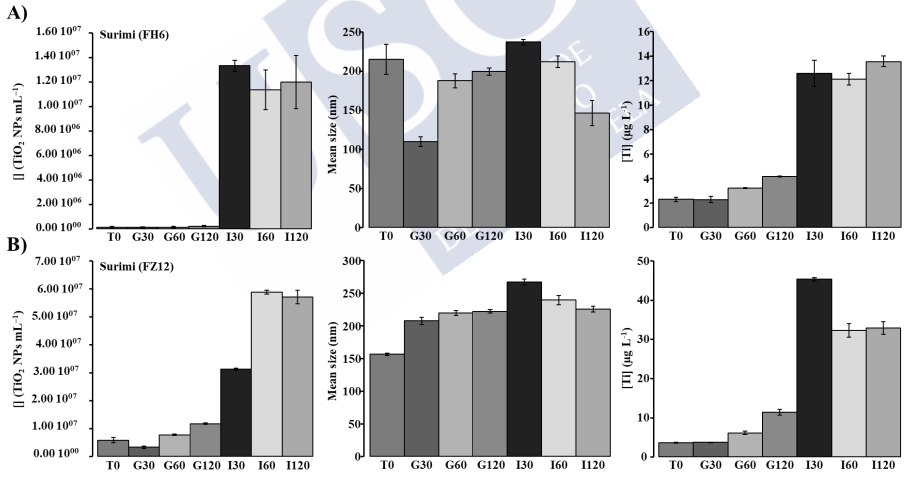

Figure 5.6. TiO_2 NPs concentrations, mean sizes and dissolved Ti concentrations at several stages of an *in vitro* gastrointestinal digestion of A) FH6 and B) FZ12 surimi samples

Variable TiO_2 NPs concentrations were measured in gastric digests when studying the fresh mussel and the variegated scallop (Figure 5.7), and a clear increase of TiO_2 NPs concentrations in the intestinal digests was only observed from variegated scallop (TiO_2 NPs concentration in the intestinal digests from mussel were lower than TiO_2 NPs concentrations in gastric digests and the initial mixture (T0), Figure 5.7). Mean sizes of the released TiO_2 NPs and the ionic Ti concentrations in mollusc samples are quite similar over the gastric and the intestinal digestion, which suggests that the released TiO_2 NPs were not degraded during the *in vitro* process (Figure 5.7). However, there is a little increase of the mean sizes of TiO_2 NPs in the intestinal digests when compared to those found in the gastric digests from surimi samples. In addition, the ionic Ti contents in the intestinal digests from surimi are also higher than those measured in the gastric digests. Similar to TiO_2 NPs standards, TEM-EDX analysis reveals the presence of chloride in the agglomerate TiO_2 NPs from gastric digests from a variegated scallop sample (Z24), whereas dispersed NPs are observed in the intestinal extracts (Figure 5.8).

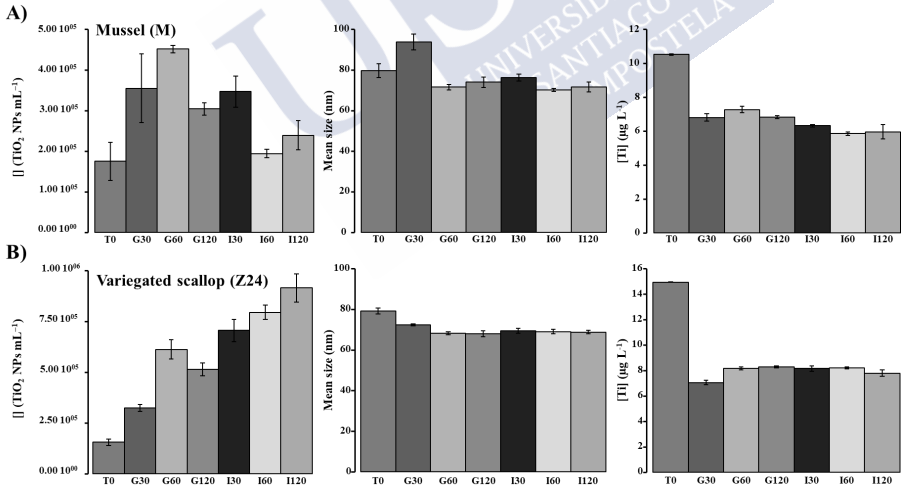

Figure 5.7. TiO_2 NPs concentrations, mean sizes and dissolved Ti concentrations at several stages of an *in vitro* gastrointestinal digestion of A) mussel-M and B) fresh variegated scallop-Z24 samples

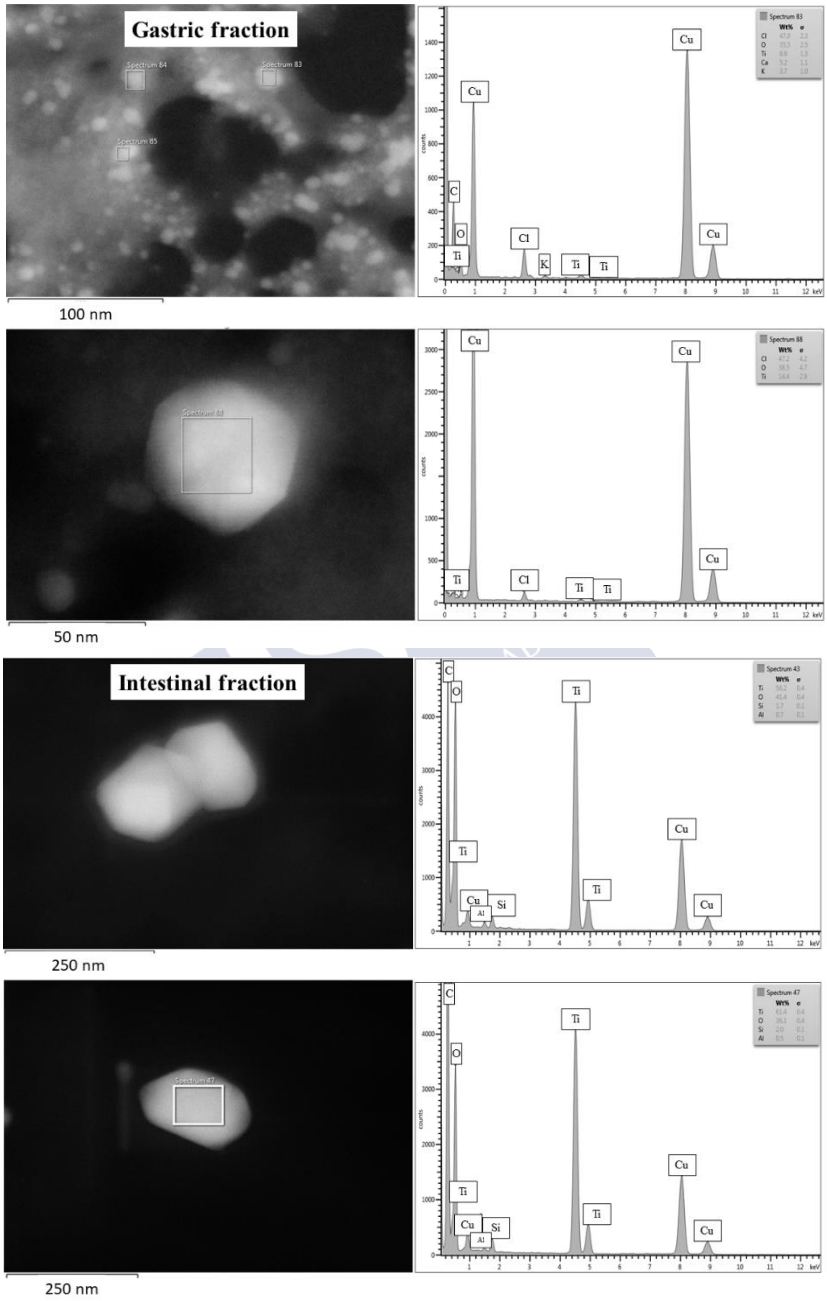

Figure 5.8. TEM images and EDX spectra of gastric and intestinal fractions from variegated scallop Z24

These findings suggest that the type of NP and the sample matrix contribute to the NPs agglomeration/dispersion phenomena under the same environmental conditions (pH, ionic strength). Therefore, results (trends) from surimi samples are quite similar to those found for experiments with 50 and 100 nm TiO_2 NPs standards, but results are different for fresh molluscs in which TiO_2 NPs are "naturally" present. These results are important because the reported literature has dealt only with the bioaccessibility of NPs from standards, but the contribution of the food matrix on the overall digestibility process must be considered.

Calculated biopersistence rates based on the EFSA guidance [21] were higher than 100% in all cases, mainly in surimi samples. This misleading result is attributed to the very low, or even negligible, extracted TiO_2 NPs from molluscs and surimi at initial conditions (T0) (Figures 5.6 and 5.7). Therefore, a biopersistence rate based on concentrations at initial conditions of the gastrointestinal process could be adequate for NPs standards but the criteria cannot be applied to the samples (NPs are still linked to the sample matrix at initial conditions). A biopersistence rate, in which the Ti mass (TiO_2 NPs concentrations) at initial gastrointestinal conditions is changed by the total TiO_2 NPs concentration in the samples [25, 27], was calculated. Values of 2 and 20% were obtained for mussels and variegated scallops, respectively. However, the biopersistence rates for surimi samples were higher than 100%, even when using this criterion. This finding is attributed to high TiO_2 (nano)particle dispersion under intestinal conditions resulting in misleading results, mainly due to the large sizes of the particles [27]. In conclusion, TiO_2 NPs do not seem be degradable in the presence of food (surimi and molluscs) matrices.

5.3.5 Ag NPs biopersistence rate in mollusc samples

Results from oyster (OP) and frozen variegated scallop (Z28) samples are summarized in Table S5.8 and plotted in Figure 5.9. Ag NPs "naturally" present in the samples have shown a different behavior than Ag NPs standards, which implies that sample matrix influence on the bioaccessibility is very important. In addition, Ag NPs (concentration and size) changes along the *in vitro* process were found to be similar in both seafood samples (Figure 5.9). Ag NPs concentration in oyster

and variegated scallop samples was lower in the gastric digests (G30, G60 and, mainly, G120) than at the beginning of the experiment (T0), findings that are not correlated to Ag NPs PSD changes because the Ag NPs mean sizes were found to decrease in the gastric digests. This behavior is similar to that found in Ag NPs standards [34, 35] and agrees with the simultaneous presence of smaller Ag NPs and large Ag NPs agglomerates reported for Ag NPs standards in *in vitro* studies [34].

An increase on the Ag NPs concentrations in the intestinal digests was observed for both samples, which implies Ag NPs dispersion under the intestinal conditions [35]. Ag NPs mean sizes remained constant along the intestinal stage and similar to those measured in the gastric digests for oyster samples, but a significant increase on mean sizes was found in intestinal digests from variegated scallops. Mean size trends were similar to ionic Ag content, which remained constant over the gastrointestinal process for oysters and was found to be higher in intestinal digests than in gastric digests from variegated scallops. In addition to agglomeration/dispersion as a consequence of the presence of macromolecules (enzymes and degradation products from sample matrix), other factors such as the high trend of Ag NPs to ionization could explain Ag NPs mean size and ionic Ag concentration changes over the *in vitro* gastrointestinal process.

Biopersistence rates were found to be different in both samples (20% in oysters and higher than 100% in variegated scallops when using the EFSA criterion). However, biopersistence rates based on Ag NPs concentrations in the samples [26] instead of Ag NPs at initial conditions (T0) have led to biopersistence values of 2 and 9% for oysters and variegated scallops, respectively, which shows a moderate influence of the sample matrix on the *in vitro* gastrointestinal digestion. The biopersistence values lower than 12 % [21] suggest that Ag NPs are degraded (ionized) during the gastrointestinal process. However, Ag NPs are highly persistent when applying the EFSA criterion (biopersistence rate based on NPs concentration at initial gastrointestinal conditions).

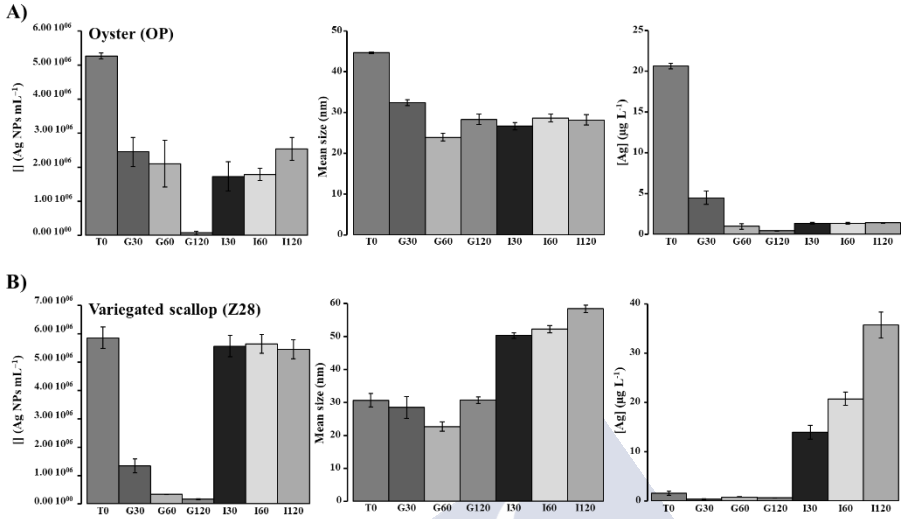

Figure 5.9. Ag NPs concentrations, mean sizes and dissolved Ag concentrations at several stages of an *in vitro* gastrointestinal digestion of A) oyster-OP and B) frozen variegated scallop-Z28 samples

5.4 CONCLUSIONS

In general, NPs agglomeration during *in vitro* gastric digestion and NPs dispersion under intestinal conditions has been observed when subjecting TiO_2 NPs and Ag NPs standards of different PSDs. However, studied Ag NPs standards have shown a high size-dependent behavior because 40 nm Ag NPs agglomeration was observed at the early stages of gastric digestion, whereas ionization phenomena appears to dominate during the gastric digestion stage for experiments with 60 nm Ag NPs standards. In addition, sample matrix constituents have been found to influence TiO_2 NPs and Ag NPs bioaccessibility. TiO_2 NPs "naturally" present in bivalve molluscs showed slow NPs release over the *in vitro* gastrointestinal digestion, while TiO_2 NPs behavior from surimi samples was quite similar to that found when studying TiO_2 NPs from E171. Regarding Ag NPs in molluscs, different trends were observed depending on the sample, and both agglomeration/dispersion and Ag NPs ionization phenomena have been found to be important.

Biopersistence rates were higher than 100% in TiO_2 NPs standards and TiO_2 NPs/TiO_2 microparticles from E171, which shows that these nano/microparticles are not degraded under simulated gastrointestinal conditions. However, Ag NPs have been found to be more degradable than TiO_2 NPs, and the biopersistence rate was dependent on the Ag NPs size. A higher digestibility of Ag NPs (lower biopersistence rate) was also found in seafood samples than that found for TiO_2 NPs in molluscs and surimi, but biopersistence rates were higher than the limit set by the EFSA (12%). Biopersistence rate in accordance with the EFSA guidance [21] was defined for studying the effect of NPs suspensions (standards and NM-based food additives). However, the application of the defined biopersistence rate to food samples is not straightforward because the NPs concentrations at the beginning of the experiment (T0 experiments) are going to be very low (NPs are linked to sample matrix components and are not going to be assessed because they have not yet been released). A biopersistence rate based on the initial NPs concentrations at T0 could thus lead to rates higher than 100% (misleading results). We therefore suggest changing the NPs concentrations at the initial gastrointestinal conditions for total NPs concentration in the sample to improve assessment when applying the EFSA guidance to food samples.

Acknowledgements

The authors wish to acknowledge the financial support of the Ministerio de Economía y Competitividad (project INNOVANANO, reference RT2018-099222-B-100), the European Union (Interreg Atlantic Area, project NANOCULTURE, reference EAPA590/2018), and the Xunta de Galicia (Grupo de Referencia Competitiva, grant number ED431C2018/19; and Program for Development of a Strategic Grouping in Materials – AEMAT, grant number ED431E2018/08). M.V. Taboada-López would like to thank the Xunta de Galicia and the European Social Fund (FSE) for the pre-doctoral grant.

5.5 REFERENCES

[1] The European Commission. Commission, Recommendation (EU) 2011/696 of 18 October 2011 on the definition of nanomaterial, Official Journal of the European Union L 275, 58 (2011) 38–40.
[2] X. Le-Guével, Overview of inorganic nanoparticles for food science applications, in M.A.V. Axelos and M. Van-de-Voorde (Ed.), Nanotechnology in Agriculture and Food Science, Wiley-VCH Weinheim, Germany, 2017, pp- 197–207.
[3] Consumer Products Inventory. An inventory of nanotechnology-based consumer products introduced on the market, http://www.nanotechproject.org/cpi (accessed on January 7th 2020).
[4] L. Holland, W. Zhong, Analytical developments in advancing safety in nanotechnology, Anal. Bioanal. Chem. 410 (2018) 6037–6039.
[5] A. Weir, P. Westerhoff, L. Fabricius, K. Hristovski, N. von Goetz, Titanium dioxide nanoparticles in food and personal care products, Environ. Sci. Technol. 46 (2012) 2242–2250.
[6] O. Geiss, J. Ponti, C. Senaldi, I. Bianchi, D. Mehn, J. Barrero, D. Gilland, R. Matissek, E. Anklan, Characterisation of food grade titania with respect to nanoparticle content in pristine additives and in their related food products, Food Addit. Contam. A 37 (2020) 236–253.
[7] Y. Yang, K. Doudrick, X. Bi, K. Hristovski, P. Herckes, P. Westerhoff, R. Kaegi, Characterization of food-grade titanium dioxide: The presence of nanosized particles, Environ. Sci. Technol. 48 (2014) 6391–6400.
[8] E.O. Ogunsona, R. Muthuraj, E. Ojogbo, O. Valerio, T.H. Mekonnen, Engineered nanomaterials for antimicrobial applications: A review. Appl. Mater. Today 18 (2020) 100473 (DOI: 10.1016/j.apmt.2019.100473).
[9] C.A. dos Santos, A.P. Ingle, M. Rai, The emerging role of metallic nanoparticles in food, Appl. Microbiol. Biot. 104 (2020) 2373–2383.
[10] L. Mei, Q, Wang, Advances in using nanotechnology structuring approaches for improving food packaging, Annu. Rev. Food Sci. Technol. 11 (2020) 339–364.
[11] R. Sharma, S.M. Jafari, S. Sharma, Antimicrobial bio-nanocomposites and their potential applications in food packaging, Food Control 12 (2020) 107086 (DOI: 10.1016/j.foodcont.2020.107086).

[12] V.K. Yemmireddy, Y.C. Hung, Selection of photocatalytic bactericidal titanium dioxide (TiO_2) nanoparticles for food safety applications, LWT-Food Sci.Technol. 61 (2015) 1–6.
[13] G.D. Venkatasubbu, R. Baskar, T. Anusuya, C.A. Seshan, R. Chelliah, Toxicity mechanism of titanium dioxide and zinc oxide nanoparticles against food pathogens, Colloid. Surface. B 148 (2016) 600–606.
[14] M. Akter, T. Sikder, M. Rahman, A.K.M. A. Ullah, K.F.B. Hossain, S. Banik, T. Hosokawa, T. Saito, M. Kurasaki, A systematic review on silver nanoparticles-induced cytotoxicity: Physicochemical properties and perspectives, J. Adv. Res. 9 (2018) 1–16.
[15] K. Murugan, Y.E. Choonara, P. Kumar, D. Bijukumar, L. C. du Toit, V. Pillay, Parameters and characteristics governing cellular internalization and trans-barrier trafficking of nanostructures, Int. J. Nanomed. 10 (2015) 2191–2206.
[16] K. Zheng, M.I. Setyawati, D.T. Leong, J. Xie, Antimicrobial silver nanomaterials, Coordin. Chem. Rev. 357 (2018) 1–17.
[17] V.K. Yemmireddy, Y.C. Hung, Effect of food processing organic matter on photocatalytic bactericidal activity of titanium dioxide (TiO_2), Int. J.Food Microbiol. 204 (2015) 75–80.
[18] D.J. McClements, H. Xiao, P. Demokritou, Physicochemical and colloidal aspects of food matrix effects on gastrointestinal fate of ingested inorganic nanoparticles, Adv. Colloid Interfac. 246 (2017) 165–180.
[19] L. Laloux, M. Polet, Y.J. Schneider, Interaction between Ingested-Engineered Nanomaterials and the Gastrointestinal Tract: *In Vitro* Toxicology Aspects, in M.A.V. Axelos and M. Van-de-Voorde (Ed.), Nanotechnology in Agriculture and Food Science, Wiley-VCH, Weinheim, Germany, 2017 pp. 311–331.
[20] E.E. Fröhlich, E. Fröhlich, Cytotoxicity of Nanoparticles Contained in Food on Intestinal Cells and the Gut Microbiota, Int. J. Mol. Sci. 17 (2016) 509–531.
[21] EFSA Scientific Committee, Guidance on risk assessment of the application of nanoscience and nanotechnologies in the food and feed chain: Part 1, human and animal health. EFSA Journal 16 (2018) 5327–5395.

[22] O.A. Sadik, N. Du, V. Kariuki, V. Okello, V. Bushlyar, Current and emerging technologies for the characterization of nanomaterials, ACS Sustain. Chem. Eng. 2 (2014) 1707–1716.
[23] R. Peters, Z. Herrera-Rivera, A. Undas, M. van der Lee, H. Marvin, H. Bouwmeester, S. Weigel, Single particle ICP-MS combined with a data evaluation tool as a routine technique for the analysis of nanoparticles in complex matrices, J. Anal. At. Spectrom. 30 (2015) 1274–1285.
[24] D. Mozhayeva, C. Engelhard, A critical review of single particle inductively coupled plasma mass spectrometry – A step towards an ideal method for nanomaterial characterization, J. Anal. At. Spectrom. 35 (2020) 1740–1783.
[25] M.V. Taboada-López, S. Iglesias-López, P. Herbello-Hermelo, P. Bermejo-Barrera, A. Moreda-Piñeiro, Ultrasound assisted enzymatic hydrolysis for isolating titanium dioxide nanoparticles from bivalve mollusk before sp-ICPMS, Anal. Chim. Acta 1018 (2018) 16–25.
[26] M.V. Taboada-López, N. Alonso-Seijo, P. Herbello-Hermelo, P. Bermejo-Barrera, A. Moreda-Piñeiro, Determination and characterization of silver nanoparticles in bivalve molluscs by ultrasound assisted enzymatic hydrolysis and sp-ICPMS, Microchem. J. 148 (2019) 652–660.
[27] M.V. Taboada-López, P. Herbello-Hermelo, R. Domínguez-González, P. Bermejo-Barrera, A. Moreda-Piñeiro, Enzymatic hydrolysis as a sample pre-treatment for titanium dioxide nanoparticles assessment in surimi (crab sticks) by single particle ICP-MS, Talanta 195 (2019) 23–32.
[28] M.R. Domínguez-González, G.M. Chiocchetti, P. Herbello-Hermelo, D. Vélez, V. Devesa, P. Bermejo-Barrera, Evaluation of iodine bioavailability in seaweed using *in vitro* methods, J. Agric. Food Chem. 65 (2017) 8435–8442.
[29] H.E. Pace, N.J. Rogers, C. Jarolimek, V.A. Coleman, C.P. Higgins, J.F. Ranvill, Determining Transport Efficiency for the Purpose of Counting and Sizing Nanoparticles via Single Particle Inductively Coupled Plasma Mass Spectrometry, Anal. Chem. 83 (2011) 9361–9369.
[30] S. Lee, X. Bi, R.B. Reed, J.F. Ranville, P. Herckes, P. Westerhoff, Nanoparticle Size Detection Limits by Single Particle ICP-MS for 40 Elements, Environ. Sci. Technol. 48 (2014) 10291–10300.

[31] W. Utembe, K. Potgieter, A. Byron Stefaniak, M. Gulumian, Dissolution and biodurability: Important parameters needed for risk assessment of nanomaterials, Part. Fibre Toxicol. 12 (2015) 11 (DOI: 10.1186/s12989-015-0088-2).
[32] L. Zhong, Y. Yu, H.Z. Lian, X. Hu, H. Fu, Y.J. Chen, Solubility of nano-sized metal oxides evaluated by using *in vitro* simulated lung and gastrointestinal fluids: implication for health risks, J. Nanopart. Res. 19 (2017) 375 (DOI: 10.1007/s11051-017-4064-7).
[33] R. Peters, E. Kramer, A.G. Oomen, Z.E. Herrera, G. Oegema, P.C. Tromp, R. Fokkink, A. Rietveld, H.J.P. Marvin, S. Weigel, A.A.C.M. Peijnenburg, H. Bouwmeester, Presence of nano-sized silica during *in vitro* digestion of foods containing silica as a food additive, ACS Nano 6 (2012) 2441–2451.
[34] P. Bove, M.A Malvindi, S. Sayaji Kote, R. Bertorelli, M. Summa, S. Sabella, Dissolution test for risk assessment of nanoparticles: a pilot study, Nanoscale 9 (2017) 6315–6326.
[35] A.P. Walczak, R. Fokkink, R. Peters, P. Tromp, Z.E. Herrera, I.M.C.M. Rietjens, Behaviour of silver nanoparticles and silver ions in an *in vitro* human gastrointestinal digestion model, Nanotoxicol. 7 (2012) 1198–1210.

5.6 SUPPLEMENTARY INFORMATION

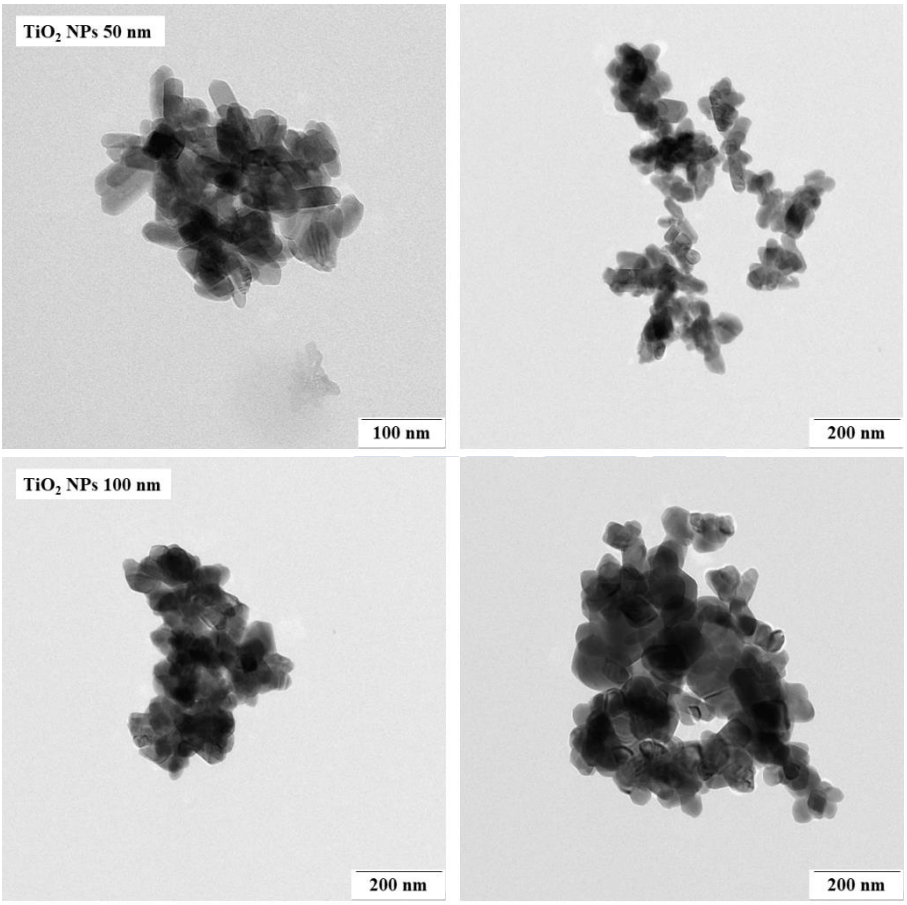

Figure S5.1. TEM characterization of 50 and 100 nm TiO_2 NPs standards

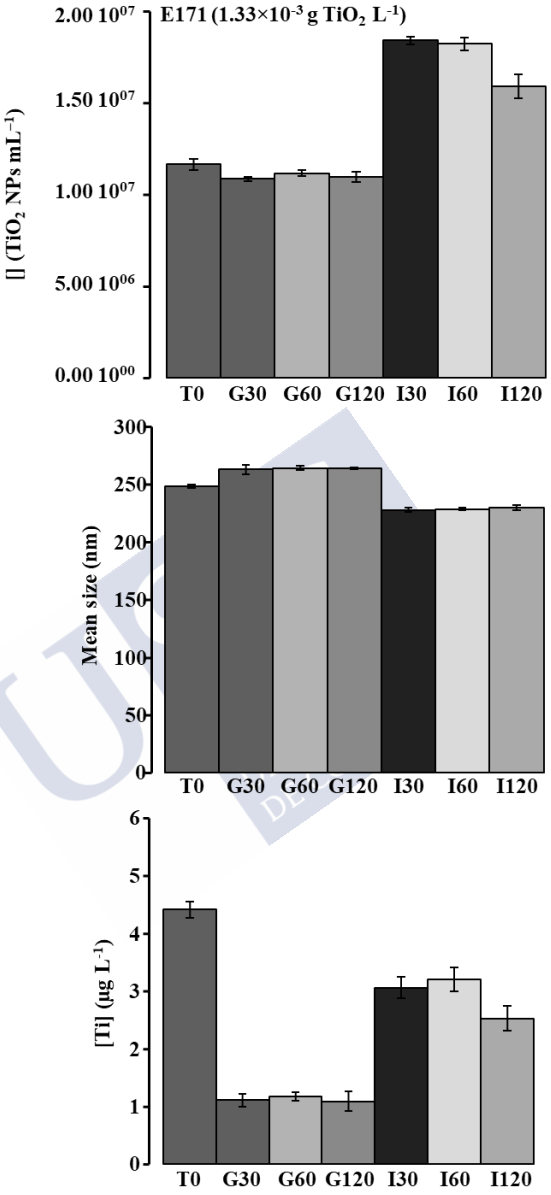

Figure S5.2. TiO_2 NPs concentrations, mean sizes and dissolved Ti concentrations at several stages of an *in vitro* gastrointestinal digestion of food additive E171 (1.33×10^{-3} g TiO_2 L^{-1})

Table S5.1. TiO_2 NPs concentrations, most frequent sizes and dissolved Ti concentrations at several stages of an *in vitro* gastrointestinal digestion of 50 nm TiO_2 NPs standard at three concentration levels

		[] (TiO_2 NPs mL^{-1})		*Most frequent size (nm)*		*[] (µg Ti L^{-1})*	
		Mean	*SD*	*Mean*	*SD*	*Mean*	*SD*
6.00×10^{-6} *g TiO_2 L^{-1}*	*STD*	1.71×10^{5}	1.61×10^{4}	38.6	4.2	2.55	0.06
	T0	1.34×10^{5}	8.44×10^{3}	50.8	1.1	0.722	0.053
	G30	2.09×10^{4}	6.02×10^{3}	53.5	2.1	0.0900	0.0357
	G60	5.39×10^{4}	1.26×10^{4}	56.7	1.8	0.0116	0.000
	G120	4.02×10^{4}	5.75×10^{3}	82.4	15.1	0.109	0.014
	I30	1.01×10^{5}	2.32×10^{4}	64.0	2.4	5.79	0.09
	I60	1.16×10^{5}	9.27×10^{3}	64.8	6.2	6.08	0.29
	I120	1.03×10^{5}	4.60×10^{4}	70.0	13.6	6.60	0.24
6.00×10^{-5} *g TiO_2 L^{-1}*	*STD*	8.07×10^{5}	4.26×10^{4}	75.7	2.1	2.98	0.08
	T0	6.98×10^{5}	6.46×10^{4}	83.3	0.5	ND	ND
	G30	6.97×10^{5}	3.74×10^{4}	83.3	6.2	0.0292	0.0099
	G60	7.31×10^{5}	1.53×10^{4}	84.9	0.4	0.206	0.046
	G120	7.02×10^{5}	1.19×10^{3}	85.5	2.6	0.0303	0.0024
	I30	1.50×10^{6}	4.88×10^{3}	74.5	3.6	0.254	0.130
	I60	1.57×10^{6}	4.17×10^{4}	69.9	4.0	0.155	0.005
	I120	1.42×10^{6}	8.69×10^{4}	75.1	2.1	0.716	0.000
6.00×10^{-4} *g TiO_2 L^{-1}*	*STD*	5.41×10^{6}	1.80×10^{4}	69.0	7.5	5.12	0.10
	T0	1.19×10^{7}	5.31×10^{5}	100	6	1.28	0.08
	G30	1.22×10^{7}	4.85×10^{5}	84.1	11.4	0.501	0.073
	G60	1.13×10^{7}	4.08×10^{5}	90.6	5.0	1.79	0.10
	G120	1.08×10^{7}	1.00×10^{6}	82.8	1.7	0.461	0.088
	I30	2.05×10^{7}	1.05×10^{5}	104	1	2.18	0.30
	I60	2.12×10^{7}	7.11×10^{5}	102	2	2.23	0.39
	I120	1.65×10^{7}	1.24×10^{6}	101	2	1.21	0.16

ND: non-detected, STD: standard

Table S5.2. TiO_2 NPs concentrations, most frequent sizes and dissolved Ti concentrations at several stages of an *in vitro* gastrointestinal digestion of 100 nm TiO_2 NPs standard at three concentration levels

		[] (TiO_2 NPs mL^{-1})		*Most frequent size (nm)*		*[] (μg Ti L^{-1})*	
		Mean	*SD*	*Mean*	*SD*	*Mean*	*SD*
6.00×10^{-5} *g TiO_2 L^{-1}*	*STD*	2.27×10^{5}	2.30×10^{4}	45.4	2.1	2.81	0.01
	T0	6.10×10^{4}	3.81×10^{3}	60.9	1.3	ND	ND
	G30	1.19×10^{5}	1.00×10^{4}	61.6	3.0	ND	ND
	G60	1.18×10^{5}	6.76×10^{3}	60.2	1.3	0.0920	0.0000
	G120	1.14×10^{5}	5.09×10^{3}	57.6	0.8	ND	ND
	I30	4.57×10^{5}	1.47×10^{3}	59.9	1.3	0.0771	0.0080
	I60	3.52×10^{5}	1.08×10^{4}	59.1	1.0	0.110	0.011
	I120	3.24×10^{5}	1.08×10^{4}	58.1	1.5	0.0790	0.0000
6.00×10^{-4} *g TiO_2 L^{-1}*	*STD*	3.53×10^{6}	4.05×10^{5}	115	11	3.06	0.43
	T0	3.56×10^{6}	7.43×10^{4}	109	6	0.316	0.138
	G30	3.37×10^{6}	1.22×10^{5}	97.8	8.9	0.314	0.088
	G60	3.37×10^{6}	1.58×10^{5}	97.6	1.8	0.366	0.042
	G120	3.79×10^{6}	2.49×10^{4}	95.4	4.4	0.290	0.048
	I30	8.45×10^{6}	7.09×10^{5}	82.5	5.8	1.13	0.07
	I60	7.63×10^{6}	7.62×10^{5}	86.3	3.7	0.864	0.167
	I120	6.37×10^{6}	6.21×10^{5}	83.8	4.6	0.757	0.291
6.00×10^{-3} *g TiO_2 L^{-1}*	*STD*	3.34×10^{7}	8.21×10^{5}	119	16	10.3	2.3
	T0	2.63×10^{7}	1.55×10^{6}	133	8	5.67	0.33
	G30	2.30×10^{7}	1.03×10^{6}	203	2	4.75	0.62
	G60	2.26×10^{7}	1.15×10^{6}	202	6	4.53	0.24
	G120	2.30×10^{7}	9.63×10^{5}	194	6	4.47	0.21
	I30	2.89×10^{7}	3.46×10^{5}	260	1	20.5	1.2
	I60	2.91×10^{7}	1.35×10^{5}	257	6	20.2	0.4
	I120	3.05×10^{7}	5.46×10^{5}	225	16	8.98	0.58

ND: non-detected, STD: standard

Table S5.3. TiO_2 NPs concentrations, mean sizes and dissolved Ti concentrations at several stages of an *in vitro* gastrointestinal digestion of food additive E171

		[] (TiO_2 NPs mL^{-1})		*Mean size (nm)*		*[] (μg Ti L^{-1})*	
		Mean	*SD*	*Mean*	*SD*	*Mean*	*SD*
1.33×10^{-3} *g TiO_2 L^{-1}*	*STD*	9.44×10^{6}	1.52×10^{5}	241	2	5.61	0.16
	T0	1.17×10^{7}	2.94×10^{5}	248	2	4.41	0.14
	G30	1.09×10^{7}	1.06×10^{5}	263	4	1.10	0.12
	G60	1.12×10^{7}	1.65×10^{5}	264	2	1.16	0.07
	G120	1.10×10^{7}	2.77×10^{5}	264	1	1.08	0.17
	I30	1.84×10^{7}	2.15×10^{5}	228	2	3.05	0.18
	I60	1.82×10^{7}	3.55×10^{5}	228	1	3.19	0.21
	I120	1.59×10^{7}	6.50×10^{5}	230	3	2.52	0.21

STD: standard

Table S5.4. Ag NPs concentrations, mean sizes and dissolved Ag concentrations at several stages of an *in vitro* gastrointestinal digestion of 40 nm Ag NPs standard at three concentration levels

		[] (Ag NPs mL^{-1})		*Mean size (nm)*		*[] (µg Ag L^{-1})*	
		Mean	*SD*	*Mean*	*SD*	*Mean*	*SD*
5.40×10^{-6} *g Ag L^{-1}*	*STD*	9.44×10^{5}	1.30×10^{5}	36.5	1.9	1.19	0.69
	T0	2.77×10^{6}	7.14×10^{5}	34.0	1.3	0.541	0.060
	G30	3.85×10^{6}	3.63×10^{5}	38.7	1.7	0.0561	0.0228
	G60	1.33×10^{6}	2.48×10^{5}	29.5	1.0	0.106	0.008
	G120	4.29×10^{5}	4.96×10^{4}	27.3	2.2	0.0145	0.0077
	I30	1.17×10^{6}	2.86×10^{5}	31.1	1.1	3.46	0.13
	I60	1.08×10^{6}	2.48×10^{5}	29.3	1.2	2.29	0.02
	I120	1.60×10^{6}	2.82×10^{4}	30.1	1.2	2.99	0.11
7.40×10^{-6} *g TiO_2 L^{-1}*	*STD*	4.61×10^{6}	3.99×10^{5}	41.7	2.7	2.78	0.13
	T0	2.01×10^{6}	2.87×10^{5}	33.1	4.7	0.862	0.261
	G30	3.32×10^{6}	5.79×10^{5}	45.4	8.2	2.38	0.11
	G60	2.70×10^{6}	3.34×10^{5}	34.4	2.0	0.0547	0.0455
	G120	2.31×10^{6}	2.88×10^{5}	33.8	1.3	0.300	0.105
	I30	1.41×10^{6}	7.54×10^{4}	34.6	1.1	4.87	0.03
	I60	1.30×10^{6}	7.34×10^{4}	33.5	1.2	4.37	0.46
	I120	1.52×10^{6}	7.53×10^{4}	31.5	1.4	3.77	0.23
9.40×10^{-6} *g TiO_2 L^{-1}*	*STD*	5.44×10^{6}	7.33×10^{4}	32.5	0.9	4.23	0.18
	T0	1.98×10^{6}	1.20×10^{6}	40.6	4.5	2.18	1.36
	G30	1.78×10^{6}	6.72×10^{5}	30.9	0.3	0.265	0.029
	G60	1.04×10^{7}	7.26×10^{5}	45.4	5.0	5.43	0.67
	G120	8.66×10^{6}	1.59×10^{6}	49.9	0.5	7.75	1.10
	I30	2.89×10^{6}	1.89×10^{5}	32.6	0.4	6.67	0.56
	I60	3.19×10^{6}	1.02×10^{5}	32.5	1.1	5.73	0.10
	I120	3.49×10^{6}	1.27×10^{5}	32.3	0.2	5.91	0.08

STD: standard

Table S5.5. Ag NPs concentrations, mean sizes and dissolved Ag concentrations at several stages of an *in vitro* gastrointestinal digestion of 60 nm Ag NPs standard at three concentration levels

		[] (Ag NPs mL^{-1})		*Mean size (nm)*		*[] (μg Ag L^{-1})*	
		Mean	*SD*	*Mean*	*SD*	*Mean*	*SD*
1.20×10^{-5} *g Ag L^{-1}*	*STD*	1.97×10^{6}	3.75×10^{5}	59.0	1.7	7.19	0.33
	T0	1.07×10^{6}	5.40×10^{5}	48.9	1.0	16.0	0.8
	G30	8.75×10^{5}	6.25×10^{4}	49.1	1.1	16.4	0.4
	G60	4.59×10^{5}	9.20×10^{4}	49.4	0.4	16.5	0.5
	G120	5.35×10^{5}	3.97×10^{4}	49.5	1.1	16.4	0.5
	I30	1.15×10^{7}	4.90×10^{5}	48.3	0.6	3.92	0.27
	I60	9.84×10^{6}	2.52×10^{5}	47.3	0.5	3.24	0.47
	I120	1.14×10^{7}	4.26×10^{5}	47.2	0.2	3.64	0.09
1.60×10^{-5} *g TiO_2 L^{-1}*	*STD*	2.59×10^{6}	1.73×10^{5}	60.4	1.2	7.82	0.60
	T0	1.29×10^{6}	1.84×10^{5}	49.7	0.1	18.3	0.9
	G30	3.07×10^{5}	1.55×10^{4}	48.8	0.9	19.1	1.1
	G60	1.32×10^{5}	6.26×10^{3}	48.0	0.6	16.9	1.2
	G120	2.79×10^{5}	2.71×10^{4}	48.5	0.3	17.8	0.7
	I30	1.28×10^{7}	9.45×10^{5}	48.9	0.5	4.58	0.25
	I60	1.19×10^{7}	1.72×10^{6}	48.4	0.6	4.20	0.45
	I120	1.31×10^{7}	3.12×10^{5}	47.8	0.2	4.26	0.06
2.00×10^{-5} *g TiO_2 L^{-1}*	*STD*	3.57×10^{6}	3.20×10^{5}	53.4	0.9	2.31	0.55
	T0	6.00×10^{6}	3.09×10^{5}	50.0	1.2	13.6	1.9
	G30	5.67×10^{6}	9.08×10^{5}	47.0	2.2	8.68	0.95
	G60	2.03×10^{6}	1.27×10^{6}	43.2	3.9	2.48	1.16
	G120	2.34×10^{6}	4.74×10^{5}	39.2	1.7	2.78	0.54
	I30	1.44×10^{6}	1.98×10^{5}	40.0	0.7	3.44	0.38
	I60	1.43×10^{7}	2.86×10^{5}	40.3	0.7	3.37	0.33
	I120	1.43×10^{7}	3.64×10^{5}	40.5	0.7	3.44	0.38

STD: standard

Table S5.6. TiO_2 NPs concentrations, mean sizes and dissolved Ti concentrations at several stages of an *in vitro* gastrointestinal digestion of surimi samples (FH6 and FZ12)

		[] (TiO_2 NPs mL^{-1})		*Mean size (nm)*		*[] (µg Ti L^{-1})*	
		Mean	*SD*	*Mean*	*SD*	*Mean*	*SD*
Fresh surimi (FH6)	*T0*	1.52×10^{5}	7.14×10^{4}	215	19	2.27	0.18
	G30	1.25×10^{5}	6.22×10^{4}	110	6	2.26	0.26
	G60	1.41×10^{5}	7.64×10^{4}	187	9	3.18	0.04
	G120	2.30×10^{5}	5.47×10^{4}	199	5	4.13	0.04
	I30	1.33×10^{7}	4.62×10^{5}	237	3	12.6	1.1
	I60	1.14×10^{7}	1.63×10^{6}	211	8	12.0	0.5
	I120	1.20×10^{7}	2.18×10^{6}	146	16	13.5	0.4
Frozen surimi (FZ12)	*T0*	5.85×10^{6}	9.24×10^{5}	157	2	3.57	0.08
	G30	3.31×10^{6}	3.82×10^{5}	208	5	3.65	0.08
	G60	7.70×10^{6}	2.54×10^{5}	220	4	6.08	0.41
	G120	1.18×10^{7}	2.82×10^{5}	222	2	11.4	0.7
	I30	3.12×10^{7}	3.74×10^{5}	267	4	45.3	0.4
	I60	5.87×10^{7}	6.60×10^{5}	239	7	32.2	1.7
	I120	5.70×10^{7}	2.47×10^{6}	226	4	32.9	1.6

Table S5.7. TiO_2 NPs concentrations, mean sizes and dissolved Ti concentrations at several stages of an *in vitro* gastrointestinal digestion of mussel (M) and fresh variegated scallop (Z24) samples

		[] (TiO_2 NPs mL^{-1})		*Mean size (nm)*		*[] (µg Ti L^{-1})*	
		Mean	*SD*	*Mean*	*SD*	*Mean*	*SD*
Mussel (M)	*T0*	1.75×10^5	4.69×10^4	79.5	3.4	10.5	0.0
	G30	3.54×10^5	8.45×10^4	93.7	4.0	6.80	0.22
	G60	4.51×10^5	9.09×10^3	71.5	1.3	7.27	0.19
	G120	3.03×10^5	1.51×10^4	73.9	2.6	6.82	0.10
	I30	3.46×10^5	3.82×10^4	76.2	1.6	6.32	0.07
	I60	1.94×10^5	1.04×10^4	70.0	0.8	5.85	0.10
	I120	2.39×10^5	3.53×10^4	71.5	2.5	5.95	0.42
Variegated scallop (Z24)	*T0*	1.55×10^5	1.49×10^4	79.1	1.4	15.0	0.0
	G30	3.24×10^5	1.63×10^4	72.3	0.6	7.04	0.18
	G60	6.12×10^5	4.77×10^4	68.1	0.7	8.16	0.13
	G120	5.13×10^5	3.19×10^4	67.9	1.4	8.28	0.10
	I30	7.06×10^5	5.50×10^4	69.3	1.3	8.14	0.23
	I60	7.94×10^5	3.53×10^4	69.0	1.2	8.20	0.07
	I120	9.14×10^5	6.93×10^4	68.8	0.8	7.79	0.27

Table S5.8. Ag NPs concentrations, mean sizes and dissolved Ag concentrations at several stages of an *in vitro* gastrointestinal digestion of oyster (OP) and frozen variegated scallop (Z28) samples

		[] (Ag NPs mL^{-1})		*Mean size (nm)*		*[] (µg Ag L^{-1})*	
		Mean	SD	Mean	SD	Mean	SD
Oyster (OP)	*T0*	5.26×10^{6}	8.71×10^{4}	44.6	0.2	20.6	0.3
	G30	2.44×10^{6}	4.29×10^{5}	32.3	0.8	4.46	0.80
	G60	2.09×10^{6}	6.80×10^{5}	23.9	0.9	0.942	0.318
	G120	6.17×10^{4}	4.51×10^{4}	28.2	1.3	0.409	0.021
	I30	1.72×10^{6}	4.32×10^{5}	26.6	0.9	1.36	0.12
	I60	1.78×10^{6}	1.81×10^{5}	28.6	1.0	1.35	0.13
	I120	2.53×10^{6}	3.40×10^{5}	28.2	1.3	1.40	0.02
Frozen variegated scallop (Z28)	*T0*	5.85×10^{6}	3.80×10^{5}	30.6	2.0	1.55	0.41
	G30	1.32×10^{6}	2.38×10^{5}	28.4	3.3	0.374	0.089
	G60	3.19×10^{5}	1.48×10^{4}	22.6	1.4	0.753	0.048
	G120	1.52×10^{5}	2.05×10^{4}	30.6	1.0	0.603	0.000
	I30	5.55×10^{6}	3.75×10^{5}	50.2	0.8	13.9	1.4
	I60	5.64×10^{6}	3.37×10^{5}	52.2	1.1	20.7	1.3
	I120	5.44×10^{6}	3.32×10^{5}	58.4	1.2	35.6	2.7

USC
UNIVERSIDADE
DE SANTIAGO
DE COMPOSTELA

CHAPTER 6

CACO-2 *IN VITRO* MODEL OF HUMAN GASTROINTESTINAL TRACT FOR STUDYING THE ABSORPTION OF TITANIUM DIOXIDE AND SILVER NANOPARTICLES FROM SEAFOOD SAMPLES

MARÍA VANESA TABOADA-LÓPEZ, BALTAZAR HIRAM LEAL-MARTÍNEZ, RAQUEL DOMÍNGUEZ-GONZÁLEZ, PILAR BERMEJO-BARRERA, PABLO TABOADA-ANTELO AND ANTONIO MOREDA-PIÑEIRO

USC
UNIVERSIDADE
DE SANTIAGO
DE COMPOSTELA

6 CACO-2 *IN VITRO* MODEL OF HUMAN GASTROINTESTINAL TRACT FOR STUDYING THE ABSORPTION OF TITANIUM DIOXIDE AND SILVER NANOPARTICLES FROM SEAFOOD SAMPLES

María Vanesa Taboada-López[1], Baltazar Hiram Leal-Martínez[2], Raquel Domínguez-González[1], Pilar Bermejo-Barrera[1], Pablo Taboada-Antelo[2], Antonio Moreda-Piñeiro[1]

[1]Trace Element, Spectroscopy and Speciation Group (GETEE), Strategic Grouping in Materials (AEMAT), Department of Analytical Chemistry, Nutrition and Bromatology. Faculty of Chemistry. Universidade de Santiago de Compostela. Avenida das Ciencias, s/n. 15782 – Santiago de Compostela, Spain.
[2]Colloids and Polymer Physics Group, Strategic Grouping in Materials (AEMAT), Department of Particle Physics. Faculty of Physics, Universidade de Santiago de Compostela. Rúa Xosé María Suárez Núñez, s/n. 15782- Santiago de Compostela, Spain.

Abstract
Titanium dioxide nanoparticles (TiO_2 NPs) are widely used in industry, as white pigment (paints, paper industry and toothpastes), photocatalysts (environmental decontamination and photovoltaic cells), inorganic UV filter (sunscreens and personal care products) and as a food additive (E171) and antimicrobial food packaging material. Silver nanoparticles (Ag NPs) are used in photonics, microelectronics, catalysis and medicine due to their catalytic activity, magnetic and optical polarizability, electrical and thermal conductivities and enhanced Raman scattering. They also have antibacterial, antifungal and antiviral activities, as well as anti-inflammatory potential. The huge increase in the use of nano-based

products, mainly metallic NPs, implies the presence of nanomaterials in the environment and, hence, the unintentional human ingestion through water or foods (gastrointestinal tract is the main pathway of NPs intake in humans).
The presence of TiO_2 NPs and Ag NPs in seafood samples was firstly established using an ultrasound assisted enzymatic hydrolysis procedure and sp-ICP-MS analysis. Several clams, cockles, mussels, razor clams, oysters and variegated scallops, which contain TiO_2 NPs and Ag NPs, were subjected to an *in vitro* digestion process simulating human gastrointestinal digestion in the stomach and in the small and large intestine to determine the bioaccessibility of these NPs. Caco-2 cells were selected as model of human intestinal epithelium for transport studies because of the development of membrane transporters that are responsible for the uptake of chemicals. Parameters as transepithelial electrical resistance (TEER) and permeability of Lucifer Yellow were studied for establishing cell monolayer integrity. TiO_2 NPs and Ag NPs transport, as well as total Ti and Ag, concentrations passing through the gastrointestinal epithelial barrier model (0-2 h) were assessed by sp-ICP-MS and ICP-MS in several molluscs.

Keywords
Titanium dioxide nanoparticles, silver nanoparticles, bioaccessibility, Caco-2 cells, transcellular transport

6.1 INTRODUCTION

Nanomaterials (NMs) are natural or manufactured materials which may contain nanosized particles in a disaggregated or aggregated/agglomerated state. A material is considered as NM if a percentage of 50% or higher of the particles, in number-sized distribution, have one or more external dimensions in the size range between 1 and 100 nm [1]. NMs have physical, chemical, biological, optical, magnetic and structural properties quite different than those shown by their bulk counterparts, which is mainly attributed to size confinement, distribution and morphology, interfacial phenomena and quantum effects in the nanoscale. These enhanced properties have led to NMs, mainly metallic nanoparticles (NPs),

to be used in several industrial applications, and also for developing improved materials/products [2, 3].

The increasing use of NMs in industry has led to concerns about their potential toxicological effects on human health and environment [4]. Specifically, NMs can be uncontrollably introduced into the aquatic environment where several of them have been proven to be toxic to aquatic plants, vertebrates and microbes [5]. Bivalve molluscs are sentinel organisms of marine environmental health, and they are useful and well recognized sensitive bioindicators for biomonitoring the potential effects of anthropogenic substances on the health of the aquatic environment. Bivalve molluscs are suspension filter feeders, so they can tolerate and accumulate potential toxic substances in their tissues. Changes on their cell and tissue physiology, behavior and biochemistry reflect the health status of the organism and the concomitant status of the surrounding environment [6]. Bivalve molluscs can uptake NPs via gills and endocytosis in the digestive system. Larger NPs and aggregates tend to accumulate in tissues in a higher extent than small or free NPs. The digestive gland is the main target organ for NPs accumulation where they can be transferred to hemolymph and circulating hemocytes. In addition to several studies that show the bioaccumulation TiO_2 NPs and Ag NPs in molluscs in controlled laboratory conditions, these NPs have been also detected in unexposed molluscs [7-9], and their uptake by humans could be expected through foods (seafood).

Oral uptake is the most important route of entry of NPs into the human body due to the presence of NPs in food, the large absorption area and the relatively high translocation rate [10]. The gastrointestinal tract acts as a barrier that prevents the penetration of unwanted food components further into the body. Ingested NPs can traverse the epithelium, enter the systemic circulation and potentially reach several organs via transcellular (epithelial and M-cells) and paracellular transports. This absorption process mainly takes place in the small and large intestine, whereas no absorbed particles may be eliminated in faeces [11, 12].

In vitro assays are useful methodologies which give some insights regarding nutrient and pollutants absorption into the human body.

Bioaccessibility is a simple model defined as the fraction of a compound which is released from the food matrix in the gastrointestinal tract and thereby made available for intestinal absorption. However, the *in vitro* model must consider the compound's absorption by the intestine. Assays based on cell lines, such as Caco-2 cells, are the best well-known models for studies of permeability, transport and absorption of nutrients/pollutants since they are derived from human colorectal adenocarcinoma and present high morphological and physiological similarity to the human intestine [10]. Caco-2 cultures and Caco-2/HT29 cocultures have been used for assessing transcellular transport and uptake of TiO_2 NPs [13, 14] and Ag NPs [15-18], and for studying *in vitro* intestinal epithelium responses of TiO_2 NPs [14, 19-27] and Ag NPs [15, 16, 28-31]. These studies have been focused on TiO_2 NPs and Ag NPs standards of several size distributions and on the manufactured E171 additive (nano-titanium) [19-21, 27]. However, the *in vitro* transcellular transport/uptake and intestinal epithelium responses for TiO_2 NPs and Ag NPs contained in food have not been studied. Most of these previous studies have used electron microscopy techniques, including scanning electron microscopy (SEM), transmission electron microscopy (TEM) and atomic force microscopy (AFM), and dynamic and static light scattering (DLS and SLS), which allow NPs visualization and counting. Inductively coupled plasma-mass spectrometry (ICP-MS) operating under the so-called single particle mode (sp-ICP-MS) provides information about the NP number concentration (counting technique) and also size distribution, allowing sensitive detection/identification of the NP's nature (mass levels down to ng L^{-1}) and the simultaneous quantification of NPs and dissolved (ionic) analyte concentration [32-34].

The benefits of sp-ICP-MS have been used in the current work for assessing TiO_2 NPs and Ag NPs concentrations and size distributions in the bioaccessible fraction, as well as in the basolateral solutions, when performing an *in vitro* Caco-2 transcellular transport model for bivalve molluscs. Total contents of Ti and Ag were also measured by ICP-MS. Although some *in vitro* studies have been performed for TiO_2 NPs and Ag NPs standards, the bioaccessibility and transcellular transport of these NPs have not been evaluated in foodstuff yet.

6.2 MATERIALS AND METHODS

6.2.1 Instrumentation

A NexION 300X ICP-MS has been used for TiO_2 NPs and Ag NPs quantification and characterization with the Syngistix™ Nano Application software (Perkin Elmer, Massachusetts, USA). An Ethos Plus microwave lab-station (Milestone, Sorisole, Italy) with 100 mL closed Teflon vessels and Teflon covers was used for assisting the acid digestion procedure. *In vitro* digestion was performed in a Boxcult temperature-controlled chamber (Stuart Scientific, Surrey, UK) with a Rotabit orbital-rocking platform shaker (J.P. Selecta, Barcelona, Spain). A 130W ultrasound probe VibraCell VCx 130 from Sonics (Connecticut, USA) was used to assist enzymatic hydrolysis. Osmometer model 210 was from Fiske (Wichelen, Belgium). Millicell ERS-2 (Electrical Resistance System) was purchased from Millipore Co. (Massachusetts, USA). FLUOstar OPTIMA fluorimeter Microplate reader from BMG Labtech (Leicester, UK) was used for Lucifer Yellow measurements. All operations were performed inside a SMH-100 laminar flow cupboard from Telstar (Tarrasa, Spain). Other equipment used were an incubator with controlled atmosphere for cell culturing (Memmert, icoMed model, Schwabach, Germany), a pH-meter model Instruments XS (Carpi Mo, Italy), a Raypa UCI-150 ultrasonic cleaner water-bath (ultrasound frequencies of 17 and 35 kHz, 325 W) from R. Espinar S.L. (Barcelona, Spain), a Laborcentrifugen 2K15 centrifuge (Sigma, Osterode, Germany), a heating bath from J.P. Selecta and a domestic Taurus blade grinder (Taurus, Barcelona, Spain).

6.2.2 Reagents

Ultrapure water of resistivity 18 MΩ cm was from a Milli-Q purification device (Millipore Co). Gold NPs solution (60 nm) for transport efficiency quantification was a certified reference material (NIST8013) from NIST (Maryland, USA). Ionic titanium ($(NH_4)_2TiF_6$ 1000 mg L^{-1}) and silver nitrate ($AgNO_3$ 1000 mg L^{-1}) stock standard solutions were purchased from Merck (Darmstadt, Germany). NexION Setup Solution (10 µg L^{-1} Be, Ce, Fe, In, Li, Mg, Pb, U in HNO_3 1%) was from Perkin Elmer. Pepsin from porcine gastric mucosa, pancreatin from porcine

pancreas, lipase from *Candida rugose* and bile salts were from Sigma Aldrich (Osterode, Germany). Hydrochloric acid (37%), from Merck, and sodium hydrogen carbonate, from Panreac (Barcelona, Spain), were used to dilute gastric and intestinal enzymes, respectively. Caco-2 cells, Lucifer Yellow and Hanks' Balanced Salt Solution (HBSS) were from Sigma Aldrich. Phosphate-Buffered Saline (PBS (1x)) was from Thermo Fisher (Dublin, Ireland). Dulbecco's Modified Eagle Medium (DMEM), trypsin (3x) and six-well Transwell® (24 mm diameter, 0.4 μm pore size polyester membrane) were from Corning (New York, USA). Sterilin black 96-well microtiter plates (400 μL) were from Thermo Fisher. Other reagents were glycerol 99.5%, D-(+)-glucose and sodium chloride (Sigma Aldrich), and hydrogen peroxide 33% (w/v) and hyperpure nitric acid 69% (w/v) from Panreac.

To avoid metal contamination, all glassware and plastic ware were washed with ultrapure water and kept in 10% (v/v) HNO_3 for 48 h and, then, rinsed several times with ultrapure water before use.

6.2.3 Seafood samples

All samples, except a frozen variegated scallop (coded as Z28), were fresh molluscs purchased in local markets (Santiago de Compostela, Spain). The molluscs were washed with ultrapure water, after removing the byssus/shell, and homogenized (approximately 1 kg) by mechanical blending. Finally, samples were labelled and kept in polyethylene bottles at -20 °C until analysis. The samples used in this study were: grooved carpet shell (*Ruditapes decussatus*, ABL), one sample; oyster (*Ostrea edulis*, OP), one sample; edible cockles (*Cerasto dermaedule*, B22 and B28), two samples; razor clams (*Ensis ensis*, N18 and N28), two samples; variegated scallops (*Chlamys varia* , Z24 and Z28), two samples; and mussels (*Mytilus galloprovincialis*, M), one sample.

6.2.4 Microwave assisted acid digestion

In order to assess the total content of Ti and Ag in molluscs, a microwave assisted acid digestion was applied using the temperature and time conditions described by Taboada-López et al. [8, 9]. Briefly, 1.0 g of wet sample was mixed with 3 mL of 69% nitric acid, 1 mL

33% hydrogen peroxide and 4 mL of ultrapure water. Each sample was digested in triplicate and two reagent blanks were prepared for each digestion batch. Acid digests were made up to 25 mL with ultrapure water and stored in plastic tubes until ICP-MS analysis.

6.2.5 NPs extraction procedure

NPs extraction from the mollusc was performed by ultrasound assisted enzymatic hydrolysis following previous optimized conditions for TiO_2 NPs [8] and Ag NPs [9]. Both procedures imply the use of pancreatin and lipase as enzymes under the conditions listed in the supplementary material (Tables S6.1 and S6.2).

6.2.6 *In vitro* procedures

6.2.6.1 *In vitro* digestion procedure (bioaccessibility assay)

The human gastrointestinal process was simulated by an *in vitro* digestion procedure consisted of two successive stages under gastric and intestinal conditions. Homogenized wet mollusc samples (2.0 g) were mixed with 20 mL of ultrapure water, and after few minutes of stabilization, the pH was adjusted at 2.0 by dropwise addition of 0.1 M HCl solution. Then, 0.15 g of gastric solution (16 g of pepsin in 100 mL of 0.1 M HCl) was added, and the Erlenmeyer flasks containing the mixture were covered with Parafilm® and incubated in the Boxcult temperature-controlled chamber at 37 °C and orbital-horizontal shaking at 150 rpm for 2 h. The gastric digests were then placed in an ice-water bath to stop the enzymatic activity and the pH was adjusted at 7.0 with 0.1 M NaOH. The intestinal stage starts by adding 5.0 mL of the intestinal solution (4 g pancreatin and 25 g bile salts in 1 L of 0.1 M $NaHCO_3$) to the flasks followed by incubation for 2 h at 37 °C and orbital-horizontal shaking at 150 rpm. The enzymatic digestion was stopped using ice-water bath and the obtained digests were centrifuged for 25 min at 4 °C and 3900 rpm. The supernatants (bioaccessible fractions) were kept in polyethylene tubes at -20 °C until analysis. Each mollusc sample was

subjected to the described procedure in triplicate and two reagent blanks were prepared for each batch.

6.2.6.2 Caco-2 cell culture and *in vitro* Caco-2 transport assay

Caco-2 cells were maintained in DMEM supplemented with 10% (v/v) fetal bovine serum, 2 mM L-glutamine, 1% (v/v) penicillin/ streptomycin, 1 mM sodium pyruvate and 1 mM non-essential aminoacids (NEAA) at 37 °C under controlled atmosphere with 95% relative humidity and 5% CO_2 flow. The medium was changed every 2 or 3 days until reaching 80% confluence. The cells were detached with 0.5 g L^{-1} trypsin and resuspended in DMEM and seeded (7.5×10^4 cells cm^{-2}) on polyester membrane inserts in 6-well plates (Transwell®). The well is divided, by the insert, into two compartments: the apical (upper) and the basolateral (lower) chambers that simulate the intestinal lumen and the serous cavity, respectively. Resuspended cells (1.5 mL) were then added to the apical chamber and 2 mL of DMEM were added to the basolateral chamber. To obtain a monolayer of Caco-2 cells, the Transwell® is placed in a temperature-controlled chamber (37 °C, 95% relative humidity and 5% CO_2 flow) and the medium was changed every 3 days. The transepithelial electrical resistance (TEER) was measured to evaluate the progress of cell monolayer formation, and a value of 250 mΩ cm^2 of TEER was considered suitable.

The bioaccessible fraction (7.5 mL) obtained after the *in vitro* digestion procedure (Section 6.2.6.1) was heated in water bath for 5 min at 90 °C to decompose the residual gastrointestinal enzymes (enzymatic activity avoidance). Glucose was added at 1 g L^{-1} and the osmolarity required for cell viability was set to 300±25 mOsm kg^{-1} by dropwise addition of 5 mM NaCl solution. The transport assay was performed by adding 1.5 mL of treated bioaccessible and Lucifer Yellow to the apical chamber and 2 mL of HBSS to the basolateral chamber. The Transwell® was incubated under the same conditions of temperature, humidity and CO_2 detailed above for 2 h. The apical and basolateral solutions were carefully removed and stored until analysis. The cell monolayer was also recovered by adding 1.0 mL of PBS to the apical chamber for washing prior to the cells' detachment with trypsin (37 °C, 95% relative humidity, 5% CO_2 flow, 4 min).

Each mollusc sample was prepared in duplicate (bioaccessible fraction) and each bioaccessible fraction was subjected to the *in vitro* Caco-2 digestion (transport assay) in triplicate. Therefore, transport is given as the mean of six independent measurements for each mollusc. Two reagent blanks were subjected to the same procedure in each assay batch.

6.2.7 Ti and Ag determination by ICP-MS

Determination of Ti and Ag in acid digests (total Ti and Ag contents), in the bioaccessible fraction (bioaccessible Ti and Ag contents) and in solutions from Caco-2 *in vitro* assays (apical and basal samples from biodistribution study and bare cells solutions as controls) were performed by ICP-MS under the operating instrumental conditions listed in Table S6.3 (supplementary material). Ge and Rh were used as internal standards for Ti and Ag determination, respectively. The standard addition calibration method covering Ti and Ag concentrations within the 0-200 μg L^{-1} range was used for measurements.

The limits of detection (LOD) and quantification (LOQ) were defined as LOD 3SD/m and LOQ 10SD/m, where *SD* is the standard deviation of eleven measurements of a blank and *m* is the slope of the standard addition curve, respectively. Regarding total Ti and Ag in molluscs (microwave assisted acid digestion and ICP-MS), the LOD and LOQ were 0.0317 and 0.106 μg g^{-1} for Ti and 0.0250 μg g^{-1} and 0.0830 μg g^{-1} for Ag, respectively. The LODs regarding Ti and Ag contents in the bioaccessible fraction and basolateral solution (*in vitro* digestion procedures and ICP-MS) were 0.0303 μg g^{-1} and 0.0140 μg g^{-1} for Ti and Ag, respectively, and the LOQs were 0.101 μg g^{-1} for Ti and 0.0456 μg g^{-1} for Ag.

6.2.8 TiO_2 NPs and Ag NPs determination by sp-ICP-MS

TiO_2 NPs and Ag NPs (particle number and size distributions) determinations were performed by ICP-MS operating in the single particle mode (sp-ICP-MS) under conditions summarized in Table S6.4 (supplementary material). Transport efficiency (TE%) was automatically assessed by Syngistix™ Nano Application software after measuring the sample introduction flow rate and analyzing a gold NPs certified reference material.

The LOD and LOQ obtained for TiO_2 NPs in the mollusc extracts were 5.28×10^6 and 1.76×10^7 NPs g^{-1}, respectively; and for Ag NPs were 4.17×10^6 (LOD) and 1.39×10^7 NPs g^{-1} (LOQ). The LOD and LOQ in the bioaccessible fraction were 2.35×10^4 and 7.85×10^4 NPs mL^{-1} for TiO_2 NPs, respectively; and 2.87×10^3 (LOD) and 9.58×10^3 NPs mL^{-1} (LOQ) for Ag NPs. Regarding the basolateral solutions, the LOD and LOQ for TiO_2 NPs were 6.70×10^3 and 2.23×10^4 NPs mL^{-1}, respectively, and 7.39×10^3 (LOD) and 2.46×10^4 NPs mL^{-1} (LOQ) for Ag NPs.

Finally, the LODs in size were 29.0 and 13.6 nm for TiO_2 NPs and Ag NPs, respectively, for all cases.

6.2.9 TEM for NPs internalization in Caco-2 cells

Caco-2 cells were seeded in 6-well plates (2 mL, 1×10^5 cells per well) and grown for 24 h at standard culture conditions. Then, 200 µL of the bioaccessible fractions (40 nm Ag NPs and 50 nm TiO_2 NPs standards and variegated scallop Z24) were added to cells. After 6 h of incubation, the NP-containing cells were washed three times with PBS, trypsinized and centrifuged at 1500 rpm for 4 min. Cell pellets were fixed with 500 µL of 1.5% (w/v) glutaraldehyde, then, included in an agar pellet, postfixed with osmium tetraoxide in 0.1 M cacodylate buffer at 1% (w/v) and, finally, pelletized with Eponate (Ted Pella Inc., California, USA). Cell sections were obtained with an ultramicrotome (UltraCut S, Leica Microsystems GmbH, Wetzlar, Germany) and were analyzed with TEM (JEOL JEM 1011, Japan).

6.3 RESULTS AND DISCUSSION

Despite there are several published papers regarding *in vitro* intestinal epithelium Caco-2 or co-culture of Caco-2 and HT29-MTX, NP uptake has been only evaluated using manufactured TiO_2 NPs and Ag NPs and E171 (mixed nano- and micro-sized TiO_2) [13-18]. There are not reports regarding *in vitro* studies for foodstuff containing NPs, and reported results for NPs slurries cannot be easily extrapolated to food since the digestion process of the latter is different and food matrix affect NPs dissolution and aggregation rates and may, therefore, influence NPs toxicity. In addition, results obtained from *in vitro* Caco-2 cells have demonstrated to be different when using NPs slurries or NPs slurries subjected to mixing with digestion simulation fluids (the latter showing a lower TiO_2 NPs uptake) [14]. Our results will be discussed in terms of bioaccessibility (maximum bioavailability) of total Ti and Ag, and TiO_2 NPs and Ag NPs from molluscs and, then, in terms of Ti and Ag, and TiO_2 NPs and Ag NPs Caco-2 transcellular transport.

6.3.1 Bioaccessibility of Ti and Ag from molluscs

The bioaccessibility percentages were calculated as given in the following equation:

$$\%\ \text{Bioaccessibility} = \frac{[\ ]_{Bioaccessible}}{[\ ]_{Total}} \times 100 \qquad \text{(Equation 6.1)}$$

where $[]_{Total}$ and $[]_{Bioaccessible}$ were the total concentration of Ti or Ag (microwave assisted acid digestion and ICP-MS assessment) and the concentration of Ti or Ag in the bioaccessible fraction (ICP-MS measurement) in mollusc samples, respectively.

As shown in Table 6.1, Ti was quantified in all studied samples, and the total Ti content varied from 0.252 μg g^{-1} (Z24) to 3.42 μg g^{-1} (N18). Nevertheless, Ag was quantified only in five out of ten samples under study (ABL, N18, OP, Z24 and Z28) with concentrations ranged from 0.0841 μg g^{-1} (N18) to 3.72 μg g^{-1} (Z28). The high Ag content in variegated scallop Z28 (frozen sample) could be attributed to an Ag-based additive used for conservation. The total Ti concentrations in the bioaccessible fractions (Table 6.1) varied between 0.0406 μg g^{-1} (B22) and 0.265 μg g^{-1} (N18). Ag was quantified only in the bioaccessible

fraction from razor clams (N18), oyster (OP) and the two variegated scallops (Z24 and Z28) samples, with total bioaccessible Ag ratios from 0.0208 μg g^{-1} (N18) to 0.754 μg g^{-1} (Z28). Therefore, bioaccessibility percentages (Table 6.1) vary from 2.9% (B22) to 89% (ABL) for Ti, and from 6.5% (OP) to 51% (Z24) for Ag, respectively.

6.3.2 Bioaccessibility of TiO_2 NPs and Ag NPs from molluscs

The bioaccessibility percentages were calculated according to Equation 6.1 but $[]_{Total}$ being now the TiO_2 NPs or Ag NPs concentrations in molluscs after the ultrasound enzymatic hydrolysis and sp-ICP-MS measurements, and $[]_{Bioaccessible}$ the concentration of TiO_2 NPs or Ag NPs in the bioaccessible fraction (sp-ICP-MS measurements).

Results show TiO_2 NPs concentrations between 2.36×10^7 and 1.25×10^8 NPs g^{-1} range, and Ag NPs from 5.92×10^8 to 1.85×10^9 NPs g^{-1}, respectively. As listed in Table 6.2, TiO_2 NPs have been quantified in all studied samples, but Ag NPs only in two samples (OP and Z28). Large mean sizes for TiO_2 NPs were ranged between 63 and 84 nm (Table 6.2) by sp-ICP-MS, and they are consequence of TiO_2 NPs agglomeration in the extract after enzymatic hydrolysis due to the presence of a high concentration of biomolecules (degraded proteins and excess of the enzymes used for sample pre-treatment) and salts (phosphate buffer to fix the optimum pH for enzymatic hydrolysis). TiO_2 NPs agglomeration has been previously reported when using simulated digestion conditions involving the presence of high chloride levels [35, 36]. Conversely, small Ag NPs (mean sizes of 25 and 26 nm) were found after sp-ICP-MS analysis.

Table 6.1. Total and bioaccessible concentrations of Ti and Ag in bivalve molluscs

	Ti			Ag		
	$[Ti]_{Total}$ (μg g^{-1})	$[Ti]_{Bioaccessible}$ (μg g^{-1})	Bioaccessibility (%)	$[Ag]_{Total}$ (μg g^{-1})	$[Ag]_{Bioaccessible}$ (μg g^{-1})	Bioaccessibility (%)
ABL	0.285±0.048	0.253±0.017	89±6	0.0983±0.0046	---[b]	---[b]
B22	1.42±0.07	0.0406±0.0065	2.9±0.5	---[a]	---[b]	---[b]
B28	1.85±0.08	0.148±0.069	8.0±3.8	---[a]	---[b]	---[b]
M	0.265±0.041	0.0741±0.018	28±6.9	---[a]	---[b]	---[b]
N18	3.42±0.19	0.265±0.063	7.7±1.8	0.0841±0.0078	0.0208±0.0014	25±2
N28	1.28±0.28	0.206±0.001	16±0	---[a]	---[b]	---[b]
OP	0.731±0.078	0.130±0.093	18±13	0.989±0.088	0.0644±0.0130	6.5±1.3
Z24	0.252±0.025	0.188±0.004	75±1	0.149±0.010	0.0758±0.0149	51±10
Z28	1.44±0.23	0.113±0.010	7.8±0.7	3.72±0.35	0.754±0.153	20±4

(a) Concentration lower than the LOQ of the method; (b) not determined

Results obtained for TiO_2 NPs in the bioaccessible fraction (Table 6.2) showed that TiO_2 NPs were bioaccessible in all studied samples, and the concentrations varied from 7.76×10^5 to 2.56×10^7 NPs per gram. Ag NPs were found to be bioaccessible in the OP and Z28 samples, and their concentrations in the bioaccessible fractions were between 9.92×10^7 and 2.38×10^8 NPs per gram (Table 6.2). This implies that bioaccessibility percentages were within 2.1-51% for TiO_2 NPs, and from 13 to 17% for Ag NPs, respectively. These bioaccessibility percentages are quite lower than those found for total Ti and total Ag (Section 6.3.1), which means that the small nanoparticulated fraction of Ti and Ag is less bioaccessible than the ionic Ti and Ag fraction.

Size distribution appears to be affected by the simulated digestion procedure (bioaccessibility assay) since slightly higher sizes (in the range of 25-40 nm) were measured for Ag NPs in the bioaccessible fractions than those found in the extracts from the samples (25-26 nm, Table 6.2). Certain differences in TiO_2 NPs size (48-136 nm in the bioaccessible fraction and 63-84 nm in the sample's extracts) have been also found.

Table 6.2. Total and bioaccessible concentrations and mean sizes of TiO_2 NPs and Ag NPs in bivalve molluscs

	TiO_2 NPs				
	Total		Bioaccessible fraction		
	NPs g^{-1}	Mean size (nm)	NPs g^{-1}	Mean size (nm)	Bioaccessibility (%)
ABL	$3.13\times10^{7}\pm7.00\times10^{6}$	78±1	$2.18\times10^{6}\pm3.35\times10^{5}$	136±12	7.0±1.1
B22	$2.88\times10^{7}\pm9.25\times10^{6}$	65±1	$1.05\times10^{6}\pm6.14\times10^{5}$	131±4	3.7±2.1
B28	$3.89\times10^{7}\pm8.64\times10^{6}$	77±1	$1.36\times10^{7}\pm8.72\times10^{6}$	106±2	24±8
M	$1.25\times10^{8}\pm1.06\times10^{7}$	84±19	$2.56\times10^{7}\pm3.64\times10^{6}$	48±1	21±3
N18	$7.56\times10^{7}\pm1.06\times10^{7}$	74±3	$8.07\times10^{6}\pm5.03\times10^{5}$	115±10	11±1
N28	$2.36\times10^{7}\pm2.54\times10^{6}$	83±2	$9.08\times10^{6}\pm3.36\times10^{6}$	113±6	42±20
OP	$3.77\times10^{7}\pm9.05\times10^{6}$	63±1	$7.76\times10^{5}\pm1.07\times10^{5}$	122±28	2.1±0.3
Z24	$4.39\times10^{7}\pm7.66\times10^{6}$	65±1	$2.24\times10^{7}\pm9.70\times10^{5}$	69±10	51±2
Z28	$8.13\times10^{7}\pm1.97\times10^{6}$	74±1	$8.73\times10^{6}\pm5.09\times10^{6}$	98±9	11±6

(a) Concentration lower than the LOQ of the method; (b) Not determined

Table 6.2. (Continued)

	Ag NPs				
	Total		Bioaccessible fraction		
	NPs g^{-1}	Mean size (nm)	NPs g^{-1}	Mean size (nm)	Bioaccessibility (%)
ABL	---[a]	---[b]	---[b]	---[b]	---[b]
B22	---[a]	---[b]	---[b]	---[b]	---[b]
B28	---[a]	---[b]	---[b]	---[b]	---[b]
M	---[a]	---[b]	---[b]	---[b]	---[b]
N18	---[a]	---[b]	---[b]	---[b]	---[b]
N28	---[a]	---[b]	---[b]	---[b]	---[b]
OP	$5.92\times10^{8}\pm1.41\times10^{7}$	25±2	$9.92\times10^{7}\pm3.99\times10^{7}$	25±1	17±7
Z28	$1.85\times10^{9}\pm2.88\times10^{8}$	26±3	$2.38\times10^{8}\pm3.23\times10^{7}$	40±3	13±2

(a) Concentration lower than the LOQ of the method; (b) Not determined

6.3.3 Ti and Ag transcellular transport in Caco-2 culture

Bioavailability of total Ti and Ag in molluscs was estimated using an intestinal epithelium model and studying the transport across intestinal epithelium (Caco-2 cells monolayer). Transport percentage is given by:

$$\%\ \text{Transport} = \frac{[\ ]_{Basal}}{[\ ]_{Bioaccessible}} \times 100 \qquad \text{(Equation 6.2)}$$

where $[]_{Basal}$ is the concentration of total Ti or Ag in basolateral solution after incubating at 37 °C (95% relative humidity and 5% CO_2 flow) for 2 h, and $[]_{Bioaccessible}$ is the total concentration in the bioaccessible fraction (initial solution of each treated bioaccessible according to Section 6.2.6.2).

The bioavailability of Ti, estimated as the percentage of Ti that was able to cross the intestinal cell monolayer (Figure 6.1), varied from 18% (B28) to 68% (OP) with a mean value of 35±18%. The Ti content in the basal chamber was lower than the LOD of the method (0.202 µg Ti L^{-1}) for B22, M and N18 samples. Ag was only quantified (concentrations higher than the LOQ of 0.304 µg Ag L^{-1}) in two samples (ABL and Z28), and the percentages of Ag transported were very low, 0.016 and 0.017% for ABL and Z28, respectively. Results showed that Ti can cross the epithelium membrane, meanwhile Ag absorption is very poor. Ag NPs in the molluscs are degraded to ionic Ag during the *in vitro* gastrointestinal procedure, which show a very low transcellular transport. The low transport percentages of Ag (ionic silver and Ag NPs) agree with those previously obtained by Abdelkhaliq et al. [18], who reported limited transport of silver as either total Ag or Ag NPs (<0.1%) after cell exposure to pristine Ag NPs and Ag NPs previously subjected to an *in vitro* gastrointestinal digestion process. These observations were mainly attributed to the significant fraction of Ag NPs that was dissolved during the *in vitro* digestion (86-92% and 48-70% for Ag NPs standards with lipoic acid and citrate coatings, respectively) [18].

6.3.4 TiO_2 NPs and Ag NPs transcellular transport in Caco-2 culture

Following the same procedure that in the former bioavailability study of Ti and Ag, a NPs transport assay with Caco-2 cells (Equation 6.2) was performed by characterizing (concentration and size distribution) TiO_2 NPs and Ag NPs by sp-ICP-MS. TiO_2 NPs were detected in all samples, except in basolateral solutions from edible cockle B22 and razor clam N18. Ag NPs were only detected in basal fractions from OP and Z28 samples. The percentage of TiO_2 NPs transported across the cellular monolayer was ranged between 17% (B28) and 82% (OP) (Figure 6.1); meanwhile, Ag NPs transport was 22±3% for the oyster (OP) sample and 2.1±0.7% for a variegated scallop (Z28). Transport through the intestinal barrier of TiO_2 NPs from digested bivalve molluscs (bioaccessible fraction) have been found to be higher than rates previously reported by other authors for TiO_2 NPs standards [14, 37]. In addition to the nature of the tested apical solutions (TiO_2 NPs contained in molluscs in our study and TiO_2 NPs standards in published papers), differences can be also attributed to the fact that the TiO_2 NPs standards were not submitted to the *in vitro* gastrointestinal digestion (TiO_2 standards directly used as slurries [34] or TiO_2 standards matched with a digestive fluid [35]). Differences on the transport of Ag NPs standards have been also reported by Abdelkhaliq et al. [18], who found lower Ag NPs transport when submitting Ag NPs to an *in vitro* digestion process in comparison with pristine Ag NPs.

Similar transport rates have been measured for total Ti (18-68%) and TiO_2 NPs (17-82%); however, quite different transport ratios were found for total Ag (0.016-0.017%) and Ag NPs (2.1-22%). As commented above, ionic Ag is poorly bioavailable (limited transcellular transport), but the small amounts of Ag NPs which remains in the bioaccessible fraction show a moderate transport through the cell barrier (bioavailability). On the other hand, Ag NPs were detected in the basolateral solutions from sample OP, but not total Ag. This finding is attributed to the better (lowest) LOD when assessing Ag NPs by sp-ICP-MS (instrumental LOD of 7.39×10^3 NPs mL^{-1}) than the LOD for total Ag determination by ICP-MS (instrumental LOD of 0.0912 µg Ag L^{-1}). Same situation was observed in mussels (M) for Ti

and TiO_2 NPs determination. Results for Ag NPs are different from those previously reported for Ag NPs standards when using the respective Ag NPs slurries [15, 17, 18] and *in vitro* digested Ag NPs [18], and the higher transcellular transport measured in our work must be related to mollusc matrix's components released during the *in vitro* procedure, which definitely affect transport through the cell monolayer.

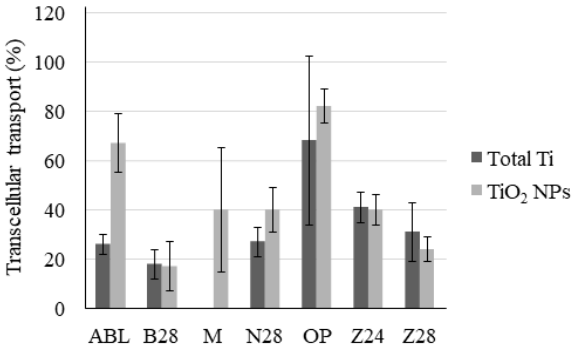

Figure 6.1. Transcellular transport (%) across Caco-2 monolayer of total Ti and TiO_2 NPs

Both TiO_2 NPs and Ag NPs size distributions have been found to be different in the apical (treated bioaccessible fraction) and basolateral and resuspended cells solutions (Figure 6.2 and 6.3). The Ag NPs mean size (Figure 6.2) in the bioaccessible solution was higher than the sizes in the apical, basolateral and resuspended cell solutions. Ag NPs size appears to affect the transcellular transport since the mean Ag NPs sizes in the basolateral and resuspended cell solutions are smaller than those mean sizes found in the apical solution probably due to the better mobility of lower-size NPs through the junctions of the cell monolayer.

Regarding TiO_2 NPs, results show a similar trend than that those observed for Ag NPs for OP and Z24 samples (Figure 6.3), that is, TiO_2 NPs mean sizes in the bioaccessible solution is higher than those found in the apical, basolateral and re-suspended solutions. However, data are different for mussel (M) for which the TiO_2 NPs mean size is smaller in the bioaccessible fraction and resuspended cell solution than in the apical and basolateral fractions.

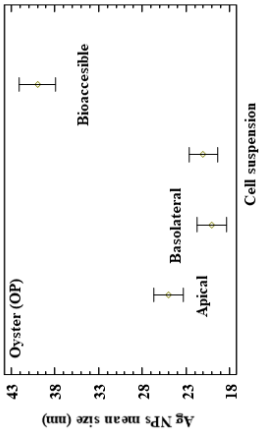

Figure 6.2. Ag NPs mean sizes (mean±SD, n=6) in apical and basolateral fractions, resuspended cell solution and bioaccessible fraction in OP sample

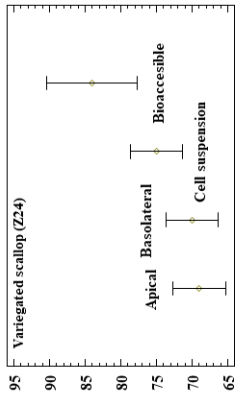

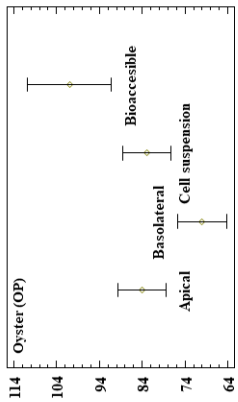

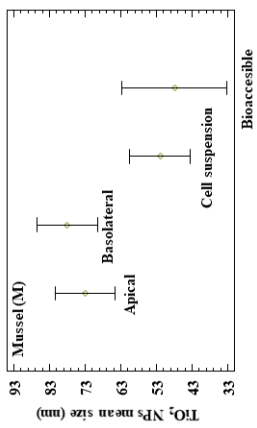

Figure 6.3. TiO_2 NPs mean sizes (mean±SD, n=6) in apical and basolateral fractions, resuspended cell solution and bioaccessible fraction in M, OP and Z24 samples

6.3.5 TiO_2 NPs and Ag NPs internalization in the Caco-2 cell monolayer

To confirm the successful incorporation of the administered NPs inside the cells, transmission electron microscopy (TEM) images were taken. It was possible to observe that control Ag NPs and TiO_2 NPs could be efficiently up-taken by the Caco-2 cells, whereas those taken from scallop extract were incorporated to a lesser extent. However, it is necessary to mention that, at a first glance, NPs seem to suffer from degradation process provided that their sizes appear to be quite smaller than the expected values. At this respect, Ag NPs standards (ca. 40 nm theoretical size) (Figure 6.4A) appeared as small dots of ca. 10-15 nm dispersed along the cell cytoplasm and entrapped inside vesicles (ca. 30-60 nm), particularly lysosomes and autophagosomes. In the case of TiO_2 NPs (Figure 6.4B), the presence of encapsulated particles inside endocytic vesicles is observed. The observation of some vesicles quite near the cell membrane would agree with a potential cell uptake regulated by an endocytic pathway. Finally, for NPs from the scallop extract (Figure 6.4C), the extent of NPs inside cells is scarce and the particles appear quite clustered inside a few vesicles along the cell cytoplasm.

6.4 CONCLUSIONS

Bivalve molluscs containing TiO_2 NPs and Ag NPs were subjected to an *in vitro* gastrointestinal digestion to determine the bioaccessibility of these NPs. Caco-2 cells were selected as human intestinal epithelium model to perform bioavailability studies. Bioaccessibility and bioavailability were assessed for total Ti and Ag (ICP-MS), and for TiO_2 NPs and Ag NPs (sp-ICP-MS).

Bioaccessibility percentages were within the 2.9-89% and 2.1-51% ranges for total Ti and TiO_2 NPs, respectively. Bioaccessibility values for Ag and Ag NPs were between 6.5-51% and 13-17%. Bioaccessibility ratios for NPs are quite lower than those found for total Ti and total Ag, which means that the small nanoparticulated fraction of Ti and Ag is less bioaccessible than the ionic Ti and Ag fraction.

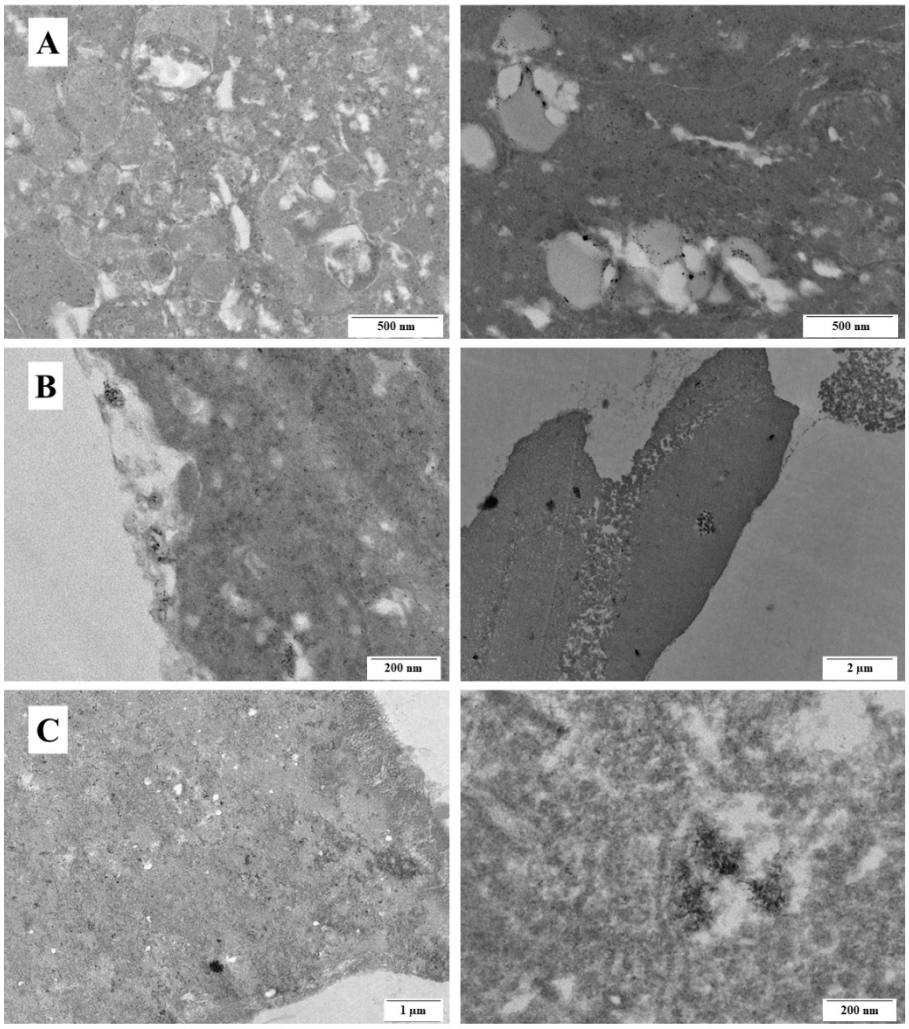

Figure 6.4. Internalization of A) 40 nm Ag NPs standard, B) 50 nm TiO_2 NPs standard and C) NPs from variegated scallop (Z24) extract in the Caco-2 cell monolayer

Regarding transport studies, we found values between 18 and 68% for Ti, and 17 and 82% for TiO_2 NPs. The bioavailability percentages for Ag and Ag NPs were within the 0.016-0.017% and 2.1-22% ranges, respectively. Results show that whereas Ag absorption is very poor, Ti can cross the intestinal membrane. Similar bioavailability percentages

were found in Ti and TiO_2 NPs, while significant differences were detected between Ag and Ag NPs. Most Ag NPs in the molluscs are degraded to ionic Ag during the *in vitro* gastrointestinal procedure, which is little bioavailable. The small amounts of Ag NPs which remains in the bioaccessible fraction show a moderate transport. Size distributions in bioaccessible fractions were higher than in apical, basolateral and cellular fractions for most of analyzed samples. Differences in NPs transport rates between standards and samples evidence the importance of the sample matrix components.

Internalization studies have shown that Ag NPs standard appeared as small dots dispersed along the cell cytoplasm and entrapped inside lysosomes and autophagosomes. In the case of TiO_2 NPs standard, we observed encapsulated particles inside endocytic vesicles. NPs from the scallop extract were less internalized than standards and only a few particles appear clustered in vesicles along the cell cytoplasm.

Acknowledgements

The authors wish to acknowledge the financial support of the Ministerio de Economía y Competitividad (project INNOVANANO, reference RT2018-099222-B-100), the European Union (Interreg Atlantic Area, project NANOCULTURE, reference EAPA590/2018), and the Xunta de Galicia (Grupo de Referencia Competitiva, grant number ED431C2018/19; and Program for Development of a Strategic Grouping in Materials – AEMAT, grant number ED431E2018/08). M.V. Taboada-López would like to thank the Xunta de Galicia and the European Social Fund (FSE) for the pre-doctoral grant.

6.5 REFERENCES

[1] The European Commission. Commission, Recommendation (EU) 2011/696 of 18 October 2011 on the definition of nanomaterial, Official Journal of the European Union L 275, 58 (2011) 38–40.

[2] J. Curtis, M. Greenberg, J. Kester, S. Phillips, G. Krieger, Nanotechnology and nanotoxicology: a primer for clinicians, Toxicol. Rev. 25 (2006) 245–260.

[3] M. Nasrollahzadeh, S.M. Sajadi, M. Sajjadi, Z. Issaabadi, An Introduction to Nanotechnology, in M. Nasrollahzadeh, M. Sajadi, M. Atarod, M. Sajjadi, Z. Isaabadi (Ed.), An Introduction to Green Nanotechnology, Academic Press, Massachusetts, USA, 2019, pp. 1–27.
[4] A. Zielińska, B. Costa, M.V. Ferreira, D. Miguéis, J.M.S. Louros, A. Durazzo, M. Lucarini, P. Eder, M.V. Chaud, M. Morsink, N. Willemen, P. Severino, A. Santini, E.B. Souto, Nanotoxicology and nanosafety: Safety-by-design and testing at a glance, Int. J. Environ. Res. Public Health. 17 (2020) 4657–4680.
[5] S. Jahan, I. Bin Yusoff, Y.B. Alias, A.F.B.A. Bakar, Reviews of the toxicity behavior of five potential engineered nanomaterials (ENMs) into the aquatic ecosystem, Toxicol. Reports 4 (2017) 211–220.
[6] C. Faggio, V. Tsarpali, S. Dailianis, Mussel digestive gland as a model tissue for assessing xenobiotics: An overview, Sci. Total Environ. 636 (2018) 220–229.
[7] C. Yin, W. Zhao, R. Liu, R. Liu, Z. Wang, L. Zhu, W. Chen, S. Liu, TiO_2 particles in seafood and surimi products: Attention should be paid to their exposure and uptake through foods, Chemosphere 188 (2017) 541–547.
[8] M.V. Taboada-López, S. Iglesias-López, P. Herbello-Hermelo, P. Bermejo-Barrera, A. Moreda-Piñeiro, Ultrasound assisted enzymatic hydrolysis for isolating titanium dioxide nanoparticles from bivalve mollusc before sp-ICP-MS, Anal. Chim. Acta 1018 (2018) 16–25.
[9] M.V. Taboada-López, N. Alonso-Seijo, P. Herbello-Hermelo, P. Bermejo-Barrera, A. Moreda-Piñeiro, Determination and characterization of silver nanoparticles in bivalve molluscs by ultrasound assisted enzymatic hydrolysis and sp-ICP-MS, Microchem. J. 148 (2019) 652–660.
[10] E. Fröhlich, E. Roblegg, Oral uptake of nanoparticles: human relevance and the role of *in vitro* systems, Arch. Toxicol. 90 (2016) 2297–2314.
[11] C. McCracken, P.K. Dutta, W.J. Waldman, Critical assessment of toxicological effects of ingested nanoparticles, Environ. Sci.: Nano 3 (2016) 256–282.

[12] M.J. Rein, M. Renouf, C. Cruz-Hernandez, L. Actis-Goretta, S.K. Thakkar, M. da Silva Pinto, Bioavailability of bioactive food compounds: A challenging journey to bioefficacy, Brit. J. Clin. Pharmaco. 75 (2013) 588–602.
[13] C. Gitrowski, A.R. Al-Jubory, R.D. Handy, Uptake of different crystal structures of TiO_2 nanoparticles by Caco-2 intestinal cells, Toxicol. Lett. 226 (2014) 264–276.
[14] Z.M. Song, N. Chen, J.H. Liu, H. Tang, X. Deng, W.S. Xi, K. Han, A. Cao, Y. Liu, H. Wang, Biological effect of food additive titanium dioxide nanoparticles on intestine: an *in vitro* study, J. Appl. Toxicol. 35 (2015) 1169–1178.
[15] L. Vila, A. García-Rodríguez, C. Cortés, R. Marcos, A. Hernández, Assessing the effects of silver nanoparticles on monolayers of differentiated Caco-2 cells, as a model of intestinal barrier, Food Chem. Toxicol. 116 (2018) 1–10.
[16] S. Imai, Y. Morishita, T. Hata, M. Kondoh, K. Yagi, J.Q. Gao, K. Nagano, K. Higashisaka, Y. Yoshioka, Y. Tsutsumi, Cellular internalization, transcellular transport, and cellular effects of silver nanoparticles in polarized Caco-2 cells following apical or basolateral exposure, Biochem. Bioph. Res. Co. 484 (2017) 543–549.
[17] M. Saez-Tenorio, J. Domenech, A. García-Rodríguez, A. Velázquez, A. Hernández, R. Marcos, C. Cortés, Assessing the relevance of exposure time in differentiated Caco-2/HT29 cocultures. Effects of silver nanoparticles, Food Chem. Toxicol. 123 (2019) 258–267.
[18] A. Abdelkhaliq, M. van der Zande, A.K. Undas, R.J.B. Peters, H. Bouwmeester, Impact of *in vitro* digestion on gastrointestinal fate and uptake of silver nanoparticles with different surface modifications, Nanotoxicology 14 (2020) 111–126.
[19] P. Pedata, G. Riccia, L. Malorni, A. Venezia, M. Cammarota, M.G. Volpe, N. Iannaccone, V. Guida, C. Schiraldi, M. Romano, G. Iacomino, *In vitro* intestinal epithelium responses to titanium dioxide nanoparticles, Food Res. Int. 119 (2019) 634–642.
[20] M. Dorier, C. Tisseyre, F. Dussert, D. Beal, M.E. Arnal, T. Douki, V. Valdiglesias, B. Laffonb, S. Fraga, F. Brandaoc, N. Herlin-Boime, F. Barreau, T. Rabilloud, M. Carriere, Toxicological impact of acute exposure to E171 food additive and TiO_2 nanoparticles on a co-culture

of Caco-2 and HT29-MTX intestinal cells, Mutat. Res. Gen. Tox. En. 845 (2019) 402980 (DOI: 10.1016/j.mrgentox.2018.11.004).
[21] M. Dorier, D. Béal, C. Tisseyre, C. Marie-Desvergne, M. Dubosson, F. Barreau, E. Houdeau, N. Herlin-Boime, T. Rabilloud, M. Carriere, The food additive E171 and titanium dioxide nanoparticles indirectly alter the homeostasis of human intestinal epithelial cells *in vitro*, Environ. Sci. Nano 6 (2019) 1549–1561.
[22] A. García-Rodríguez, L. Vila, C. Cortés, A. Hernández, R. Marcos, Effects of differently shaped TiO_2NPs (nanospheres, nanorods and nanowires) on the *in vitro* model (Caco-2/HT29) of the intestinal barrier, Part. Fibre Toxicol. 15 (2018) 33 (DOI: 10.1186/s12989-018-0269-x).
[23] K. Krüger, K. Schrader, M. Klempt, Cellular Response to Titanium Dioxide Nanoparticles in Intestinal Epithelial Caco-2 Cells is Dependent on Endocytosis-Associated Structures and Mediated by EGFR, Nanomaterials 7 (2017) 79 (DOI: 10.3390/nano7040079).
[24] K. Krüger, F. Cossais, H. Neve, M. Klempt, Titanium dioxide nanoparticles activate IL8-related inflammatory pathways in human colonic epithelial Caco-2 cells, J. Nanopart. Res. 16 (2014) 2402–2414.
[25] B.A. Koeneman, Y. Zhang, P. Westerhoff, Y. Chen, J.C. Crittenden, D.G. Capco, Toxicity and cellular responses of intestinal cells exposed to titanium dioxide, Cell. Biol. Toxicol. 26 (2010) 225–238.
[26] S. Tada-Oikawa, G. Ichihara, H. Fukatsu, Y. Shimanuki, N. Tanaka, E. Watanabe, Y. Suzuki, M. Murakami, K. Izuoka, J. Chang, W. Wu, Y. Yamada, S. Ichihara, Titanium Dioxide Particle Type and Concentration Influence the Inflammatory Response in Caco-2 Cells, Int. J. Mol. Sci. 17 (2016) 576–588.
[27] I. Singh Sohal, G.M. DeLoid, K.S. O'Fallon, P. Gaines, P. Demokritou, D. Bello, Effects of ingested food-grade titanium dioxide, silicon dioxide, iron (III) oxide and zinc oxide nanoparticles on an *in vitro* model of intestinal epithelium: Comparison between monoculture vs. a mucus-secreting coculture model, NanoImpact 17 (2020) 100209 (DOI: 10.1016/j.impact.2020.100209).
[28] N. Chen, Z.M. Song, H. Tang, W.S. Xi, A. Cao, Y. Liu, H. Wang, Toxicological effects of Caco-2 cells following short-term and long-term exposure to Ag nanoparticles, Int. J. Mol. Sci. 17 (2016) 974–991.

[29] M. Polet, L. Laloux, S. Cambier, J. Ziebel, A.C. Gutleb, Y.J. Schneider, Soluble silver ions from silver nanoparticles induce a polarised secretion of interleukin-8 in differentiated Caco-2 cells, Toxicol. Lett. 325 (2020) 14–24.
[30] S.C. Sahu, J. Zheng, L. Graham, L. Chen, J. Ihrie, J.J. Yourick, R.L. Sprando, Comparative cytotoxicity of nanosilver in human liver HepG2 and colon Caco2 cells in culture J. Appl. Toxicol. 34 (2014) 1155–1166.
[31] A.A.M. Kämpfer, P. Urbán, R. La Spina, I. Ojea Jiménez, N. Kanase, V. Stone, A. Kinsner-Ovaskainen, Ongoing inflammation enhances the toxicity of engineered nanomaterials: Application of an *in vitro* co-culture model of the healthy and inflamed intestine, Toxicol. In Vitro 63 (2020) 104738 (DOI: 10.1016/j.tiv.2019.104738).
[32] F. Laborda, J. Jiménez-Lamana, E. Bolea, J.R. Castillo, Critical considerations for the determination of nanoparticle number concentrations, size and number size distributions by single particle ICP-MS, J. Anal. At. Spectrom. 28 (2013) 1220–1232.
[33] D.M. Schwertfeger, J.R. Velicogna, A.H. Jesmer, R.P. Scroggins, J.I. Princz, Single Particle-Inductively Coupled Plasma Mass Spectroscopy Analysis of Metallic Nanoparticles in Environmental Samples with Large Dissolved Analyte Fractions, Anal. Chem. 88 (2016) 9908–9914.
[34] S.A. Pergantis, T.L. Jones-Lepp, E.M. Heithmar, Hydrodynamic chromatography online with single particle-inductively coupled plasma mass spectrometry for ultratrace detection of metal-containing nanoparticles, Anal. Chem. 84 (2012) 6454–6462.
[35] W. Utembe, K. Potgieter, A. Byron Stefaniak, M. Gulumian, Dissolution and biodurability: Important parameters needed for risk assessment of nanomaterials, Part. Fibre Toxicol. 12 (2015) 11 (DOI: 10.1186/s12989-015-0088-2).
[36] L. Zhong, Y. Yu, H.Z. Lian, X. Hu, H. Fu, Y.J. Chen, Solubility of nano-sized metal oxides evaluated by using *in vitro* simulated lung and gastrointestinal fluids: implication for health risks, J. Nanopart. Res. 19 (2017) 375–385.
[37] J.S. Hwang, J. Yu, H.M. Kim, J.M. Oh, S.J. Choi, Food Additive Titanium Dioxide and Its Fate in Commercial Foods, Nanomaterials 9 (2019) 1175–1194.

6.6 SUPPLEMENTARY INFORMATION

Table S6.1. Ultrasound assisted enzymatic hydrolysis conditions for TiO_2 NPs extraction from bivalve molluscs

Parameter	*Value*
Mass of sample	1.0 g
Pancreatin and lipase concentration	3.0 g L^{-1}
Volume of enzymatic solution	7.5 mL
Ultrasonication amplitude	60%
Ultrasonication time	10 min
Ultrasonication Mode	Continuous

Table S6.2. Ultrasound assisted enzymatic hydrolysis conditions for Ag NPs extraction from bivalve molluscs

Parameter	*Value*
Mass of sample	1.0 g
Pancreatin and lipase concentration	2.0 g L^{-1}
Volume of enzymatic solution	10 mL
Ultrasonication amplitude	80%
Ultrasonication time	10 min
Ultrasonication Mode	Continuous

Table S6.3. Operating ICP-MS parameters for total Ti and Ag determination

	Ti	*Ag*
Parameter	*Value*	*Value*
Nebulization Gas Flow	0.95 mL min^{-1}	0.87 mL min^{-1}
Auxiliary Gas Flow	1.2 mL min^{-1}	1.2 mL min^{-1}
Plasma Gas Flow	16 mL min^{-1}	16 mL min^{-1}
Radiofrequency power	1600 W	1600 W
Analyte (m/z)	48.9479	106.905
IS (m/z)	73.9211	102.905

Table S6.4. Operating sp-ICP-MS parameters for TiO_2 NPs and Ag NPs determination

Operating parameters regarding single particle measurements		
Analyte	Ti	Ag
Mass	48.9479 uma	106.905 uma
Density	4.23 g cm^{-3}	10.49 g cm^{-3}
Mass Fraction	59.9 %	100 %
Ionization efficiency	100 %	100 %
Sample Flow Rate	0.41–0.45 mL min^{-1}	0.41–0.45 mL min^{-1}
Dwell time	100 µs	50 µs
Sampling time	100 s	100 s
Mode	Standard	Standard
Operating conditions of ICP-MS		
Nebulization gas flow: 0.95 mL min^{-1}; Auxiliary gas flow:1.2 mL min^{-1}; Plasma gas flow: 16 mL min^{-1}; Radiofrequency power: 1600 W		

USC
UNIVERSIDADE
DE SANTIAGO
DE COMPOSTELA

PART IV. CHARACTERIZATION OF NPS PROTEIN CORONA IN HEMOLYMPH OF BIVALVE MOLLUSCS

USC
UNIVERSIDADE
DE SANTIAGO
DE COMPOSTELA

CHAPTER 7

TITANIUM DIOXIDE NANOPARTICLES PROTEIN CORONA CHARACTERIZATION AND QUANTIFICATION IN HEMOLYMPH OF BIVALVE MOLLUSCS

MARÍA VANESA TABOADA-LÓPEZ, ISABEL PAZ-VILARCHAO, RAQUEL DOMÍNGUEZ-GONZÁLEZ, PILAR BERMEJO-BARRERA AND ANTONIO MOREDA-PIÑEIRO

USC
UNIVERSIDADE
DE SANTIAGO
DE COMPOSTELA

7 TITANIUM DIOXIDE NANOPARTICLES PROTEIN CORONA CHARACTERIZATION AND QUANTIFICATION IN HEMOLYMPH OF BIVALVE MOLLUSCS

María Vanesa Taboada-López, Isabel Paz-Vilarchao, Raquel Domínguez-González, Pilar Bermejo-Barrera, Antonio Moreda-Piñeiro

Trace Element, Spectroscopy and Speciation Group (GETEE), Strategic Grouping in Materials (AEMAT), Department of Analytical Chemistry, Nutrition and Bromatology. Faculty of Chemistry. Universidade de Santiago de Compostela. Avenida das Ciencias, s/n. 15782 – Santiago de Compostela, Spain.

Abstract

Due to their high reactivity, nanoparticles (NPs) in contact with biological mediums form a shell of proteins on their surface. This structure is called "protein corona" and it is divided into "soft corona" (low affinity proteins), "hard corona" (high affinity proteins) and "interfacial corona". Protein corona formation affects the properties of NPs and their further behavior. A mesocosm system using clams as bio-indicators has been used to expose clams to commercial titanium dioxide nanoparticles (TiO_2 NPs) standards of several size distributions and nano- and micro-titanium from the food additive E171. TiO_2 NPs-protein corona complexes were studied in the hemolymph. Four independent tanks were settled (one control, one for 50 nm TiO_2 NPs, one for 100 nm TiO_2 NPs and one for E171) with 30 specimens in each tank. Filtered marine water was used as a medium, and an aeration system was installed in all tanks. Clams were fed every two days with *in vitro* cultured phytoplankton. TiO_2 NPs concentrations were increased progressively from 0 to 14 mg L^{-1} (2 mg L^{-1} increments) for eighteen days. One specimen per tank was sampled before any addition, at the ninth day of exposure and at the last day of the experiment

(eighteenth day). Hemolymph, extracted from each sampled clam, was subjected to centrifugation for separating bound (pellet) and non-bound proteins (supernatant). Then, evolution in the profile of protein corona over time was studied in re-suspended pellets by liquid chromatography coupled with tandem mass spectrometry (LC-MS/MS) for protein identification, and by sequential window acquisition of all theoretical spectra-mass spectrometry (SWATH-MS) for protein quantification.

Keywords
Titanium dioxide nanoparticles, clams, hemolymph, protein corona, SWATH-MS

7.1 INTRODUCTION

The European Commission (EC) defines a nanomaterial (NM) as a natural, incidental or manufactured material containing unbound particles or aggregates where 50% or more of the particles have one or more external dimensions in the size range of 1-100 nm [1]. Nowadays, there are more than 1800 listed consumer products which contain NMs [2] and their widespread utilization implies the unavoidable release to the environment. At the same time, there is no clear information about the effects of this "nanowaste" on humans or environment, so studies related to nanotoxicology are becoming urgent [3].

More than 90 of the aforementioned listed products contain titanium dioxide nanoparticles (TiO_2 NPs) [2]. Similar to bulk TiO_2, their respective NPs have high visible light reflectance and no absorption in the visible region, so they are used as pigments in paints, coatings, plastics, inks, foods, medicines and toothpastes. TiO_2 NPs can be used also in sunscreens and personal care products because they are UV blockers [4], in the energy sector (hydrogen storage, photovoltaics…) and also in sensors [5]. TiO_2 NPs are also present in the food additive E171 since several studies have shown that E171 contains TiO_2 NPs in a number-based fraction of 17-36% [6, 7].

Due to the high surface reactivity of NPs, macromolecules (proteins, lipids and polysaccharides) present in biological fluids tend to be absorbed onto NPs surfaces. The formed complex is called "biological corona" and,

more specifically, absorbed proteins form the "protein corona". Protein corona formation is a dynamic process, so the composition of corona changes over time. High abundance proteins are first absorbed, but then, they are replaced by low abundance proteins with exhibit a high affinity to NPs (Vroman effect). Protein corona can be divided in "hard corona", "soft corona" and "interfacial corona". Hard corona is formed by high affinity proteins whose residence times are high, so its composition is more stable. Soft corona consists of low affinity proteins which are not close to NPs and are more exchangeable. Interfacial corona is the layer of hard corona tightly bound on NPs [8]. It comprises a combination of NP-protein (interfacial and hard corona) and protein-protein (soft corona) interactions. These interactions imply association constants related to the NP-protein contact frequency, whereas dissociation constants depend on the binding energy of the complexes [9]. Van der Waals, H-bonds, electrostatic, hydrophobic and π-π stacking are the main interactions that contribute to corona formation [10]. This process is conditioned by intrinsic properties of the NPs and by the biological environment [11, 12]. The presence of NPs can affect the activity of specific proteins during the formation of protein corona promoting conformational changes, misfolding or aggregation [13, 14]. Besides, proteins can cause changes in the properties of NPs [13]. Understanding protein corona nature is essential to predict the behavior of NPs in biological systems since the formation of these complexes gives NPs a new biological identity which controls their interactions and, therefore, their biological fate, distribution and toxicity [15-17].

There are some experiments regarding protein corona formation after the *in vitro* exposure of NPs to hemolymph of marine invertebrates [18, 19] and plasma from fish [20, 21]. Assays have led to the identification of putative C1q domain containing protein (MgC1q6) as the only component of the hard corona when exposing hemolymph of mussel (*Mytilus galloprovincialis*) to polystyrene NPs (PS-NPs) [18]. *In vitro* experiments with hemolymph of *M. galloprovincialis* have also shown a protein corona of Cu, Zn-superoxide dismutase for negative charge CeO_2 NPs, whereas neutral charged CeO_2 NPs did not form any corona [19]. Finally, the composition of polyvinylpyrrolidone-coated silver NPs (PVP-Ag NPs) protein corona has been reported to be gender-specific since egg-specific

proteins such vitellogenin (VTG) and zona pellucida (ZP) were found to form a soft corona during *in vitro* experiments with plasma of smallmouth bass (*Micropterus dolomieu*) [20]. VTG was also reported to form part of corona after *in vitro* experiments with SiO_2 NPs exposed to zebrafish plasma, verifying also the evidence of sex-specific NP uptake [21]. As can be seen, published studies imply *in vitro* experiments for assessing protein corona in NPs exposed to biological fluids (plasma from fish and hemolymph from mussels), but studies regarding protein corona in hemolymph from specimens previously exposed to NPs have not been reported.

Before analyzing protein corona composition, its separation from non-bound NPs and proteins is required. Separation techniques such as centrifugation, size exclusion chromatography, cloud point extraction, differential centrifugal sedimentation, capillary electrophoresis and gel electrophoresis are applicable. Centrifugation is commonly used because it is low time-consuming and affordable, allowing corona complexes sedimentation at the bottom (pellet) and isolation from free compounds which remains in the supernatant. Pellets can be washed to remove remaining unbound NPs or proteins before protein corona qualitative characterization by sodium dodecyl sulphate-polyacrylamide gel electrophoresis (SDS-PAGE) or qualitative and quantitative analysis by mass spectrometry (MS)-based techniques [10, 22, 23].

In this study, we propose a mesocosm system using clams as bio-indicators to evaluate the protein corona formation around TiO_2 NPs in hemolymph samples. Commercial standards of different nominal sizes (50 and 100 nm) and food additive E171, containing nano- and micro-titanium, were administered to clams over a period of eighteen days. Protein corona in isolated hemolymph have been evaluated at the beginning, at the middle (ninth day) and at the last day of the experiment (eighteenth day). Separation between bound (pellet) and non-bound proteins and NPs (supernatant) in hemolymph was performed by centrifugation. Evolution of protein corona composition over time has been analyzed in re-suspended pellets for protein identification (liquid chromatography-tandem mass spectrometry, LC-MS/MS) and for protein quantification (sequential window acquisition of all theoretical spectra-mass spectrometry, SWATH-MS).

7.2 MATERIALS AND METHODS

7.2.1 Instrumentation

Micro liquid chromatography (micro-LC) Ekspert nLC425 system (AB Sciex, Massachusetts, USA) coupled to high speed Triple TOF 6600 System mass spectrometer (AB Sciex) with a micro flow source was used for protein identification and quantification. Trap column, coupled on-line with the analytical column, was a YMC-TRIART C18 (3 mm particle size and 120 Å pore size) from YMC Technologies, Teknokroma (Barcelona, Spain). Analytical column was a silica reversed phase column Chrom XP C18 (150×0.30 mm, 3 mm particle size and 120 Å pore size) from AB Sciex. A NexION 300X ICP-MS system (Perkin Elmer, Massachusetts, USA) was used for TiO_2 NPs quantification and characterization with the Syngistix™ Nano Application software (Perkin Elmer). A JEM-1010 transmission electron microscope (TEM) coupled to energy dispersive X-ray (EDX) detector from JEOL (Tokyo, Japan) was used for TiO_2 NPs standards and E171 characterization. Other laboratory devices consist of a Laborcentrifugen 2K15 ultracentrifuge (Sigma, Osterode, Germany), a Boxcult temperature-controlled incubation chamber (Stuart Scientific, Surrey, UK) equipped with a Rotabit orbital-rocking platform shaker (J.P. Selecta, Barcelona, Spain), a Raypa UCI–150 ultrasonic cleaner water-bath (R. Espinar S.L., Barcelona, Spain), a ThermoMixer from Eppendorf (Hamburg, Germany), a Thermo Savant SPD121P-115 SpeedVac with a Thermo Scientific UVS400SPD vacuum system from ThermoFisher (Massachusetts, USA), a Power Pac Basic power supply (Bio-Rad, California, USA) for SDS-PAGE and a UVP PhotoDoc-It Imaging System (Analytik Jena, Jena, Germany) for gel image acquisition.

7.2.2 Reagents

Ultrapure water (18 MΩ cm resistivity) was obtained from a Milli-Q purification device (Millipore Co., Massachusetts, USA). TiO_2 NPs stock solutions were prepared from TiO_2 nanopowder (rutile 99.9%) of 50 and 100 nm purchased from US Research Nanomaterials (Texas, USA). Food additive E171 was from Minerals-Water (Rainham, UK). Methanol

and chloroform were from Panreac (Barcelona, Spain). Ammonium bicarbonate and formic acid were from Fluka (Steinheim, Germany). Phosphate-buffered saline (PBS) was from ThermoFisher. All reagents and solvents used in proteomics were HPLC-grade: sodium dodecyl sulphate (SDS) from Panreac; dithiothreitol (DTT), iodoacetamide (IAA), 30% acrylamide/bis-acrylamide solution (37.5:1), glycerol 86–88%, Tris-base, Coomassie Brilliant Blue R250 (CBB) and Sigma Marker (6.5–200 kDa) from Sigma-Aldrich (Missouri, USA); *β*-mercaptoethanol from Merck (Darmstadt, Germany); bromophenol-blue from Riedel-de Haen (Seelze, Germany); and modified porcine trypsin from Promega (Wisconsin, USA). Methanol for proteomics, acetonitrile and acetic acid were from Scharlau (Barcelona, Spain). Tryptic peptides used as external calibrants for SWATH-MS were from PepcalMix (AB Sciex).

7.2.3 Exposure experiment

7.2.3.1 Nanoparticle suspensions

Suspensions of TiO_2 NPs standards (50 nm and 100 nm) and food additive E171 (nano- and micro-titanium) at 1000 mg L^{-1} were prepared in ultrapure water from the solid reagents. Characterization of these materials was performed by TEM analysis which showed a particle size distribution from 30 to 86 nm (mean size of 51 nm) for 50 nm TiO_2 NPs standard, from 36 to 142 nm (mean size of 74 nm) for 100 nm TiO_2 NPs standard and from 32 to 249 nm (mean size of 114 nm) for E171 (images in supplementary material, Figures S7.1-7.3). All standard solutions were highly aggregated. The stock solutions of 1000 mg L^{-1} were stored at 8 °C and were sonicated (ultrasonic water-bath) for 10 min before their addition to the tanks.

7.2.3.2 Mesocosms system

Atlantic surf clams (*Spisula solidissima*) 3-4 cm long were selected as bioindicators. They came from a shellfish farm located in Rianxo (Galicia, Spain). Four independent tanks containing 30 specimens each were settled: one tank for control, one tank for TiO_2 NPs 50 nm exposure, one for TiO_2 NPs 100 nm exposure and one for E171 exposure.

Filtered marine water (5 L) was used as medium (seawater was changed every two days), and the tanks were kept at 15.5±2 °C with continuous aeration. Concentrations of TiO_2 NPs and E171 were increased progressively from 0 (first day) to 14 mg L^{-1} (eighteenth day) by 2 mg L^{-1} increments every two days. The added volume of NPs suspensions was 10 mL (each 2 mg L^{-1} addition). Clams were fed with *in vitro* cultured phytoplankton (10 mL of the mixture of three collected cultures) the same days that NP addition was carried out. One specimen per tank was sampled before any exposure (T0), after nine days (T1) and after eighteen days (T2) of exposure.

7.2.3.3 *In vitro* phytoplankton culture

In vitro cultured phytoplankton consists of two flagellate species (*Tetraselmis suecica* and *Isochrysis galbana*) and one diatom (*Chaetoceros igafa*). Individual culture of three species was carried out using 1 L glass bottles, previously sterilized. Culture media was sterilized filtered marine seawater (salinity 35 PSU) enriched with nutrients [24]. Cultures were submitted to 12 h light-12 h dark cycles with a light intensity of 15-25 klux. Temperature was set between 18-22 °C. An aeration system, supplemented with CO_2 for ensuring pH value below 8, was installed (250 mL min^{-1}). Every two days, 150 mL of each culture were removed and replaced with an equal volume of fresh, sterilized and supplemented marine seawater

7.2.4 Hemolymph extraction

The hemolymph was extracted from the posterior adductor muscle of each clam using a 1 mL sterile syringe with a 29 G1/2" needle (BD, New Jersey, USA). With the needle removed, the hemolymph was collected in 2 mL Eppendorf tubes and they were frozen at -20 °C until analysis.

7.2.5 Sample preparation

7.2.5.1 Protein corona isolation

Extracted hemolymph (500 µL) was submitted to centrifugation at 15300 rpm and 4 °C for 15 min to separate protein corona (pellet) and free NPs and un-bonded proteins (supernatant). Pellets were then washed by adding 500 µL of PBS, vortexed and centrifuged (12000 rpm, 4 °C, 10 min). Supernatant was discarded and washed pellets were resuspended in 500 µL of PBS and homogenized using a vortex. Resuspended pellets and supernatants were stored at -20 °C before analysis.

7.2.5.2 Supernatant cleansing

Individual supernatants (500 µL) were mixed with 2 mL of methanol, 0.5 mL of chloroform and 1.5 mL of ultrapure water. Mixtures were homogenized in vortex and centrifuged at 3900 rpm for 10 min at 4 ºC. Top layer (methanol-water) was discarded and 2 mL of methanol were added to chloroform layer, which contained proteins. After homogenizing in vortex, centrifugation was performed at same conditions as mentioned before. Supernatants were removed and precipitates were resuspended in 500 µL of PBS. This cleansing procedure have been already reported by García-Otero et al. [25]. Clean supernatants were kept at -20 ºC.

7.2.5.3 One dimensional SDS-PAGE

Each sample (24 µL) was mixed with 4 µL of SDS-PAGE loading buffer (10% w/v SDS, 40 mM Tris-Base, pH 6.8, 50% v/v glycerol, 0.1% v/v bromophenol blue and 10% v/v β-mercaptoethanol). Denaturalization was performed by heating at 100 °C for 5 min. Then, samples were loaded into a 10% acrylamide/bis-acrylamide, stacking gel, 12.5% acrylamide/bis-acrylamide, running gel (1 mm thickness). Separation was performed at 80 V (constant voltage) and the run was interrupted when the front penetrated 3 mm into the running gel. Coomasie Blue was used for gel staining at room temperature under continuous agitation for 2 h. Gels were distained with methanol-acetic acid (45%-7.5%)

under agitation for 12 h and washed with ultrapure water before being scanned.

7.2.5.4 In-gel protein digestion

Protein bands were excised from gels and rinsing was carried out using a 50 mM NH_4HCO_3 in 50% methanol solution. A solution containing 10 mM DTT in 50 mM NH_4HCO_3 and 55 mM IAA in aqueous 50 mM NH_4HCO_3 were used for reduction and alkylation of proteins, respectively. Proteins were washed with 50 mM NH_4HCO_3 in 50% methanol, dehydrated by adding acetonitrile and they were dried in a SpeedVac. A solution containing 20 g μL^{-1} of modified porcine trypsin prepared in 20 mM NH_4HCO_3 was added to dried gel bands and the mixture was incubated at 37 °C for 16 h. Extraction of peptides was performed with 40 µL of a solution containing 60% acetonitrile and 0.5% formic acid by incubating at 37 °C for 20 min (each sample by triplicate). Finally, extracted peptides were pooled, concentrated in a SpeedVac and stored at -20 °C.

7.2.6 Protein identification by mass spectrometry (LC-MS/MS) and data analysis

The separation of digested peptides by reverse phase LC was performed by injecting 4 µL of the sample. Loading pump flow rate was set at 10 µL min^{-1} to deliver an aqueous 0.1% formic acid solution. The flow rate of the micro-pump was 5 µL min^{-1} using gradient elution conditions. Peptides separation was carried out using a 25 min gradient elution from 2 to 90% of mobile phase B (mobile phase A consisted of 2% acetonitrile and 0.1% formic acid in ultrapure water and mobile phase B was 0.1% formic acid in acetonitrile).

Triple TOF spectrometer (Analyst TF v1.7.1 software from AB Sciex) conditions were: ion spray voltage floating 5500 V, curtain gas 25, collision energy 10 and ion source gas 25. Switching criteria was fixed to ions with a mass to charge ratio (*m/z*) higher than 350 and lower than 1400, charge state of 2-5, mass tolerance of 250 ppm and 200 counts per second (cps) as abundance threshold. Exclusion time of former target ions was 15 s.

Automatic calibration was performed every 4 h using tryptic peptides as external calibrants.

7.2.7 Protein quantification by SWATH-MS

7.2.7.1 Spectral library creation

Shotgun (data-dependent acquisition, DDA) was selected for MS/MS spectral library creation by micro-LC-MS/MS. Samples for every group were pooled including equal proportions of each one for assuring a good representation of all peptides and proteins. Separation of peptides in 4 µL (4 mg) of pooled samples was performed by micro-LC at a flow rate of 5 µL min^{-1} using an analytical column Chrom XP C18 (150×0.30 mm, 3 mm particle size and 120 Å pore size). Mobile phases A and B were 0.1% formic acid in water and 0.1% formic acid in acetonitrile, respectively, and the gradient run consisted of a three stages program: 5% to 95% B for 30 min, 5 min at 90% B and 5 min at 5% B for column equilibration (40 min each run).

Eluted peptides were sequentially injected into the Triple TOF operating in DDA and positive ion modes. Micro-source voltage was set at 2600 V and survey was performed between 400 and 1250 m/z during 250 ms. Sixty-five top peptides from survey were submitted to MS/MS scan from 100 to 1500 m/z for 25 ms (2.8 s total cycle time). Precursor ions are fragmented and added to a dynamic exclusion list for 15 s, whereas singly charged ions were excluded.

ProteinPilot v5.0.1 software (AB Sciex) was used for peptide and protein identification over Mollusca Uniprot database. False Discovery Rate (FDR) was fixed at 1%. Spectral library for further SWATH was created with MS/MS spectra of identified peptides and proteins. SWATH peak extraction was performed by the add-in SWATH Acquisition MicroApp v2.0 (AB Sciex) for PeakView v2.2 software (AB Sciex). Only peptides with a confidence score above 99%, after search in ProteinPilot database, were included in the spectral library.

7.2.7.2 Relative quantification by SWATH-MS acquisition

Triple TOF micro-LC-MS/MS system working at data-independent acquisition (DIA) mode was used for acquiring SWATH-MS data (twenty-four samples: twelve pellets and twelve supernatants). Each sample (4 μL) was analyzed under the same gradient conditions used for spectral library creation but with SWATH-MS acquisition method. It consisted of one cycle repetition of acquisition of sixty-five TOF MS/MS scans (from 400 to 1500 m/z) of overlapping sequential precursor isolation window of variable width (1 m/z overlap) from 400 to 1250 m/z mass range (50 ms). The total cycle time was 6.3 s and the width of every sixty-five variable windows was optimized for each sample set based on the ion density found in DDA runs. SWATH variable window calculator worksheet from AB Sciex was used for this purpose.

7.2.7.3 Data analysis

PeakView software with SWATH Acquisition MicroApp was used to targeted data extraction of fragment ion chromatogram traces from SWATH runs. Data processing is based on previously created spectral library from Shotgun data. Selection criteria were more than ten peptides per protein and, at least, seven fragments per peptide, based on signal intensity. Shared and modified peptides were excluded. For ion chromatograms extraction, 5 min windows and 30 ppm widths were selected. Quantitation by SWATH was applied to proteins included in the ion library.

Retention time of selected peptides for each protein must be realigned in every run according to iRT spiked peptides in all samples. For each selected fragment ion, ion chromatogram was extracted. PeakView provided an FDR value and a score for each corresponding peptide based on their chromatographic and spectral components. Only peptides with FDR lower than 1% were quantified. Total peak area for one peptide was obtained after adding the individual areas of all assigned fragment ions.

Integrated peak area files were processed using MarkerView software (AB Sciex) for relative quantitation analysis. Three different files (individual ions quantitative information, total intensity of different ions corresponding to one peptide and total intensity of different peptides

associated with one protein) were exported. This software performs a DIA quantification method and the processing algorithms can find chromatographic and spectral peaks from raw SWATH data with high accuracy. Minor variations in mass and retention time values were compensated due to data alignment performed by MarkerView, which guaranteed that compounds which were in different samples would be accurately compared.

The sum of individual peak areas from all peptides and transitions from every replicate of each sample were used for performing a global normalization which prevents the effects of possible sample loss during preparation. Principal Component Analysis (PCA) was applied to sample comparison. The mean MS peak area of all protein was extracted from the biological replicates of each sample. Then, Student's *t*-test analysis was used to establish comparisons between samples according to the sums of averaged area of all transitions which corresponded to the same protein. This statistical analysis showed the most significant variables that can be used to make distinctions between two groups and they were distinguished using p-value. Selection criteria for differentially expressed proteins were p-value below 0.05 and fold change above 1.5.

7.3 RESULTS AND DISCUSSION

7.3.1 TiO_2 NPs-protein corona separation from free NPs and proteins in hemolymph from clams

Operational conditions (ultracentrifugation speed and time) were studied for separating TiO_2 NPs-protein corona complexes from free TiO_2 NPs and un-bonded proteins in hemolymph from clams. The conditions were established by using hemolymph isolated from unexposed clams mixed with 50 nm TiO_2 NPs (~ 10^{10} TiO_2 NPs mL^{-1}) and incubated at 37 °C and 180 rpm (orbital-horizontal shaking) for 1 h. The supernatants (free TiO_2 NPs and un-boded proteins) and the pellets (TiO_2 NPs-protein corona) after ultracentrifugation were analyzed by single particle-inductively coupled plasma-mass spectrometry (sp-ICP-MS) to assess TiO_2 NPs and by one dimensional SDS-PAGE to assess protein corona and un-bonded proteins. Two tested centrifugation speeds

(15300 and 12000 rpm) resulted in a more compact pellet when using 15300 rpm, pellet which was found to be stable after a further washing stage with PBS (4 °C, 12000 rpm, 10 min) for removing free TiO_2 NPs and un-bonded proteins adsorbed onto the pellet. After fixing the ultracentrifugation speed at 15300 rpm, several ultracentrifugation times were tested and, as shown in Figure 7.1B, the presence of proteins in the pellets were always observed at any ultracentrifugation time. However, the TiO_2 NPs concentration was found to diminish slightly when using large ultracentrifugation times. The shortest ultracentrifugation time (15 min) was, therefore, selected.

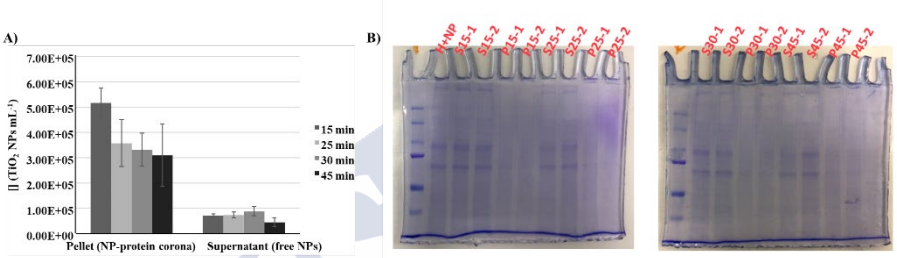

Figure 7.1. A) TiO_2 NPs concentration and B) proteins in pellets and supernatants after several ultracentrifugation times: H+NPs means hemolymph plus TiO_2 NPs before centrifugation, P means pellet and S means supernatant

7.3.2 Protein corona identification in hemolymph from clams exposed to TiO_2 NPs

Shotgun proteomics have been used to identify protein corona in hemolymph from clams exposed to TiO_2 NPs (50 and 100 nm) and food additive E171. Venn diagrams were plotted with FunRich v3.1.3 software (open access) to establish comparisons between samples. Common and non-common proteins in every group have been therefore listed.

7.3.2.1 Protein corona changes over time

Regarding unexposed clams, pellets (NP-protein corona complexes) were obtained since small amounts of TiO_2 NPs can be present in bivalve molluscs [26]. Therefore, nine proteins in pellets from

control samples (hemolymph from non-exposed clams) were found to remain constant from the beginning (PC-1 at T0, Figure 7.2A) to the end (PC-3 at T2, Figure 7.2A) of the experiment. Most of these proteins are part of cytoskeleton (beta-actin, myosin heavy chain and cytoplasmic actin), while others are related to binding molecules such as DNA (histone H4), actin (filamin-C) and sialic acid (sialic acid-binding lectin). Other invariable protein corona found were citrate synthase, which is involved in tricarboxylic acid cycle; complement component C3, that is part of immune system; and voltage-dependent anion channel 2-like protein, which enables transmembrane transference of anions in a voltage-dependent way. If comparisons are made between two long sampling periods (for instance, T0/T2, five proteins), the number of common proteins is higher than those found when comparing short sampling times (T0/T1 or T1/T2, two proteins). These findings suggest changes on the protein corona over time. Regarding uncommon proteins (corona proteins that were found only at specific sampling times), fourteen proteins were identified in the pellet of control samples at T0 (PC-1), three proteins at T1 (PC-2) and sixty-four proteins at T2 (PC-3) (proteins given in supplementary material, Table S7.1). The number of identified peptides and the sequence coverage (ratio between number of amino acids in all peptides that were identified and the number of amino acids in a protein sequence), with individual confidence of 95% or better, are also listed in Table S7.1. Differences on the number and type of protein corona at the three sampling times could be attributed to stress as a consequence of the static conditions and feeding periods of the experiment [27, 28]. In addition, the number of proteins (common and uncommon proteins) that interact which the NPs naturally present in the hemolymph increases over time (Figure 7.1A).

Results after exposure to 50 nm TiO_2 NPs (P50-1 at T0, P50-2 at T1 and P50-3 at T2) showed similar results than those obtained for unexposed clams. Therefore, six common proteins all over the experiment were identified (Figure 7.2B), five of them were previously identified in control samples (beta-actin, cytoplasmic actin, histone H4, complement component C3 and citrate synthase). The remaining protein was heat

shock protein 22 (isoform 1), protein related to stress response. When comparing two sampling periods, high similarities have been observed between P50-1 and P50-3 (nine proteins), whereas five proteins were found in TiO_2 NPs corona at sampling time T0 (P50-1) and T1 (P50-2) and seven common proteins form the corona at sampling times T1 and T2 (P50-2 and P50-3) as shown in Figure 7.2B. Finally, nine uncommon proteins were identified at T0, four proteins at T1 and sixty-two proteins at T2 (Table S7.2, supplementary material). Similar to the experiment with unexposed clams, a higher number of proteins were found in the corona at the end of exposure experiment (T2) than at other sampling times, which can be a consequence of the TiO_2 NPs exposure and also to the large time of the experiment.

Evolution of protein corona composition after exposing to 100 nm TiO_2 NPs standards (P100-1, P100-2 and P100-3 at T0, T1 and T2, respectively, Figure 7.2C) has revealed that fifteen proteins remain bonded to the TiO_2 NPs over all exposition process. Two proteins of the fifteen identified common proteins were found to form protein corona of control (PC) and 50 nm TiO_2 NPs exposed (P50) samples (beta-actin and complement component C3), whereas four proteins were only included in PC corona (myosin heavy chain, filamin-C, voltage-dependent anion channel 2-like protein and citrate synthase) and one protein (heat shock protein 22 isoform 1) was exclusive to P50 corona. In addition, cytoskeleton proteins (paramyosin, actin-3 and tubulin alpha chain), actin binding protein (alpha-actinin), ubiquitin and ferritin were also found. As it was mentioned before for 50 nm TiO_2 NPs exposure, the highest number of common proteins was detected at the beginning and at the end of the experiment (P100-1 and P100-3). Forty-two uncommon proteins in P100-1, eight proteins in P100-2 and thirty-two proteins in P100-3 were also identified (Table S7.3, supplementary material). Unlike previous cases, protein corona which contained a greater number of proteins was found at the beginning of the experiment (P100-1), and the number of proteins linked to TiO_2 NPs decreases over time and after adding higher TiO_2 NPs concentrations.

Finally, only one protein (beta-actin) was found to remain constant in corona composition in hemolymph from clams exposed to food additive E171 at three studied times (Figure 7.2D). This protein was also found in the corona when exposing to 50 and 100 nm TiO_2 NPs standards and in control samples. When comparing corona proteins at the beginning of the experiment (PE171-1) and after nine days of exposition (PE171-2), a high number of proteins (twenty-four proteins) were found to be common in both coronas. However, only one protein remains bonded to the NPs after eighteen days of exposure to E171, which implies a great corona change from the beginning (thirty-eight proteins, PE171-1) to the end of the experiment (one protein, PE171-3). The list of the uncommon proteins identified in each corona (thirty-eight proteins in PE171-1, fourteen proteins in PE171-2 and one protein in PE171-3) are given in Table S7.4 (supplementary material). These findings (lower number of proteins linked to TiO_2 NPs over time and at after adding higher TiO_2 NPs concentrations) are quite similar than those obtained for exposition experiment with 100 nm TiO_2 NPs and they could be explained taking in mind the higher size distribution of 100 nm TiO_2 NPs and the large nano(micro) particles in E171.

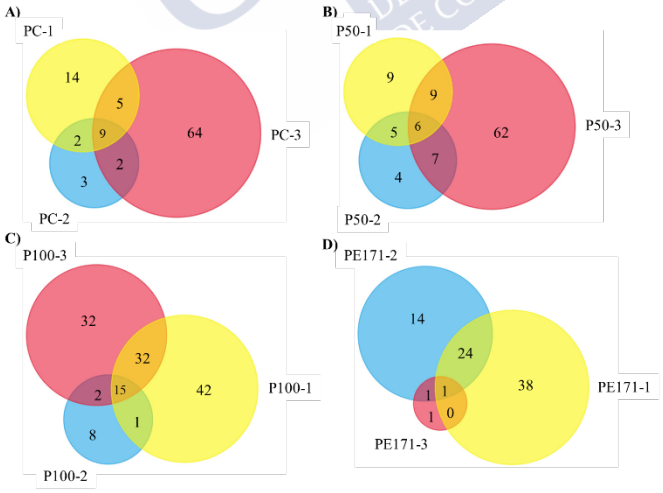

Figure 7.2. Venn diagrams of identified corona proteins (1% FDR) in hemolymph of A) controls, B) samples exposed to 50 nm TiO_2 NPs, C) samples exposed to 100 nm TiO_2 NPs and D) samples exposed to food additive E171

7.3.2.2 Influence of NPs characteristics on protein corona

Figure 7.3 summarizes the comparisons among hemolymph samples from controls and clams exposed to several NPs at same concentrations and sampling times as an attempt to evaluate the influence of the TiO_2 NPs characteristics (mainly size distribution) on the corona composition. Before any addition (Figure 7.3A), the number of uncommon proteins was relatively high: nine proteins in PC-1, six proteins in P50-1, forty-seven proteins in P100-1 and eighteen proteins in PE171-1 (supplementary material, Table S7.5). Therefore, huge variability between samples existed even before exposure. The greatest number of common proteins among the four groups was found at T0. These nine common proteins were cytoskeleton proteins (actin, actin-2, actin-3, putative paramyosin 3, beta-actin and filamin-C), ferritin, citrate synthase and complement component C3. Comparisons between two tanks at the beginning of the experiment (T0) have led to observe many similarities in corona composition, and twenty-one common proteins were found between P100-1 and PE171-1 samples, sixteen common proteins between P50-1 and P100-1 and eighteen common proteins between P50-1 and PE171-1. A moderate number of common proteins were also found when comparing the corona composition of hemolymph from unexposed clams, and fifteen, sixteen and eighteen common proteins were found after comparing control sample PC-1 with P50-1, P100-1 and PE171-1, respectively.

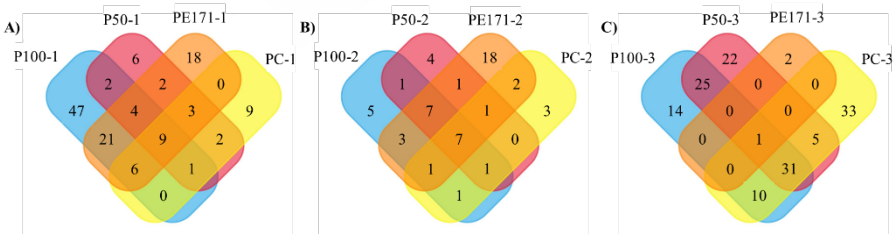

Figure 7.3. Venn diagrams of identified corona proteins (1% FDR) in hemolymph of controls (PC) and clams exposed to NPs (P50, P100 and PE171) A) before any exposure (T0), B) at the ninth day of exposure (T1) and C) at the end of experiment (T2)

Corona composition in hemolymph from control and exposed clams began to be more different after the ninth day of exposure to TiO_2 NPs (8 mg L^{-1}) and the number of common proteins in the corona of the four groups diminishes. Therefore, seven proteins were identified and four of these proteins (beta-actin, ferritin, citrate synthase and complement component C3) were also found in the corona at T0. The remaining three proteins were histone H4, cytoplasmatic actin and voltage-dependent anion channel 2-like protein. The decrease on the number of common proteins was due to the increase in differences in coronas caused by the presence TiO_2 NPs of different size distribution. The highest similarity in corona composition has been found between corona from P100-2 and PE171-2 samples (eighteen common proteins). In addition, common proteins in the corona from control clams (PC-2) and exposed clams were also found to diminish when compared to T0: nine proteins when comparing to P50-2, ten proteins for P100-2 and eleven proteins for PE171-2. These findings are attributed to the influence of the higher TiO_2 NPs concentration and the different size distribution on the corona composition. Number of the uncommon proteins was also found to decrease in comparison to the identified proteins at the beginning of the experiment (T0): three proteins identified in PC-2, four proteins in P50-2, five proteins in P100-2 and eighteen in PE171-2 (supplementary material, Table S7.6).

At the end of the experiment, only one protein (beta-actin) was identified in the corona of all samples. Beta-actin forms part of all studied coronas at any time and condition. Unlike previous scenarios, a high number of shared proteins were found in P50-3 and P100-3 (fifty-seven proteins). Only one protein was detected in common between P50-3 and PE171-3 and between P100-3 and PE171-3, which is attributed to the low number of proteins detected in coronas from PE171-3 hemolymph. Comparisons between control (PC-3) and exposed clams (P50-3 and P100-3) have led to a higher number of common proteins than those identified at T0 and T1 (thirty-seven and forty-two, respectively). There was only one common protein between PE171-3 and PC-3 but, again, the low number of detected proteins in PE171-3 sample could be the reason. Uncommon proteins (supplementary material, Table S7.7) have consisted of thirty-three proteins for unexposed clams (PC-3), twenty-two

and fourteen proteins for exposed clams to 50 nm TiO_2 NPs (P50-3) and 100 nm TiO_2 NPs (P100-3), respectively, and two proteins for exposed clams to E171 (PE171-3).

In conclusion, more differences on the corona composition between unexposed (PC) and exposed (P50, P100 and PE171) clams were observed at the middle (T1) and at the end (T2) of the experiment, and effects of NPs on protein corona composition seem to be established after large exposure time. Common proteins present in the coronas of exposed clams to 50 and 100 nm TiO_2 NPs (P50 and P100) were also found to be increased over time, and NPs size distribution does not seem to affect corona composition at high NPs concentrations and large exposure times.

7.3.3 Protein quantification by SWATH-MS analysis

A library containing 266 identified proteins from all samples was created before SWATH-MS analysis. Principal Components Analysis (PCA) was applied to all samples measured by triplicate, and the first two principal components accounts 90.6% of variance among samples (the first principal component, C1, explained 88.4% of variance while the second principal component, C2, explained 2.2%). Therefore, PCA (Figure 7.4) indicated that there were some differences among control (unexposed clams) and exposed clams at the studied times. There was a clear separation of hemolymph based on the corona composition for every group of samples at the several sampling times (T0, T1 and T2). Samples P100-1, PE171-1, P100-3, P50-3 and PC-3 have shown negative C2 scores, whereas positive scores for C1 were obtained for the remaining samples. Exposed clams (P50-1, P100-2 and PE171-2) and unexposed clams (PC-1 and PC-2) formed a grouping, while exposed clams P50-2 and PE171-3 were dispersed.

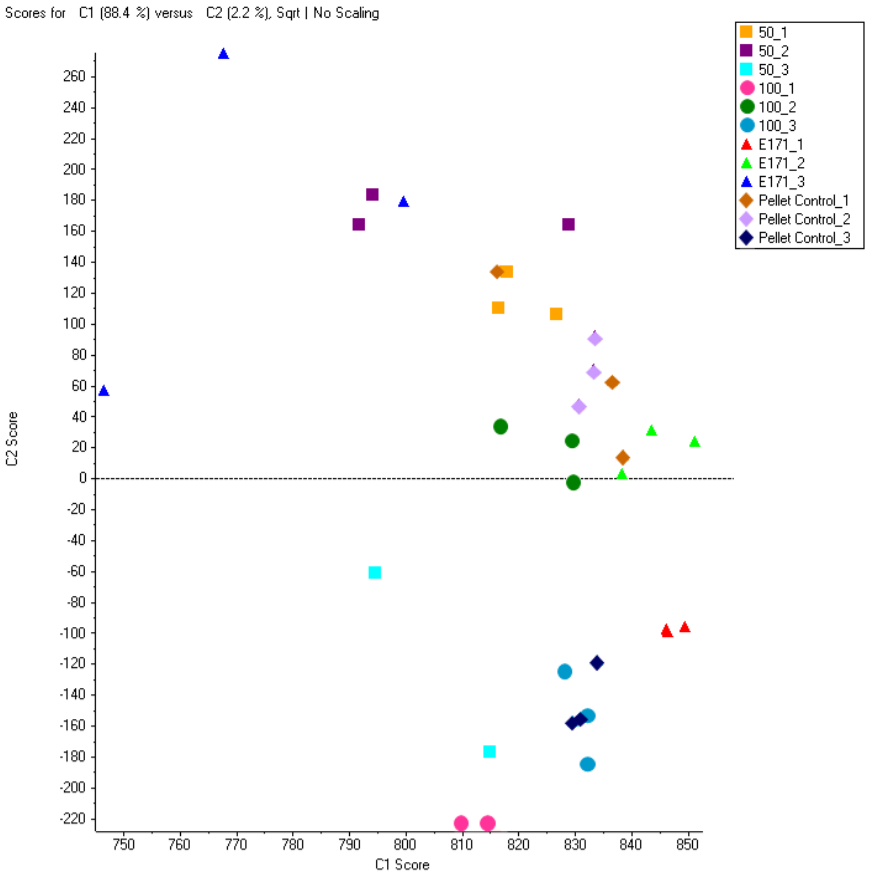

Figure 7.4. PCA of the log2 transformed SWATH areas for controls and hemolymph of exposed clams at rising NPs concentration and exposure times

7.3.3.1 Differentially expressed corona proteins: Evolution over time

SWATH files were load over the new created library and quantitative analysis were performed to determine changes on the relative protein concentrations (proteins which concentrations are increased or decreased between groups).

Changes on protein corona from control samples (hemolymph from un-exposed clams) have consisted of a decrease on the concentration of ferritin and cytoskeleton proteins (tubulin alpha and beta chain, among others) over time (Table 7.1). On the contrary, heat shock protein (stress related proteins) was found to be overexpressed (increased concentrations) along the experiment. Therefore, clams appear to increase their metabolic stress over time although they were not exposed to TiO_2 NPs. Complement components C3 and C1q, proteins related to innate immunity, were found to be overexpressed at the beginning of the experiment, whereas the concentration of catalase and histone H2A were found to be increased at the middle and at the end of the experiment. Catalase is related to the responses to oxidative stress, so its overexpression is indicative of oxidative metabolism. Histones are involved in packaging DNA in the chromatin structures. Talin-1, putative filamin-A-like protein (isoform X7) and ribosomal-related proteins (26S proteasome non-ATPase regulatory subunit 2 and putative 40S ribosomal protein S18) were found also overexpressed at the end of the experiment. Both talin-1 and filamin-A proteins are actin-binding proteins, while ribosomal proteins participate in regulation of catabolic process and translation, respectively.

Table 7.1. Significant proteins (p-value<0.05) in comparisons between control samples at different times (PC-1, PC-2 and PC-3)

		Protein	Specie	UniProt ID	p-value	Fold Change
PC-1 vs. PC-2	↑PC-1	Phosphoenolpyruvate carboxykinase [GTP]	*Crassostrea gigas*	K1QEA6	0.0251000	Infinity
		Myosin heavy chain, striated muscle	*Mizuhopecten yessoensis*	A0A210Q4E0	0.0168953	6.5309260
		Tubulin alpha chain	*Octopus bimaculoides*	A0A0L8G5J8	0.0395575	4.5387541
		Visual G-protein beta subunit	*Doryteuthis pealeii*	Q6TQF6	0.0133082	4.0018828
		Ferritin	*Ruditapes philippinarum*	U3GS70	0.0191281	3.7808948
		Complement C1q-like protein 2	*Ruditapes philippinarum*	A0A0U3AA90	0.0408918	2.8233446
		Putative filamin-A-like protein isoform X7	*Pinctada fucata*	A0A194AJE0	0.0039369	2.2941750
		Dihydropyrimidinase	*Crassostrea gigas*	K1PGY5	0.0095845	2.0243650
		Histone H2A	*Lottia gigantea*	V4B4B8	0.0408882	1.7464368
		Putative paramyosin-3	*Pinctada fucata*	A0A194AJD6	0.0134596	1.7278486
		Phosphoglycerate mutase	*Mizuhopecten yessoensis*	A0A210R2C8	0.0175281	5.5186849
		Tubulin beta chain	*Arion vulgaris*	A0A0B7B670	0.0480409	2.9794920
		Complement component C3	*Ruditapes decussatus*	C0JPJ2	0.0350887	2.9143721

Table 7.1. (Continued)

PC-2 vs. PC-3	Protein	Specie	UniProt ID	p-value	Fold Change
↓PC-1	Ubiquitin	*Biomphalaria glabrata*	Q9BH32	0.0155399	2.8888791
	Heat shock protein 22 isoform 1	*Ruditapes philippinarum*	C8CBN4	0.0172588	1.8646072
	HSP70 protein	*Ruditapes philippinarum*	A0A023W7L5	0.0260740	1.5877672
↑PC-2	Phosphoglycerate mutase	*Mizuhopecten yessoensis*	A0A210R2C8	0.0014503	6.8146362
	Myosin heavy chain, non-muscle	*Mizuhopecten yessoensis*	A0A210QSX4	0.0080505	4.9387045
	Superoxide dismutase	*Ruditapes philippinarum*	J7FII1	0.0109435	4.5801159
	Triosephosphate isomerase	*Lottia gigantea*	V4AUY5	0.0171992	4.5054474
	Elongation factor Tu	*Mizuhopecten yessoensis*	A0A210PGD1	0.0007125	3.8527527
	Ubiquitin	*Biomphalaria glabrata*	Q9BH32	0.0152683	3.5482640
	Sialic acid-binding lectin	*Ruditapes philippinarum*	C8CBM9	0.0030702	3.5360718
	Peptidyl-prolyl cis-trans isomerase	*Ruditapes philippinarum*	C8CBN3	0.0008501	3.0573572
	Galectin	*Ruditapes philippinarum*	B1AAP1	0.0214312	2.8090906
	Putative paramyosin-3	*Pinctada fucata*	A0A194AJD6	0.0072461	2.7597046

Table 7.1. (Continued)

PC-2 vs. PC-3	Protein	Specie	UniProt ID	p-value	Fold Change
↑PC-2	Putative paramyosin-3	*Pinctada fucata*	A0A194AJD6	0.0072461	2.7597046
	Complement component C3	*Ruditapes decussatus*	C0JPJ2	0.0149678	2.4184697
	Ezrin/radixin/moesin	*Aplysia californica*	Q45R39	0.0109390	1.8742535
	Ferritin	*Ruditapes philippinarum*	U3GS70	0.0268787	1.7834487
	Tropomyosin	*Ruditapes philippinarum*	B7XC71	0.0033367	1.7521684
	Phosphoenolpyruvate carboxykinase [GTP]	*Crassostrea gigas*	K1QEA6	0.0317364	Infinity
↑PC-3	26S proteasome non-ATPase regulatory subunit 2	*Mizuhopecten yessoensis*	A0A210QZJ7	0.0315249	Infinity
	Fructose-bisphosphate aldolase	*Meretrix meretrix*	E3VWM3	0.0164731	Infinity
	Catalase	*Corbicula fluminea*	A0A1P8NQK0	0.0159670	Infinity
	Talin-1	*Crassostrea gigas*	K1PI02	0.0037818	Infinity
	Tubulin beta chain	*Lottia gigantea*	V4BLC8	0.0032154	Infinity
	Enolase	*Crassostrea gigas*	K1QX37	0.0064354	7.4786752
	Tubulin beta chain	*Mizuhopecten yessoensis*	A0A210R050	0.0011484	5.9755218

Table 7.1. (Continued)

	Protein	Specie	UniProt ID	p-value	Fold Change
PC-2 vs. PC-3	↓PC-3	Actin-2	*Mizuhopecten yessoensis*	A0A210QJE2	0.0116470	2.9186927
		Heat shock protein 22 isoform 1	*Ruditapes philippinarum*	C8CBN4	0.0078523	2.8236961
		Putative filamin-A-like protein isoform X7	*Pinctada fucata*	A0A194AJE0	0.0131316	2.5518666
		Histone H2A	*Lottia gigantea*	V4B4B8	0.0033108	2.0985696
		Arginine kinase	*Paphia undulata*	C3VUU4	0.0079977	1.8212072
		Voltage-dependent anion channel 2-like protein	*Haliotis diversicolor*	D7RP02	0.0445530	1.7699477
		HSP70 protein	*Ruditapes philippinarum*	A0A023W7L5	0.0007722	1.7408813
PC-1 vs. PC-3	↓PC-1	Ferritin	*Ruditapes philippinarum*	U3GS70	0.0115081	6.7430320
		Tubulin alpha chain	*Octopus bimaculoides*	A0A0L8G5J8	0.0263352	5.0404905
		Putative paramyosin-3	*Pinctada fucata*	A0A194AJD6	0.0006861	4.7683516
		Ferritin	*Ruditapes decussatus*	A0A067XHZ5	0.0147309	4.3921588
		Ferritin	*Ruditapes decussatus*	A0A067XI00	0.0278245	4.1308497
		Myosin heavy chain, striated muscle	*Mizuhopecten yessoensis*	A0A210Q4E0	0.0250955	3.6999337

Table 7.1. (Continued)

PC-1 vs. PC-3	Protein	Specie	UniProt ID	p-value	Fold Change
↓PC-1	Elongation factor Tu	*Mizuhopecten yessoensis*	A0A210PGD1	0.0021951	3.2722619
	Visual G-protein beta subunit	*Doryteuthis pealeii*	Q6TQF6	0.0138954	2.4500000
	Actin-related protein 3	*Crassostrea gigas*	K1QLZ1	0.0257362	2.2761222
	Fibrinogen-related protein 5	*Mytilus galloprovincialis*	E6ZCD7	0.0231704	2.2477161
	Tropomyosin	*Ruditapes philippinarum*	B7XC71	0.0117695	1.7654214
	Alpha-actinin, sarcomeric	*Crassostrea gigas*	K1RH58	0.0014749	1.5549295
↓PC-3	Sarcoplasmic calcium-binding protein	*Meretrix lusoria*	O61284	0.0334344	Infinity
	Talin-1	*Crassostrea gigas*	K1PI02	0.0037818	Infinity
	Tubulin beta chain	*Lottia gigantea*	V4BLC8	0.0032154	Infinity
	Ribosomal protein L12	*Argopecten irradians*	Q8ITA1	0.0022618	Infinity
	Tubulin beta chain	*Mizuhopecten yessoensis*	A0A210R050	0.0012733	9.2282543
	Adenosylhomocysteinase	*Octopus bimaculoides*	A0A0L8G425	0.0012066	6.2244621
	Heat shock protein 22 isoform 1	*Ruditapes philippinarum*	C8CBN4|	0.0040034	5.2650842

Table 7.1. (Continued)

PC-1 vs. PC-3	Protein	Specie	UniProt ID	p-value	Fold Change
↓PC-3	Putative 40S ribosomal protein S18	*Pinctada fucata*	A0A194ANH2|	0.0154937	4.8462029
	Tubulin alpha chain	*Lottia gigantea*	V3ZTB1	0.0160885	4.8379208
	Tubulin beta chain	*Arion vulgaris*	A0A0B7B670	0.0061528	3.1284737
	HSP70 protein	*Ruditapes philippinarum*	A0A023W7L5	0.0001469	2.7641143
	Glutathione peroxidase A	*Ruditapes philippinarum*	C8CBM2	0.0419250	2.4895609

Concentrations of protein corona in hemolymph from clams exposed to 50 nm TiO_2 NPs have been found to be time-dependent (Table 7.2). High concentrations of ferritin were found at the beginning of the experiment (un-exposed clams at T0, P50-1) and this protein was found to be reduced after TiO_2 NPs exposure. The trend for complement components (C3 and C1q) was similar than that found for control samples (higher concentrations at the beginning of the experiment and at the early stages of exposure), and similar findings have been found for enzymes such as alpha-mannosidase and phosphoenolpyruvate carboxykinase (GTP). Putative filamin-A-like protein (isoform X7) and alpha-actinin are the only overexpressed proteins in the corona at the end of the exposure (highest TiO_2 NPs concentration). Regarding filamin-A protein, overexpression at the end of the experiment was also found for control hemolymph, and the overexpression of this proteins could be not directly (only) related to TiO_2 NPs uptake. Un-bonded proteins (free proteins in the supernatants after centrifugation) such as histones (H2A, H2B and H4) have been found to be overexpressed, but these proteins were not found in the corona. In addition, concentrations of free putative filamin-A-like protein, superoxide dismutase and sarcoplasmic calcium-binding protein were also higher at the end of the experiment and at the middle of the experiment when compared to initial conditions. On the contrary, un-bonded ferritin and complement components (C3 and C1q) concentrations were reduced. Decrement on free complement components C3 and C1q could indicate an immunodeficiency caused by TiO_2 NPs exposure, whereas the increment on un-bonded superoxide dismutase concentration could be related to oxidative stress responses (although this protein did not show affinity for 50 nm TiO_2 NPs).

Table 7.2. Significant proteins (p-value<0.05) in comparisons between samples exposed to 50 nm TiO_2 NPs at different NPs concentrations and times (P50-1, P50-2 and P50-3)

P50-1 vs. P50-2		Protein	Specie	UniProt ID	p-value	Fold Change
↓P50-1		Isocitrate dehydrogenase [NADP]	*Mizuhopecten yessoensis*	A0A210QYM1	0.0357168	4.9001013
		Ferritin	*Ruditapes philippinarum*	U3GS70	0.0215071	3.5694625
		Peptidyl-prolyl cis-trans isomerase	*Ruditapes philippinarum*	C8CBN3	0.0047240	3.3447893
		Myosin heavy chain	*Onchidium struma nom. nud.*	A0A1P8C5A6	0.0213384	2.5480114
		Complement component C3	*Ruditapes decussatus*	C0JPJ2	0.0034782	2.4356984
		Ferritin	*Ruditapes decussatus*	A0A067XI00	0.0147841	1.7875972
↓P50-2		Sarcoplasmic calcium-binding protein	*Mizuhopecten yessoensis*	Q9U5C3	0.0194481	3.4926379
		Retinal dehydrogenase 1	*Mizuhopecten yessoensis*	A0A210Q6W9	0.0447320	2.7855105
		78 kDa glucose-regulated protein	*Conus novaehollandiae*	H8XWJ4	0.0223090	2.5049771
		Tubulin beta chain	*Pinctada fucata*	A0A194AQ74	0.0219864	1.8343592
		Alpha-1,4 glucan phosphorylase	*Lottia gigantea*	V4ALJ5	0.0393302	1.6481927

Table 7.2. (Continued)

P50-2 vs. P50-3	Protein	Specie	UniProt ID	p-value	Fold Change
↓P50-2	Beta-glucuronidase	*Lottia gigantea*	V4A2U2	0.0161181	1.4874937
	Alpha-mannosidase	*Crassostrea gigas*	K1QII0	0.0237862	0.9119328
	Phosphoenolpyruvate carboxykinase [GTP]	*Crassostrea gigas*	K1QEA6	0.014105	0.8253419
	Elongation factor Tu	*Mizuhopecten yessoensis*	A0A210PGD1	0.0004184	0.7779047
	Ubiquitin	*Biomphalaria glabrata*	Q9BH32	0.0477494	0.7074324
	Beta-glucuronidase	*Mizuhopecten yessoensis*	A0A210PUW7	0.0233464	0.5392514
	Glutathione peroxidase A	*Ruditapes philippinarum*	C8CBM2	0.0478564	0.5101066
	Complement component C3	*Ruditapes decussatus*	C0JPJ2	0.0254001	0.4880047
	Complement C1q-like protein 2	*Ruditapes philippinarum*	A0A0U3AA90	0.0490353	0.4372268
	Tropomyosin	*Ruditapes philippinarum*	B7XC71	0.0108534	0.3625167
↓P50-3	Putative filamin-A-like protein isoform X7	*Pinctada fucata*	A0A194AJE0	0.0263184	3.0577519
	Alpha-actinin, sarcomeric	*Crassostrea gigas*	K1RH58	0.0026967	1.7071192

Table 7.2. (Continued)

P50-1 vs. P50-3	Protein	Specie	UniProt ID	p-value	Fold Change
↓P50-1	Complement component C3	*Ruditapes decussatus*	C0JPJ2	0.0007738	7.492525
	Multidrug resistance-associated protein 1	*Crassostrea gigas*	K1PZ06	0.0036800	7.3615299
	Ferritin	*Ruditapes philippinarum*	K4HXI8	0.0280269	5.7942862
	Sodium/potassium-transporting ATPase subunit alpha	*Mizuhopecten yessoensis*	A0A210Q4Z0	0.0092436	5.7118813
	Elongation factor Tu	*Mizuhopecten yessoensis*	A0A210PGD1	0.0001277	4.2521836
	Transgelin-like protein-2	*Mytilus galloprovincialis*	A0A0K0YB45	0.0250828	4.1299950
	Alpha-mannosidase	*Crassostrea gigas*	K1QII0	0.0257803	4.0463078
	Complement C1q-like protein 2	*Ruditapes philippinarum*	A0A0U3AA90	0.0275626	3.9650116
	ATP synthase subunit beta	*Pinctada fucata*	A0A194AL63	0.0221311	3.8420887
	Dihydropyrimidinase	*Crassostrea gigas*	K1PGY5	0.0395081	3.512478
	Phosphoenolpyruvate carboxykinase [GTP]	*Crassostrea gigas*	K1QEA6	0.0172833	3.3638706
	Ferritin	*Ruditapes decussatus*	A0A067XI00	0.0449434	3.0138459

Table 7.2. (Continued)

P50-1 vs. P50-3	Protein	Specie	UniProt ID	p-value	Fold Change
↓P50-1	Sodium/potassium-transporting ATPase subunit alpha	*Tridacna squamosa*	A0A288PNI3	0.0195394	3.0112192
↓P50-3	Alpha-actinin, sarcomeric	*Crassostrea gigas*	K1RH58	0.0019164	2.7964849
	Putative filamin-A-like protein isoform X7	*Pinctada fucata*	A0A194AJE0	0.0267686	2.5644898

Over subjecting clams to 100 nm TiO_2 NPs, actin-binding proteins (talin-1 and filamin-C), phosphoenolpyruvate carboxykinase, catalase and heat shock protein were found to be reduced in the protein corona (Table 7.3). Similarly, cytoskeleton proteins (tubulin, paramyosin and myosin heavy chain) and fibrinogen-related protein were also found to be more concentrated at the beginning of the experiment (unexposed clams). Ferritin in the corona was also reduced, whereas putative filamin-A-like protein (isoform X7) and HSP90 were overexpressed. These findings have been also observed from un-exposed clams and clams exposed to 50 nm TiO_2 NPs. Mixed results have been observed for histones H2A and H2B (reduced at the middle and overexpressed at the end of the experiment) and for sialic acid-binding lectin, alpha-actinin and complement C1q-like protein (overexpressed at the middle and reduced at the end of the experiment).

Concerning un-bonded proteins, stress markers (catalase and heat shock protein) increased along with NPs concentration but the maximum value was reached before exposure, whereas free ferritin was reduced. Proteins such as sarcoplasmic calcium-binding protein, complement component C3, histones (H2A, H2B and H4) and talin-1 were also found overexpressed. The latter was reduced in the corona, which implies talin-1 replacement. In addition to talin-1 exchange (Vroman effect), these findings suggested that histones (H2A and H2B) and complement C1q-like protein have high affinity to 100 nm TiO_2 NPs since their absence as un-bounded proteins.

Table 7.3. Significant proteins (p-value<0.05) in comparisons between samples exposed to 100 nm TiO_2 NPs at different NPs concentrations and times (P100-1, P100-2 and P100-3)

		Protein	Specie	UniProt ID	p-value	Fold Change
P100-1 vs. P100-2	↑P100-1	Talin-1	*Crassostrea gigas*	K1PI02	0.0005744	Infinity
		Filamin-C	*Crassostrea gigas*	K1PW06	0.0012353	Infinity
		Tubulin beta chain	*Mizuhopecten yessoensis*	A0A210R050	0.0016047	Infinity
		Tubulin beta chain	*Lottia gigantea*	V4BLC8	0.0176175	Infinity
		Elongation factor Tu	*Biomphalaria glabrata*	A0A0U3EBQ1	0.0230373	Infinity
		Catalase	*Corbicula fluminea*	A0A1P8NQK0	0.0358463	Infinity
		Paramyosin	*Haliotis discus discus*	E5RSV6	0.0007899	8.1419512
		14-3-3 protein zeta	*Crassostrea gigas*	K1P9N7	0.0269208	7.0483325
		Adenosylhomocysteinase	*Octopus bimaculoides*	A0A0L8G425	0.0037528	6.2445405
		Phosphoenolpyruvate carboxykinase, cytosolic [GTP]	*Crassostrea gigas*	K1Q760	0.0378026	3.5306864
		Putative paramyosin-3	*Pinctada fucata*	A0A194AJD6	0.0009542	3.3782340
		Histone H2B	*Azumapecten farreri*	A2CI31	0.0128329	3.1369220

Table 7.3. (Continued)

P100-1 vs. P100-2	Protein	Specie	UniProt ID	p-value	Fold Change
↓P100-1	Heat shock protein 22 isoform 1	*Ruditapes philippinarum*	C8CBN4	0.0013862	2.7864414
	Histone H2A	*Lottia gigantea*	V4B4B8	0.0081223	2.3862546
	Myosin heavy chain, striated muscle	*Mizuhopecten yessoensis*	A0A210Q4E0	0.0391608	2.3649466
↓P100-2	Sialic acid-binding lectin	*Ruditapes philippinarum*	C8CBM9	0.0003140	10.4925112
	Fibrinogen-related protein 5	*Mytilus galloprovincialis*	E6ZCD7	0.0005376	6.1572559
	Dihydropyrimidinase	*Crassostrea gigas*	K1PGY5	0.0274352	6.0518889
	Elongation factor Tu	*Mizuhopecten yessoensis*	A0A210PGD1	0.0124906	3.3899471
	78 kDa glucose-regulated protein	*Conus novaehollandiae*	H8XWJ4	0.0179069	2.6501730
	Sarcoplasmic calcium binding protein	*Ruditapes philippinarum*	O97050	0.0491842	1.9716440
	Alpha-actinin, sarcomeric	*Crassostrea gigas*	K1RH58	0.0489097	1.8532373

Table 7.3. (Continued)

P100-2 vs. P100-3	Protein	Specie	UniProt ID	p-value	Fold Change
↓P100-2	Ferritin	*Ruditapes philippinarum*	K4HXI8	0.0318333	9.8462902
	Beta-glucuronidase	*Lottia gigantea*	V4A2U2	0.0175567	7.7339991
	Sialic acid-binding lectin	*Ruditapes philippinarum*	C8CBM9	0.0001258	5.4431749
	Cytosolic 10-formyltetrahydrofolate dehydrogenase	*Mizuhopecten yessoensis*	A0A210R6J6	0.0023511	5.2840319
	Dihydropyrimidinase	*Crassostrea gigas*	K1PGY5	0.0094009	3.0730575
	Elongation factor Tu	*Mizuhopecten yessoensis*	A0A210PGD1	0.0068825	2.6227159
	Complement C1q-like protein 3	*Ruditapes philippinarum*	A0A0U3CDP6	0.0113542	2.5903254
	Ubiquitin	*Biomphalaria glabrata*	Q9BH32	0.0484904	2.4770642
	Ferritin	*Ruditapes philippinarum*	U3GS70|	0.0053817	2.3852248
	Retinal dehydrogenase 1	*Mizuhopecten yessoensis*	A0A210Q6W9	0.0388664	2.3451896
	Ferritin	*Ruditapes decussatus*	A0A067XI00	0.0116203	2.2968737

Table 7.3. (Continued)

P100-2 vs. P100-3	Protein	Specie	UniProt ID	p-value	Fold Change
↓P100-2	Sarcoplasmic calcium binding protein	*Ruditapes philippinarum*	O97050	0.0100584	2.2382533
	Citrate synthase	*Biomphalaria glabrata*	A0A2C9K6D3	0.0321746	1.7062287
↓P100-3	Tubulin alpha chain	*Crassostrea gigas*	K1R473	0.0416569	Infinity
	Tubulin beta chain	*Mizuhopecten yessoensis*	A0A210R050	0.0057170	Infinity
	Putative filamin-A-like protein isoform X7	*Pinctada fucata*	A0A194AJE0	0.0051218	4.5354231
	Myosin heavy chain, striated muscle	*Mizuhopecten yessoensis*	A0A210Q4E0	0.0274077	2.7635040
	Putative paramyosin-3	*Pinctada fucata*	A0A194AJD6	0.0284300	2.4712711
	Tubulin beta chain	*Arion vulgaris*	A0A0B7B670	0.0345805	2.4300089
	Histone H2A	*Lottia gigantea*	V4B4B8	0.0078245	2.2604905
	HSP90 protein	*Ruditapes philippinarum*	A0A023W7V2	0.0137218	2.0164056
	Histone H2B	*Azumapecten farreri*	A2CI31	0.0105779	1.8446464

Table 7.3. (Continued)

P100-1 vs. P100-3	↓P100-1	Protein	Specie	UniProt ID	p-value	Fold Change
		Talin-1	*Crassostrea gigas*	K1PI02	0.0005744	Infinity
		Tubulin beta chain	*Lottia gigantea*	V4BLC8	0.0176175	Infinity
		Catalase	*Corbicula fluminea*	A0A1P8NQK0	0.0358463	Infinity
		Catalase	*Haliotis diversicolor*	G5DD16	0.0483616	8.4133107
		Cytosolic 10-formyltetrahydrofolate dehydrogenase	*Mizuhopecten yessoensis*	A0A210R6J6	0.0051686	7.7232152
		Paramyosin	*Haliotis discus discus*	E5RSV6	0.0485499	4.2089065
		Ferritin	*Ruditapes decussatus*	A0A067XI00	0.0034801	3.2930481
		Adenosylhomocysteinase	*Octopus bimaculoides*	A0A0L8G425	0.0236873	2.8464854
		Citrate synthase	*Biomphalaria glabrata*	A0A2C9K6D3	0.0103128	2.8045163
		Phosphoenolpyruvate carboxykinase, cytosolic [GTP]	*Crassostrea gigas*	K1Q760	0.0172936	2.5806487
		Glutathione peroxidase A	*Ruditapes philippinarum*	C8CBM2	0.0012159	2.3494575
		Heat shock protein 22 isoform 1	*Ruditapes philippinarum*	C8CBN4	0.0291205	2.1951327

Table 7.3. (Continued)

P100-1 vs. P100-3	Protein	Specie	UniProt ID	p-value	Fold Change
↓P100-1	Sarcoplasmic calcium-binding protein	*Mizuhopecten yessoensis*	Q9U5C3	0.0112894	1.9130140
	Histone H2B	*Azumapecten farreri*	A2CI31	0.0476586	1.7005547
	Ferritin	*Ruditapes philippinarum*	U3GS70	0.0364343	1.5495406
↓P100-3	Fibrinogen-related protein 5	*Mytilus galloprovincialis*	E6ZCD7	0.0020411	7.2869314
	Alpha-mannosidase	*Crassostrea gigas*	K1QII0	0.0078718	4.8930073
	Putative filamin-A-like protein isoform X7	*Pinctada fucata*	A0A194AJE0	0.0213443	3.9996955
	Phosphoglycerate kinase	*Crassostrea gigas*	K1QCC1	0.0316246	3.2911826
	Alpha-1,4 glucan phosphorylase	*Lottia gigantea*	V4ALJ5	0.0498339	2.8634688
	HSP90 protein	*Ruditapes philippinarum*	A0A023W7V2	0.0139360	2.1625510
	78 kDa glucose-regulated protein	*Conus novaehollandiae*	H8XWJ4	0.0274319	2.0598982
	Triosephosphate isomerase	*Lottia gigantea*	V4AUY5	0.0403528	1.6147199

Finally, results from food additive E171 exposure (Table 7.4) show that catalase, talin-1 and calcium-related proteins (calcium-transporting ATPase and sarcoplasmic calcium binding protein) are overexpressed in the corona, while histones (H4 and H2B) and complement component C3 are reduced. The increment on catalase concentration could be related to oxidative stress, although heat shock protein (other stress protein) was reduced. Several proteins, such as ferritin, complement C1q-like protein 2 and phosphoenolpyruvate carboxykinase were overexpressed at the middle of the exposure. Other proteins, such as superoxide dismutase [Cu-Zn], showed increased concentrations at high E171 concentrations and exposure times (overexpression at the end of the experiment, while not statistically significant differences were found at the middle of the experiment and at initial conditions). Superoxide dismutase [Cu-Zn] is an enzyme involved in the stress oxidative response and the overexpression of this protein alongside catalase could suggest a stress response to E171 exposure.

Concerning un-bonded proteins, heat shock protein and cytochrome c oxidase were overexpressed, but these proteins were not found in the corona (null affinity to nano(micro)particles in the food additive E171). Free histones (H2A and H4) were found to be reduced, similarly to that found in hemolymph from clams exposed to 50 and 100 nm TiO_2 NPs. Overexpression of catalase and superoxide dismutase [Cu-Zn] in the corona and the overexpression of un-bonded heat shock protein and cytochrome c oxidase could be related to an oxidative stress response to TiO_2 nano(micro)particles in E171. In addition, the reduction of complement component C3 and histones (H2B and H4) in the corona could imply immunologic system impairment and deficiencies in DNA packaging by E171 exposure.

Table 7.4. Significant proteins (p-value<0.05) in comparisons between samples exposed to food additive E171 at different concentrations and times (PE171-1, PE171-2 and PE171-3)

PE171-1 vs. PE171-2	Protein	Specie	UniProt ID	p-value	Fold Change
↓PE171-1	Actin-3	*Crassostrea gigas*	K1QHY0	0.0009453	16.5060593
	14-3-3 protein zeta	*Crassostrea gigas*	K1P9N7	0.0309014	4.5163052
	Succinate dehydrogenase [ubiquinone] flavoprotein subunit, mitochondrial	*Lottia gigantea*	V3ZLV6	0.0355801	3.5851241
	Putative 40S ribosomal protein S18	*Pinctada fucata*	A0A194ANH2	0.0394059	2.5359423
	Sialic acid-binding lectin	*Ruditapes philippinarum*	C8CBM9	0.0022599	2.2272847
	Myosin heavy chain	*Onchidium struma nom. nud.*	A0A1P8C5A6	0.0139935	1.8243345
	Myosin heavy chain isoform A	*Octopus bimaculoides*	V6A729	0.0383228	1.8069902
	Histone H4	*Lottia gigantea*	V4A0D9	0.0009580	1.5635391
	Adenosylhomocysteinase	*Octopus bimaculoides*	A0A0L8G425	0.0009267	6.5166326
	Fructose-bisphosphate aldolase	*Lottia gigantea*	V4A4F2	0.0014303	4.5464067
	Phosphoenolpyruvate carboxykinase, cytosolic [GTP]	*Crassostrea gigas*	K1Q760	0.0136658	4.3976485

Table 7.4. (Continued)

		Protein	Specie	UniProt ID	p-value	Fold Change
PE171-1 vs. PE171-2	↑PE171-2	Glutathione peroxidase A	*Ruditapes philippinarum*	C8CBM2	0.0060076	4.0833819
		Retinal dehydrogenase 2	*Mizuhopecten yessoensis*	A0A210QHZ3	0.0281702	3.7307340
		ATP synthase subunit beta	*Pinctada fucata*	A0A194AL63	0.0277259	3.6953969
		Catalase	*Haliotis diversicolor*	G5DD16	0.0012876	3.6861820
		Complement C1q-like protein 2	*Ruditapes philippinarum*	A0A0U3AA90	0.0049315	2.7067480
		Phosphoglycerate kinase	*Crassostrea gigas*	K1QCC1	0.0343376	2.7016467
		Elongation factor Tu	*Mizuhopecten yessoensis*	A0A210PGD1	0.0004426	2.4223859
		Phosphoenolpyruvate carboxykinase [GTP]	*Crassostrea gigas*	K1QEA6	0.0151522	2.1795240
		Actin-related protein 3	*Crassostrea gigas*	K1QLZ1	0.0349355	2.1784463
		Calcium-transporting ATPase	*Mizuhopecten yessoensis*	O96039	0.0096638	2.0377499
		Sarcoplasmic calcium binding protein	*Ruditapes philippinarum*	O97050	0.0309454	2.0175106
		Ferritin	*Ruditapes decussatus*	A0A067XI00	0.0386842	1.9991569
		HSP70 protein	*Ruditapes philippinarum*	A0A023W7L5	0.0060269	1.5760214

Table 7.4. (Continued)

PE171-2 vs. PE171-3	Protein	Specie	UniProt ID	p-value	Fold Change
↓PE171-2	Citrate synthase	*Biomphalaria glabrata*	A0A2C9K6D3	0.0023471	11.8718105
	Adenosylhomocysteinase	*Octopus bimaculoides*	A0A0L8G425	0.0008938	7.9045432
	Complement C1q-like protein 2	*Ruditapes philippinarum*	A0A0U3AA90	0.0030045	6.4960717
	Histone H2B	*Azumapecten farreri*	A2CI31	0.0434082	4.7793958
	Glutathione peroxidase A	*Ruditapes philippinarum*	C8CBM2	0.0065764	4.7157957
	Voltage-dependent anion channel 2-like protein	*Haliotis diversicolor*	D7RP02	0.0101941	4.0923444
	Retinal dehydrogenase 2	*Mizuhopecten yessoensis*	A0A210QHZ3	0.0363724	3.9249686
	Phosphoenolpyruvate carboxykinase, cytosolic [GTP]	*Crassostrea gigas*	K1Q760	0.0300039	3.7872663
	Complement component C3	*Ruditapes decussatus*	C0JPJ2	0.0072975	2.4646676
	Galectin	*Ruditapes philippinarum*	B1AAP1	0.0493285	2.1073448
	Histone H4	*Lottia gigantea*	V4A0D9	0.0022945	1.9678442

Table 7.4. (Continued)

PE171-2 vs. PE171-3		Protein	Specie	UniProt ID	p-value	Fold Change
↓PE171-3		Talin-1	*Crassostrea gigas*	K1PI02	0.0122852	Infinity
		Superoxide dismutase [Cu-Zn]	*Ruditapes philippinarum*	J7FI85	0.0499451	4.2673882
		Clathrin heavy chain	*Crassostrea gigas*	K1PNR3	0.0327303	2.8486850
		Myosin heavy chain, striated muscle	*Mizuhopecten yessoensis*	A0A210Q4E0	0.0239769	2.1853349
		Tropomyosin	*Ruditapes philippinarum*	B7XC71	0.0136809	2.0265467
		Alpha-1,4 glucan phosphorylase	*Lottia gigantea*	V4AL J5	0.0027013	1.5453371
PE171-1 vs. PE171-3						
↓PE171-1		14-3-3 protein zeta	*Crassostrea gigas*	K1P9N7	0.0003466	Infinity
		Citrate synthase	*Biomphalaria glabrata*	A0A2C9K6D3	0.0104750	13.8205791
		Myosin heavy chain	*Onchidium struma nom. nud.*	A0A1P8C5A6	0.0098597	6.2462582
		Histone H2B	*Azumapecten farreri*	A2CI31	0.0026188	6.0355987
		Actin-3	*Crassostrea gigas*	K1QHY0	0.0061522	4.7354179

Table 7.4. (Continued)

PE171-1 vs. PE171-3	Protein	Specie	UniProt ID	p-value	Fold Change
↓PE171-1	Histone H4	*Lottia gigantea*	V4A0D9	0.0002335	3.0768013
	Fascin	*Biomphalaria glabrata*	A0A2C9JG25	0.0464751	2.8991090
	Voltage-dependent anion channel 2-like protein	*Haliotis diversicolor*	D7RP02	0.0121926	2.4803589
	Complement C1q-like protein 2	*Ruditapes philippinarum*	A0A0U3AA90	0.0452866	2.3999544
	Heat shock protein 22 isoform 1	*Ruditapes philippinarum*	C8CBN4	0.0417098	2.3973459
	Galectin	*Ruditapes philippinarum*	B1AAP1	0.0487401	2.0816840
	Complement component C3	*Ruditapes decussatus*	C0JPJ2	0.0387554	1.8380756
↓PE171-3	Talin-1	*Crassostrea gigas*	K1PI02	0.0250580	6.6560924
	Catalase	*Haliotis diversicolor*	G5DD16	0.0148415	6.6024978
	Actin-related protein 3	*Crassostrea gigas*	K1QLZ1	0.0261401	5.8549875
	Phosphoglycerate kinase	*Crassostrea gigas*	K1QCC1	0.0127030	5.3141204
	Arginine kinase	*Paphia undulata*	C3VUU4	0.0487950	4.6340077

Table 7.4. (Continued)

PE171-1 vs. PE171-3	↓PE171-3	Protein	Specie	UniProt ID	p-value	Fold Change
		Myosin heavy chain, non-muscle	*Mizuhopecten yessoensis*	A0A210QSX4	0.0203327	3.6060649
		Dihydropyrimidinase	*Crassostrea gigas*	K1PGY5	0.0127477	3.3944513
		Sarcoplasmic calcium binding protein	*Ruditapes philippinarum*	O97050	0.0499233	3.2316237
		Tropomyosin	*Ruditapes philippinarum*	B7XC71	0.0067989	2.3511686
		Arginine kinase two-domain chain	*Spisula sachalinensis*	O77052	0.0145903	2.0898700
		Myosin heavy chain, striated muscle	*Mizuhopecten yessoensis*	A0A210Q4E0	0.0239164	1.5399290

7.4 CONCLUSIONS

The analysis of hemolymph from clams (*Spisula solidissima*) exposed to TiO_2 NPs (50 and 100 nm) and food additive E171 at different exposure times (nine days, 8 mg L^{-1}; eighteen days, 14 mg L^{-1}) has shown high variability in protein profile in TiO_2 NP-protein complexes and un-bounded protein, even before TiO_2 NPs exposure. Exposure at 50 nm TiO_2 NPs has led to the presence of fibrinogen-related and sarcoplasmic calcium binding proteins at middle conditions (nine days, 8 mg L^{-1}), whereas alpha-actinin and putative filamin-A-like proteins have been found to be more concentrated at the end of the experiment (eighteen days, 14 mg L^{-1}). Changes on protein corona in hemolymph from clams exposed to 50 nm TiO_2 NPs have also shown a decrement in complement components (C3 and C1q), which are related to innate immunity, whereas the concentration of unbounded superoxide dismutase (oxidative stress marker) and histones was found to be increased. Results regarding exposure to 100 nm TiO_2 NPs have shown that heat shock protein forms part of the corona, as well as ATP synthase (subunit beta), which concentration is higher when the exposition time and TiO_2 NPs concentration increase. In addition, 100 nm TiO_2 NPs showed high for histones (H2A and H2B) and low affinity for complement component C3. Coronas from food additive E171 was found to consist of complement C1q-like protein, histones (H2A and H2B) and proteins such as talin-1, catalase and superoxide dismutase. Catalase and superoxide dismutase were found to be increased in the corona for long exposure times, whereas the concentration of unbounded cytochrome c oxidase increased over time in supernatants. These variations could be related to stress oxidative produced by E171 exposure. In addition, there was a decrease in unbounded complement component C3 concentration, so immunologic system could be affected. In general, since the decrease in complement components and the increment in stress marker, TiO_2 NPs could cause alterations in immune system and oxidative stress.

Acknowledgements
The authors wish to acknowledge the financial support of *Ministerio de Economía y Competitividad* (project INNOVANANO, reference RT2018-099222-B-100), and *Xunta de Galicia* (*Grupo de Referencia Competitiva*, grant number ED431C2018/19; and Program for Development of a Strategic Grouping in Materials – AEMAT, grant number ED431E2018/08). Authors also thank to Proteomics Platform from Health Research Institute of Santiago de Compostela (IDIS) for proteomics analysis; Margarita Vilas-Cruz (Acuario at the Faculty of Biology, University of Santiago de Compostela) for clams mesocosmos facilities; and Professor Ana M. Otero-Casal (Aquiculture and Biotechnology Group at University of Santiago de Compostela) for phytoplankton culture. M.V. Taboada-López thanks the *Xunta de Galicia* and the European Social Fund (FSE) for the pre-doctoral grant.

7.5 REFERENCES

[1] The European Commission. Commission, Recommendation (EU) 2011/696 of 18 October 2011 on the definition of nanomaterial, Official Journal of the European Union L 275. 58 (2011) 38–40.
[2] Consumer Products Inventory. An inventory of nanotechnology-based consumer products introduced on the market, http://www.nanotechproject.org/cpi (accessed on March 30th 2020).
[3] G. Bystrzejewska-Piotrowska, J. Golimowski, P.L. Urban, Nanoparticles: Their potential toxicity, waste and environmental management, Waste Manag. 29 (2009) 2587–2595.
[4] Y. Lan, Y. Lu, Z. Ren, Mini review on photocatalysis of titanium dioxide nanoparticles and their solar applications, Nano Energy 2 (2013) 1031–1045.
[5] X. Chen, S.S. Mao, Titanium dioxide nanomaterials: Synthesis, properties, modifications and applications, Chem. Rev. 107 (2007) 2891–2959.
[6] O. Geiss, J. Ponti, C. Senaldi, I. Bianchi, D. Mehn, J. Barrero, D. Gilland, R. Matissek, E. Anklan, Characterisation of food grade titania with respect to nanoparticle content in pristine additives and in their related food products, Food Addit. Contam. A 37 (2020) 236–253.

[7] Y. Yang, K. Doudrick, X. Bi, K. Hristovski, P. Herckes, P. Westerhoff, R. Kaegi, Characterization of Food-Grade Titanium Dioxide: The Presence of Nanosized Particles, Environ. Sci. Technol. 48 (2014) 6391–6400.
[8] N. Liu, M. Tang, J. Ding, The interaction between nanoparticles-protein corona complex and cells and its toxic effect on cells, Chemosphere. 245 (2020) 125624 (DOI: 10.1016/j.chemosphere.2019.125624).
[9] C. Ge, J. Tian, Y. Zhao, C. Chen, R. Zhou, Z. Chai, Towards understanding of nanoparticle–protein corona, Arch. Toxicol. 89 (2015) 519–539.
[10] B. Kharazian, N.L. Hadipour, M.R. Ejtehadi, Understanding the nanoparticle-protein corona complexes using computational and experimental methods, Int. J. Biochem. Cell Biol. 75 (2016) 162–174.
[11] M. Neagu, Z. Piperigkou, K. Karamanou, A.B. Engin, A.O. Docea, C. Constantin, C. Negrei, D. Nikitovic, A. Tsatsakis, Protein bio-corona: critical issue in immune nanotoxicology, Arch. Toxicol. 91 (2017) 1031–1048.
[12] I. Dewald, O. Isakin, J. Schubert, T. Kraus, M. Chanana, Protein Identity and Environmental Parameters Determine the Final Physicochemical Properties of Protein-Coated Metal Nanoparticles, J. Phys. Chem. C. 119 (2015) 25482–25492.
[13] D.K. Ban, S. Paul, Protein corona over silver nanoparticles triggers conformational change of proteins and drop in bactericidal potential of nanoparticles: Polyethylene glycol capping as preventive strategy, Colloid. Surface. B. 146 (2016) 577–584.
[14] H. Yang, M. Wang, Y. Zhang, X. Liu, S. Yu, Y. Guo, S. Yang, L. Yang, Detailed insight into the formation of protein corona: Conformational change, stability and aggregation, Int. J. Biol. Macromol. 135 (2019) 1114–1122.
[15] S. Zanganeh, R. Spitler, M. Erfanzadeh, A.M. Alkilany, M. Mahmoudi, Protein corona: Opportunities and challenges, Int. J. Biochem. Cell Biol. 75 (2016) 143–147.
[16] L. Canesi, T. Balbi, R. Fabbri, A. Salis, G. Damonte, M. Volland, J. Blasco, Biomolecular coronas in invertebrate species: Implications in the environmental impact of nanoparticles, NanoImpact 8 (2017) 89–98.
[17] L. Canesi, I. Corsi, Effects of nanomaterials on marine invertebrates, Sci. Total Environ. 565 (2015) 933–940.

[18] L. Canesi, C. Ciacci, R. Fabbri, T. Balbi, A. Salis, G. Damonte, K. Cortese, V. Caratto, M.P. Monopoli, K. Dawson, E. Bergami, I. Corsi, Interactions of cationic polystyrene nanoparticles with marine bivalve hemocytes in a physiological environment: Role of soluble hemolymph proteins, Environ. Res. 150 (2016) 73–81.
[19] M. Sendra, M. Volland, T. Balbi, R. Fabbri, M.P. Yeste, J.M. Gatica, L. Canesi, J. Blasco, Cytotoxicity of CeO_2 nanoparticles using *in vitro* assay with *Mytilus galloprovincialis* hemocytes: Relevance of zeta potential, shape and biocorona formation, Aquat. Toxicol. 200 (2018) 13–20.
[20] J. Gao, L. Lin, A. Wei, M.S. Sepúlveda, Protein corona analysis of silver nanoparticles exposed to fish plasma, Environ. Sci. Technol. Lett. 4 (2017) 174–179.
[21] Y. Hayashi, T. Miclaus, S. Murugadoss, M. Takamiya, C. Scavenius, K. Kjaer-Sorensen, J. Enghild, U. Strähle, C. Oxvig, C. Weiss, D. Sutherland, Female versus male biological identities of nanoparticles determine the interaction with immune cells in fish, Environ. Sci.: Nano 4 (2017) 895–906.
[22] L. Zeng, J. Gao, Y. Liu, J. Gao, L. Yao, X. Yang, X. Liu, B. He, L. Hu, J. Shi, M. Song, G. Qu, G. Jiang, Role of protein corona in the biological effect of nanomaterials: Investigating methods, Trac-Trend. Anal. Chem. 118 (2019) 303–314.
[23] D. Baimanov, R. Cai, C. Chen, Understanding the Chemical Nature of Nanoparticle-Protein Interactions, Bioconjug. Chem. 30 (2019) 1923–1937.
[24] S. Pereira, A. Otero, *Haematococcus pluvialis* bioprocess optimization: Effect of light quality, temperature and irradiance on growth, pigment content and photosynthetic response, Algal Res. 51 (2020) 102027 (DOI: 10.1016/j.algal.2020.102027).
[25] N. García-Otero, E. Peña-Vázquez, M.C. Barciela-Alonso, P. Bermejo-Barrera, A. Moreda-Piñeiro, Two-Dimensional Isoelectric Focusing OFFGEL and Microfluidic Lab-on-Chip Electrophoresis for Assessing Dissolved Proteins in Seawater, Anal. Chem. 85 (2013) 5909–5916.
[26] M.V. Taboada-López, S. Iglesias-López, P. Herbello-Hermelo, P. Bermejo-Barrera, A. Moreda-Piñeiro, Ultrasound assisted enzymatic hydrolysis for isolating titanium dioxide nanoparticles from bivalve mollusc before sp-ICP-MS, Anal. Chim. Acta 1018 (2018) 16–25.

[27] E.M. Foekema, N.H.B.M. Kaag, K.J.M. Kramer, K. Long, Mesocosm validation of the marine No Effect Concentration of dissolved copper derived from a species sensitivity distribution, Sci. Total Environ. 521–522 (2015) 173–182.
[28] M.E. Ledger, R.M.L. Harris, P.D. Armitage, A.M. Milner, Realism of model ecosystems: An evaluation of physicochemistry and macroinvertebrate assemblages in artificial streams, Hydrobiologia 617 (2009) 91–99.

7.6 SUPPLEMENTARY INFORMATION

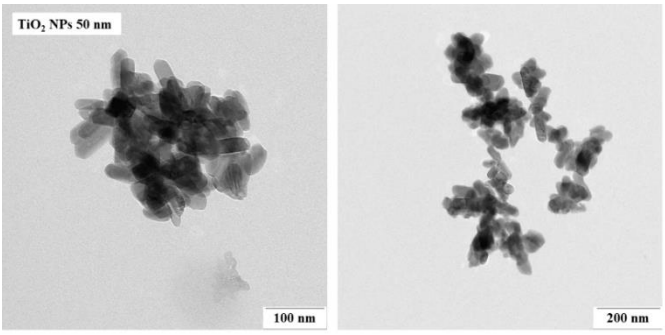

Figure S7.1. TEM images of 50 nm TiO_2 NPs standard

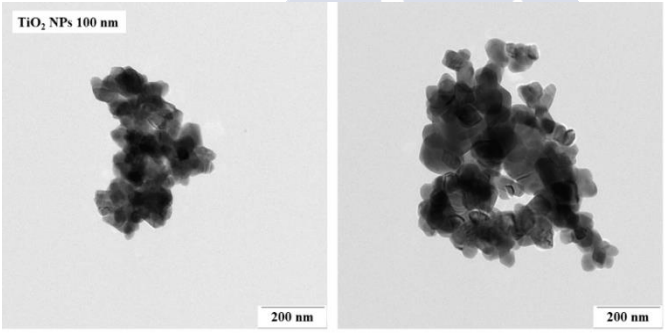

Figure S7.2. TEM images of 100 nm TiO_2 NPs standard

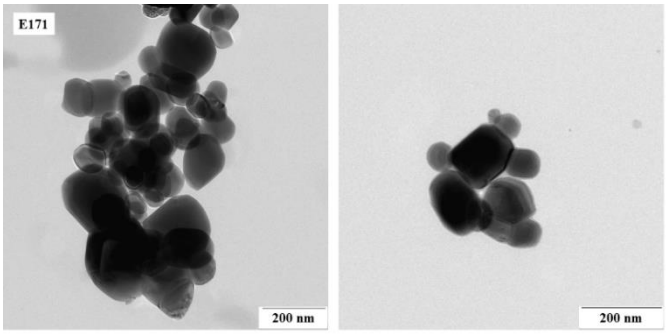

Figure S7.3. TEM images of food additive E171

Table S7.1. Uncommon proteins over time in control samples

	Protein	Specie	UniProt ID	Peptides (95%)	% Cov (95%)
PC-1	Myosin heavy chain, striated muscle	*Mizuhopecten yessoensis*	A0A210QNK6	5	2.8
	Tubulin alpha chain	*Lottia gigantea*	V4CGI5	3	10.9
	Putative paramyosin-3	*Pinctada fucata*	A0A194AJD6	2	2.8
	ADP, ATP carrier protein	*Mizuhopecten yessoensis*	A0A210PS96	2	8.3
	Actin	*Azumapecten farreri*	Q7YZD7	24	44.7
	Complement C1q-like protein 2	*Ruditapes philippinarum*	A0A0U3AA90	2	16.0
	ATP synthase subunit alpha	*Octopus bimaculoides*	A0A0L8IA38	1	2.2
	Elongation factor 1-alpha	*Lottia gigantea*	V4AP92	1	2.6
	Heat shock protein 78	*Hyriopsis cumingii*	X2KNR4	1	2.6
	Myosin heavy chain	*Onchidium struma nom. nud.*	A0A1P8C5A6	4	1.9
	Alpha macroglobulin	*Azumapecten farreri*	Q6TL26	1	0.5
	Ferritin	*Biomphalaria glabrata*	A0A2C9LWC4	1	3.4
	Myosin heavy chain, striated muscle	*Crassostrea gigas*	K1QRU8	2	2.4
	ATP synthase subunit beta	*Biomphalaria glabrata*	A0A2C9KBD6	1	1.4

Table S7.1. (Continued)

	Protein	Specie	UniProt ID	Peptides (95%)	% Cov (95%)
PC-2	Tubulin beta chain	*Biomphalaria glabrata*	A0A2C9JVM1	4	14.1
	Tubulin alpha chain	*Lottia gigantea*	V4CDJ4	3	10.9
	Myosin heavy chain isoform A	*Sepia officinalis*	V6A720	1	0.6
PC-3	Tubulin beta chain	*Lottia gigantea*	V3ZL01	34	61.0
	Tubulin alpha chain	*Crassostrea gigas*	K1QII6	32	41.7
	HSP90 protein	*Ruditapes philippinarum*	A0A023W7V2	6	8.8
	HSP70 protein	*Ruditapes philippinarum*	A0A023W7L5	7	11.6
	Heat shock protein 22 isoform 1	*Ruditapes philippinarum*	C8CBN4	8	53.2
	Arginine kinase	*Paphia undulata*	C3VUU4	5	10.3
	Clathrin heavy chain	*Crassostrea gigas*	K1PNR3	4	3.8
	ADP-ribosylation factor	*Crassostrea gigas*	K1PTH4	3	4.1
	Tubulin beta chain	*Arion vulgaris*	A0A0B7B670	31	62.0
	Tubulin alpha chain	*Lottia gigantea*	V3ZGT0	26	41.6
	Alpha-1,4 glucan phosphorylase	*Lottia gigantea*	V4ALJ5	2	4.0

Table S7.1. (Continued)

	Protein	Specie	UniProt ID	Peptides (95%)	% Cov (95%)
PC-3	40S ribosomal protein S2	*Mizuhopecten yessoensis*	A0A210PH18	2	8.6
	40S ribosomal protein SA	*Crassostrea gigas*	K1R4D4	2	9.2
	78kDa glucose regulated protein	*Crassostrea gigas*	Q75W49	5	6.5
	Cytochrome c oxidase subunit 2	*Ruditapes philippinarum*	Q8WF42	2	4.2
	Fructose-bisphosphate aldolase	*Meretrix meretrix*	E3VWM3	2	6.0
	Tubulin alpha chain	*Lottia gigantea*	V3ZTB1	2	6.4
	Ras-related protein Rab-7a	*Crassostrea gigas*	K1PZ08	3	14.2
	Glutathione S-transferase B	*Ruditapes philippinarum*	C8CBM0	2	9.8
	Galectin	*Ruditapes philippinarum*	B1AAP1	2	6.5
	Tubulin alpha chain	*Lottia gigantea*	V3YVR5	23	32.2
	Tubulin beta chain	*Lottia gigantea*	V4AVP5	27	50.2
	Tubulin beta chain	*Mizuhopecten yessoensis*	A0A210R050	31	50.1
	Calcium-transporting ATPase	*Mizuhopecten yessoensis*	O96039	1	2.3
	Glutathione peroxidase A	*Ruditapes philippinarum*	C8CBM2	2	8.9

Table S7.1. (Continued)

	Protein	Specie	UniProt ID	Peptides (95%)	% Cov (95%)
PC-3	Elongation factor 1-alpha	*Azumapecten farreri*	K9L279	3	7.4
	Sodium/potassium-transporting ATPase subunit alpha	*Tridacna squamosa*	A0A288PNI3	1	1.6
	Tubulin beta chain	*Lottia gigantea*	V4A0A3	15	15.5
	Calcium-transporting ATPase	*Octopus bimaculoides*	A0A0L8FX15	1	1.7
	Tubulin beta chain	*Lottia gigantea*	V4BLC8	9	19.1
	PL10-like protein	*Haliotis asinina*	C7EAA2	1	1.8
	ATP synthase subunit beta	*Pinctada fucata*	A0A194AL63	9	27.7
	Ras-related protein Rab-11B	*Crassostrea gigas*	K1QX44	1	7.6
	Dolichyl-diphosphooligosaccharide-protein glycosyltransferase 48 kDa subunit	*Lottia gigantea*	V3ZEM0	1	2.5
	Ribosomal protein S13	*Argopecten irradians*	Q8ITB0	1	8.1
	Cytosolic 10-formyltetrahydrofolate dehydrogenase	*Mizuhopecten yessoensis*	A0A210R6J6	1	1.9
	Tubulin beta chain	*Pinctada fucata*	A0A194AQ74	31	58.0
	Beta-actin 2	*Sinonovacula constricta*	V9I358	21	37.5

Table S7.1. (Continued)

	Protein	Specie	UniProt ID	Peptides (95%)	% Cov (95%)
PC-3	Tubulin beta chain	*Pinctada fucata*	A0A194AQ74	31	58.0
	Beta-actin 2	*Sinonovacula constricta*	V9I358	21	37.5
	Tubulin beta chain	*Lymnaea stagnalis*	A0A1D8KD44	14	16.1
	Myosin heavy chain, striated muscle	*Crassostrea gigas*	K1RSS3	3	2.1
	40S ribosomal protein S18	*Biomphalaria glabrata*	A0A2C9JC73	1	5.3
	Catalase	*Lottia gigantea*	V4B843	1	2.6
	Protein kinase C	*Lottia gigantea*	V4B6K8	1	1.8
	T-complex protein 1 subunit delta	*Lottia gigantea*	V4B496	1	2.5
	Rab GDP dissociation inhibitor	*Lottia gigantea*	V3ZWK7	1	4.3
	Protein disulfide-isomerase	*Lottia gigantea*	V3ZNZ0	1	1.6
	Coatomer subunit gamma	*Lottia gigantea*	V3ZH42	1	1.4
	Sarcoplasmic calcium binding protein	*Ruditapes philippinarum*	O97050	1	9.9
	Puromycin-sensitive aminopeptidase	*Crassostrea gigas*	K1R866	1	2.3
	T-complex protein 1 subunit beta	*Crassostrea gigas*	K1R294	1	2.8

Table S7.1. (Continued)

	Protein	Specie	UniProt ID	Peptides (95%)	% Cov (95%)
PC-3	Glucose dehydrogenase [acceptor]	*Crassostrea gigas*	K1QZJ5	1	1.3
	26S proteasome non-ATPase regulatory subunit 2	*Crassostrea gigas*	K1QDM2	1	1.7
	Putative phosphoglycerate mutase	*Crassostrea gigas*	K1QBL3	1	5.6
	TNF receptor-associated factor 3	*Crassostrea gigas*	K1PDY7	2	1.9
	40S ribosomal protein S7	*Biomphalaria glabrata*	A0A2C9JPX3	1	6.2
	Actin-related protein 2/3 complex subunit 4	*Mizuhopecten yessoensis*	A0A210R0V6	1	6.5
	Ras GTPase-activating-like protein IQGAP1	*Mizuhopecten yessoensis*	A0A210QG69	1	0.7
	Putative 60S ribosomal protein L7-like protein	*Pinctada fucata*	A0A194AM17	1	4.1
	Ubiquitin	*Ruditapes philippinarum*	A0A1P8SD54	2	32.5
	Arginine kinase	*Meretrix lyrata*	C3VUU3	5	8.5
	Isocitrate dehydrogenase [NADP]	*Mizuhopecten yessoensis*	A0A210QYM1	1	1.8
	Phosphoglycerate kinase	*Lottia gigantea*	V4ADA9	2	7.7
	Paramyosin	*Mizuhopecten yessoensis*	A0A210R0B2	1	1.2
	Myosin essential light chain	*Pecten maximus*	Q9U7E2	1	7.6

Table S7.2. Uncommon proteins over time in samples exposed to 50 nm TiO_2 NPs

	Protein	Specie	UniProt ID	Peptides (95%)	% Cov (95%)
P50-1	Ferritin	*Ruditapes philippinarum*	U3GS70	4	24.7
	ATP synthase subunit beta	*Pinctada fucata*	A0A194AL63	2	6.1
	Actin 2	*Crassostrea gigas*	Q8TA69	21	45.0
	Elongation factor Tu	*Biomphalaria glabrata*	A0A0U3EBQ1	1	3.8
	Sarcoplasmic calcium binding protein	*Ruditapes philippinarum*	O97050	1	9.9
	Cell cycle regulator Mat89Bb-like protein	*Crassostrea gigas*	K1PUA7	1	4.3
	Elongation factor Tu	*Mizuhopecten yessoensis*	A0A210PGD1	1	1.9
	Histone H4	*Octopus bimaculoides*	A0A0L8GSZ5	5	17.6
	ATP synthase subunit alpha	*Mizuhopecten yessoensis*	A0A2C9K8Q4	1	0.0
P50-2	Ubiquitin	*Pinctada fucata*	V5IWR5	1	21.1
	Retinol dehydrogenase 14	*Mizuhopecten yessoensis*	A0A210QLE1	1	3.1
	Heat shock protein 90	*Paphia undulata*	L0BTB2	1	1.9
	ATP synthase subunit beta	*Lottia gigantea*	V4AQP1	1	1.9

Table S7.2. (Continued)

	Protein	Specie	UniProt ID	Peptides (95%)	% Cov (95%)
P50-3	Myosin heavy chain	*Onchidium struma nom. nud.*	A0A1P8C5A6	18	9.7
	Tubulin alpha chain	*Crassostrea gigas*	Q5H7U8	13	42.4
	ATP synthase subunit alpha	*Lottia gigantea*	V4A6V0	6	16.1
	HSP70 protein	*Ruditapes philippinarum*	A0A023W7L5	5	8.5
	Calcium-transporting ATPase	*Mizuhopecten yessoensis*	O96039	4	5.6
	Myosin heavy chain, non-muscle	*Mizuhopecten yessoensis*	A0A210QSX4	9	4.5
	Filamin-A	*Mizuhopecten yessoensis*	A0A210QAC9	5	2.4
	Clathrin heavy chain	*Crassostrea gigas*	K1PNR3	4	4.2
	HSP90 protein	*Ruditapes philippinarum*	A0A023W7V2	4	7.0
	Calcium-transporting ATPase	*Crassostrea gigas*	K1QA13	4	6.9
	Arginine kinase	*Paphia undulata*	C3VUU4	2	6.5
	Myosin heavy chain, striated muscle	*Mizuhopecten yessoensis*	A0A210Q4E0	12	5.8
	Isocitrate dehydrogenase [NADP]	*Mizuhopecten yessoensis*	A0A210QYM1	2	4.5
	Arginine kinase two-domain chain	*Spisula sachalinensis*	O77052	3	4.3

Table S7.2. (Continued)

	Protein	Specie	UniProt ID	Peptides (95%)	% Cov (95%)
P50-3	Non-muscle myosin II heavy chain	*Doryteuthis pealeii*	Q8SWQ7	5	2.9
	Beta-actin isotype 1	*Lymnaea stagnalis*	A0A1D8KD32	48	54.8
	Ras GTPase-activating-like protein IQGAP1	*Mizuhopecten yessoensis*	A0A210QG69	3	1.9
	Malate dehydrogenase	*Mizuhopecten yessoensis*	A0A210QWL4	2	6.7
	Triosephosphate isomerase	*Crassostrea ariakensis*	H9LJ32	2	10.0
	Visual G-protein beta subunit	*Doryteuthis pealeii*	Q6TQF6	1	3.5
	Actin-related protein 2/3 complex subunit 4	*Octopus bimaculoides*	A0A0L8FI18	2	13.1
	Ubiquitin	*Biomphalaria glabrata*	Q9BH32	1	12.5
	Fructose-bisphosphate aldolase	*Meretrix meretrix*	E3VWM3	2	10.2
	Enolase	*Crassostrea gigas*	K1QX37	1	0.8
	14-3-3 protein zeta	*Crassostrea gigas*	K1P9N7	2	3.3
	Septin-2	*Crassostrea gigas*	K1PY30	1	1.7
	Transgelin-like protein-2	*Mytilus galloprovincialis*	A0A0K0YB45	4	9.6
	Putative filamin-A-like protein isoform X7	*Pinctada fucata*	A0A194AJE0	1	3.6

Table S7.2. (Continued)

	Protein	Specie	UniProt ID	Peptides (95%)	% Cov (95%)
P50-3	Cytochrome c oxidase subunit 2	*Ruditapes philippinarum*	Q8WF42	1	1.9
	Complement C1q-like protein 2	*Ruditapes philippinarum*	A0A0U3AA90	3	8.4
	Complement C1q-like protein 3	*Ruditapes philippinarum*	A0A0U3CDP6	1	8.6
	Profilin	*Lottia gigantea*	V4A7Z0	1	10.0
	Calcium-transporting ATPase	*Octopus bimaculoides*	A0A0L8FX15	3	5.8
	Coatomer subunit gamma	*Lottia gigantea*	V3ZH42	1	1.4
	Dolichyl-diphosphooligosaccharide-protein glycosyltransferase 48 kDa subunit	*Lottia gigantea*	V3ZEM0	1	2.5
	Ras-related protein Rab-11B	*Crassostrea gigas*	K1QX44	1	7.6
	Ras-related protein Rab-7a	*Crassostrea gigas*	K1PZ08	1	6.3
	Calcium-transporting ATPase	*Hyriopsis cumingii*	A0A0U1ZY67	4	6.0
	40S ribosomal protein SA	*Meretrix meretrix*	K4M440	1	4.2
	Histone H3	*Crassostrea gigas*	K1Q9K6	1	2.7
	Myosin essential light chain	*Pecten maximus*	Q9U7E2	1	7.6

Table S7.2. (Continued)

	Protein	Specie	UniProt ID	Peptides (95%)	% Cov (95%)
P50-3	Protein kinase C	*Lottia gigantea*	V4B6K8	1	1.8
	Kyphoscoliosis peptidase	*Mizuhopecten yessoensis*	A0A210QLF5	1	1.1
	Galectin	*Ruditapes philippinarum*	B1AAP1	1	3.6
	Phosphoglycerate kinase	*Crassostrea gigas*	K1QCC1	1	3.7
	Putative phosphoglycerate mutase	*Crassostrea gigas*	K1QBL3	1	5.6
	Myosin essential light chain	*Hyriopsis cumingii*	J9UEN7	1	8.4
	Glyceraldehyde-3-phosphate dehydrogenase	*Haliotis discus discus*	B6RB30	1	3.8
	Propionyl-CoA carboxylase beta chain, mitochondrial	*Mizuhopecten yessoensis*	A0A210PUA9	1	2.6
	Methylmalonyl-CoA mutase, mitochondrial	*Mizuhopecten yessoensis*	A0A210PW47	1	1.5
	Endoplasmin	*Mizuhopecten yessoensis*	A0A210PZR8	1	1.5
	Tubulin alpha chain	*Octopus bimaculoides*	A0A0L8HMY5	9	25.6
	Protein disulfide-isomerase	*Lottia gigantea*	V3ZNZ0	1	1.6
	Peptidyl-prolyl cis-trans isomerase	*Mizuhopecten yessoensis*	A0A210Q9T6	1	4.8
	Tubulin beta chain	*Lottia gigantea*	V3YY74	15	30.2

Table S7.2. (Continued)

	Protein	Specie	UniProt ID	Peptides (95%)	% Cov (95%)
P50-3	Cystatin B	*Ruditapes philippinarum*	M9NV28	1	12.1
	Receptor of Activated Kinase C 1	*Mya arenaria*	Q08G56	1	3.8
	Polycystin-1	*Crassostrea gigas*	K1RLH5	1	0.3
	TNF receptor-associated factor 3	*Crassostrea gigas*	K1PDY7	1	1.9
	Calcium-transporting ATPase	*Tridacna squamosa*	A0A288MAH8	3	4.6
	Muscle myosin heavy chain	*Sepia esculenta*	B2ZTQ6	7	3.4
	Pyruvate kinase	*Crassostrea gigas*	Q0KHB6	1	2.3

Table S7.3. Uncommon proteins over time in samples exposed to 100 nm TiO_2 NPs

	Protein	Specie	UniProt ID	Peptides (95%)	% Cov (95%)
P100-1	Actin 2	*Crassostrea gigas*	Q8TA69	52	68.9
	Tubulin alpha chain	*Mizuhopecten yessoensis*	A0A210Q0A8	17	45.0
	Histone H4	*Octopus bimaculoides*	A0A0L8GSZ5	14	35.7
	ATP synthase subunit alpha	*Lottia gigantea*	V4A6V0	7	16.1
	Tropomyosin	*Ruditapes philippinarum*	B7XC71	7	26.4
	Phosphoenolpyruvate carboxykinase, cytosolic [GTP]	*Mizuhopecten yessoensis*	A0A210R642	5	8.4
	Radixin	*Crassostrea gigas*	K1PUJ1	4	8.0
	Sodium/potassium-transporting ATPase subunit alpha	*Tridacna squamosa*	A0A288PNI3	3	5.3
	Histone H2B	*Azumapecten farreri*	A2CI31	7	28.8
	Catalase	*Corbicula fluminea*	A0A1P8NQK0	3	9.2
	ADP-ribosylation factor	*Crassostrea gigas*	K1PTH4	3	4.1
	Calcium-transporting ATPase	*Tridacna squamosa*	A0A288MAH8	6	8.3
	Retinal dehydrogenase 2	*Mizuhopecten yessoensis*	A0A210QHZ3	4	8.4
	10-formyltetrahydrofolate dehydrogenase	*Lottia gigantea*	V4B2Z6	2	2.9

Table S7.3. (Continued)

	Protein	Specie	UniProt ID	Peptides (95%)	% Cov (95%)
P100-1	Actin	*Azumapecten farreri*	Q7YZD7	35	50.5
	Catalase	*Haliotis diversicolor*	G5DD16	2	6.6
	Methylmalonate-semialdehyde dehydrogenase [acylating], mitochondrial	*Mizuhopecten yessoensis*	A0A210PP78	3	7.2
	Malate dehydrogenase	*Mizuhopecten yessoensis*	A0A210QWL4	2	6.7
	Heat shock protein 22 isoform 2	*Ruditapes philippinarum*	C8CBN5	2	10.9
	Pyruvate carboxylase, mitochondrial	*Crassostrea gigas*	K1QHI5	2	1.5
	Adenosylhomocysteinase	*Crassostrea gigas*	K1RW85	3	7.2
	Ferritin	*Ruditapes philippinarum*	U3GS70	1	6.5
	Pyruvate carboxylase	*Biomphalaria glabrata*	A0A2C9JXN7	1	1.1
	Sodium/potassium-transporting ATPase subunit alpha	*Mizuhopecten yessoensis*	A0A210Q4Z0	2	3.8
	Triosephosphate isomerase	*Crassostrea ariakensis*	H9LJ32	1	6.0
	Cytosolic 10-formyltetrahydrofolate dehydrogenase	*Mizuhopecten yessoensis*	A0A210R6J6	2	3.3
	Multidrug resistance-associated protein 1	*Crassostrea gigas*	K1PZ06	1	1.0

Table S7.3. (Continued)

	Protein	Specie	UniProt ID	Peptides (95%)	% Cov (95%)
P100-1	Propionyl-CoA carboxylase beta chain, mitochondrial	*Mizuhopecten yessoensis*	A0A210PUA9	3	7.5
	Tubulin beta chain	*Pinctada fucata*	A0A194AQ74	25	62.7
	Putative methylmalonate-semialdehyde dehydrogenase [acylating], mitochondria	*Crassostrea gigas*	K1R252	1	2.1
	Glycogen [starch] synthase	*Biomphalaria glabrata*	A0A2C9JZ16	1	2.1
	Phosphoenolpyruvate carboxykinase, cytosolic [GTP]	*Crassostrea gigas*	K1Q760	2	4.6
	Ras-related protein Rab-1	*Crassostrea gigas*	K1RBB8	1	6.0
	Serine hydroxymethyltransferase	*Biomphalaria glabrata*	A0A2C9K569	1	2.2
	Methylmalonyl-CoA mutase, mitochondrial	*Mizuhopecten yessoensis*	A0A210PW47	1	1.5
	4-hydroxyphenylpyruvate dioxygenase	*Crassostrea gigas*	K1QX22	1	0.6
	Endoplasmin	*Mizuhopecten yessoensis*	A0A210PZR8	2	3.0
	Myosin essential light chain	*Pecten maximus*	Q9U7E2	1	7.6
	Enolase	*Crassostrea gigas*	K1QX37	1	0.8
	Cytochrome c oxidase subunit 3	*Ruditapes philippinarum*	Q8WF35	1	2.7

Table S7.3. (Continued)

	Protein	Specie	UniProt ID	Peptides (95%)	% Cov (95%)
P100-1	Monomeric sarcosine oxidase	*Mizuhopecten yessoensis*	A0A210Q8T8	1	3.0
	Dipeptidas	*Crassostrea gigas*	K1QKG0	1	2.4
P100-2	Tubulin beta chain	*Aplysia californica*	Q86D82	2	7.1
	Tubulin alpha chain	*Lottia gigantea*	V4C3J7	3	9.3
	Ubiquitin	*Pinctada fucata*	V5IWR5	1	21.1
	Glyceraldehyde-3-phosphate dehydrogenase	*Mizuhopecten yessoensis*	A0A210R5L9	1	3.0
	Alpha-actinin, sarcomeric	*Mizuhopecten yessoensis*	A0A210Q538	4	5.8
	Triosephosphate isomerase	*Lottia gigantea*	V4AUY5	1	6.0
	Alpha macroglobulin	*Azumapecten farreri*	Q6TL26	1	0.5
	Heat shock protein 70	*Laternula elliptica*	A2TF45	1	2.6
P100-3	Tubulin alpha chain	*Lottia gigantea*	V4CDJ4	13	34.2
	ATP synthase subunit alpha	*Mizuhopecten yessoensis*	A0A210QGA8	3	5.6
	78 kDa glucose-regulated protein	*Conus novaehollandiae*	H8XWJ4	4	8.6
	Fructose-bisphosphate aldolase	*Meretrix meretrix*	E3VWM3	6	14.0

Table S7.3. (Continued)

	Protein	Specie	UniProt ID	Peptides (95%)	% Cov (95%)
P100-3	Phosphoglycerate kinase	*Crassostrea gigas*	K1QCC1	2	8.1
	Ubiquitin	*Biomphalaria glabrata*	Q9BH32	2	19.5
	Tubulin alpha chain	*Mizuhopecten yessoensis*	A0A210Q0I1	8	30.6
	Actin-related protein 3	*Crassostrea gigas*	K1QLZ1	1	5.0
	Histone H3	*Crassostrea gigas*	K1Q9K6	2	2.7
	Ezrin/radixin/moesin	*Biomphalaria glabrata*	Q963F9	1	1.7
	Complement C1q-like protein 3	*Ruditapes philippinarum*	A0A0U3CDP6	1	8.6
	Sarcoplasmic calcium binding protein	*Ruditapes philippinarum*	O97050	1	10.0
	Putative filamin-A-like protein isoform X7	*Pinctada fucata*	A0A194AJE0	1	3.6
	Beta-actin isotype 1	*Lymnaea stagnalis*	A0A1D8KD32	40	49.5
	ATP synthase subunit alpha	*Crassostrea gigas*	K1R6Z7	3	6.0
	Ras GTPase-activating-like protein IQGAP1	*Mizuhopecten yessoensis*	A0A210QG69	1	0.7
	Protein kinase C	*Lottia gigantea*	V4B6K8	1	1.8
	6-phosphogluconate dehydrogenase, decarboxylating	*Lottia gigantea*	V4AME8	1	2.1

Table S7.3. (Continued)

	Protein	Specie	UniProt ID	Peptides (95%)	% Cov (95%)
P100-3	C-type lectin	*Ruditapes philippinarum*	W6JJB5	1	1.7
	40S ribosomal protein SA	*Meretrix meretrix*	K4M440	1	4.2
	Pyruvate kinase	*Biomphalaria glabrata*	A0A2C9JVJ4	1	2.1
	Glyceraldehyde-3-phosphate dehydrogenase	*Haliotis discus discus*	B6RB30	2	3.8
	Peptidyl-prolyl cis-trans isomerase	*Mizuhopecten yessoensis*	A0A210Q9T6	1	4.8
	Alpha-1,4 glucan phosphorylase	*Biomphalaria glabrata*	A0A2C9KFK2	3	5.8
	Protein disulfide-isomerase	*Crassostrea gigas*	K1Q6X5	1	1.6
	Polycystin-1	*Crassostrea gigas*	K1RLH5	1	0.3
	Visual G-protein beta subunit	*Doryteuthis pealeii*	Q6TQF6	1	3.2
	Fascin	*Biomphalaria glabrata*	A0A2C9JG25	1	2.0
	Profilin	*Lottia gigantea*	V4A7Z0	1	10.0
	PL10-like protein	*Haliotis asinina*	C7EAA2	1	1.4
	Tubulin beta chain	*Lottia gigantea*	V4A0A3	7	11.6
	ATP synthase subunit beta	*Lottia gigantea*	V4AQP1	7	13.9

Table S7.4. Uncommon proteins over time in samples exposed to food additive E171

	Protein	Specie	UniProt ID	Peptides (95%)	% Cov (95%)
PE171-1	Tubulin alpha chain	*Crassostrea gigas*	K1QII6	10	30.4
	Myosin heavy chain isoform A	*Octopus bimaculoides*	V6A729	6	3.8
	ATP synthase subunit alpha	*Pinctada fucata*	Q000T7	4	10.3
	Galectin	*Ruditapes philippinarum*	B1AAP1	5	15.9
	Actin 2	*Crassostrea gigas*	Q8TA69	39	56.7
	Myosin heavy chain, striated muscle	*Mizuhopecten yessoensis*	A0A210Q4E0	6	3.8
	Ubiquitin	*Biomphalaria glabrata*	Q9BH32	2	19.5
	Phosphoenolpyruvate carboxykinase, cytosolic [GTP]	*Mizuhopecten yessoensis*	A0A210R642	2	5.4
	Actin	*Azumapecten farreri*	Q7YZD7	43	51.1
	Actin-related protein 3	*Crassostrea gigas*	K1QLZ1	2	12.1
	Myosin heavy chain	*Onchidium struma nom. nud.*	A0A1P8C5A6	6	3.7
	Histone H3	*Crassostrea gigas*	K1Q9K6	1	2.7
	Actin-related protein 2/3 complex subunit 4	*Octopus bimaculoides*	A0A0L8FI18	1	6.5
	Ferritin	*Ruditapes philippinarum*	U3GS70	1	6.5

Table S7.4. (Continued)

	Protein	Specie	UniProt ID	Peptides (95%)	% Cov (95%)
PE171-1	Myosin heavy chain, non-muscle	*Mizuhopecten yessoensis*	A0A210QSX4	6	3.9
	14-3-3 protein zeta	*Crassostrea gigas*	K1P9N7	2	3.3
	Sodium/potassium-transporting ATPase subunit alpha	*Tridacna squamosa*	A0A288PNI3	1	1.6
	Malate dehydrogenase	*Mizuhopecten yessoensis*	A0A210QWL4	1	3.2
	Protein disulfide-isomerase	*Crassostrea gigas*	K1Q6X5	1	1.6
	Cytochrome c oxidase subunit 2	*Ruditapes philippinarum*	Q8WF42	1	1.9
	ADP-ribosylation factor	*Crassostrea gigas*	K1PTH4	3	4.1
	Ras-related protein Rab-7a	*Crassostrea gigas*	K1PZ08	1	6.3
	Sarcoplasmic calcium binding protein	*Ruditapes philippinarum*	O97050	1	13.3
	Putative phosphoglycerate mutase	*Crassostrea gigas*	K1QBL3	1	5.6
	Glycogen [starch] synthase	*Biomphalaria glabrata*	A0A2C9JZ16	1	2.2
	Histone H2B	*Azumapecten farreri*	A2CI31	5	28.8
	Endoplasmin	*Mizuhopecten yessoensis*	A0A210PZR8	1	1.5
	Ferritin	*Ruditapes philippinarum*	K4HXI8	1	6.4

Table S7.4. (Continued)

	Protein	Specie	UniProt ID	Peptides (95%)	% Cov (95%)
PE171-1	Actin-related protein 2	*Crassostrea gigas*	K1QFS4	1	3.6
	Alpha-2-macroglobulin-like protein 1	*Mizuhopecten yessoensis*	A0A210QRJ0	1	0.5
	Metalloendopeptidase	*Biomphalaria glabrata*	A0A2C9JFH7	1	1.1
	TNF receptor-associated factor 3	*Crassostrea gigas*	K1PDY7	1	1.9
	Glyceraldehyde-3-phosphate dehydrogenase	*Haliotis discus discus*	B6RB30	1	3.8
	Four and a half LIM domains protein 2	*Mizuhopecten yessoensis*	A0A210Q6K0	1	2.3
	Ras-related protein Rab-2	*Crassostrea gigas*	K1QBM3	1	6.2
	Tubulin alpha chain	*Octopus bimaculoides*	A0A0L8HMY5	8	22.0
	Tubulin beta chain	*Crassostrea gigas*	K1QAJ5	7	24.5
	Enolase	*Crassostrea gigas*	K1QX37	1	0.8
PE171-2	Tubulin alpha chain	*Crassostrea gigas*	K1R473	8	23.8
	ATP synthase subunit alpha	*Mizuhopecten yessoensis*	A0A210QGA8	5	11.6
	Ezrin/radixin/moesin	*Biomphalaria glabrata*	Q963F9	2	3.2
	ATP synthase subunit beta	*Pinctada fucata*	A0A194AL63	5	13.8

Table S7.4. (Continued)

	Protein	Specie	UniProt ID	Peptides (95%)	% Cov (95%)
PE171-2	Isocitrate dehydrogenase [NADP]	*Mizuhopecten yessoensis*	A0A210QYM1	1	1.8
	Methylmalonate-semialdehyde dehydrogenase [acylating], mitochondrial	*Mizuhopecten yessoensis*	A0A210PP78	2	3.8
	Elongation factor Tu	*Biomphalaria glabrata*	A0A0U3EBQ1	1	3.8
	Beta-glucuronidase	*Lottia gigantea*	V4A2U2	1	1.5
	Glutathione peroxidase A	*Ruditapes philippinarum*	C8CBM2	1	4.4
	Ras GTPase-activating-like protein IQGAP1	*Mizuhopecten yessoensis*	A0A210QG69	1	0.7
	Catalase	*Paphia textile*	V5W832	2	4.7
	14-3-3 zeta	*Haliotis diversicolor*	W8E7M6	1	3.7
	Beta-actin 2	*Sinonovacula constricta*	V9I358	20	40.2
	Actin	*Todarodes pacificus*	D3GBA7	21	41.2
PE171-3	Myosin heavy chain	*Pecten maximus*	Q9U7E3	1	0.7

Table S7.5. Uncommon proteins in PC, P50, P100 and PE171 samples at T0

	Protein	Specie	UniProt ID	Peptides (95%)	% Cov (95%)
PC-1	Myosin heavy chain, striated muscle	*Mizuhopecten yessoensis*	A0A210QNK6	5	2.8
	ADP, ATP carrier protein	*Mizuhopecten yessoensis*	A0A210PS96	2	8.3
	ATP synthase subunit alpha	*Octopus bimaculoides*	A0A0L8IA38	1	2.2
	Ezrin/radixin/moesin	*Biomphalaria glabrata*	Q963F9	1	1.5
	Elongation factor 1-alpha	*Lottia gigantea*	V4AP92	1	2.6
	Heat shock protein 78	*Hyriopsis cumingii*	X2KNR4	1	2.6
	Ubiquitin	*Pinctada fucata*	V5IWR5	1	21.1
	Ferritin	*Biomphalaria glabrata*	A0A2C9LWC4	1	3.4
	ATP synthase subunit beta	*Biomphalaria glabrata*	A0A2C9KBD6	1	1.4
P50-1	Tubulin beta chain	*Aplysia californica*	Q86D82	4	11.1
	ATP synthase subunit beta	*Pinctada fucata*	A0A194AL63	2	6.1
	Elongation factor Tu	*Biomphalaria glabrata*	A0A0U3EBQ1	1	3.8
	Cell cycle regulator Mat89Bb-like protein	*Crassostrea gigas*	K1PUA7	1	4.3

Table S7.5. (Continued)

	Protein	Specie	UniProt ID	Peptides (95%)	% Cov (95%)
P50-1	Elongation factor Tu	*Mizuhopecten yessoensis*	A0A210PGD1	1	1.9
	ATP synthase subunit alpha	*Mizuhopecten yessoensis*	A0A210QGA8	1	0.0
P100-1	Tubulin beta chain	*Arion vulgaris*	A0A0B7B670	29	66.2
	Tubulin alpha chain	*Mizuhopecten yessoensis*	A0A210Q0A8	17	45.0
	ATP synthase subunit alpha	*Lottia gigantea*	V4A6V0	7	16.4
	Calcium-transporting ATPase	*Mizuhopecten yessoensis*	O96039	7	9.8
	Tropomyosin	*Ruditapes philippinarum*	B7XC71	7	26.4
PE171-1	HSP70 protein	*Ruditapes philippinarum*	A0A023W7L5	5	10.5
	HSP90 protein	*Ruditapes philippinarum*	A0A023W7V2	5	8.7
	Radixin	*Crassostrea gigas*	K1PUJ1	4	8.0
	Arginine kinase	*Paphia undulata*	C3VUU4	4	9.9
	Catalase	*Corbicula fluminea*	A0A1P8NQK0	3	9.2
	Calcium-transporting ATPase	*Tridacna squamosa*	A0A288MAH8	6	8.3
	Glutathione peroxidase A	*Ruditapes philippinarum*	C8CBM2	3	15.5

Table S7.5. (Continued)

	Protein	Specie	UniProt ID	Peptides (95%)	% Cov (95%)
PE171-1	Retinal dehydrogenase 2	*Mizuhopecten yessoensis*	A0A210QHZ3	4	8.4
	Isocitrate dehydrogenase [NADP]	*Mizuhopecten yessoensis*	A0A210QYM1	4	8.5
	Tubulin beta chain	*Mizuhopecten yessoensis*	A0A210R050	23	51.5
	10-formyltetrahydrofolate dehydrogenase	*Lottia gigantea*	V4B2Z6	2	2.9
	Arginine kinase two-domain chain	*Spisula sachalinensis*	O77052	3	5.7
	Catalase	*Haliotis diversicolor*	G5DD16	2	6.6
	Methylmalonate-semialdehyde dehydrogenase [acylating], mitochondrial	*Mizuhopecten yessoensis*	A0A210PP78	3	7.2
	Transgelin-like protein-2	*Mytilus galloprovincialis*	A0A0K0YB45	3	10.2
	Non-muscle myosin II heavy chain	*Doryteuthis pealeii*	Q8SWQ7	4	2.5
	Heat shock protein 22 isoform 2	*Ruditapes philippinarum*	C8CBN5	2	10.9
	Pyruvate carboxylase, mitochondrial	*Crassostrea gigas*	K1QHI5	2	1.5
	Adenosylhomocysteinase	*Crassostrea gigas*	K1RW85	3	7.2
	Alpha-1,4 glucan phosphorylase	*Lottia gigantea*	V4ALJ5	1	1.9

Table S7.5. (Continued)

	Protein	Specie	UniProt ID	Peptides (95%)	% Cov (95%)
PE171-1	Pyruvate carboxylase	*Biomphalaria glabrata*	A0A2C9JXN7	1	1.1
	Ras-related protein Rab-11B	*Crassostrea gigas*	K1QX44	1	7.6
	Sodium/potassium-transporting ATPase subunit alpha	*Mizuhopecten yessoensis*	A0A210Q4Z0	2	3.8
	Triosephosphate isomerase	*Crassostrea ariakensis*	H9LJ32	1	6.0
	Cytosolic 10-formyltetrahydrofolate dehydrogenase	*Mizuhopecten yessoensis*	A0A210R6J6	2	3.3
	Multidrug resistance-associated protein 1	*Crassostrea gigas*	K1PZ06	1	1.0
	Propionyl-CoA carboxylase beta chain, mitochondrial	*Mizuhopecten yessoensis*	A0A210PUA9	3	7.5
	Tubulin beta chain	*Pinctada fucata*	A0A194AQ74	25	62.7
	Calcium-transporting ATPase	*Crassostrea gigas*	K1QA13	5	8.5
	Calcium-transporting ATPase	*Octopus bimaculoides*	A0A0L8FX15	5	8.9
	Putative methylmalonate-semialdehyde dehydrogenase [acylating], mitochondrial	*Crassostrea gigas*	K1R252	1	2.1
	Phosphoenolpyruvate carboxykinase, cytosolic [GTP]	*Crassostrea gigas*	K1Q760	2	4.6
	Ras-related protein Rab-1A	*Crassostrea gigas*	K1RBB8	1	6.0
	Serine hydroxymethyltransferase	*Biomphalaria glabrata*	A0A2C9K569	1	2.2

Table S7.5. (Continued)

	Protein	Specie	UniProt ID	Peptides (95%)	% Cov (95%)
PE171-1	Methylmalonyl-CoA mutase, mitochondrial	*Mizuhopecten yessoensis*	A0A210PW47	1	1.5
	Calcium-transporting ATPase	*Hyriopsis cumingii*	A0A0U1ZY67	5	7.6
	Succinate dehydrogenase [ubiquinone] flavoprotein subunit, mitochondrial	*Lottia gigantea*	V3ZLV6	1	2.1
	4-hydroxyphenylpyruvate dioxygenase	*Crassostrea gigas*	K1QX22	1	0.6
	Myosin essential light chain	*Pecten maximus*	Q9U7E2	1	7.6
	Cytochrome c oxidase subunit 3	*Ruditapes philippinarum*	Q8WF35	1	2.7
	Monomeric sarcosine oxidase	*Mizuhopecten yessoensis*	A0A210Q8T8	1	3.0
	Dipeptidase	*Crassostrea gigas*	K1QKG0	1	2.4
	Tubulin alpha chain	*Crassostrea gigas*	K1QII6	10	30.4
	ATP synthase subunit alpha	*Pinctada fucata*	Q000T7	4	10.3
	Ubiquitin	*Biomphalaria glabrata*	Q9BH32	2	19.5
	Heat shock protein 90	*Paphia undulata*	L0BTB2	2	3.6
	Actin-related protein 3	*Crassostrea gigas*	K1QLZ1	2	12.1

Table S7.5. (Continued)

	Protein	Specie	UniProt ID	Peptides (95%)	% Cov (95%)
PE171-1	Histone H3	*Crassostrea gigas*	K1Q9K6	1	2.7
	Actin-related protein 2/3 complex subunit 4	*Octopus bimaculoides*	A0A0L8FI18	1	6.5
	Heat shock protein 70	*Laternula elliptica*	A2TF45	1	2.6
	Protein disulfide-isomerase	*Crassostrea gigas*	K1Q6X5	1	1.6
	Ferritin	*Ruditapes philippinarum*	K4HXI8	1	6.4
	Actin-related protein 2	*Crassostrea gigas*	K1QFS4	1	3.6
	Alpha-2-macroglobulin-like protein 1	*Mizuhopecten yessoensis*	A0A210QRJ0	1	0.5
	TNF receptor-associated factor 3	*Crassostrea gigas*	K1PDY7	1	1.9
	Glyceraldehyde-3-phosphate dehydrogenase	*Haliotis discus discus*	B6RB30	1	3.8
	Four and a half LIM domains protein 2	*Mizuhopecten yessoensis*	A0A210Q6K0	1	2.3
	Ras-related protein Rab-2	*Crassostrea gigas*	K1QBM3	1	6.2
	Tubulin alpha chain	*Octopus bimaculoides*	A0A0L8HMY5	8	22.0
	Tubulin beta chain	*Crassostrea gigas*	K1QAJ5	7	24.5

Table S7.6. Uncommon proteins in PC, P50, P100 and PE171 samples at T1

	Protein	Specie	UniProt ID	Peptides (95%)	% Cov (95%)
PC-2	Tubulin beta chain	*Biomphalaria glabrata*	A0A2C9JVM1	4	14.1
	Tubulin alpha chain	*Lottia gigantea*	V4CDJ4	3	10.9
	Myosin heavy chain isoform A	*Sepia officinalis*	V6A720	1	0.7
P50-2	Tubulin alpha chain	*Lottia gigantea*	V4CGI5	2	5.3
	Myosin heavy chain isoform A	*Octopus bimaculoides*	V6A729	1	0.7
	Retinol dehydrogenase 14	*Mizuhopecten yessoensis*	A0A210QLE1	1	3.1
	ATP synthase subunit beta	*Lottia gigantea*	V4AQP1	1	1.9
P100-2	Tubulin beta chain	*Aplysia californica*	Q86D82	2	7.1
	Tubulin alpha chain	*Lottia gigantea*	V4C3J7	3	9.3
	Glyceraldehyde-3-phosphate dehydrogenase	*Mizuhopecten yessoensis*	A0A210R5L9	1	3.0
	Alpha-actinin, sarcomeric	*Mizuhopecten yessoensis*	A0A210Q538	4	5.8
	Triosephosphate isomerase	*Lottia gigantea*	V4AUY5	1	6.0

Table S7.6. (Continued)

	Protein	Specie	UniProt ID	Peptides (95%)	% Cov (95%)
PE171-2	Tubulin alpha chain	*Crassostrea gigas*	K1R473	8	23.8
	Myosin heavy chain, striated muscle	*Crassostrea gigas*	K1RSS3	2	1.2
	Complement C1q-like protein 2	*Ruditapes philippinarum*	A0A0U3AA90	2	15.9
	Ezrin/radixin/moesin	*Biomphalaria glabrata*	Q963F9	2	3.2
	Clathrin heavy chain	*Crassostrea gigas*	K1PNR3	1	0.7
	ATP synthase subunit beta	*Pinctada fucata*	A0A194AL63	5	13.8
	Isocitrate dehydrogenase [NADP]	*Mizuhopecten yessoensis*	A0A210QYM1	1	1.8
	Histone H4	*Octopus bimaculoides*	A0A0L8GSZ5	7	26.9
	Methylmalonate-semialdehyde dehydrogenase [acylating], mitochondrial	*Mizuhopecten yessoensis*	A0A210PP78	2	3.8
	Elongation factor Tu	*Biomphalaria glabrata*	A0A0U3EBQ1	1	3.8
	Beta-glucuronidase	*Lottia gigantea*	V4A2U2	1	1.5
	Putative paramyosin-3	*Pinctada fucata*	A0A194AJD6	1	1.2
	Glutathione peroxidase A	*Ruditapes philippinarum*	C8CBM2	1	4.4
	Ras GTPase-activating-like protein IQGAP1	*Mizuhopecten yessoensis*	A0A210QG69	1	0.7

Table S7.6. (Continued)

	Protein	Specie	UniProt ID	Peptides (95%)	% Cov (95%)
PE171-2	Catalase	*Paphia textile*	V5W832	2	4.7
	14-3-3 zeta	*Haliotis diversicolor*	W8E7M6	1	3.7
	Beta-actin 2	*Sinonovacula constricta*	V9I358	20	40.2
	Actin	*Todarodes pacificus*	D3GBA7	21	41.2

Table S7.7. Uncommon proteins in PC, P50, P100 and PE171 samples at T2

	Protein	Specie	UniProt ID	Peptides (95%)	% Cov (95%)
PC-3	Tubulin beta chain	*Lottia gigantea*	V3ZL01	34	61.0
	Tubulin alpha chain	*Crassostrea gigas*	K1QII6	32	41.7
	Actin 2	*Crassostrea gigas*	Q8TA69	34	53.
	ADP-ribosylation factor	*Crassostrea gigas*	K1PTH4	3	4.1
	Tubulin alpha chain	*Lottia gigantea*	V3ZGT0	26	41.6
	40S ribosomal protein S2	*Mizuhopecten yessoensis*	A0A210PH18	2	8.6
	40S ribosomal protein SA	*Crassostrea gigas*	K1R4D4	2	9.2
	78kDa glucose regulated protein	*Crassostrea gigas*	Q75W49	5	6.5
	Glutathione S-transferase B	*Ruditapes philippinarum*	C8CBM0	2	9.8
	Tubulin beta chain	*Lottia gigantea*	V4AVP5	27	50.2
	Elongation factor 1-alpha	*Azumapecten farreri*	K9L279	3	7.4
	Sodium/potassium-transporting ATPase subunit alpha	*Tridacna squamosa*	A0A288PNI3	1	1.6
	Tubulin beta chain	*Lottia gigantea*	V4BLC8	9	19.1
	ATP synthase subunit beta	*Pinctada fucata*	A0A194AL63	9	27.7

Table S7.7. (Continued)

	Protein	Specie	UniProt ID	Peptides (95%)	% Cov (95%)
PC-3	Ribosomal protein S13	*Argopecten irradians*	Q8ITB0	1	8.1
	Cytosolic 10-formyltetrahydrofolate dehydrogenase	*Mizuhopecten yessoensis*	A0A210R6J6	1	1.9
	Tubulin beta chain	*Pinctada fucata*	A0A194AQ74	31	58.0
	Beta-actin 2	*Sinonovacula constricta*	V9I358	21	37.5
	Tubulin beta chain	*Lymnaea stagnalis*	A0A1D8KD44	14	16.1
	40S ribosomal protein S18	*Biomphalaria glabrata*	A0A2C9JC73	1	5.3
	Catalase	*Lottia gigantea*	V4B843	1	2.6
	T-complex protein 1 subunit delta	*Lottia gigantea*	V4B496	1	2.5
	Rab GDP dissociation inhibitor	*Lottia gigantea*	V3ZWK7	1	4.3
	Puromycin-sensitive aminopeptidase	*Crassostrea gigas*	K1R866	1	2.3
	T-complex protein 1 subunit beta	*Crassostrea gigas*	K1R294	1	2.8
	Glucose dehydrogenase [acceptor]	*Crassostrea gigas*	K1QZJ5	1	1.3
	26S proteasome non-ATPase regulatory subunit 2	*Crassostrea gigas*	K1QDM2	1	1.7
	40S ribosomal protein S7	*Biomphalaria glabrata*	A0A2C9JPX3	1	6.2

Table S7.7. (Continued)

	Protein	Specie	UniProt ID	Peptides (95%)	% Cov (95%)
PC-3	Actin-related protein 2/3 complex subunit 4	*Mizuhopecten yessoensis*	A0A210R0V6	1	6.5
	Putative 60S ribosomal protein L7-like protein	*Pinctada fucata*	A0A194AM17	1	4.1
	Arginine kinase	*Meretrix lyrata*	C3VUU3	5	8.5
	Phosphoglycerate kinase	*Lottia gigantea*	V4ADA9	2	7.7
	40S ribosomal protein S7	*Biomphalaria glabrata*	A0A2C9JPX3	1	6.2
	Sialic acid-binding lectin	*Ruditapes philippinarum*	C8CBM9	1	5.1
P50-3	Tubulin beta chain	*Aplysia californica*	Q86D82	21	42.3
	Tubulin alpha chain	*Crassostrea gigas*	Q5H7U8	13	42.4
	ATP synthase subunit alpha	*Lottia gigantea*	V4A6V0	6	16.1
	Filamin-A	*Mizuhopecten yessoensis*	A0A210QAC9	5	2.4
	Malate dehydrogenase	*Mizuhopecten yessoensis*	A0A210QWL4	2	6.7
	Triosephosphate isomerase	*Crassostrea ariakensis*	H9LJ32	2	10.0
	Actin-related protein 2/3 complex subunit 4	*Octopus bimaculoides*	A0A0L8FI18	2	13.1
	Enolase	*Crassostrea gigas*	K1QX37	1	0.8

Table S7.7. (Continued)

	Protein	Specie	UniProt ID	Peptides (95%)	% Cov (95%)
P50-3	Septin-2	*Crassostrea gigas*	K1PY30	1	1.7
	Actin	*Azumapecten farreri*	Q7YZD7	47	52.7
	Kyphoscoliosis peptidase	*Mizuhopecten yessoensis*	A0A210QLF5	1	1.1
	Myosin essential light chain	*Hyriopsis cumingii*	J9UEN7	1	8.4
	Propionyl-CoA carboxylase beta chain, mitochondrial	*Mizuhopecten yessoensis*	A0A210PUA9	1	2.6
	Methylmalonyl-CoA mutase, mitochondrial	*Mizuhopecten yessoensis*	A0A210PW47	1	1.5
	Endoplasmin	*Mizuhopecten yessoensis*	A0A210PZR8	1	1.5
	Tubulin alpha chain	*Octopus bimaculoides*	A0A0L8HMY5	9	25.6
	Tubulin beta chain	*Lottia gigantea*	V3YY74	15	30.2
	Cystatin B	*Ruditapes philippinarum*	M9NV28	1	12.1
	Receptor of Activated Kinase C 1	*Mya arenaria*	Q08G56	1	3.8
	Calcium-transporting ATPase	*Tridacna squamosa*	A0A288MAH8	3	4.6
	Muscle myosin heavy chain	*Sepia esculenta*	B2ZTQ6	7	3.4
	Pyruvate kinase	*Crassostrea gigas*	Q0KHB6	1	2.3

Table S7.7. (Continued)

	Protein	Specie	UniProt ID	Peptides (95%)	% Cov (95%)
P100-3	Tubulin alpha chain	*Lottia gigantea*	V4CDJ4	13	34.2
	Succinate dehydrogenase [ubiquinone] flavoprotein subunit, mitochondrial	*Lottia gigantea*	V3ZLV6	3	7.0
	78 kDa glucose-regulated protein	*Conus novaehollandiae*	H8XWJ4	4	8.6
	Tubulin alpha chain	*Mizuhopecten yessoensis*	A0A210Q0I1	8	30.6
	Actin-related protein 3	*Crassostrea gigas*	K1QLZ1	1	5.0
	ATP synthase subunit alpha	*Crassostrea gigas*	K1R6Z7	3	6.0
	6-phosphogluconate dehydrogenase, decarboxylating	*Lottia gigantea*	V4AME8	1	2.1
	C-type lectin	*Ruditapes philippinarum*	W6JJB5	1	1.7
	Ferritin	*Ruditapes decussatus*	A0A067XI00	1	4.3
	Pyruvate kinase	*Biomphalaria glabrata*	A0A2C9JVJ4	1	2.1
	Alpha-1,4 glucan phosphorylase	*Biomphalaria glabrata*	A0A2C9KFK2	3	5.8
	Protein disulfide-isomerase	*Crassostrea gigas*	K1Q6X5	1	1.6
	Fascin	*Biomphalaria glabrata*	A0A2C9JG25	1	2.0
	ATP synthase subunit beta	*Lottia gigantea*	V4AQP1	7	13.9

Table S7.7. (Continued)

	Protein	Specie	UniProt ID	Peptides (95%)	% Cov (95%)
PE171-3	Histone H4	*Octopus bimaculoides*	A0A0L8GSZ5	1	4.4
	Myosin heavy chain	*Pecten maximus*	Q9U7E3	1	0.7

USC
UNIVERSIDADE
DE SANTIAGO
DE COMPOSTELA

V. DISCUSSION

USC
UNIVERSIDADE
DE SANTIAGO
DE COMPOSTELA

DISCUSSION

This thesis has focused on determining TiO_2 NPs and Ag NPs in foodstuff (crab sticks and bivalve molluscs) and evaluating their potential risks on humans when ingesting food products containing NPs. In addition, protein corona associated with NPs in hemolymph of bivalve molluscs has been studied.

A. Determination of TiO_2 NPs and Ag NPs in crab sticks and bivalve molluscs

Food additive E171 contains nano- and micro-Ti. The percentage of TiO_2 NPs in E171 is within 17-36%, according to previous studies. Crab stick samples that may contain this food additive have been analyzed for total Ti and TiO_2 NPs concentrations. The total Ti content was determined using microwave assisted acid digestion followed by ICP-MS analysis. Acid digestion method was validated using a certified reference material with indicative Ti content. For TiO_2 NPs, an enzymatic extraction protocol was optimized and validated. Eleven out of twenty-two analyzed samples showed Ti concentrations higher than the LOQ of the method (0.210 μg g^{-1}). These concentrations varied from 0.248 to 12.6 μg Ti g^{-1}. Surimi samples containing the highest total Ti concentrations were subjected to the optimized enzymatic hydrolysis and sp-ICP-MS measurement. Extraction protocol was validated, and good stability, accuracy and repeatability were obtained. TiO_2 NPs were detected in seven samples and concentrations ranged from 1.96×10^7 to 1.19×10^8 TiO_2 NPs g^{-1}. Regarding size distributions, mean sizes varied from 65 to 217 nm. Three different size distribution profiles were observed among different samples: (1) high proportion of TiO_2 NPs of small size and a very small amount of large TiO_2 NPs; (2) TiO_2 NPs of small and large sizes; and (3) wide TiO_2 NPs size distributions. This fact is related to the different types of TiO_2 NPs present in E171 (NPs, microparticles

and aggregates). In addition, TiO_2 NPs may come from shellfish and fish used for preparing crab sticks.

In reference to bivalve molluscs, two ultrasound assisted enzymatic hydrolysis procedures have been successfully optimized and validated for TiO_2 NPs and Ag NPs extraction. Bivalve molluscs, as filter-feeders, accumulate contaminants in their tissues so they are considered sentinels of environmental health. NPs are emerging pollutants, so TiO_2 NPs and Ag NPs present in bivalve mollusc samples may come from the several applications of these new materials (sunscreens, textiles, paints, food industry…) and their inappropriate disposal in waste water treatment plants. Clams, cockles, mussels, razor clams, oysters and variegated scallops were studied. For total Ti and Ag determination, the same microwave assisted acid digestion procedure was applied prior the ICP-MS measurements. Ti was found in the eleven analyzed samples in the range of 0.285-3.42 μg Ti g^{-1}, while only seven samples had Ag ranged between 0.0841 and 3.72 μg Ag g^{-1}. TiO_2 NPs were found in all samples, while Ag NPs were quantified in five samples. TiO_2 NPs concentrations were from 2.36×10^7 to 1.25×10^8 TiO_2 NPs g^{-1}, and the highest concentrations were found in mussels and variegated scallops, whereas razor clams showed the lowest TiO_2 NPs concentration. Considering Ag NPs concentrations, values varied from 1.56×10^7 to 1.85×10^9 Ag NPs g^{-1}. Variegated scallops, oysters and Japanese clams showed the highest Ag NPs contents, while the lowest level was found in Atlantic clams. Levels of Ag NPs and TiO_2 NPs, as well as Ag and Ti, were similar. The majority of analyzed samples showed most frequent sizes of 50 and 25 nm for TiO_2 NPs and Ag NPs, respectively. The size distributions for TiO_2 NPs were broader than for Ag NPs. TiO_2 NPs and Ag NPs presence in commercially available bivalve molluscs may imply a clear spread of these emerging pollutants in the marine environment, especially TiO_2 NPs which were present in all studied molluscs.

In general, TiO_2 NPs concentrations in bivalve molluscs were similar to those found in crab stick samples. Size distributions were narrower in bivalve molluscs than in crab sticks, and large NPs were not found. NPs in bivalve molluscs are present due to their presence in

the environment, they do not come from E171, and organisms tend to absorb small NPs rather than large ones.

The presence of Ag NPs in bivalve molluscs has been also evaluated by enzymatic hydrolysis and AF4-UV-ICP-MS analysis. Samples containing Ag NPs, according to previous enzymatic extraction and sp-ICP-MS results, were used in this study. Ag NPs were coeluted with proteins in the enzymatic extract as observed in UV spectra. This interaction was not observed in sp-ICP-MS due to the fact that proteins were eliminated in the plasma. AF4-UV-ICP-MS fractograms showed different elution profiles and, therefore, different Ag NPs size distributions. The differences between AF4-UV-ICP-MS and sp-ICP-MS results are possibly due to more moderate enzymatic extraction conditions and interaction with proteins over hydrolysis and measurement in the first scenario.

B. Evaluation of potential risk of TiO_2 NPs and Ag NPs in humans through the ingestion of food products containing NPs

According to EFSA guidance, published in 2018, several TiO_2 NPs and Ag NPs standards, as well as food additive E171 and foodstuff containing these NPs (crab sticks and bivalve molluscs), have been analyzed to obtain their biopersistence rate (Stage 0). In general, NPs agglomeration during the *in vitro* gastric digestion and NPs dispersion under intestinal conditions were observed. Ag NPs showed a size-dependent behavior. Sample matrix has been found to affect TiO_2 NPs and Ag NPs release. TiO_2 NPs behavior in surimi samples was quite similar to that found in TiO_2 NPs standards and E171, while TiO_2 NPs present in bivalve molluscs showed slow NPs release along the *in vitro* gastrointestinal digestion. Ag NPs in molluscs have shown different tendencies depending on the sample.

Biopersistence rates were higher than 100% in TiO_2 NPs standards and TiO_2 NPs/ TiO_2 microparticles from E171. Ag NPs have been found to be more degradable than TiO_2 NPs and their biopersistence rate was dependent on the size. Ag NPs were less biopersistent than TiO_2 NPs in food samples. All biopersistence rates were higher than the limit set by the EFSA (12%), so these NPs are

not degraded under simulated gastrointestinal digestion and further studies are needed to assess their risk.

EFSA guidance establish *in vitro* toxicity testing approaches as the next step (Stage 1). *In vitro* models are based on primary cells or cell lines that represent the gastrointestinal tract. If NPs translocate through the gastrointestinal barrier, they might enter the systemic circulation and reach other organs. Concentrations of Ti and Ag in bivalve molluscs, as well as TiO_2 NPs and Ag NPs, were established by methods described above. Several samples, containing TiO_2 NPs and Ag NPs, were subjected to an *in vitro* digestion process simulating the human gastrointestinal digestion in stomach and in small and large intestine to determine their bioaccessibility. In addition, transport of Ti, Ag, TiO_2 NPs and Ag NPs through the gastrointestinal epithelial barrier (0-2 h) has been assessed.

The bioaccessibility percentages varied from 2.9 (cockles) to 89% (grooved carpet shell) for Ti, and from 6.5 (oysters) to 51% (fresh variegated scallops) for Ag. Regarding the NPs, the bioaccessibility percentages were between 2.1 and 51% for TiO_2 NPs, and 13-17% for Ag NPs. These bioaccessibility percentages were quite lower than those found for total Ti and total Ag, which means that NPs are less bioaccessible than their ionic counterparts. The bioaccessibility percentages of TiO_2 NPs were higher than Ag NPs, which agreed with their high biopersistence rates (Stage 0).

Size distribution did not appear to be highly affected by the simulated digestion procedure compared to those observed in the enzymatic extracts. Slightly smaller Ag NPs (16-22 nm) were found in the bioaccesible fractions than in the enzymatic extracts (22-25 nm). Same trend was observed for TiO_2 NPs and smaller sizes were obtained in the bioaccesible fractions (54-83 nm) in comparison with the enzymatic extracts (60-84 nm).

Ti bioavailability varied from 18 (cockles) to 68% (oysters), while the percentage of Ag transport was very low (0.017% for grooved carpet shells and 0.016% for frozen variegated scallops). Meanwhile Ti can cross the epithelium membrane, Ag absorption is very poor. The percentage of TiO_2 NPs transported across cellular monolayer varied from 17 (cockles) to 82% (oysters). Ag NPs

transport ranged from 2.1 (frozen variegated scallop) to 22% (oysters). Similar transport rates have been measured for total Ti and TiO_2 NPs, but quite different transport rates were found for total Ag and Ag NPs.

Both TiO_2 NPs and Ag NPs size distributions have been found to be different in the apical fraction, basolateral fraction and resuspended cells solutions. Sizes in the bioaccesible fractions were higher than in apical, basolateral and cellular fractions for most of analyzed samples.

Further genotoxicity studies and dissolution under lysosomal conditions are necessary to complete the Stage 1 of EFSA guidance.

C. Study of protein corona associated with TiO_2 NPs in hemolymph of bivalve molluscs

Clams were exposed to 50 and 100 nm TiO_2 NPs (commercial standards) and food additive E171 in a mesocosm system. Concentrations were progressively increased and one specimen per tank was sampled before any addition (0 mg L^{-1}), at the 9^{th} day of exposure (8 mg L^{-1}) and at the last day of the experiment (14 mg L^{-1}). Hemolymph was extracted from each clam.

Hemolymph was centrifugated and protein corona evolution profile was qualitatively and quantitatively analyzed by LC-MS/MS and SWATH-MS, respectively.

High variation in protein profile of different samples have been already detected even before NPs addition. It was observed that affinity of NPs for proteins also changed with concentration and NPs size. Interactions with proteins related to DNA packaging (histones), innate immunity (complement components C3 and C1q) and stress markers (heat shock proteins, catalase and superoxide dismutase) have been observed. Protein-NP interaction may cause alterations in protein function, which may significantly affect cellular roles. In addition, an increase in oxidative stress markers in corona and supernatants was found.

Strong interaction of NPs with proteins has also been observed when using AF4-UV-ICP-MS for analyzing enzymatic extracts containing Ag NPs.

USC
UNIVERSIDADE
DE SANTIAGO
DE COMPOSTELA

VI. CONCLUSIONS

USC
UNIVERSIDADE
DE SANTIAGO
DE COMPOSTELA

CONCLUSIONS

Part I. Enzymatic hydrolysis for NPs assessment by sp-ICP-MS

A. Enzymatic hydrolysis as a sample pre-treatment for TiO_2 NPs assessment in surimi (crab sticks) by sp-ICP-MS

An enzymatic hydrolysis procedure for TiO_2 NPs extraction from crab sticks has been successfully optimized and validated and the measurements were performed by sp-ICP-MS. The total Ti concentrations were determined by ICP-MS. The optimized method showed good repeatability, sensitivity and high analytical recovery.

Ti was quantified in eleven samples out of the twenty-two and the concentrations were ranged from 2.29 to 12.6 μg g^{-1}. These samples were subjected to the enzymatic hydrolysis and the obtained concentrations were within 1.96×10^{7}-1.19×10^{8} TiO_2 NPs g^{-1}. Size distribution of TiO_2 NPs was quite variable among several analyzed samples which may be due to the different types of TiO_2 NPs included in E171 (NPs, micrometric particles and aggregates) and the possible contribution of TiO_2 NPs present in shellfish and fish used for preparing surimi-based products.

TiO_2 NPs presence in the enzymatic extracts was confirmed by TEM analysis.

B. Ultrasound assisted enzymatic hydrolysis for isolating TiO_2 NPs from bivalve mollusk before sp-ICP-MS

Assessment of TiO_2 NPs in bivalve molluscs has been performed by ultrasound assisted enzymatic hydrolysis followed by sp-ICP-MS measurement. Total Ti concentration was analyzed by ICP-MS after a microwave assisted acid digestion. Good repeatability (concentration and size), low LOD and LOQ and analytical recovery around 100% were obtained.

Eleven bivalve molluscs were analyzed and Ti and TiO_2 NPs were found in all samples with concentrations range 0.285-3.42 μg g^{-1} (for Ti) and 2.36×10^7-1.25×10^8 NPs g^{-1} (for TiO_2 NPs). Most frequent size values were similar for all samples (53-69 nm).

The presence of NPs in enzymatic extracts was confirmed by DLS analysis.

C. Determination and characterization of Ag NPs in bivalve molluscs by ultrasound assisted enzymatic hydrolysis and sp-ICP-MS

An ultrasound assisted enzymatic hydrolysis procedure has been optimized and validated for the characterization and quantification of Ag NPs in bivalve molluscs by sp-ICP-MS. Total Ag content was also determined. The method was repeatable, sensitive and accurate.

Seven samples out of eleven contained Ag (0.0841-3.72 μg g^{-1}). Ag NPs concentrations were from 1.56×10^7 to 1.85×10^9 NPs g^{-1}. The highest Ag NPs levels were found in variegated scallops, oysters and Japanese clams, while Atlantic clams showed the lowest concentration.

Ag NPs presence in the enzymatic extracts was confirmed by SEM analysis.

Part II. Optimization of separation of NPs by AF4 coupled with different detectors

D. AF4-UV-ICP-MS for detecting and quantifying Ag NPs in seafood after enzymatic hydrolysis

AF4 technique coupled with UV spectroscopy and ICP-MS was used to detect and quantify Ag NPs in bivalve molluscs. An enzymatic hydrolysis treatment was performed before the analysis. Good membrane recoveries have been obtained (49 -121%).

Four bivalve molluscs were analyzed for total Ag content (microwave assisted acid digestion and ICP-MS measurement) and for determining Ag NPs by the proposed method. Total Ag concentrations were ranged between 1.6×10^2 and 3.7×10^3 μg kg^{-1}, while Ag levels in AF4 fractions were between 4.1×10^1 (oysters) and 2.3×10^2 μg kg^{-1} (frozen variegated scallop). AF4-UV-ICP-MS fractograms showed

different elution profiles and, therefore, different size distributions. UV spectra indicated that Ag NPs coelute with proteins.

Part III. Evaluation of potential risk of TiO_2 NPs and Ag NPs in humans through the ingestion of food products containing NPs

E. Biopersistence rate of metallic NPs in the gastrointestinal human tract (Stage 0 of the EFSA guidance for nanomaterials risk assessment)

Stage 0 of EFSA guidance for risk analysis of the use of NMs in food and feed chain consists of evaluating whether the NMs are degraded under the human digestion conditions. An *in vitro* gastrointestinal digestion was performed to assess the biopersistence rate of TiO_2 NPs (50 and 100 nm) and Ag NPs (40 and 60 nm) in standards, bivalve molluscs and crab sticks, as well as food additive E171. All measurements were performed by sp-ICP-MS.

NPs agglomeration at the gastric stage and NPs dispersion during intestinal digestion were observed in most of the experiments. Ag NPs have shown a size-dependent behavior in standards. TiO_2 NPs in bivalve molluscs were progressively released, while TiO_2 NPs in crab sticks followed a similar behavior to standards and E171. Ag NPs in bivalve molluscs showed different tendencies depending on the sample.

Higher degradation rate of Ag NPs compared to TiO_2 NPs have been observed in standards and bivalve molluscs. All biopersistence rates were higher than the limit established by EFSA guidance (12%).

F. Caco-2 in vitro model of human gastrointestinal tract for studying the absorption of TiO_2 NPs and Ag NPs from seafood samples

Bioaccessibility and bioavailability percentages of Ti, TiO_2 NPs, Ag and Ag NPs in bivalve molluscs have been analyzed. Caco-2 cells were selected as human intestinal epithelium model. The stability of cellular monolayer was monitored by TEER measurement and Lucifer Yellow transport.

Bioaccessibility percentages were between 2.9 and 89% for total Ti and 2.1-51% for TiO_2 NPs. Bioaccessibility percentages varied

from 6.5 to 51% for Ag and from 13 to 17% for Ag NPs. NPs showed less bioaccessibility than their ionic counterparts. Bioavailability percentages for Ti were within a range of 18-68%, while they varied from 17 to 82% for TiO_2 NPs. Ag and Ag NPs have shown bioavailability percentages within 0.016-0.017% and 2.1-22%, respectively. Ti and TiO_2 NPs showed similar bioavailability percentages, while significant differences were observed between Ag and Ag NPs.

Higher size distributions were obtained in bioaccesible fractions compared to basolateral, cellular and apical fractions for most of the analyzed samples.

Part IV. Characterization of NPs protein corona in hemolymph of bivalve molluscs

G. TiO_2 NPs protein corona characterization and quantification in hemolymph of bivalve molluscs

Clams were exposed to TiO_2 NPs standards (50 and 100 nm) and food additive E171. Concentrations were progressively increased from 0 to 14 mg L^{-1} over 18 days. One specimen per tank was sampled before any addition, at the 9^{th} exposure day (8 mg L^{-1}) and at the last day of the experiment. Hemolymph was extracted for all sampled specimens and centrifuged to isolate corona proteins.

Qualitative analysis by LC-MS/MS showed that 50 nm TiO_2 NPs had high affinity for fibrinogen-related and sarcoplasmic calcium binding proteins. At high concentration, alpha-actinin and putative filamin-A-like proteins were more affined. 100 nm TiO_2 NPs showed strong affinity for histone H4. They also interacted with heat shock protein and, when NPs concentration increased, they formed coronas with ATP synthase (subunit beta). Food additive E171 was associated with complement C1q-like protein and histones (H2A and H2B) and, at high concentrations, it was associated with talin-1, catalase, superoxide dismutase and ferritin.

Quantification of proteins has been performed by SWATH-MS. Complement components (C3 and C1q) were reduced over time in the corona upon using 50 nm TiO_2 NPs, while there was an increment in

stress markers in the supernatants. During 100 nm TiO_2 NPs exposure, high affinity for histones (H2A and H2B) was observed. In food additive E171 studies, catalase and superoxide dismutase concentrations increased in the corona over time. These variations could be related to oxidative stress.

As global conclusions, the presence of TiO_2 NPs and Ag NPs has been demonstrated in foodstuff (crab sticks and bivalve molluscs). NPs present in bivalve molluscs may be an indication of the spread of these emerging pollutants in the marine environment. In the aforementioned food products, TiO_2 NPs and Ag NPs were biopersistent and bioaccesible over human gastrointestinal digestion. TiO_2 NPs have shown high bioavailability percentages, so they can easily reach systemic circulation and other organs. Therefore, further nanotoxicological studies are required. Finally, the reduction of proteins related to the immune system and the increase of stress markers in corona proteins in the hemolymph of bivalve molluscs exposed to TiO_2 NPs may be considered as an indication of the impairment of immunity and oxidative stress in these organisms.

USC
UNIVERSIDADE
DE SANTIAGO
DE COMPOSTELA

ANNEX I. RESUMO

USC
UNIVERSIDADE
DE SANTIAGO
DE COMPOSTELA

RESUMO

Dende que Richard Feynman introducise o concepto de nanociencia no ano 1959, a evolución da nanotecnoloxía non se detivo. Engloba diversas áreas, como a química, a ciencia dos materiais, a medicina, a toxicoloxía, a ecotoxicoloxía e a industria. A Comisión Europea (EC) definiu no ano 2011 un nanomaterial (NM) como un material natural, incidental ou manufacturado no que o 50% ou máis das súas partículas libres ou agregadas teñen unha ou mais dimensións externas no rango de tamaño entre 1 e 100 nm. As nanoláminas, os nanotubos e as nanopartículas (NPs) posúen unha, dúas e tres dimensións en dita escala nanométrica, respectivamente. Estes NMs presentan propiedades fisicoquímicas, electrónicas, ópticas e mecánicas moi novidosas, ademais dunha elevada reactividade.

O dióxido de titanio (TiO_2) foi comercializado por primeira vez no ano 1916. Pódese atopar baixo o nome de óxido de titanio (IV), titanio branco ou pigmento branco 6 en pinturas e E171 como aditivo alimentario. Tradicionalmente, usábase como pigmento en pinturas, recubrimentos, plásticos, tintas e comida. As TiO_2 NPs presentan unha maior actividade fotocatalítica, así como dispersión da luz e opacidade. Son tamén axentes antimicrobianos. Empréganse en fotovoltaica, fotocatálise e medicina. Ademais, inclúense en cosméticos como escudo contra a radiación ultravioleta (UV).

As NPs de prata (Ag) son moi populares debido a que presentan propiedades fisicoquímicas novidosas, como elevada condutividade eléctrica e térmica, estabilidade química, actividade catalítica e comportamento óptico non lineal. Teñen propiedades antimicrobianas fronte a bacterias Grampositivas e Gramnegativas, fungos e virus. Están incluídas como un dos NMs mais empregados con fins comerciais. Destaca a súa utilización en campos como a catálise, a electrónica, a

óptica, o medio ambiente, a industria téxtil, os produtos de coidado persoal, a industria alimentaria e a medicina.
Os efectos da nanotecnoloxía sobre os seres humanos e o medio ambiente son descoñecidos en gran medida. A nanotecnoloxía pretende identificar, manexar e reducir os potenciais efectos adversos causados polos NMs. Debido ás propiedades únicas que presentan, estes materiais poden provocar efectos desfavorables que non foran observados nos materiais masivos. As rutas principais de entrada dos NMs no organismo son a inxestión, a inhalación e a penetración cutánea. O seu comportamento é unha combinación dos procesos de absorción, distribución, metabolismo e excreción (ADME).
A nanotecnoloxía utilizouse en varias etapas da produción alimentaria, como o procesamento, o embalaxe, o almacenamento e o consumo. Existe preocupación acerca do uso directo dos NMs en produtos alimentarios, a súa migración dende os embalaxes ou sensores ás matrices alimentarias e o seu uso durante a etapa de produción, xa que poden levar a unha exposición humana non intencionada a través da inxestión. O proceso de dixestión pode afectar ás características fisicoquímicas dos NMs (disolución e agregación), alterando a súa toxicidade. Os estudos de bioaccesibilidade (fracción dun compoñente que é liberado dende unha matriz alimentaria nos fluídos dixestivos) e biodispoñibilidade (fracción que cruza a parede gastrointestinal e é capaz de alcanzar a circulación sistémica) son de gran importancia.
Os NMs son considerados contaminantes emerxentes e a súa presencia pode causar efectos adversos. Unha vez no medio ambiente, os NMs son sometidos a procesos de transformación físicos, químicos ou biolóxicos marcados polas propiedades dos NMs e as condicións ambientais. Os tres compartimentos ambientais afectados son o aéreo ou atmosférico, os solos e a auga. Especificamente, os NMs poden ser liberados no mar, onde os organismos bivalvos que habitan o fondo mariño (sedentarios e filtradores) son dianas para a acumulación e toxicidade de contaminantes. Estes poden penetrar a través das branquias ou o sistema dixestivo e traspasar á hemolinfa ou a outros órganos.
Cando os NMs entran en contacto cos fluídos biolóxicos, a interacción dos NMs coas proteínas do medio resulta na formación dunha coroa proteica cuxa composición, anchura e conformación dependen das

propiedades dos NMs, da natureza do medio e da duración da exposición. Esta estrutura divídese en "coroa dura" (proteínas de alta afinidade que interaccionan directamente co NM) e "coroa branda" (proteínas debilmente unidas que interaccionan coas proteínas da "coroa dura"). A proteína coroa confírelle aos NMs unha nova identidade que marcará o seu transporte, mecanismo de captación e localización intracelular.

A análise dos NMs implica a súa detección e cuantificación (concentración en masa e número), xunto coa súa caracterización física (tamaño, forma e propiedades superficiais) e química (composición do núcleo e posible recubrimento). Acostuma a ser necesaria a preparación previa das mostras antes da súa análise, por exemplo, mediante métodos de dixestión enzimática ou ácida. Técnicas derivadas da espectrometría de masas con plasma de acoplamento indutivo (ICP-MS) poden empregarse para a caracterización e cuantificación de NPs, como ICP-MS en modo de detección de partículas individuais (sp-ICP-MS) ou ICP-MS xunto coa técnica de fraccionamento en campo de fluxo con fluxo asimétrico (AF4-ICP-MS). Outras técnicas, como a microscopía electrónica de barrido (SEM) ou de transmisión (TEM) e a dispersión dinámica da luz (DLS) empréganse para a caracterización das NPs.

Esta tese dividiuse en catro partes principais: (1) a optimización de métodos de extracción enzimáticos de TiO_2 NPs e Ag NPs presentes en produtos do mar (moluscos bivalvos) e derivados (paus de caranguexo); (2) a optimización da separación das NPs nos extractos enzimáticos de moluscos bivalvos mediante a técnica AF4 xunto con distintos detectores; (3) a avaliación do risco potencial de TiO_2 NPs e Ag NPs en humanos a través da inxestión de produtos alimentarios que conteñen estas NPs; e (4) caracterización das proteínas coroa asociadas a NPs na hemolinfa de moluscos bivalvos.

Parte I. Hidrólise enzimática para a análise de NPs por sp-ICP-MS

A. Hidrólise enzimática como método de pretratamento para a avaliación de TiO_2 NPs en paus de caranguexo por sp-ICP-MS

Un método de pretratamento de mostras de paus de caranguexo baseado na hidrólise enzimática foi optimizado e validado para o illamento de TiO_2 NPs incluídas como parte do aditivo alimentario E171. Mostras de paus de caranguexo, frescas e conxeladas, foron mercadas en supermercados locais e homoxeneizadas mediante trituración. A concentración total de titanio (Ti) foi analizada mediante ICP-MS, previa dixestión ácida asistida por microondas. Para a extracción de TiO_2 NPs, un volume de 7.5 mL dunha disolución de pancreatina e lipasa (8 g L^{-1}), preparada nun tampón de 0.2 M NaH_2PO_4/0.2 M NaOH a pH 7.4, foi incubada con 1.0 g de mostra homoxeneizada a 37 ºC con axitación (200 rpm) durante 12 h. Os extractos foron centrifugados (8 ºC, 3900 rpm, 10 min) e almacenados a 4 ºC. A análise dos extractos diluídos empregando glicerol 1% (v/v) levouse a cabo por sp-ICP-MS.

Non se observou efecto matriz, polo tanto, empregáronse calibrados acuosos de Ti iónico. Obtivéronse bos valores de repetibilidade, en termos de desviación estándar relativa (RSD%), de 25 e 8% para a concentración e tamaño de TiO_2 NPs, respectivamente. A sensibilidade expresouse empregando o límite de detección (LOD) e o límite de cuantificación (LOQ). Os seus valores foron 5.10×10^5 e 1.70×10^6 NPs g^{-1}, respectivamente. O LOD foi 31.3-37.1 nm para o tamaño de TiO_2 NPs. Os valores de recuperación analítica con estándares de TiO_2 NPs de 50 e 100 nm foron 108±5% e 105±4%.

Unicamente once das vinte e dúas mostras analizadas contiñan Ti. O método de extracción optimizado aplicouse a estas mostras e atopáronse concentracións entre 1.96×10^7 e 1.19×10^8 TiO_2 NPs g^{-1}. A distribución de tamaños obtida foi moi diferente entre mostras (valores de tamaño mais frecuentes entre 42 e 75 nm e tamaños medios entre 65 e 217 nm).

A presenza de TiO_2 NPs foi corroborada mediante a análise dos extractos enzimáticos por TEM despois dun tratamento con peróxido de hidróxeno e quentamento para eliminar ou diminuír a carga de materia orgánica presente.

B. Hidrólise enzimática asistida por ultrasóns para illar TiO_2 NPs de moluscos bivalvos antes da súa medida por sp-ICP-MS

A caracterización e cuantificación de TiO_2 NPs en mostras de moluscos bivalvos foi levada a cabo mediante sp-ICP-MS previa hidrólise enzimática acelerada por ultrasóns. Analizáronse un total de once mostras de moluscos bivalvos, frescos e conxelados, adquiridos en mercados e supermercados locais. As mostras foron lavadas con auga ultrapura e homoxeneizadas mediante trituración. O contido total de Ti nas mostras foi analizado mediante ICP-MS, despois dun proceso de dixestión ácida asistida por microondas. Para a extracción de TiO_2 NPs, 7.5 mL dunha disolución das enzimas pancreatina e lipasa (3 g L^{-1}), preparada en 0.2 M NaH_2PO_4/0.2 M NaOH a pH 7.4, foron engadidos a 1.0 g de mostra. A mestura foi sometida a ultrasonicación (60% de amplitude) durante 10 min nun baño de xeo. Os extractos centrifugados (8 ºC, 3900 rpm, 25 min) e diluídos con glicerol 1% (v/v) foron medidos por sp-ICP-MS.

Utilizáronse calibrados acuosos de Ti iónico ao non observarse efecto matriz. RSD% do 17 e 3% foron obtidas para a concentración e tamaño de TiO_2 NPs ao longo de todo o proceso. Os LOD e LOQ para a concentración de TiO_2 NPs foron 5.28×10^6 e 1.76×10^7 NPs g^{-1}, respectivamente. O LOD en tamaño calculado en base aos criterios 3σ e 5σ foron 24.4 e 30.4 nm. Estudouse a recuperación analítica cun estándar de TiO_2 NPs de 50 nm a dúas concentracións (7 e 14 µg L^{-1}) e obtívose un valor medio de 95±6%.

Mostras de ameixas, berberechos, mexillóns, navallas, ostras e zamburiñas foron analizadas. Todas elas contiñan Ti e TiO_2 NPs. Acháronse concentracións totais de Ti entre 0.285 e 3.42 µg g^{-1}. Con respecto ás concentración de TiO_2 NPs, o valor mais alto atopouse en mexillóns ($1.25\times10^8\pm1.06\times10^7$ NPs g^{-1}), mentres que unha mostra de

navalla tiña a concentración mais baixa ($2.36\times10^7\pm2.54\times10^6$ NPs g^{-1}). As mostras presentaron tamaños máis frecuentes de TiO_2 NPs similares (53-69 nm).

A presenza de NPs foi confirmada mediante DLS en distintos extractos enzimáticos. A maioría das mostras mostraron índices de polidispersión maiores a 1.1 e dúas distribucións de tamaño.

C. Determinación e caracterización de Ag NPs en moluscos bivalvos mediante hidrólise enzimática asistida por ultrasóns e sp-ICP-MS

Mostras de moluscos bivalvos (ameixas, berberechos, mexillóns, navallas, ostras e zamburiñas) foron tratadas mediante hidrólise enzimática acelerada por ultrasóns para a caracterización e cuantificación de Ag NPs. Os moluscos bivalvos, adquiridos en mercados e supermercados locais, foron lavados con auga ultrapura e triturados. Para a determinación do contido total de Ag, as mostras foron sometidas a unha dixestión ácida asistida por microondas e analizadas por ICP-MS. As Ag NPs foron extraídas engadindo 10 mL dunha disolución enzimática de pancreatina e lipasa (2 g L^{-1}), preparada en 0.2 M NaH_2PO_4/0.2 M NaOH a pH 7.4, a 1.0 g de mostra. A mestura someteuse a ultrasonicación (80% de amplitude) durante 10 min nun baño de xeo. Os extractos enzimáticos foron centrifugados (8 ºC, 3900 rpm, 25 min) e diluídos empregando glicerol 1% (v/v) antes da súa análise por sp-ICP-MS.

Ao non observarse efecto matriz, traballouse con calibrados acuosos de Ag iónica. As RSD% foron de 8 e 3% para a determinación da concentración e tamaño das Ag NPs. No referente á sensibilidade, os LOD e LOQ foron 4.17×10^6 e 1.39×10^7 Ag NPs g^{-1}. O LOD en tamaño calculouse empregando diferentes métodos e obtivéronse valores entre 13 e 23 nm. Os valores de recuperación analítica con estándares de Ag NPs de 40 e 60 nm foron 109±10% e 92±2%, respectivamente.

En sete das once mostras analizadas, atopáronse concentracións totais de Ag entre 0.0841 y 3.72 µg g^{-1}. Con respecto á concentración de Ag NPs (1.56×10^7-1.85×10^9 Ag NPs g^{-1}), as concentracións mais altas analizadas foron as de zamburiñas, ostras e ameixas xaponesas,

mentres que as ameixas atlánticas presentaron a concentración mais baixa.

Para a confirmación da presenza de Ag NPs nos extractos enzimáticos, levouse a cabo unha análise por SEM despois dun tratamento con peróxido de hidróxeno e quentamento.

Parte II. Optimización da separación de NPs mediante a técnica AF4 xunto con distintos detectores

D. AF4-UV-ICP-MS para a detección e cuantificación de Ag NPs en moluscos bivalvos despois dunha hidrólise enzimática

Desenvolveuse un método de separación empregando a técnica AF4 xunto con espectroscopía UV e ICP-MS para a detección e cuantificación de Ag NPs en moluscos bivalvos (ameixas, ostras e zamburiñas). Aproximadamente 1.0 g de cada mostra foi pretratado mediante hidrólise enzimática con 10 mL dunha disolución de pancreatina e lipasa (2.0 g L^{-1}), preparada en 0.2 M Trizma® con pH axustado a 7.4. A mestura foi incubada a 37 ºC durante 12 h nun forno equipado cun rotor circular. Os residuos sólidos foron eliminados mediante centrifugación (8 °C, 3900 rpm, 25 min).

A separación na canle do sistema AF4 levouse a cabo cunha membrana de celulosa rexenerada (10 kDa, 350 µm espaciador) e unha disolución 5 mM Tris-HCl como fase móbil. Durante a etapa de enfoque (4.0 min), empregáronse fluxos de introdución e de enfoque de 0.20 e 3.0 mL min^{-1}, respectivamente. Na etapa de elución, o fluxo cruzado foi de 3.0 mL min^{-1} durante 15 min, seguido dun decaemento lineal durante 7.5 min e unha etapa de lavado de 9.4 min.

Os moluscos bivalvos foron analizados para a determinación do contido total de Ag (dixestión ácida asistida por microondas e análise por ICP-MS) e de Ag NPs polo método proposto. As concentracións máis alta e máis baixa de Ag nas fraccións de AF4 atopáronse nunha mostra de zamburiña conxelada e de ostra, respectivamente. Tódalas concentracións estaban dentro do rango 4.1×10^{1}-2.3×10^{2} µg Ag kg^{-1}, mentres que os contidos totais de Ag tiñan valores entre 1.6×10^{2} e

3.7×10^3 µg Ag kg^{-1}. Os fractogramas AF4-UV-ICP-MS mostran diferentes distribucións de tamaño de Ag NPs debido ao diferente perfil de elución. As recuperacións da membrana obtidas para as distintas mostras tiñan valores entre 49 e 121%. Ademais, nos espectros UV obsérvase a elución simultánea das Ag NPs con proteínas, o que suxire certa interacción entre ambas.

Parte III. Avaliación do risco potencial de TiO_2 NPs e Ag NPs en humanos a través da inxestión de produtos alimentarios que conteñen NPs

E. Cálculo da porcentaxe de biopersistencia de NPs metálicas no tracto gastrointestinal humano (Etapa 0 da guía EFSA para a análise de riscos de NMs)

Seguindo as recomendacións da guía EFSA para a análise dos riscos dos NMs en alimentos e na cadea alimentaria, levouse a cabo unha aproximación *in vitro* dunha dixestión gastrointestinal humana para avaliar a biopersistencia de TiO_2 NPs e Ag NPs en estándares e alimentos. Dous tamaños (TiO_2 NPs de 50 e 100 nm e Ag NPs de 40 e 60 nm) a tres niveis de concentración foron estudados. Ademais, avaliáronse o aditivo alimentario E171 e mostras de moluscos bivalvos e paus de caranguexo que contiñan NPs. Os volumes correspondentes dos estándares e disolución de E171, ou 5.0 g das mostras, foron engadidos a matraces Erlenmeyer e completouse o volume a 50 mL con auga ultrapura. O pH axustouse a 2.0 cunha disolución de 0.6 M HCl. Unha concentración de 7.5 mg mL^{-1} de disolución gástrica (0.16 g mL^{-1} pepsina en 0.1 M HCl) foi engadida. As mostras incubáronse durante 2 h a 37 °C con axitación orbital-horizontal (150 rpm). A dixestión gástrica parouse introducindo as mostras nun baño de xeo. O pH da mestura foi axustado a 7.0 empregando 0.2 M NaOH, seguido da adición de 25% (v/v) de disolución intestinal (4 g L^{-1} pancreatina e 25 g L^{-1} sales biliares en 0.1 M $NaHCO_3$). As mostras incubáronse outras 2 h coas condicións anteriormente mencionadas. A concentración das NPs, a súa distribución de tamaños e o contido iónico foron analizados ao inicio

inicio da dixestión (T0) e a tres tempos diferentes (30, 60 e 120 min) durante as etapas gástrica e intestinal. As medidas leváronse a cabo mediante sp-ICP-MS.

En xeral, observouse aglomeración das NPs durante a etapa gástrica e dispersión das NPs durante a etapa intestinal. As Ag NPs mostraron un comportamento condicionado polo tamaño. Mentres que no estándar de Ag NPs de 40 nm as NPs aglomeráronse durante a etapa gástrica, no estándar de 60 nm dominou a ionización. Ademais, a matriz dos alimentos demostrou influír na biopersistencia das NPs. As TiO_2 NPs en moluscos bivalvos liberáronse dunha maneira progresiva ao longo da dixestión gastrointestinal a diferenza das incluídas en mostras de paus de caranguexo, que seguen un comportamento parecido aos estándares e ao E171. As Ag NPs en moluscos seguen tendencias diferentes en función da mostra.

Os estándares de TiO_2 NPs e o aditivo alimentario E171 non se degradaron durante a dixestión. Observouse que as Ag NPs nos estándares eran menos biopersistentes que as TiO_2 NPs. Unha maior degradación das Ag NPs con respecto a TiO_2 NPs tamén se atopou nas mostras. En tódolos casos, as porcentaxes de biopersistencia calculadas foron maiores a 12% (o límite marcado pola EFSA).

F. Caco-2 como modelo in vitro do tracto gastrointestinal humano para o estudo da absorción de TiO_2 NPs e Ag NPs presentes en moluscos bivalvos

Diferentes mostras de moluscos bivalvos que contiñan TiO_2 NPs e Ag NPs foron sometidas a unha aproximación *in vitro* dunha dixestión gastrointestinal humana para determinar a bioaccesibilidade destas NPs. Seleccionáronse células Caco-2 como mellor aproximación do epitelio intestinal humano para levar a cabo os estudos de transporte. Tanto a bioaccesibilidade como o transporte foron analizados para os contidos totais de Ti e Ag e para TiO_2 NPs e Ag NPs mediante medidas por ICP-MS e sp-ICP-MS, respectivamente.

As células Caco-2 mantivéronse en medio Eagle modificado por Dulbecco (DMEM) enriquecido con 10% (v/v) soro fetal bovino, 2 mM

L-glutamina, 1% (v/v) penicilina/estreptomicina, 1 mM piruvato sódico e 1 mM aminoácidos non esenciais (NEAA) a 37 ºC, humidade relativa 95% e 5% CO_2. O medio cambiouse cada 2 ou 3 días (80% de confluencia). Separáronse as células con tripsina e engadíronse (7.5×10^4 células cm^{-2}) aos insertos con membrana de poliéster das placas Transwell®. 1.5 mL das células resuspendidas en DMEM engadíronse ao compartimento apical e 2 mL de DMEM ao compartimento basolateral. Mediuse a resistencia epitelial transmembrana (TEER) ata que alcanzou un valor de 250 mΩ cm^2. Un volume de 7.5 mL da fracción bioaccesible (mostras dixeridas seguindo o protocolo especificado na sección anterior) quentáronse a 100 ºC durante 5 min para desactivar as enzimas. Engadiuse glucosa (1 g L^{-1}) e axustouse a osmolaridade (250-300 mOsm kg^{-1}) con cloruro sódico 10 mM. O ensaio de transporte realizouse engadindo este bioaccesible tratado e co marcador Lucifer Yellow ao compartimento apical (1.5 mL) e a solución salina equilibrada de Hank (HBSS) ao compartimento basolateral (2 mL). Os Transwell® incubáronse baixo as condicións anteriormente mencionadas. Pasadas 2 h, recolléronse as fraccións apical e basal e as células recuperáronse engadindo tampón fosfato salino (PBS) ao compartimento apical para lavar e tripsina para despegalas.

As porcentaxes de bioaccesibilidade foron dende 2.9 ata 89% para Ti e dende 6.5 ata 51% para Ag, mentres que os porcentaxes de bioaccesibilidade para TiO_2 NPs e Ag NPs estaban entre 2.1-51% e 13-17%, respectivamente. No referente ao transporte, atopáronse valores entre 18 e 68% para Ti e entre 0.016 e 0.017% para Ag. Os valores de transporte para TiO_2 NPs e Ag NPs estaban entre 17-82% e 2.1-22%, respectivamente. Os transportes de Ti e TiO_2 NPs foron similares, mentres que se observaron diferenzas entre Ag e Ag NPs. Os tamaños nas fraccións bioaccesibles foron maiores que nas fraccións apicais, basolaterais e nas células para a maioría das mostras.

Parte IV. Caracterización das proteínas coroa asociadas a NPs na hemolinfa de moluscos bivalvos

G. Caracterización e cuantificación da coroa proteica asociada a TiO_2 NPs na hemolinfa de moluscos bivalvos

Ameixas foron expostas a estándares de TiO_2 NPs de 50 e 100 nm e ao aditivo alimentario E171, que contén nano- e micro-Ti. Preparáronse catro tanques (1 control, 1 TiO_2 NPs 50 nm, 1 TiO_2 NPs 100 nm e 1 E171) con 30 espécimes de ameixa cada un. Empregouse auga mariña filtrada como medio e instaláronse sistemas de aireación. As ameixas alimentáronse cada dous días con fitoplancto cultivado *in vitro*. As concentracións dos estándares de TiO_2 NPs e E171 aumentáronse de maneira progresiva, en incrementos de 2 mg L^{-1}, dende 0 a 14 mg L^{-1} durante 18 días. Tomouse un espécime por tanque ao inicio do experimento (0 mg L^{-1}), ao noveno día (8 mg L^{-1}) e o último día da exposición (14 mg L^{-1}), e extraeuse a hemolinfa.

Seleccionouse a centrifugación como método de separación das proteínas coroa (sedimento) e as proteínas libres (fase líquida) na hemolinfa. O perfil de evolución das proteínas coroa ao longo do experimento foi estudado cualitativa e cuantitativamente mediante cromatografía líquida xunto con espectrometría de masas en tándem (LC-MS/MS) e por espectrometría de masas con adquisición secuencial de todo o espectro teórico (SWATH-MS), respectivamente.

Detectouse unha enorme variabilidade no perfil de proteínas entre espécimes incluso antes da exposición ás NPs. A afinidade destas NPs polas proteínas foi cambiando ao longo do tempo. Durante a exposición a TiO_2 NPs de 50 nm, produciuse unha diminución da concentración dos compoñentes do complemento (C3 e C1q) relacionados coa inmunidade innata. A concentración da superóxido dismutasa (marcador de estrés oxidativo) e das histonas aumentaron, pero non estableceron interacción con ditas NPs. Cando a exposición se levou a cabo con TiO_2 NPs de 100 nm, observouse alta afinidade polas histonas (H2A e H2B) e baixa afinidade polo compoñente C3 do complemento. As proteínas "heat shock", marcadores de estrés, formaban parte das coroa xunto

coa ATP sintasa (subunidade beta). O aditivo E171 presentou elevada afinidade pola proteína C1q do complemento, histonas (H2A e H2B), talina-1, catalasa e superóxido dismutasa. A concentración da enzima citocromo c oxidasa aumentou progresivamente pero non interaccionou coas NPs. Ademais, tamén se produciu unha diminución da concentración do compoñente C3 do complemento. En xeral, a diminución da concentración dos compoñentes do complemento e o incremento dos marcadores de estrés poderían estar relaciones con alteracións no sistema inmunolóxico e estrés oxidativo causados polas TiO_2 NPs.

USC
UNIVERSIDADE
DE SANTIAGO
DE COMPOSTELA

USC
UNIVERSIDADE
DE SANTIAGO
DE COMPOSTELA

ANNEX II. LIST OF PUBLICATIONS

USC
UNIVERSIDADE
DE SANTIAGO
DE COMPOSTELA

LIST OF PUBLICATIONS

During the development of this Doctoral thesis the following works have been published in scientific journals:

- M.V. Taboada-López, P. Herbello-Hermelo, R. Domínguez-González, P. Bermejo-Barrera, A. Moreda-Piñeiro, Enzymatic hydrolysis as a sample pre-treatment for titanium dioxide nanoparticles assessment in surimi (crab sticks) by single particle ICP-MS, Talanta 195 (2019) 23-32 (DOI: 10.1016/j.talanta.2018.11.023).

Impact factor (2019): 5.339 Times cited: 8

Position in "Analytical Chemistry" ranking (2019): 11/86

M.V. Taboada-López's contribution: investigation, formal analysis and writing (original draft)

- M.V. Taboada-López, S. Iglesias-López, P. Herbello-Hermelo, P. Bermejo-Barrera, A. Moreda-Piñeiro, Ultrasound assisted enzymatic hydrolysis for isolating titanium dioxide nanoparticles from bivalve mollusk before sp-ICP-MS, Anal. Chim. Acta 1018 (2018) 16-25 (DOI: 10.1016/j.aca.2018.02.075).

Impact factor (2018): 5.256 Times cited: 8

Position in "Analytical Chemistry" ranking (2018): 10/84

M.V. Taboada-López's contribution: investigation, formal analysis and writing (original draft)

- M.V. Taboada-López, N. Alonso-Seijo, P. Herbello-Hermelo, P. Bermejo-Barrera, A. Moreda-Piñeiro, Determination and characterization of silver nanoparticles in bivalve molluscs by ultrasound assisted enzymatic hydrolysis and sp-ICP-MS, Microchem. J. 148 (2019) 652-660 (DOI: 10.1016/j.microc.2019.05.023).

Impact factor (2019): 3.594 Times cited: 1

Position in "Analytical Chemistry" ranking (2019): 19/86

M.V. Taboada-López's contribution: investigation, formal analysis and writing (original draft)

USC
UNIVERSIDADE
DE SANTIAGO
DE COMPOSTELA

USC
UNIVERSIDADE
DE SANTIAGO
DE COMPOSTELA